1994

Effects Of Line Inclination On The Hydrodynamics Of Riser Transport In The Non-slugging Dense Phase Flow Regime

Gupta Supriya Sen

EFFECTS OF LINE INCLINATION ON THE HYDRODYNAMICS OF RISER TRANSPORT IN THE NON-SLUGGING DENSE PHASE FLOW REGIME

by

Supriya Kumar Sen Gupta

Faculty of Engineering Science

Department of Chemical & Biochemical Engineering

Submitted in partial fulfilment

of the requirements for the degree of

Doctor of Philosophy

Faculty of Graduate Studies

The University of Western Ontario

London, Ontario, Canada

December 1993

National Library
of Canada

Acquisitions and
Bibliographic Services Branch

395 Wellington Street
Ottawa, Ontario
K1A 0N4

Bibliothèque nationale
du Canada

Direction des acquisitions et
des services bibliographiques

395, rue Wellington
Ottawa (Ontario)
K1A 0N4

Your file Votre reference

Our file Notre reference

ISBN 0-315-90580-8

Canada

ABSTRACT

The present work was undertaken to evaluate the effects of slight line inclinations ($\theta \leq 18°$ from the vertical) on the hydrodynamics of non-slugging dense phase upwards cocurrent gas-solids flows. Previous research and operating experience has focused on the dilute phase flow regime where $[\partial(\partial P/\partial z)]/\partial U_g > 0$. This thesis is restricted to the regime where $[\partial(\partial P/\partial z)]/\partial U_g < 0$ and for which refluxing of particles, without slug flow, dominates in the flow patterns.

Experiments were conducted with 197 μm sand particles and 441 μm glass beads in a 3.2 cm diameter Plexiglas tube. Use of the two particle sizes (Geldart Group B powders) enabled the characterization of different systems : the first with sand, showed a slow transition from the non-slugging dense (reflux flows) to the dense slugging regime; the other using glass beads, collapsed abruptly into a slugging flow with a slight decrease of gas velocity near the choking point.

The pressure gradient and solids holdup (α) in the fully developed riser test section increased linearly with both the solids flux (50 - 300 kg/m^{2}s) and solids mass loading ratio (5 - 40), but decreased with the gas velocity for both sand (4.5 - 12 m/s) and glass beads (6 - 16 m/s). The solids-wall

frictional pressure gradient contributed between -25% and 25% of the total gradient, and was negative whenever there was solids refluxing at the wall. A 2-parameter semi-empirical model was developed which was successfully employed for the correlation of negative solids-wall friction factors.

A lifting efficiency of 2-phase transport in oblique risers (η) was defined, which decreased with θ, from 75% (of the theoretical single particle lifting efficiency in dilute phase transport), to 35-45% for $\theta \geq 11°$. The decrease of η was attributed to extensive refluxing near choking. A previous study has shown that $\eta < 10\%$ for dilute phase transport.

The dominant frequency from the power spectrum of the pressure gradient time series was 5 Hz for sand and 3 Hz for glass beads. The pressure gradient time series could be stochastically modelled with a linear stationary ARIMA model of the form AR(2) or AR(3).

ACKNOWLEDGEMENTS

The author would like to express his sincere gratitude to the Natural Science and Engineering Research Council for research funding of this project. Gratitude is expressed to thesis supervisor Dr. John Beeckmans, whose guidance and helpful suggestions throughout the course of this work were invaluable towards its successful completion.

Grateful acknowledgement is also made to the many helpful comments of the Advisory Committee panel comprised of Drs. M.A. Bergougnou and C. Briens. Use of the laboratory space provided by Dr. M.A. Bergougnou is sincerely appreciated.

Dr. Z. Shen and Mr. S. Afara are thanked for their assistance in the laboratory and for some inspired comments during the course of the program. Construction of the pneumatic transport rig and auxiliary equipment by the U.W.O. mechanical shop is gratefully appreciated. The author thanks the assistance of the U.W.O. Electrical Shop in the construction and commissioning phases of this project.

Page

TABLE OF CONTENTS

Page

Page

Page

LIST OF TABLES

Page

LIST OF FIGURES

Page

LIST OF FIGURES

LIST OF FIGURES

LIST OF FIGURES

LIST OF FIGURES

LIST OF FIGURES

LIST OF FIGURES

Page

LIST OF APPENDICES

Page

THESIS NOMENCLATURE

Symbol	Units	Description
A	$[m^2]$	Cross-sectional pipe area
d_p , D_p	[m , μm]	Particle Diameter
D, D_t	[m]	Tube Diameter
$E_{diss.}$	[-]	Fractional Energy Dissipated
Fr	[-]	Froude Number
f_s	[-]	Solids-Wall Friction Factor
f_g	[-]	Gas-Wall Friction Factor
g	$[m/s^2]$	Gravitational constant
H	[m]	Test section height
L	[m]	Test section length
P_i	[Pa , kPa]	Pressure signals
$\Delta P/L$	[Pa/m]	Pressure gradient
r	[m]	Radial coordinate
R	[m]	Pipe radius
R^2	[- , %]	Correlation squared statistic
Re	[-]	Reynolds Number
U_{gs}	[m/s]	Gas velocity uncorrected for voidage
U_g , U_{gc}	[m/s]	Gas velocity voidage corrected, Choking Velocity
U_t	[m/s]	Terminal particle velocity
U_p , U_s	[m/s]	Mean particle or solids velocity
U_{slip}	[m/s]	Slip velocity
u_{mf}	[m/s]	Minimum Fluidization velocity
W_{sf} , W_s	[kg/s]	Solids flowrate, Solids Flux

Thesis Nomenclature Cont'd

Symbol	Units	Description
ε_c , ε	[m^3/m^3]	Choking voidage, Mean Voidage
μ_g	[kg/m/s]	Gas viscosity
ρ_p or ρ_s	[kg/m^3]	Particle or solid density
ρ_g	[kg/m^3]	Gas density
Φ	[-]	Radial coordinate
θ	[°]	Line inclination, degrees
α , α_s	[m^3/m^3]	Solids volumetric holdup
μ	As applicable	Mean of Distribution
σ	As applicable	Standard deviation of Distribution
ψ	[-]	Skewness of Distribution
κ	[-]	Kurtosis of Distribution
Γ	[Pa^2]	Coherence of Power Spectrum
P_i	[Pa , kPa]	Pressure signals
η_{gross} , η_{net} , η_p	[%]	Gross, Net, Particle Lifting Efficiency
ξ	[%]	Absolute average deviation
τ	[s]	Time lag in time series study
ΔP_m	[Pa/m]	Total pressure gradient including acceleration terms
ΔP_{fs}	[Pa/m]	Solids-wall frictional pressure drop
Rp (τ)	[-]	Autocorrelation
Φ (τ)	[-]	Partial Autocorrelation
M_s	[kg]	Mass of solids between pinch valves
Δt , Δt_{pv}	[ms]	Pinch valve closure time difference
β	[bytes]	Signal intensity
ΔU_g	[J]	Energy consumption of gas phase
ΔU_s	[J]	Potential energy gain of solid phase

Thesis Nomenclature Cont'd

ACRONYM	DESCRIPTION
PDF	Probability Density Function
PSD	Particle Size Distribution
AAD ; AD	Absolute average deviation; Average deviation
VEL.	Velocity
CORR.	Correlation

BACKGROUND

Because of the lack of work in the non-slugging dense phase regime to date (even for horizontal and vertical pipe configurations) there is a noticeable lack of design guidelines available in the literature for risers operating in this regime (Leung, 1980). The effects of line inclination on the pressure gradient, solids holdup and pump power requirements are mostly unknown. The current design practice is to use the correlations developed for vertical and horizontal lines in off-vertical pipes for small angles of inclination (Rose and Duckworth, 1969a). Although this method may be accurate enough for dilute phase flows where particles are all entrained, it is not suitable for non-slugging flows because of the refluxing of particles and multiple flow patterns which are possible with inclined lines.

A slight line inclination can change the flow pattern from annular to choking flow. The solids holdup in the inclined lines cannot be predicted from vertical line correlations. Neither can the choking velocity be established from data on vertical transport lines. Expansion of the existing database on non-slugging flows is necessary to be able to generate reliable correlations for the prediction of pressure gradient, choking velocity, solids refluxing, and solids holdup, from the basic design variables such as solids loading and pipe diameter. A slight line inclination in the non-slugging dense phase (in lieu of the elbow connecting straight pipes) could save

power and decrease attrition of expensive particles. It may also significantly reduce operating maintenance due to wear of the equipment from sandblasting action of the particles on elbow-connected pipes. Since most commercial risers operate in the non-slugging regime (Rhodes et al., 1992a), it is important to determine how the power consumption in this regime compares with dilute phase transport.

OBJECTIVES

The objectives of this thesis were, using the vertical line as a standard for comparison, to:

1. Investigate the effect of small line inclinations (up to 18° from the vertical) on the hydrodynamics of the non-slugging dense phase flow regime, on the basis of time-averaged pressure gradient signals and solids holdup measurements, for 197 μm (sand) and 441 μm (glass beads) particles.

2. Evaluate the effect of small line inclinations on the overall lifting efficiency of pneumatic transport, η , under conditions of solids refluxing with deposition at the pipe walls; Using η as a basis, compare non-slugging dense phase transport (this work), with dilute phase transport from the work of Zaltash (1987).

3. Identify experimental and derived parameters (using statistical and time-series methods for analysis of pressure gradient data) which could be used to characterise non-slugging dense phase flows;

4. Address the significance of line inclination on the 2-phase flow stability in the low gas velocity regime, including the effects on solids refluxing, solids deposition, and transition to choking solids suspensions.

5. Correlate the observed variables including pressure gradient and solids holdup with the independent variables : solids flux, gas velocity, particle size, and line inclination.

1 : LITERATURE REVIEW

1.1. INTRODUCTION TO PNEUMATIC CONVEYING

Although there is an abundance of literature available for pneumatic transport in vertical and horizontal lines, there is a dearth of knowledge for oblique risers in the non-slugging dense phase (Klinzing et al., 1989). This is despite numerous references with regard to the use of oblique risers in the literature, particularly with application in the petroleum industry for catalytic cracking of gas oils (Rhodes et al., 1992a).

Zenz and Othmer (1960) have noted that references are frequently made to the advisability of employing diagonals, rather than vertical runs, whenever possible in piping systems in which material must be conveyed to a higher level. Such installation would reduce the sharp 90° elbow pressure losses and should also decrease the abrasive action of the solid material at the elbows (Rohatgi, 1988). Another area of inclined pneumatic transport, which has not received much attention to date, is the transition of the dilute phase to the non-slugging dense phase. The transition is diffuse and a quantitative method for its prediction is presently not available (Leung and Wiles, 1976).

The common procedure for two-phase flow design (Kokal and Stanislav, 1989) has been to use the correlations developed for vertical and horizontal

lines in off-vertical pipes for small angles of inclination, such as the work of Rose and Duckworth (1969 a,b,c) for dilute phase inclined pneumatic transport lines. This practice can lead to significant errors and large uncertainties in the design phase since some transitions are sensitive to the line inclination. Moreover, such methods are not applicable in the non-slugging dense regime where extensive solids refluxing is known to occur.

The first study on the effect of line inclination on gas-solids hydrodynamics was done by Zenz (1957). He showed that for line inclinations less than 45° *from the horizontal*, particles tended to sediment along the lower half-radius of the pipe, and slid slowly down the tube. If the transport line was further inclined to 67.5° (from the horizontal), at a gas velocity of 5.2 m/s, aggregates were observed, approximately 0.2 m apart. A reduction of gas velocity below 3 m/s resulted in the transition to choking and slug flow. Using 300 μm magnetite particles no changes in flow characteristics were observed when the line was inclined less than 10° from the vertical. At higher line inclinations clusters of solids formed in the tube. This eventually led to slugging conditions or to a tapered layer of solids, settling out on the underside of the tube. Myler (1987) observed retrograde dunes at various inclinations in a 0.0508 m diameter tube which resulted in a maximum in pressure drop fluctuations at those sites.

Ocone et al. (1993) have presented a mathematical model using the equations of motion to predict the hydrodynamics of inclined (dense) pneumatic transport. They observed that, when calculating the stress of the assembly of particles, it is necessary to take into account forces transmitted between particles at points of sustained, rolling, and sliding contact. Their frictional model is capable of predicting the down flowing solids layer at the wall when the line is inclined. It also predicts the asymmetry of the solids holdup profile in inclined ducts.

1.2 ZENZ PLOT

1.2.1 VERTICAL LINES

The selection of an appropriate gas velocity in the design of a pneumatic transport rig is critical to avoid excessive gas requirements and high pressure drops, or unstable slugging flow. Fig. 1.2.1 (Arastoopour, 1986) shows the relationship between the pressure gradient and the gas velocity, commonly referred to as the Zenz plot. The curve OA represents the profile without any solids, or with gas alone in an otherwise empty tube. Curve BCD represents the cocurrent pneumatic transport. Between points C and B the pressure gradient rises because the gas-wall frictional forces dominate. At point C there is a minimum, and between C and D the pressure gradient again rises because of the increasing solids inventory in the line. This type of flow is called dense phase flow and particles are no

Fig. 1.2.1: Effect of Gas Velocity on Pressure Gradient

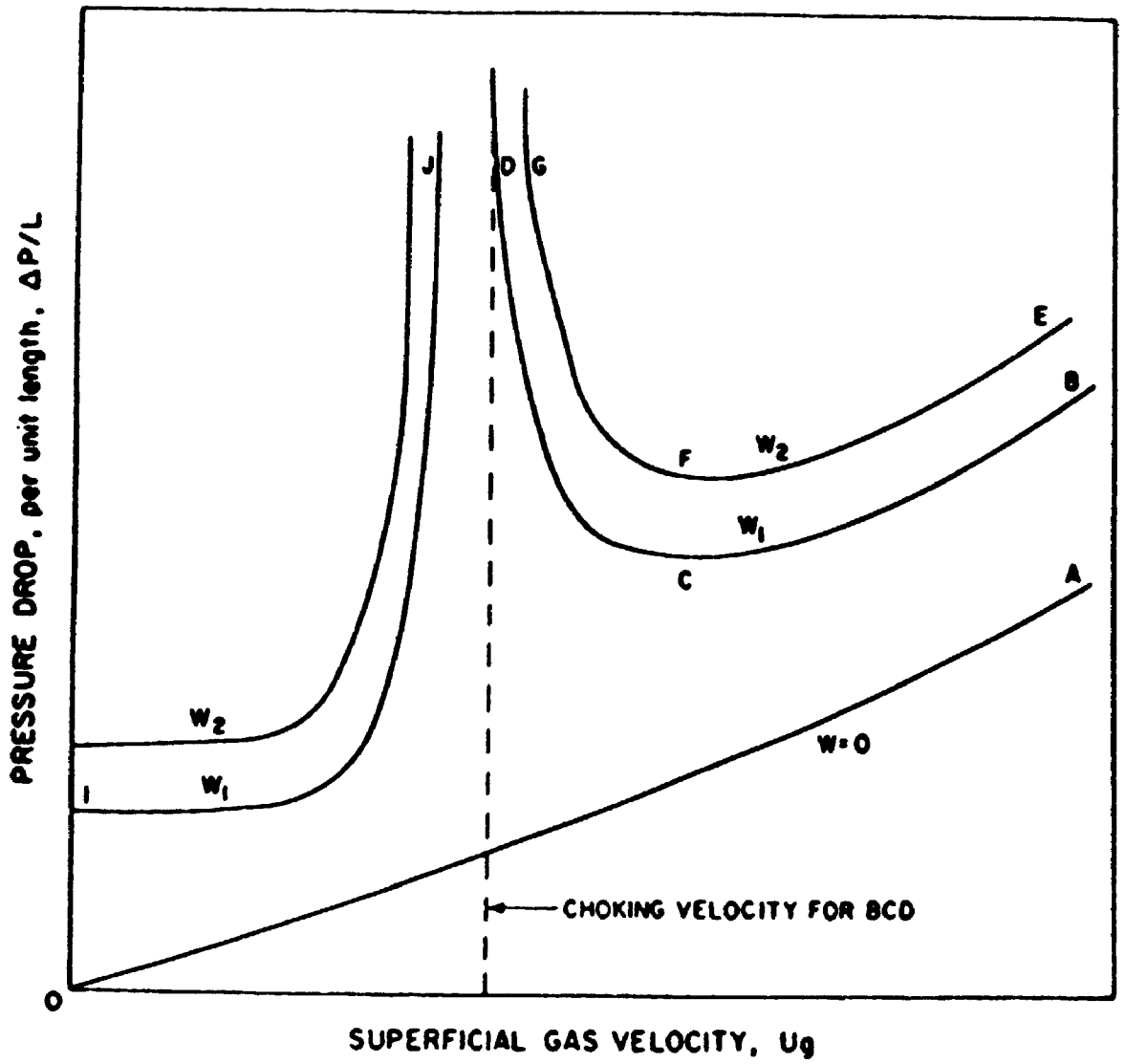

longer in a uniform suspension. This is the flow regime of the present thesis research.

Curve 'IJ' represents the countercurrent gas-solids transport system. An increase in gas velocity results in more drag force on the solids particles, and lower particle velocities, which increases solids inventory and pressure drop.

The region between points C and B refers to dilute phase conveying which has most often been reported in the literature. Slugging dense phase conveying necessitates a higher line pressure drop (Sandy et al., 1970), and gas requirements are much lower than for dilute phase transport. Because of the low solids velocity in dense phase transport, which causes less attrition, it is more desirable for transporting expensive and fragile particles. The transition from dilute to dense phase conveying may be a sharp transition, which results in the collapse of the suspension into slugs and unstable flow. In the dense slugging regime, if the gas velocity is further decreased, the slip velocity is no longer able to support the particles, and the transition from a slugging to a packed or moving bed occurs.

1.2.2 INCLINED LINES

Zenz (1957) showed that the pressure gradient decreased with line

inclination (measured from the vertical) in dilute phase pneumatic transport where $[\partial(\partial P/\partial z)]/\partial U_g > 0$, and this has subsequently been verified by Zaltash (1987). For the non-slugging dense phase regime where $[\partial(\partial P/\partial z)]/\partial U_g < 0$, however, the reverse was apparent (Zenz, 1957); the pressure gradient increased with line inclination (Fig. 1.2.2) for the range of gas velocities between 3 and 7 m/s and a solids flux of 20 to 70 kg/m^{2}s. Zenz noted that for gas velocities above 7 m/s the particles were carried in a well-dispersed stream. Clusters of particles were observed to form for gas velocities slightly below the velocity at the minima of the pressure gradient curves, which were alternately broken and reformed. The restriction of the tube cross section at the cluster-forming sites resulted in the increase of pressure drop observed. With a further reduction of gas velocity the aggregates became more permanent, eventually merging to form bases for the layers of particles settling out in the tube.

Klinzing et al. (1989) studied the effect of line inclination on the hydrodynamics of dilute phase suspensions (gas velocity regime to the right of the Zenz plot minimum). In accordance with Zenz (1957), Klinzing et al. observed that the pressure gradient increased as the pipe was raised from the horizontal orientation for dilute phase transport. The increase was attributed to changes in static head and solids friction factor. The gas velocity at minimum pressure drop was observed to increase with line

Fig. 1.2.2: Effect of Line Inclination on Pressure Gradient (Zenz, 1957)

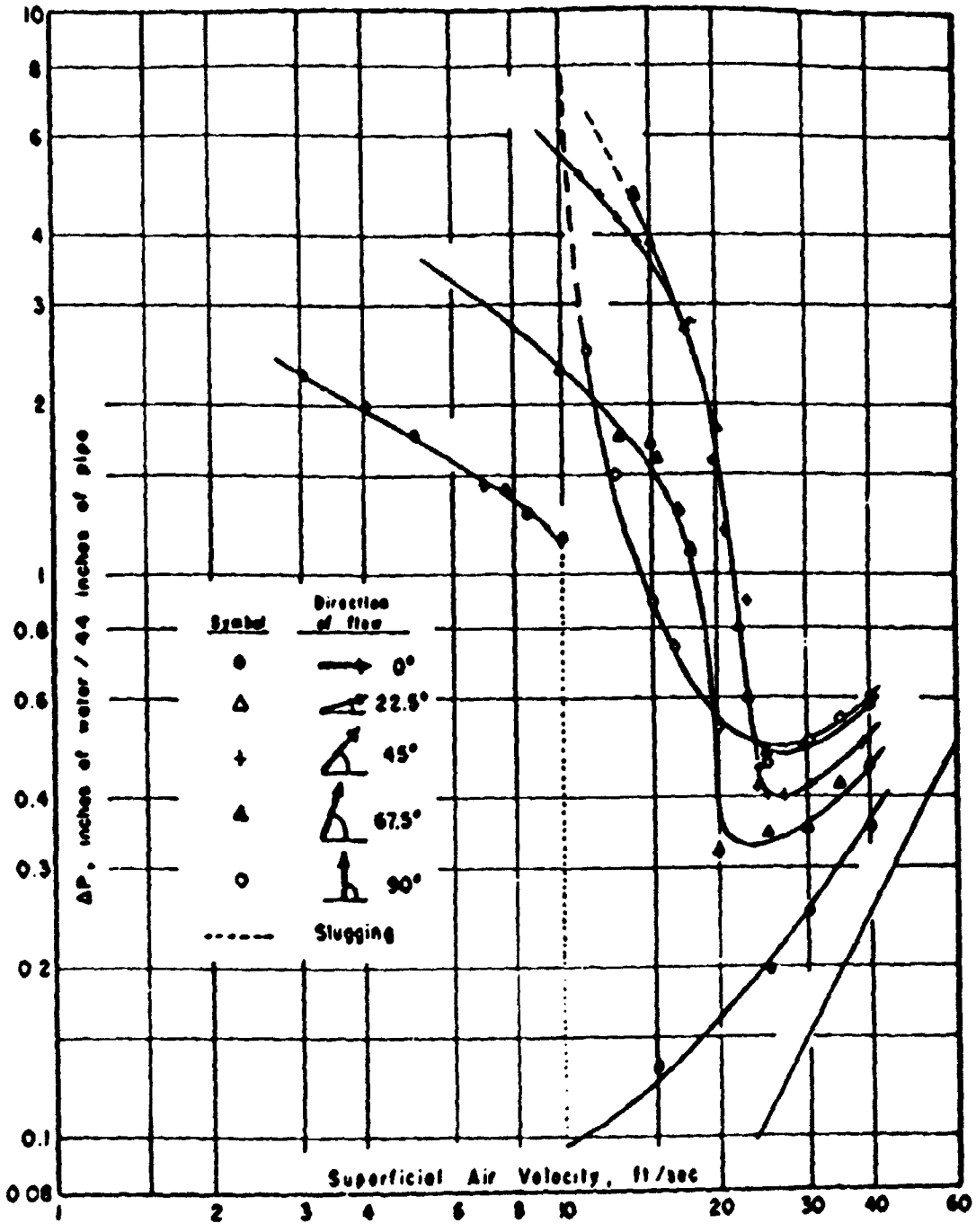

inclination (from horizontal). The pressure gradient increased with solids flux but decreased with pipe diameter. The ratio of solids mass flux in the upper section to the lower section of the pipe decreased with gas velocity, although the effect of inclination on this ratio was inconclusive.

1.3 CHOKING

1.3.1 DEFINITION AND FLOW CHARACTERISATION

The choking velocity, which is the most critical parameter in the design of any pneumatic conveying installation, is usually associated with the minimum gas velocity for smooth transmission of a solids stream, or reversal of solids flowrates (Staub, 1980). When the gas velocity is decreased beyond point D in Fig. 1.2.1, the dilute suspension of solids collapses resulting in slugging flow. The pipe is in the so called choking condition, and the velocity corresponding to point D referred to as the choking velocity. Choking results in large pressure drops and pressure-drop fluctuations. Although the operation near choking will result in a minimum gas requirement, the choking region is very unstable. As the solids flux increases from W_1 to W_2 the curve is shifted upwards.

The flow chart in Fig. 1.3 shows the two possible classes of flow characteristics as the gas velocity is reduced from a high value at the same solid flowrate. In general, systems that follow the left hand branch of the

Fig. 1.3 : Flow Patterns in Riser Transport
(Leung, 1980)

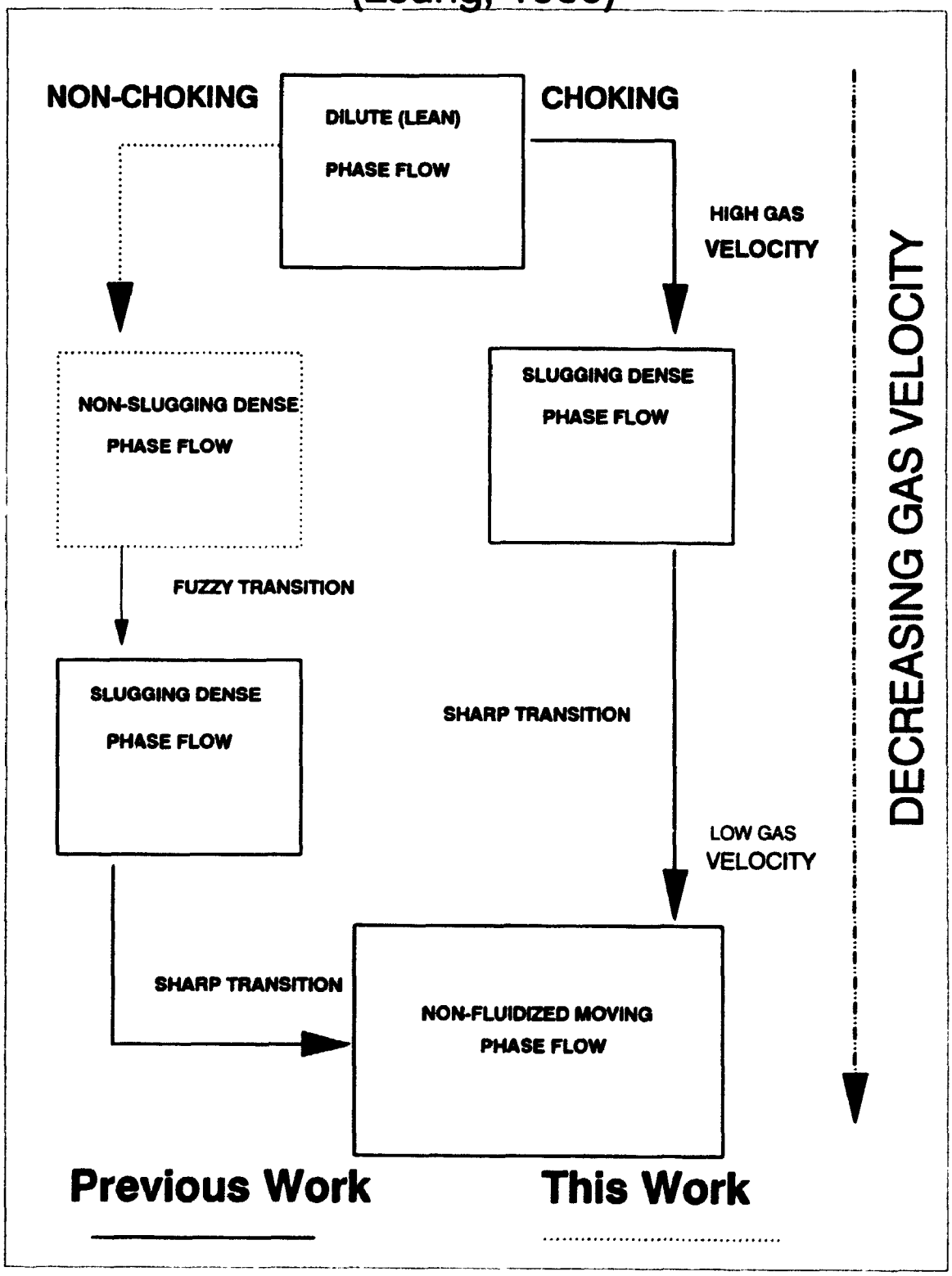

chart are defined as non-choking, while those that resemble the right hand branch are the choking type of system (Leung et al., 1978). For a non-choking system (Leung, 1980) there are four possible flow patterns as the gas velocity is reduced at constant solids flux. These are:

1. Dilute (lean) phase pneumatic transport
2. Non-slugging dense phase flow (fast fluidization, circulating fluidized bed, or riser transport)
3. Slugging dense phase flow
4. Packed-bed (moving bed) flow

The primary difference between the left and right branches is that in "non choking systems" it is possible to have solids refluxing without the occurrence of solids slugs in the line. However, this non-slugging flow (with incipient solids refluxing) will eventually lead to slugging dense phase conveying via a fuzzy transition, as the gas velocity is lowered at constant solids flux. This type of system is normally encountered with Geldart Group A powders, and sometimes with Group B powders.

For a "choking system" there is no intermediate flow regime between dilute flow and slugging flows, and it is generally applicable to Geldart Group D powders, and some Geldart Group B powders. In this study, Geldart Group B powders were investigated.

Yousfi and Gau (1974 a,b) observed four distinct transitions in their vertical riser as the solids concentration was increased. They were a dilute phase, a concentrated phase, the formation of bundles (later named clusters by subsequent workers) and an unstable phase, giving rise to slugging flow. Mok et al. (1989) have shown that there exist three distinct flow regimes in vertical pneumatic transport based on a plot of solids holdup versus solids flowrate at constant gas velocity. They have been named 'dilute', 'dense 1', and 'dense 2'. The dilute phase is right of the Zenz minimum. The dense 1 and dense 2 regimes (studied within the context of this research) represent the fast fluidization and transition to slugging dense regimes respectively.

Almost all of the research and operating experience to date has focused on the flow regime between C and B (dilute phase) in Fig. 1.2.1. The scope of the present research is restricted to the region of the curve between points C and D, where refluxing of particles dominates the flow patterns for vertical and inclined lines. This flow regime has been referred to as "non-slugging dense phase conveying" by Leung (1980) and "fast fluidization" by Yerushalmi et al. (1976). The fast fluidization flow regime is the hydrodynamic flow regime encountered in circulating fluidized beds and in some commercial-scale riser systems (Gajdos and Bierl, 1978).

1.3.2 CRITERIA FOR PREDICTION OF CHOKING

Leung (1980) found that at velocities close to choking, a slight decrease of gas velocity at the same flowrate, or a slight increase of solids flux at constant gas velocity, will significantly increase the pressure drop in the transport line. Due to the high amplitude of the pressure fluctuations in this region, the choking point cannot usually be precisely defined. The operating stability and pressure fluctuations depend upon the properties of gas and solids, solids and gas flowrates, void fraction, size of tube, particle-size distribution, and the solids feeding mechanism to the transport line. Yousfi and Gau (1974 a,b) specified the following criterion for choking to occur (equation 1) :

$$\frac{U_t^2}{gd_p} \equiv Fr_{d_p} > 140 \qquad (1)$$

where d_p is the particle diameter. Yang (1976) specified a criterion based on pipe diameter, D, for choking to occur, given by equation (2).

$$\frac{U_t^2}{gD} \equiv Fr_D > 0.12 \qquad (2)$$

Depending upon the properties of the system a pneumatic transport rig may be of the non-choking variety. As a general qualitative guide fine particles in large tubes tend to exhibit the non-choking phenomenon, while coarse particles in small tubes give rise to choking systems. In the literature the

choking criterion was first described by Zenz and Othmer (1960). Yousfi and Gau (1974), Yang (1975, 1983), and Smith (1978) analysed the choking and non-choking systems. Leung (1980) compared the latter three analyses with limited experimental data and found weaknesses in all of the systems. Since Yang's correlation (1983) accounts for pipe size his equation is recommended. The choking velocity, U_{gc} and voidage, ε_c , are computed

$$\frac{2gD(\epsilon_c^{-4.7} - 1)}{(U_{gc} - U_t)^2} = 0.01 \qquad (3)$$

with two sets of nonlinear equations which are solved to estimate parameters. These are given by equations (3) and (4):

$$U_p = (U_{gc} - U_t)(1 - \epsilon_c) \qquad (4)$$

where : U_p is the solids velocity, U_t is the terminal velocity, and D is the pipe diameter.

The terminal velocity of the particles can be computed from equation (5) for $0.4 < Re_p < 500$:

$$U_t = \left(\frac{4}{225} \frac{(\rho_p - \rho_g)^2 g^2}{\rho_g \mu_g} \right)^{\frac{1}{3}} d_p \qquad (5)$$

where d_p is the mean particle diameter.

1.3.3 CORRELATIONS

Punwani et al. (1976) have compared the available correlations for choking velocity such as those by Zenz and Othmer (1960), Rose and Duckworth (1969), Leung et al. (1971), Yousfi and Gau (1974), Knowlton and Bachavin (1976), and Yang (1975), with the available experimental data in the literature. Yang (1983) successfully compared his modified correlation with low-pressure experimental data on choking. The limitation of all these models is that they are based on small-scale units. It is unclear how reliable they would be for larger rigs. The validity of any choking correlation is questionable until the choking mechanism is better understood and defined.

1.4 FLOW REGIME CHARACTERISATION

Two types of dense conveying are possible depending upon the characteristics of the gas-solid-tube system. In slugging dense conveying, particles are conveyed upwards in slugs or bubbles. In the other, known as non-slugging dense conveying, clusters of particles appear and solids are conveyed with considerable amounts of internal recirculation. A further decrease in the gas velocity results in slugging, and ultimately a packed moving bed.

1.4.1 NON-SLUGGING DENSE PHASE FLOWS

For non-slugging dense phase conveying the transition between the dilute phase and dense phase conveying is diffuse. When the gas velocity is reduced at a given solid rate in the dilute phase mode, the solid concentration increases in the tube. No equation has been published for predicting the demarcation of this transition. It is the non-slugging dense phase conveying with line inclination which has been studied in this research. Previous work on inclined pneumatic transport at the University of Pittsburgh initiated by Klinzing et al. has focused exclusively on the dilute phase flows (Zaltash, 1987; Myler, 1987; Rohatgi, 1988).

Gianetto et al. (1990) have indicated that the non-slugging dense flow regime could be modelled as a plug flow reactor with longitudinal dispersion, presumably to account for the down flowing pipe-wall solids. Amos et al. (1993) have developed a model for gas mixing based on the assumption of a radially dispersed plug flow in the core, and a well-mixed side stream in the annulus. They found that the radial Peclet number, Pe, could be related to the mixture Reynolds number by: $Pe = 3.23Re_m^{0.297}$.

Bader et al. (1988) have shown that the axial dispersion coefficient is less than 1613 cm^2/s, and contributes little to overall gas dispersion in the reactor, while the radial dispersion coefficient had an average value of 38.7

cm^2/s. Tsuo and Gidaspow (1990) have noted that a one-dimensional model is not appropriate because cluster formation and reverse particle flow are not considered; a transient model in two dimensions is required. Their model assumes a generalization of the Navier-Stokes equations for two fluids, with a solids viscosity determined from riser experiments.

Leung and Wiles (1976) have found that for non-slugging systems, the internal solids recirculation can result in a negative solids friction factor due to solid down-flow at the wall. Wirth and Seiter (1991) have shown that the velocity of the falling solids layer ranges from 1 to 3 m/s. Grace (1990) estimated it at between 0.5 and 1.5 m/s.

1.4.2 FAST FLUIDIZATION AND RISER TRANSPORT

Leung and Wiles (1976) have shown that the regime of flows studied within the scope of the present study for sand can be classified as fast fluidization, and the rig used to collect data is a circulating fluidized bed (CFB). Westphalen (1991) has noted that typical gas velocities for CFB operation are 1 - 10 m/s, and the solids flux can range from 10 to 200 kg/m^2s. These are also the conditions which have been used within the context of this thesis.

Fast fluidization or non-slugging dense phase transport has attracted

considerable interest in recent years. Some general features of the flow regime are summarized below:

1. Pressure gradient in the tube decreases rapidly with an increase in gas velocity at constant solids flux.
2. Pressure gradient increases with solids flux at constant gas velocity.
3. Slip velocities are high and can be an order of magnitude above the free-fall velocity of single particles, typically used to compute particle velocities in dilute phase transport.
4. Solid volumetric concentrations are high, depending upon the tube diameter, before slugging sets in.
5. The transition from the lean phase to non-slugging dense phase is diffuse.
6. At low gas velocity within this regime, it is possible to have down-flow of solids near the wall of the pipe, although the net solid flow is upwards. This gives rise to the possibility of negative wall friction or negative frictional pressure drops.

The flow regimes studied here can also be called riser flow based on the observations of White and Dry (1989). Grace (1990) noted that the primary difference between fast fluidized beds and riser reactors is related to suspension density. In fast beds the solids fraction ranges from 2 to 15%,

while in riser reactors the solids fraction is typically less than 5%. The solids flux in the fast bed can be less than 200 kg/m^{2}s, but is usually between 400 - 900 kg/m^{2}s in the riser (Bi and Zhu, 1993). Moreover, the gas velocities in the riser are between 8 - 30 m/s, compared with 5 - 9 m/s in the fast bed. Another important difference is that in fast beds the flow develops over virtually the entire length of the bed. In risers the flow is developed over most of the transport length. The fast fluidization regime is observed for small pipe diameters; the first fast bed reactor was a 4 cm diameter column with a 5 cm dipleg (Shingles and McDonald, 1988). In this thesis the riser and dipleg diameters were 3.175 cm.

1.5 VOIDAGE PROFILE IN RISERS IN NON-SLUGGING FLOW REGIME

With the advent of the era on research in circulating fluidized bed (CFB) flows (or non-slugging dense phase), more effort has been placed on development of reliable correlations for estimation of line voidage. Both theory (Ocone et al., 1993) and experiment (Grace, 1990) show high solids concentrations near the wall of the riser corresponding to porosities of 0.75 to 0.85, but much higher porosities, 0.95 to 0.98, at the centre of the riser. Pita and Sundaresan (1993) demonstrated that in a commercial-scale riser the solids holdup increases from 1.9% (v/v) at the center to 17.1% (v/v) at the pipe wall. They also observed that lateral segregation of particles was

sensitive to the inlet injection configuration of the 2-phase suspension.

Wirth and Seiter (1991) showed that the solids concentration in the wall region is about three times that of the core. Berker and Tulig (1986) have shown that the bulk density of the suspension increases from about 25 kg/m^3 at 0.8R, to 325 kg/m^3 at 1R for a gas velocity of 15.2 m/s and a solids flux of 122 kg/m^2s, conditions similar to those used here. A small layer free of solids, about 1 mm thick, exists immediately adjacent to the wall. Lee (1991) has estimated the solids-free zone to be about 8% of the pipe radius for 400 μm particles (the diameter of glass beads particle size used in this research) and 10% for 200 μm particles (the diameter of the sand particles used in this work).

Zhang and Tung (1991) have developed an empirical correlation which is capable of predicting the radial dependence of voidage in the non-slugging dense regime, $\varepsilon(r)$, from the volume-averaged voidage (ε), assuming its symmetry around the pipe. The correlation has been tested over a range of pipe diameters (3 - 30 cm), particle sizes (34 - 75 μm), gas velocities (1 - 5 m/s), and solid fluxes (1 - 300 kg/m^2s). Its form is given by equation (6).

where $\phi(r)$ is the ratio of radial distance to pipe radius (r/R), and $\varepsilon(r)$ is the voidage at any radial coordinate. Using equation (6) it is possible to

$$\varepsilon(r) = \varepsilon^{(0.191 + \phi^{2.5} + 3\phi^{15})} \quad (6)$$

estimate the radial profile in any comparably operated CFB, knowing only the average solids holdup at a given axial coordinate.

Rhodes et al. (1992b) have found a linear semi-empirical relationship that is able to predict the radial dependence of the solids holdup in vertical risers, which is given by equation (7).

$$\frac{1 - \epsilon(r)}{1 - \epsilon} = 2\left(\frac{r}{R}\right)^2 \quad (7)$$

The correlation is robust and is able to handle the entire range of conditions studied in the current research.

The assumption of radial symmetry of solids around the circumference of the pipe, as used by Zhang and Tung (1991), may be erroneous for riser transport, where gas velocities are typically between 10 and 20 m/s, and solids fluxes range up to 600 kg/m^{2}s (Matsen, 1976). Asymmetry of the radial profile has been reported by Bartholomew and Casagrande (1957), Saxton and Worley (1970), Schuurmans (1980), Kwauk et al. (1985), Galtier et al. (1989), Rhodes et al. (1989), Azzi et al. (1990), and Martin et al. (1992). In each case lateral segregation of solids was apparent, and there

was asymmetry around the circumference of the pipe.

Azzi et al. (1991), using commercial risers with diameters between 0.71 and 0.95 m, found that the solids bulk movement was skewed towards the left side of the pipe, while the gas flowed mostly through the right. Arena et al. (1988) found that the length of the cluster of solids was 1 m in the dense lower phase, but increased to 3 m between the transition zone and the more dilute upper zone. Rhodes et al. (1992c) observed smaller swarms of particles, even in dilute conveying, whose diameter was about 1 mm, and which fell at a velocity of 1 m/s at the pipe boundaries.

Dry and Christensen (1988) have noted the presence of density inversion zones or solids waves in fast bed risers which appear to be asymmetric around the pipe. Their results indicate that the radial nonuniformity is irregular in the axial direction. Their observations imply that there is extreme lateral segregation in some parts of the pipe, followed by more uniform and leaner radial profiles. Adewumi and Arastoopour (1986) from a model of upwards gas-solid flow, were able to predict experimental data with an asymmetric radial profile for solids velocity. The authors found that the model predicted a local circulation or vortex motion. This was thought to be due to the exchange of particles between the core and annulus. Part of the solid material was carried in the form of strands or

clusters, while the remainder was carried as a fully suspended flow.

1.6 ESTIMATION OF PRESSURE GRADIENT

1.6.1 CALCULATION OF TOTAL PRESSURE DROP

The total measured pressure drop can be subdivided into several components. According to Hariu and Molstat (1949) the expression for total pressure drop is given by equation (8).

$$\Delta P_m = \Delta P_{ag} + \Delta P_{as} + \Delta P_{pg} + \Delta P_{ps} + \Delta P_{fg} + \Delta P_{fs} \qquad (8)$$

The terms ΔP_{ag} and ΔP_{as} represent the pressure drops due to acceleration of the gas and solids phases respectively. Both can be neglected when the flow is fully developed. The terms ΔP_{pg} and ΔP_{ps} are the pressure drops necessary to sustain the columns of both phases, or simply the static heads of both phases. The last two terms of equation (8), ΔP_{fg} and ΔP_{fs} , represent the frictional pressure drops of the gas and solid phases.

In the fully developed region where acceleration effects can be ignored, the expression for pressure gradient in inclined lines (Rohatgi, 1988) is given by equation (9) .

$$\left(\frac{\Delta P}{L}\right) = \left((1 - \epsilon)\rho_p + \epsilon\rho_g \right) g\cos\theta + \frac{2\rho_g f_s (1 - \epsilon) U_p^2}{D} + \frac{2\rho_g f_g \epsilon U_g^2}{D} \quad (9)$$

(i) *(ii)* *(iii)* *(iv)*

The first term, *(i)*, accounts for the pressure gradient due to solids holdup in the line. The second term *(ii)*, represents the pressure gradient due to the mass of gas in the line, which is usually negligible in comparison to *(i)*. Term *(iii)* is the contribution to the pressure gradient of solids-wall frictional losses, and is also referred to as the *residual pressure gradient* in this research. It is usually obtained by difference between the observed total pressure gradient and the other three terms, which can all be independently estimated. The fourth term *(iv)* is the pressure gradient due to gas-wall frictional losses. While it is dominant for dilute transport (Fig. 1.2.1), it is minor for the non-slugging dense phase.

1.6.2 EFFECTS OF LINE INCLINATION AND TUBE DIAMETER

Rose and Duckworth (1969 a,b,c) presented a fundamental analysis of how the effect of line inclination could be incorporated into the pressure drop equation for inclined lines operated in dilute phase flow. They noted that in inclined lines, the acceleration length was not affected by line inclination. However, Dhodapkar et al. (1987) showed that the length of the acceleration zone increases with angle of inclination measured from the horizontal.

They found an acceleration length of 5 to 10 pipe diameters at the vertical, which increased linearly with inclination, to 55 pipe diameters in the horizontal position. The length was strongly affected by wall-to-particle diameter ratio in the horizontal transport region only.

Pita and Sudaresan (1991) using the Sinclair/Jackson -1989 model, studied the effect of tube radius on pressure gradient. For a solids flux of 150 kg/m^2s and a gas velocity of 4.5 m/s (conditions used within this research), the pressure gradient was minimized for a tube diameter of 3 to 6 cm (compared with a 3.2 cm tube used in this research). Ocone et al. (1993) observed a minimum in the pressure gradient at a tube diameter of 10 cm based on their model.

1.7 SOLIDS FRICTION FACTOR

Usually the frictional component of the solids phase is expressed

$$\frac{\Delta P_p}{L} = \frac{2 f_s \rho_p (1 - \epsilon) U_p^2}{D} \qquad (10)$$

analogously to that employed for the gas phase using equation (10). Here, D denotes the diameter of the pipe and f_s designates the frictional coefficient of the particulate phase. Correlations for f_s are given by Capes and Nakamura (1973), Konno and Saito (1969), and Yang (1988).

Capes and Nakamura :

$$f_s = 0.048\ U_p^{-1.22} \qquad (11)$$

Konno and Saito :

$$f_s = 0.0285\ g d_p^{0.5}\ U_p^{-1} \qquad (12)$$

Yang :

$$f_s = 0.00315 \left(\frac{1 - \epsilon}{\epsilon^3} \right) \left(\frac{(1 - \epsilon) U_t}{U_g - U_p} \right)^{-0.979} \qquad (13)$$

Rose and Duckworth (1969) presented an expression to compute the combined friction factor for gas with solids and the tube wall for inclined lines. Using the data of Zenz (1957) for inclined lines, the authors developed an empirical correlation to calculate the solids velocity given the angle of inclination. This was subsequently used to obtain the mixture friction factor. The solids friction factor could be obtained by subtracting the gas phase friction factor from the mixture friction factor.

1.8 PRESSURE DROP CORRELATIONS AND HYDRODYNAMICS

The predictive models that have been developed in the literature for describing gas-solids systems fall into two general categories, namely the empirical approach and the fundamental hydrodynamic approach. In the

former, empirical correlations are developed for predicting the important design variables, such as pressure drop and choking velocity. The empirical correlations are limited to the particular data base (Adewumi and Arastoopour, 1990), and the hydrodynamic models are generally restricted to narrow particle-size distributions. Michaelides and Roy (1987) compared pressure drop correlations from 14 different sources and concluded that Michaelides and Roy (1987) was the best for vertical pneumatic transport, with an average absolute deviation of 30%. There are presently no correlations available for inclined non-slugging dense phase flows. A crude estimate of pressure drop for inclined dilute phase flows can be gleaned from the nomograph methods given by Rose and Duckworth (1969).

Zaltash et al. (1989) used a thermodynamic approach to model dilute phase inclined pneumatic transport. The van der Waals (VDW) equation of state was assumed because it was thought to have the capability to predict the existence of two distinct phases. Its use depended on the existence of the two coexisting phases and the critical state in gas-solid transport. Three parameters in the VDW equation were required to be estimated including a^*, (which accounts for particle-particle interactions), b^*, (which accounts for the finite size of particles, and for cluster tendencies), and the constant R^*, (which was computed from the ideal gas analog). Knowledge of these parameters would allow the estimation of pressure gradient at any line

inclination in dilute phase transport. Prediction of these three parameters would eliminate the need for experimental data on particle velocity. Zaltash (1987) noted that the two parameters a^* and b^* decreased with increasing particle size and pipe diameter. This implies that particle clustering would decrease with a coinciding increase of the pipe diameter and particle size. The overall conclusion was that the VDW analog was capable of describing two separate phases which could coexist in equilibrium states (dilute and dense phase).

1.9 PARTICLE AND SLIP VELOCITIES

The particle velocity, U_p , can be determined from solids holdup and solids flowrate, W_{sf} , through equation (14).

$$U_p = \frac{W_{sf}}{(\rho_p A \alpha_p)} \tag{14}$$

The actual superficial gas velocity, U_g, should be corrected for the modified cross sectional area available for flow due to solids constriction of the line, by equation (15).

$$U_g = U_{gs} (1 - \alpha) \tag{15}$$

$$U_{slip} = U_g - U_p \tag{16}$$

The actual slip velocity, U_{slip}, can be computed from the difference of U_g and U_p (equation 16).

The particle velocity calculated from equation (14) was compared in this thesis with several correlations from the literature. They include Konno and Saito (1969), Hinkle-IGT (Institute of Gas Tech., 1978), Yang (1973), Matsen (1982), Myler (1987), and Zaltash (1987). With exception of Zaltash (1987) these correlations (equations 17-24) were not developed for inclined lines. They are as follows:

Konno and Saito :

$$U_p = U_g - U_t \tag{17}$$

Hinkle-IGT :

$$U_p = U_g \left(1 - 0.68 d_p^{0.92} \rho_p^{0.5} \rho_g^{-0.2} D^{-0.54} \right) \tag{18}$$

Yang :

$$U_p = U_g - U_t \left(\left(1 + \frac{f_p U_p^2}{2gD} \right) \epsilon^{4.7} \right)^{0.5} \tag{19}$$

Zaltash:

$$\frac{U_p}{(gD)^{0.5}} = \left(\left(\frac{U_g}{(gD)^{0.5}}\right) - \left(\frac{U_t}{(gD)^{0.5}}\right)^{0.877}\right)(1 - 0.5\sin\theta)^{0.0765}\left(\frac{D}{d_p}\right)^{0.031}\left(\frac{\rho_p}{\rho_g}\right)^{-0.0321} \qquad (20)$$

Matsen :

$$U_p = U_g - 10.8\ U_t\ (1 - \epsilon)^{0.293} \qquad (21)$$

$$\frac{U_{slip}}{U_T} = 1 \qquad [(1 - \epsilon) < 0.0003] \qquad (22)$$

$$(0.9997 > \varepsilon > 0.91)$$

Myler :

$$U_p = \left(U_g - U_t^{0.71}\right) D^{0.019} \qquad (23)$$

Matsen (1982) has given a correlation to predict the slip velocity, U_{slip}, if the voidage of the suspension is known (equations 23/24).

$$\frac{U_{slip}}{U_T} = 10.8\,(1 - \varepsilon)^{0.293} \qquad [\,(1 - \varepsilon) > 0.0003\,] \qquad (24)$$

Geldart and Rhodes (1985) have stated that high slip velocities in non-slugging systems can be explained on the basis of the radial nonuniformities. They note that where a dense annular layer of solids has been experimentally confirmed, the idea of average slip velocity has no physical meaning and can be misleading. Patience et al. (1992) observed that the ratio between gas velocity and particle velocity was about 2. They suggested that this ratio could be used for the scale-up of vertical riser reactors.

Mok et al. (1989) also observed that in the fast fluidization regime, the assumption of the equivalence of slip velocity and terminal velocity is invalid. They noted that the slip velocity increases rapidly with solids fluxes between 80 and 160 kg/m^{2}s at constant gas velocity for vertical lines, but remains constant thereafter. The assumption of equivalence was also demonstrated to be faulty at high gas velocities in the dilute phase flows.

Zaltash's results (1987) indicate that the assumption of constant slip velocity (equation 16) is invalid even for dilute phase transport. For the

vertical line and 450 μm glass beads, the slip velocity increased from virtually zero (at a 25 m/s gas velocity) to 7 m/s (at a gas velocity of 12 m/s). For 60 degree inclination from the vertical a slip velocity variation of nearly 10 m/s was observed over the range of gas velocities between 10 and 35 m/s.

2 : EXPERIMENTAL APPARATUS

2.1 PNEUMATIC TRANSPORT LINE

A schematic flowsheet of the experimental apparatus is shown in Fig. 2.1. The apparatus was designed, constructed, and commissioned in this project as part of the thesis requirements. The computer-aided data acquisition system, peripherals, and associated software for data collection and analysis were also prepared as part of the thesis research requirements. The pneumatic transport rig extended over three floors and was housed in The University of Western Ontario's fluidization laboratory.

In this thesis the angle of inclination, θ, refers to the angle as measured from the vertical pipe orientation, *except where specifically noted.* The angle of inclination was measured in two ways. The first method involved the use of a carpenter's protractor to set the angle. A second method of line inclination determination was by direct measurement of line lengths, and then utilizing trigonometric principles. Knowledge of the horizontal and vertical distances at any axial coordinate along the riser allowed

Fig. 2.1: Experimental Apparatus

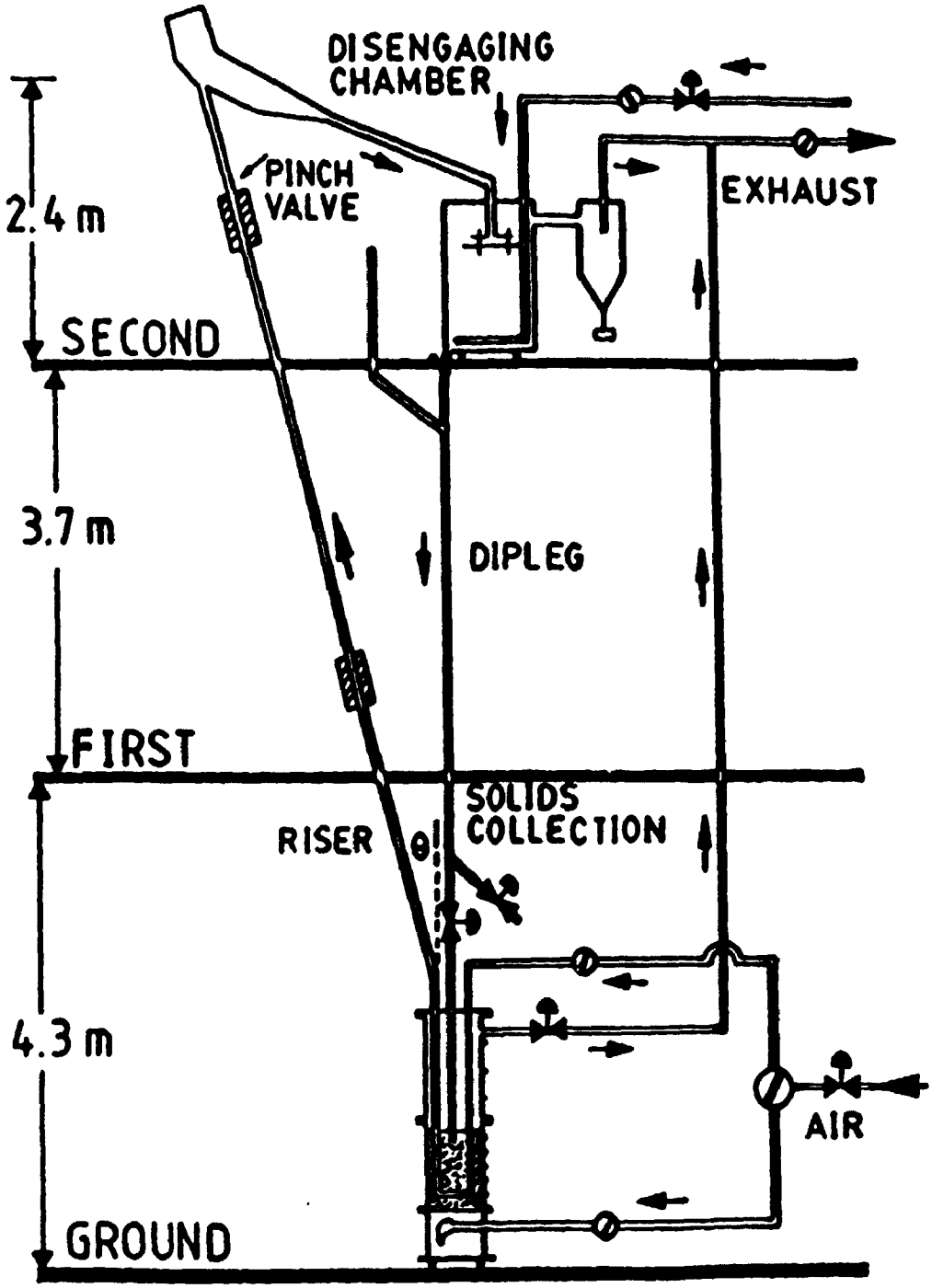

computation of the angle with four digit precision, although the reported values were rounded off to the closest nominal degree. Vertical distances were measured in conjunction with a tape measure and plumb bob. The inclined length was also measured, giving an independent estimate of the accuracy of the inclination angle.

Solids were transported pneumatically with air over a distance of approximately 10 metres after being injected into the line from the fluidized bed feeder on the ground floor. The dimensions of the riser are shown in Fig. 2.1. The pneumatic transport line was constructed of a 31.7 mm (inside diameter) Plexiglas tube which allowed flow visualization. Tube lengths of approximately two metres were connected by 8 cm diameter external flanges, to form a pipe length of about ten metres in total length. Pressure taps were glued on to the Plexiglas tube at 1.5 m intervals. The taps were bored from the outside so that the fitting was flush with the inside of the tube. This prevented solids blockage in the line and allowed static pressure measurement at the tube wall. The use of pressure taps along the tube was to determine the entry length required for fully developed two-phase suspension pipe flow. For all except three of the pressure taps, the lines were connected to water manometers. These provided static pressure measurements over the length of the riser and a quick visual scan of the pressure profile. Three of the taps were connected to electronic pressure

transducers. The electrical signals from the transducers were fed to a computer-aided data acquisition system for subsequent time series analysis.

The entire pipe length with pinch valves (used for solids holdup measurement) and outlet expansion chamber was supported by an aluminum channel, which was open on the front side to allow observation of the flow structure of the two-phase mixture. The aluminum channel ensured that the Plexiglas tube remained rigid, and that there was no sagging of the pipe due to its weight in an inclined position. It also prevented a double angle of inclination in the depth plane (projected normally to Fig. 2.1). A double angle of inclination can occur if the weight of the pipe is not supported from a single overhead pivot point. The dimensions of the channel measured 13 cm in width and 7.5 cm in depth. The tube was firmly affixed to the channel with bolted brace supports, placed at 1 metre intervals. The entire pipe with valves and pressure connections was attached to a pivot point, located 15 cm above the upper pinch valve on the top floor. The pivot point is not shown in Fig. 2.1 to maintain clarity of the figure. The pivot allowed the angle of line inclination to be conveniently adjusted in the direction indicated.

2.2 SEPARATION OF SOLIDS FROM GAS

The solids-gas suspension was transported through 10 m of Plexiglas tube

before being discharged into a conical impingement unit (25 cm top diameter) situated on the top floor. The geometry of the structure was such that the impinging suspension fell on to the downcomer, angled off to the right, instead of back into the riser. Visual observations and static pressure measurements on the line preceding the structure confirmed that solids were not being deflected back into the transport line. Although the primary purpose of the expanded section was to reduce the momentum of the suspension, it was fairly efficient for separation of the solids from the gas. The solids were observed to flow as a continuous cluster along the lower side of the pipe, while the gas stream flowed above it. The solids with gas flowed smoothly out of the downcomer and into a disengaging chamber mounted on castors on the top floor.

Further separation of solids from air was possible through use of a carbon steel disengaging chamber, which was 1.5 m in height and 0.3 m in diameter. A Plexiglas top flange allowed visual observations of the flow conditions inside of the vessel. Twin deflector plates with adjustable spacing allowed solids to be separated from the rising gas stream. Solids were forced to flow radially outward to the wall of the chamber by the momentum of the gas stream, and were subsequently removed from the bottom of the chamber.

The combination of the expanded downcomer with the disengaging chamber separated over 99.8% of the incoming solids. The remaining fines entrained in the off-gas were separated with a cyclone. The chamber was fluidized with air at a velocity slightly above u_{mf} to ensure that solids flowed homogeneously through the dipleg, and this practice also prevented accumulation of solids within the vessel. Solids could then be returned continuously back to the fluidized bed feeder on the ground floor at the same rate at which they were collected in the chamber. Any build-up of solids in the chamber could be detected by measurement of the pressure drops on the two fluidized beds. It could also be verified by visual observation indicating a decrease in suspension density in the riser. The air flow from the disengaging chamber was combined with the outlet flow from the riser and the fluidized bed feeder, and was exhausted to the atmosphere.

2.3 PRESSURE GRADIENT AND STATIC PRESSURE MEASUREMENTS

The upstream static pressure and pressure drop across the test section were measured by two pressure transducers. The first, a Schaevitz model P-3091 series transducer, was used to detect the static pressure at a point 1.765 m below the lower pinch valve. The second, a Setra model C-239 model transducer, was used to measure the pressure drop between the 4.769 m distance between the pinch valves. The start of the test section was

approximately 4 m from the injection point at the base of the fluidized bed feeder, and was situated over 100 pipe diameters from the solids-gas entrance. From Dhodapkar et al. (1987) it is known that the entry length in such flows is less than 50 pipe diameters, so that fully developed flow conditions were ensured for all runs. This was verified independently by static pressure measurements along the riser.

The pressure gradient transducer could detect differences of up to 1400 Pa/m, while the static pressure transducer range extended up to 14000 Pa; the precision of the instruments were better than 5 Pa/m and 50 Pa respectively. The transducers were mounted within close proximity of the relevant pressure taps. Calibration curves for the static and pressure gradient transducers are shown in Figs. A1 and A2 respectively (Appendix A). The calibrations of the transducers were routinely checked with water manometer measurements to ensure reliable collection of data. All calibrations had a linear R^2 of 0.99 or more.

The pressure taps were mounted flush with the inside diameter of the Plexiglas tube. A thin strip of fine mesh screen (25 μm) was butt-welded on to the surface of the brass Swagelok tube fittings, so as to prevent solids from entering the transducers. This entire length of the test section was in the fully developed two-phase flow condition. From experiment it was

confirmed that the static pressure profile did not change with the axial coordinate in the test section.

The data acquisition APPLESOFT BASIC program (Appendix B) was written such that the static pressure was sampled first followed by the pressure drop. The sampling frequency of 12 Hz that was used, was based upon the Nyquist criterion (Press et al., 1986). The frequency was well below the maximum of 215 Hz for the compiled BASIC program, determined for the transducer/computer tandem. The response time for the transducer itself was less than 1 ms according to the manufacturer's specifications. The sampling frequency was established based upon spectral analysis data (§ 4.10) which indicated that there were low frequency fluctuations (<10 Hz) in the system. A total of 2050 signals from each of two transducers were collected.

2.4 MEASUREMENT OF AIR FLOWRATE

Air flowrates were calculated from the upstream static pressure and pressure drop across a square-edged orifice plate, equipped with corner taps. The orifice plates were constructed in-house, and were mounted with external flange connections to fit the 1.27, 1.91, 3.2, and 3.8 cm pipes used to transport air. A number of plates with different orifice diameters were machined so that the plates could easily be changed for a variety of

different flow conditions. The orifice plates are illustrated schematically in Fig. 2.1 by the circles (flanges) with two solid lines (representing orifice plates) inside. Taylor Instrument model 3402T series transducers with a 0-5 V output signal, were used for pressure data acquisition. The output from the pressure transducer was fed to an A/D converter, and subsequently to an Apple IIe microcomputer. The transducer had a working range of 1.7 to 10 kPa differential and a maximum applied pressure of 6800 kPa. The maximum error of the unit was 40 Pa.

A computer-aided data acquisition program was employed to convert output from the Taylor transducer, to a signal between 0 and 255 bytes for the 8 bit Applied Engineering A/D card that was used. This 0-255 byte output was subsequently converted to a pressure equivalent using a predetermined linear calibration curve (Figs. A3, A4; Appendix A), which was incorporated into the data acquisition program. The precision of the transducers was greater than 40 Pa. Equations for the linear calibration of the transducers are given in Appendix A. The signals were collected and stored in data files on diskettes for subsequent analysis.

2.5 SOLIDS VOLUME FRACTION WITH PINCH VALVES

2.5.1 DIMENSIONS OF PINCH VALVES

The solids holdup was measured by the weight of solids trapped between

two simultaneously closing pinch valves enclosing the 4.769 m test section. The Series SGE 1.5 in. (3.8 cm) pinch valves used in this study were industrial grade, and consisted of an inner rubber lining, which was encased in a stainless steel outer frame (Appendix C). The inner rubber lining (Section B of the valve; Appendix C) had an inside diameter of 3.175 cm, which was the same as the pneumatic transport tube. The diameter at the entrance and exit points was larger, however, to accommodate the pipe wall thickness so as not to change the tube cross section as the suspension passed through it. This criterion (of constant pipe cross-section) was essential to minimize perturbations in the flow pattern which could result in unaccountable pressure losses in the system. An absence of pressure loss was confirmed experimentally from pressure measurements before and after the valves.

Each pinch valve was 26 cm in length, 12.1 cm in width, and weighed 7.7 kg. The SGE valve was constructed of a split housing constructed of cast aluminum, and was manufactured in the normally open position. The minimum applied pressure required for closure of the rubber linings was determined to be 275 kPa. The SGE pinch valve was chosen for this application because of its reliability in pneumatic transport lines based on industrial operating experience

2.5.2 PINCH VALVE OPERATION

Situated on opposite sides of the pinch valve and radially outward from the tube wall (Section F; Appendix C), were two female pipe connections of 0.5 inch (1.27 cm) diameter. These two pipe fittings were inlets to the valve, which allowed air to be transmitted to the surface of the rubber lining from the compressed air line. Operation of the SGE valve was by the application of air pressure (via the University compressed air line) through the pipe connection in the housing, to the annular volume surrounding the elastomeric tube. As pressure was applied, the central portion of the tube collapsed from opposite sides. In this configuration the pinch valve was closed. Complete closure of the valve was verified with leak-proof tests prior to the installation of the valves on the aluminum channel.

The two pinch valves were physically located at the base of the second and third floors, and were securely mounted with brace supports to the aluminum channel. The transport line was not stressed in any way from the weight of the pinch valves. Immediately upstream of both pinch valves were three-way electrically-operated solenoid valves. The solenoid valves were closed remotely from the central control panel located on the ground floor, and were in the normally closed configuration. When actuated, air was transmitted to both sides of the pinch valve until pressures were equilibrated and flow stopped. The length of tube between the air line and

the annular space was kept as small as physically possible. When the solenoid valve was re-opened the air collected in the annular space was rapidly exhausted by the third port of the three-way valve. The release of air pressure resulted in the opening of the pinch valves.

It was determined that for applied pressures of up to 275 kPa the difference of pinch valve closure time was linearly dependent on applied pressure, after which there was no such dependence. To ensure minimum closure time of the pinch valves, an air pressure of between 485 and 550 kPa was applied. The electrical valves were placed a minimal upstream distance of about 0.2 m from the pinch valves.

2.5.3 PINCH VALVE CLOSURE TIME

Fig. 2.5 schematically illustrates how the closure time (elapsed time between the closure of both valves) was measured. Four specially constructed plastic flanges were machined to fit the inner end-lining section of the pinch valve (shown in Appendix C). Two of these were fitted with small light bulbs at their centre-points. The other two were equipped with photodetectors, also positioned at their centre-points. The two flanges with light bulbs were placed above the pinch valves. The other two (with photodetectors) were positioned beneath the pinch valves. At the moment of bottom valve (#2) closure a millivolt signal was initiated (as registered by

the indicator), and the initiation of this signal was observed remotely by a hand-held voltameter. The millivolt signal originating from valve #2 was terminated when valve #1 (top) closed. The sensing indicator was calibrated so that one millivolt was equivalent to one millisecond of elapsed time between successive closures. Hence, the millivolt signal recorded by the voltameter represented the difference of closure time between the two valves in milliseconds.

Through repeated measurements it was found that the difference of closure time between the two pinch valves ranged between three to twenty milliseconds. This difference decreased with the number of valve actuations immediately preceding the closure, to a maximum of about 10 closures. The variation of closure time with the number of actuations was due to the elasticity of the rubber lining which increased after having being stressed. The closure time was estimated to be between 3 to 10 ms for all runs in this study. The error associated with the closure time of the valves will be addressed in §2.9.

2.6 FLUIDIZED BED FEEDER

2.6.1 CONSTRUCTION OF THE BED

The fluidized bed solids feeder shown in Fig. 2.6 was used to inject solids into the inclined riser. The bed was 1.52 m in height and 25 cm in

Fig. 2.5 : Pinch Valve Closure Measurement

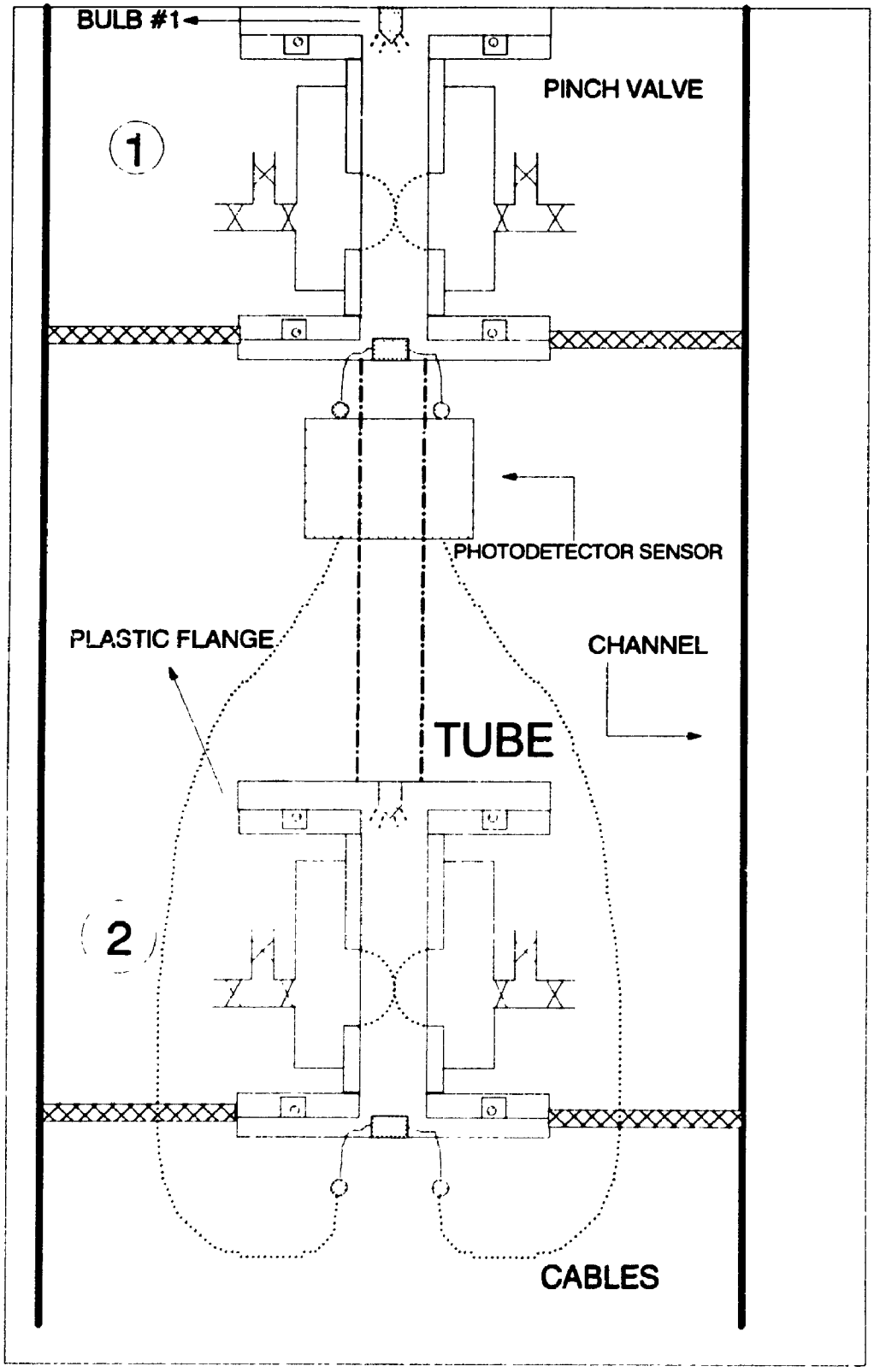

diameter. It was mounted on castors so that the position of the rig could be adjusted when the inclination angle, θ, of the riser was reset. Air from the University's compressed air line entered the fluidized bed at two points. Fluidizing air was injected into the windbox to maintain the bed at about five times the minimum fluidization velocity, and in a state of bubbling fluidization. Visual observations indicated that the bed was homogeneously and uniformly fluidized. There were no apparent bypassing zones in any area of the bed.

Between 65% to 75% of the inlet fluidizing air was continuously exhausted by the globe valve situated at the top of the bed. A secondary source of inlet air was fed through the top of the 255 mm diameter fluidized bed into a U-tube constructed of copper. This was the primary source of pneumatic transport air used to transport solids through the riser. A secondary source of riser air flow (exhaust flow) originated from the 25%-35% of fluidizing air injected into the riser with the pneumatic transport air flow. The ratio of flowrates was quantified by mass balance for each run performed. It was found that the percentage of fluidizing air injected into the riser increased with the solids flux in the line. This was expected since the pressure drop at the orifice location was raised to increase the solids flux in the riser.

There was approximately a 0.5 m transport disengaging height (TDH) in the

Fig. 2.6: Fluidized Bed Feeder

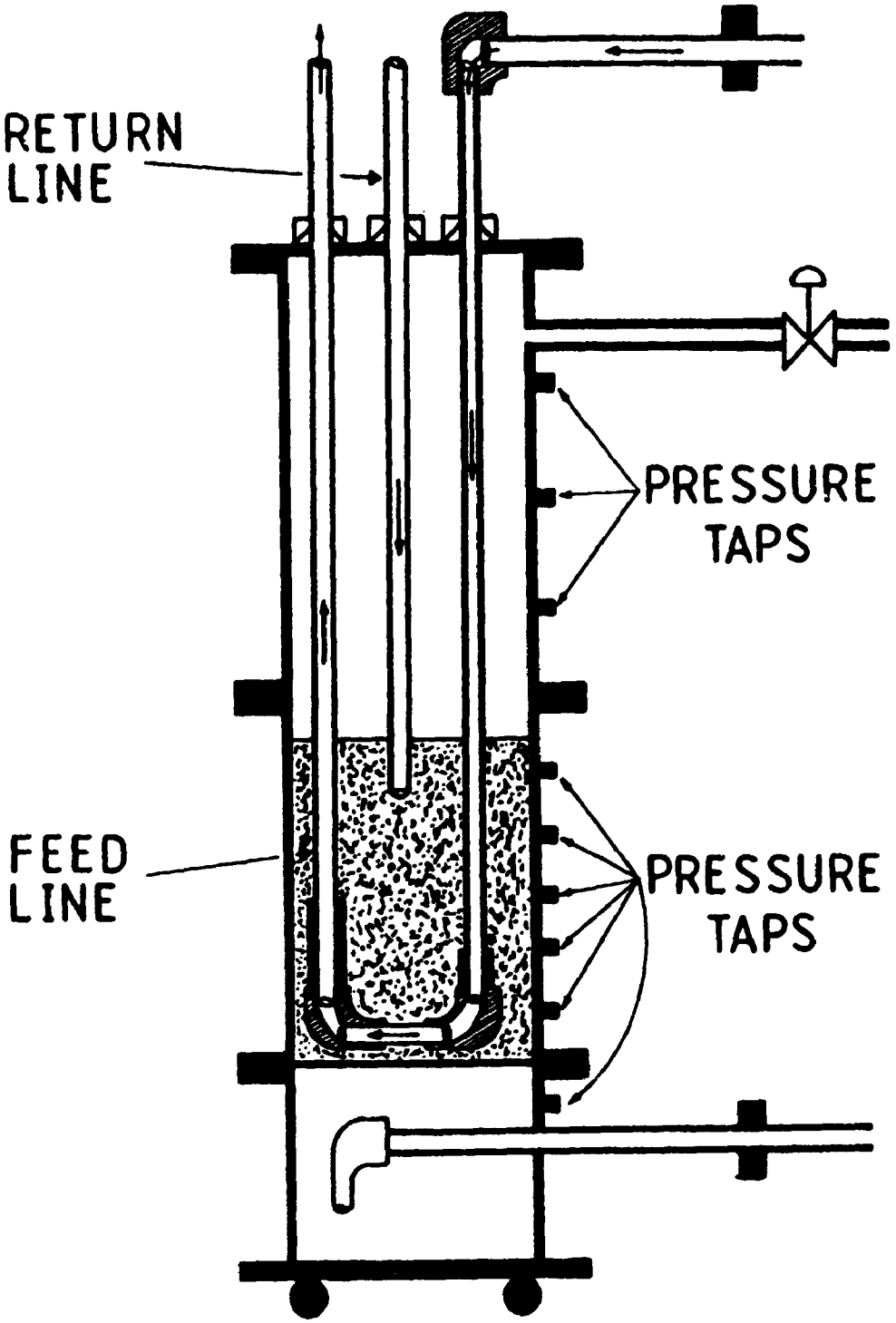

bed, minimizing solids carryover into the air exhaust line. The bed had a removable Plexiglas cover which permitted observation of internals. The design of the bed was modelled after Muzyka's (1985) line at UTC, Compiegne, France. A major modification to that design was the provision for removable flanges on all Plexiglas connector locations. Removable flanges allowed the tubes to be immersed to varying solids levels in the bed, which permitted greater flexibility and ease of operation.

The orifice through which the solids to the transport line were injected, was a hole drilled on the face of a 31.8 mm diameter carbon steel tube, 15 cm in length (shown on the left bottom side of fluidized bed feeder; Fig. 2.6). This piece was removable, allowing the orifice diameter to be changed when a different solids flux was required. The orifice diameter was varied between 0.95 cm and 2.5 cm for these experiments. Solids could be injected because the bed pressure at the orifice was maintained at a static pressure of 50 to 200 cm of water above that in the pneumatic transport line. The solids flux could be adjusted by modifying this pressure with an air regulator situated upstream of the fluid bed feeder. After passing through a U-loop about 10 cm from the bottom of the bed, the pneumatic transport air in the riser picked up injected solids from the fluidized bed. The horizontal air-solids jet changed direction (by 90°) upon entry to the transport line.

A flexible rubber tube of the same inside diameter as the Plexiglas riser (3.2 cm) was used as the transport line between the riser tube immersed in the fluidized bed feeder (from the U-loop exit) to the base of the riser. Sleeves with gear clamps were used to strap the flexible hose to the riser and feeder connecting points. Use of a flexible tube, in lieu of the more rigid Plexiglas, was required for adjustment of the angle of inclination of the riser.

2.6.2 HEIGHT OF THE FLUIDIZED BED OF SOLIDS

Pressure taps located axially at 5 cm intervals along the fluidized bed were used to determine the height of solids, and to assess whether steady-state operation had been attained. The height of solids in the bed was varied between 0.3 and 0.7 m above the injection point, depending upon the solids flux in the line. For those experiments with a solids flux greater than about 100 kg/m^{2}s, an extra inventory of solids was added to the system at the disengaging chamber outlet.

In a few of the earlier commissioning runs the bed height dropped to a level below the base of the return line dipleg. In such cases it was necessary to stop the run and change the positioning of the dipleg or increase the solids inventory in the system. The former was preferred because the removable flanges were easily adjusted to allow dipleg positioning. If the solids level dropped below the level of the injection point on the dipleg it was visually

evident, since the density of the suspension thinned from non-slugging dense to homogeneous dilute-phase flow, and the flow became unsteady.

When the pressure gradient across the bed became invariant with time, steady state was assumed. All taps were connected to water manometers and Dwyer Instruments Magnehelic pressure gauges for fast on-line static pressure measurement. A globe valve in the air exhaust line from the bed was used to regulate its pressure.

2.6.3 SOLIDS RETURN LINE DIPLEG OPERATION

The return line dipleg immersed in solids along the centre-line of the bed allowed recycling of separated solids. By immersing the dipleg outlet into the bed of solids, gas bypassing into the solids return line was avoided.

Vibrators were installed along the dipleg at the midpoint, and just prior to injection of the bed, as a precautionary step to prevent bridging of solids in the line. All flanges holding the air transport line and solids return dipleg to the bed could be moved along the outside of the tube (above the top cover; Fig. 2.6), which allowed the height of the tubes to be conveniently adjusted. The flexibility permitted by these adjustable flanges allowed a wider range of solids fluxes to be tested at a given gas velocity.

The solids return dipleg was constructed from the identical Plexiglas tube as used for the riser, except near the inlet of the fluidized bed. There, grounded copper piping was used to minimize electrostatic effects. Use of copper sections with the Plexiglas tube minimized buildup of electrostatic charges in the line as outlined by Ally (1981). The various grounding points included copper piping, nuts and bolts used to connect flanges, pressure taps (at 1 m intervals along the pipe), the feeder, and disengaging chamber. It was determined experimentally that there was no significant effect of humidifying the inlet air -even up to 95% RH- to the transport line; no difference of test section pressure drop was noted. Hence, the practice of air humidification was subsequently discontinued for all future runs.

The observations made here are in agreement with Muzyka (1985) for similar flow conditions. Wolny and Kabata (1985) observed that there was no correlation between the radial distribution of particle concentration and relative humidity or particle electrostatic charge. Rhodes et al. (1992c) observed that the effect of static electricity in riser systems was negligible, and in particular, for the range of experimental conditions covered by this research.

2.7 OPERATING PROCEDURES

2.7.1 PRE-STARTUP PROCEDURES

Before the start of an experiment several preparatory steps were required. This included setting the angle from a pivot on the top floor from which the riser was suspended. In addition to changing the line orientation it was also necessary to position the auxiliary equipment such as : the fluidized bed, disengaging chamber, and dipleg. All vinyl tubing connecting pressure taps were reconnected when the angle of inclination for the apparatus was reset.

The flowrates of air to various parts of the system were calculated a priori. Appropriate plates with orifice diameters ranging from 1 to 3 cm were installed so that reliable static pressure and pressure drop readings could be taken from the Magnehelic gauges. All gauges were periodically calibrated, and green miriam fluid in manometers was changed if there was some visual evidence of impurities in the fluid.

The pneumatically operated pinch valves were actuated in quick succession 5 to 10 times prior to the start of an experiment. This was to reduce the stiffness of the rubber lining by stressing it with successive closures. By actuating the valves at high frequency and for a period of about 1 minute,

the flexibility of the rubber lining in the valves was established and the minimal closure time of the valves could be assumed.

2.7.2 MINIMUM FLUIDIZATION VELOCITY

For 197μm (Sauter mean diameter) sand particles, u_{mf} was determined (by experiment) to be 3.8 cm/s; for 441μm glass beads the value of u_{mf} was 14.0 cm/s. Fig. 2.7 shows how the minimum fluidization velocity was determined in the lab for the sand particles. On the plot of bed pressure drop versus superficial gas velocity, the point of minimum fluidization is represented at the intersection of the oblique and horizontal lines (indicated by a dotted arrow in Fig. 2.7), and where the pressure drop in the bed does not increase further with the superficial gas velocity.

The empirical method of Kunii and Levenspiel (1969) gave a value of 3.2 cm/s for u_{mf} of these sand particles, in comparison with the 3.8 cm/s experimental result. The empirical value of 14.0 cm/s for glass beads (obtained in a similar manner as the sand particles) was close in magnitude to the predicted u_{mf} value of 16.5 cm/s predicted by Kunii and Levenspiel. It should be noted that the correlation uses the average particle size d_p. Considering that both types of particles had broad particle size distributions (Figs. 2.10.1 and 2.10.2, §2.10), there is good agreement between experiment and the correlation.

Fig. 2.7: Minimum Fluidizing Velocity for 197 μm Sand

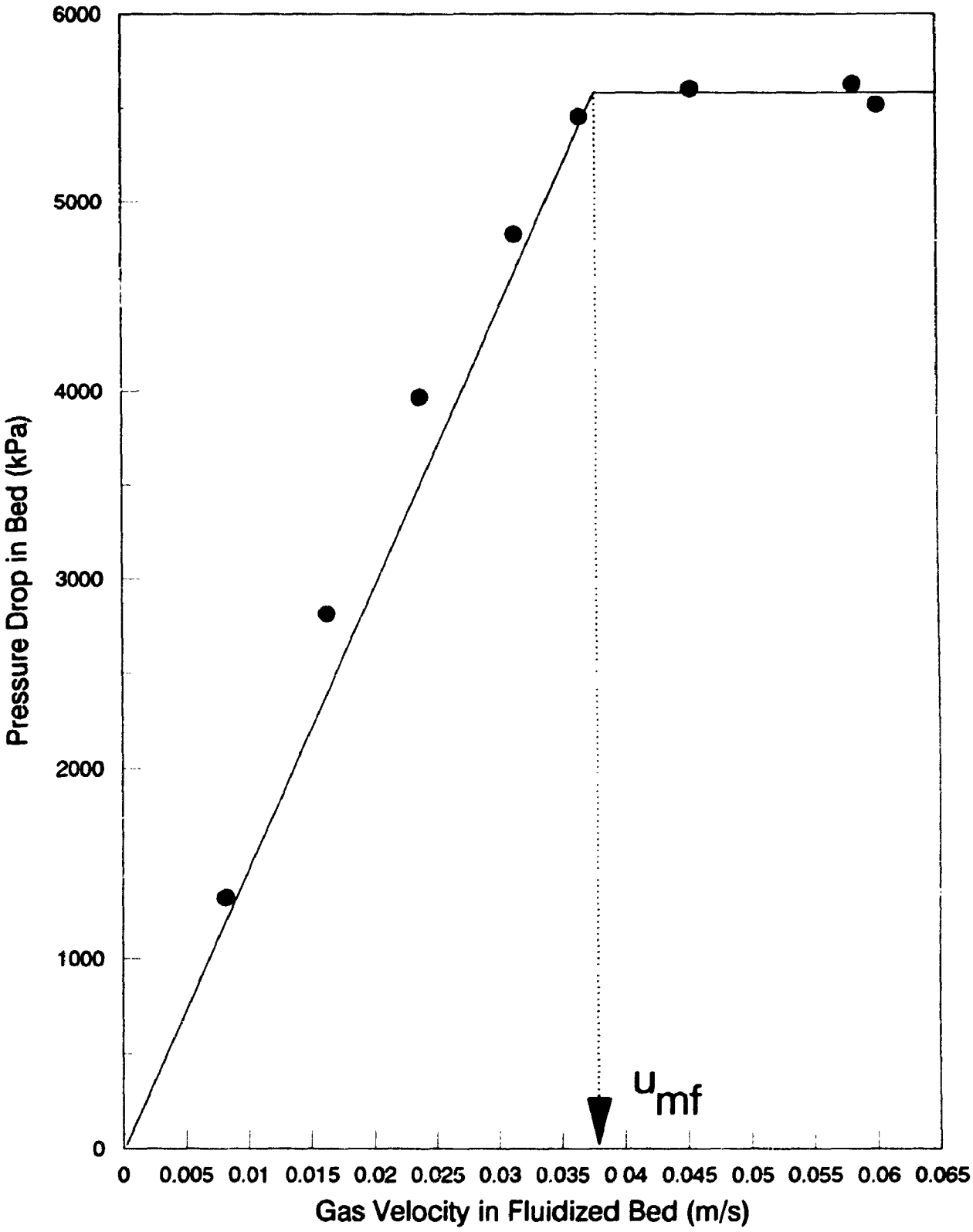

2.7.3 FLUIDIZED BED FEEDER PRE-STARTUP PROCEDURES

To ensure that particles were not segregated in the feeder, the bed was fluidized with the top cover off for half an hour at 10 u_{mf}, prior to the start of the run. During an experiment, however, it was usually maintained at about 5 u_{mf}. The top cover was disconnected so that massive amounts of solids would not be injected into the transport line (connected by flange connections to the top cover), which could cause tube blockage or slug flow upon start-up. Visual observations indicated that the bed was in a state of turbulent fluidization. Fluidization of the particles collected in the upper disengaging chamber was also carried out in the same manner and at the same time.

While the two beds were fluidizing the solids orifice injection nozzle piece in the solids feeder was adjusted to one suitable for the solids flux range being investigated. The positioning of the U-loop bend (Fig. 2.6) and dipleg was also modified depending upon the equilibrium height of bed solids that was expected for the run. It was known from operating experience that plugging of the dipleg return line was sensitive to the solids inventory in the system. This entailed that close monitoring of the total solids in the system was necessary.

2.8 START-UP PROCEDURES

2.8.1 AIR FLOWRATE AND SOLIDS FLUX MEASUREMENTS

Air flow to the disengaging chamber was initiated by a switch on the ground floor using an electrically-operated solenoid valve. The flow to the upper chamber fluidized the solids there, and decreased the level of solids in the chamber to the valve-outlet level. The pinch valves were turned on and off rapidly (with full flow to the transport line) to apply back pressure at the point of solids injection. This loosened any particles that may have been wedged in the orifice from a previous experiment. This practice was particularly necessary for solids fluxes above 100 kg/m^2s.

The air flow to the pneumatic transport line was gradually increased to the desired transport line velocity. Fluidizing air to the feeder was then initiated and the air flowrate in the fluidized bed was elevated to about $5u_{mf}$.

2.8.2 DATA ACQUISITION

The computer software written for data acquisition was executed following the pre-startup procedures. The compiled BASIC program was designed to run in two different modes (Appendix B). In the first, the mean and standard deviation of the test section pressure drop and upstream static

pressure, were displayed for every 200 points collected from each transducer. The number of points averaged was left as a variable in the program, but 200 points seemed to be the optimal number. By closely observing the change of pressure gradient in the test section with each successive computation, it was possible to determine when steady state had been achieved with 95% confidence. After 10 iterations for the test section pressure drop and static pressure (representing 2000 sampling points for each transducer), two other (Taylor) transducers (Appendix A; Figs. A3, A4) were used to measure the air flowrate to the transport line. This was measured by sensing pressure drop and upstream pressure across the square-edged orifice corner taps shown in Fig. 2.1.

When steady state had been attained (as determined by the method outlined above) the second mode of the computer program was executed. A total of 2050 signals were collected from each of the two transducers. The signals were obtained by sampling the static pressure which was followed by the pressure gradient. The two signals were stored in computer memory as separate arrays. At the end of the sampling period the program stored the raw data on diskette, and also computed an average and standard deviation of the data. The average and 95% confidence band of the static pressure, pressure gradient, and transport line air flowrate (expressed as a superficial gas velocity) were printed. The original mode of data collection

(averaging of 200 points) was then resumed automatically.

2.8.3 VALIDATION OF STEADY-STATE

Steady state for the two-phase flow was confirmed by a time series study (§ 4.9), performed after the completion of all the experiments. The slopes of the time series for both the pressure gradient and static pressure data were separately computed by linear regression. A zero slope at the 95% confidence level would indicate steady state conditions, and this was regularly observed.

2.8.4 SOLIDS FLOWRATE MEASUREMENT

Following the pressure data collection period the solids flowrate was determined. The solids flowrate was measured on the ground floor of the lab. It was necessary to attain solids transport velocity conditions in the riser prior to fluidizing the bed. If this procedure was not carried out solids were injected into the riser through the dipleg which resulted in line blockage and termination of the run.

The flow of solids to the line could be adjusted by increasing the upstream pressure to the bed by regulator or throttling the globe valve downstream of the bed. Although there was independent control of solids flowrate to the system, by adjusting the pressure differential in the bed, the flux was not

known before being measured externally.

Immediately above the fluid bed feeder and auxiliary piping connections, there were two ball valves plumbed into the return line dipleg. By closing the valve in the return line, and simultaneously opening the other to divert the flow, solids were collected for a 30 second interval. It was determined experimentally that a longer period of solids diversion from the system could result in depletion of the bed and a change in riser hydrodynamic flow conditions. By timing the solids collected over a 30 s interval the time-averaged solids flowrate in the riser, W_{sf}, was determined. The valve in the return line was subsequently opened and the other was closed. The solids collected were weighed and recycled back into the system by re-injecting them through the Y-shaped injector configuration situated on the top floor (Fig. 2.1), close to the disengaging chamber outlet solids valve. It was verified that there were no significant changes in the flow hydrodynamics in the system by monitoring the test section pressure drop before and after the solids flowrate measurement, using the method outlined in Section 2.8.2.

2.8.5 SOLIDS HOLDUP MEASUREMENT

After the solids flowrate was determined, and the collected solids were re-injected into the line, the system was allowed to restabilize itself to the hydrodynamic flow condition that existed prior to the start of the solids

measurement. The program was executed in mode 1 showing the pressure drop and static pressure across the line after 200 points were averaged. When 10 successive displayed values were the same as the data collected prior to solids flow measurement within 95% confidence, the program was terminated and the solids holdup was measured. If a persistent offset from the original pressure data was noted after solids flowrate measurement, the experiment was redone. Otherwise, the pinch valves were actuated and all air flows were stopped.

The weight of solids collected between the valves (solids holdup) was measured by disconnecting the rubber tubing connecting the vertical pipe (mounted in the fluidized bed feeder) to the Plexiglas riser. The lower pinch valve was remotely opened from the ground floor. All solids trapped between the two valves then dropped into a container on the ground floor. Solids in the line below the lower pinch valve had been cleared prior to opening the lower valve. Solids collected in the line above the upper valve were not collected until that valve was opened. Solids trapped between valves were weighed on a top loading weight scale. Since the volume of the test section was known, the weight of the solids collected was easily converted to an equivalent average solids volume fraction.

Although not required, the solids holdup in the region above the test section

was also obtained by opening the upper pinch valve after the test-section holdup had been determined. Since both regions were in the fully developed region the holdups measured from the two sections should have been equivalent. A check was made on the consistency between the two data, and if they did not agree within 10%, the experiment was replicated.

The solids holdup was always the last measurement made in an experiment. This ensured that any disturbance that could have been propagated through the system by shutting it down for solids holdup measurement, was not manifested in the pressure gradient and other measurements. Following the solids holdup measurement the apparatus was prepared for the next run.

A particle size analysis of the solids in the system was done periodically. This indicated that there was no significant loss of fines from the system, and attrition was minimal.

2.8.6 REPRODUCIBILITY OF MEASUREMENTS

To ensure the integrity of the data collected, a series of replicates were obtained on pressure profiles for the fluidized bed and the riser. Fig. 2.8.1 shows replicate data on the fluidized bed feeder. The discontinuity in the curve (at about 800 mm) where the two oblique lines intersect, represents

Fig. 2.8.1 : Axial Pressure Profile of Fluid Bed

Replicate Experiments

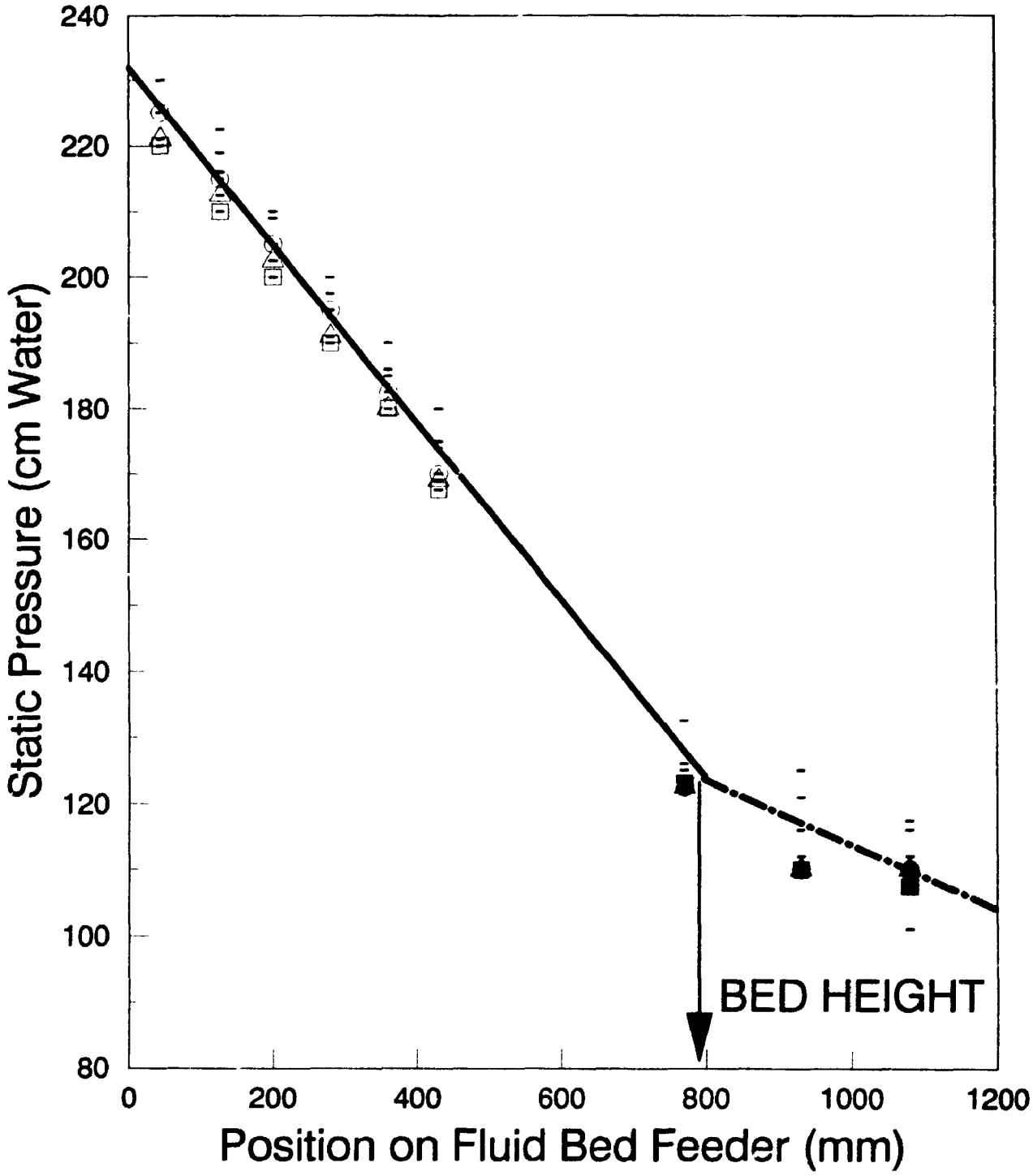

the bed level. All measurements are within close proximity of each other, indicating excellent reproducibility of experimental data.

Fig. 2.8.2 shows the static pressure profile along the vertical riser for several replicate experiments conducted in the non-slugging dense phase at a solids flux of 196 kg/m^{2}s and a gas velocity of 6.0 m/s. The curve is linear so that the test section is in the region of fully developed suspension flow. The replicate data points (for representative experiments 13-21) are within the expected error margins of each other. The same test was carried out on the inclined lines with the same margin of deviation. The methods of data collection are therefore considered to be reliable.

2.8.7 OTHER MEASUREMENTS

The ambient room temperature (20 -24°C), atmospheric pressure (720 - 780 mm Hg), and pressure drops and upstream pressures to the various orifice plates were recorded on the operating data sheet. Pressure drops across regulators and valves were also monitored during all runs. The flowrates were obtained by computation from standard orifice plate equations obtained in Chemical Engineering handbooks. The flowrates to the fluid bed feeder, transport line, outlet from the fluid bed feeder, inlet to the disengaging chamber, and total exhaust were compiled for each experiment. A mass balance was routinely done at the end of each experiment. This not

Fig. 2.8.2 : Axial Pressure Profile of Riser

Vertical Line Replicate Experiments

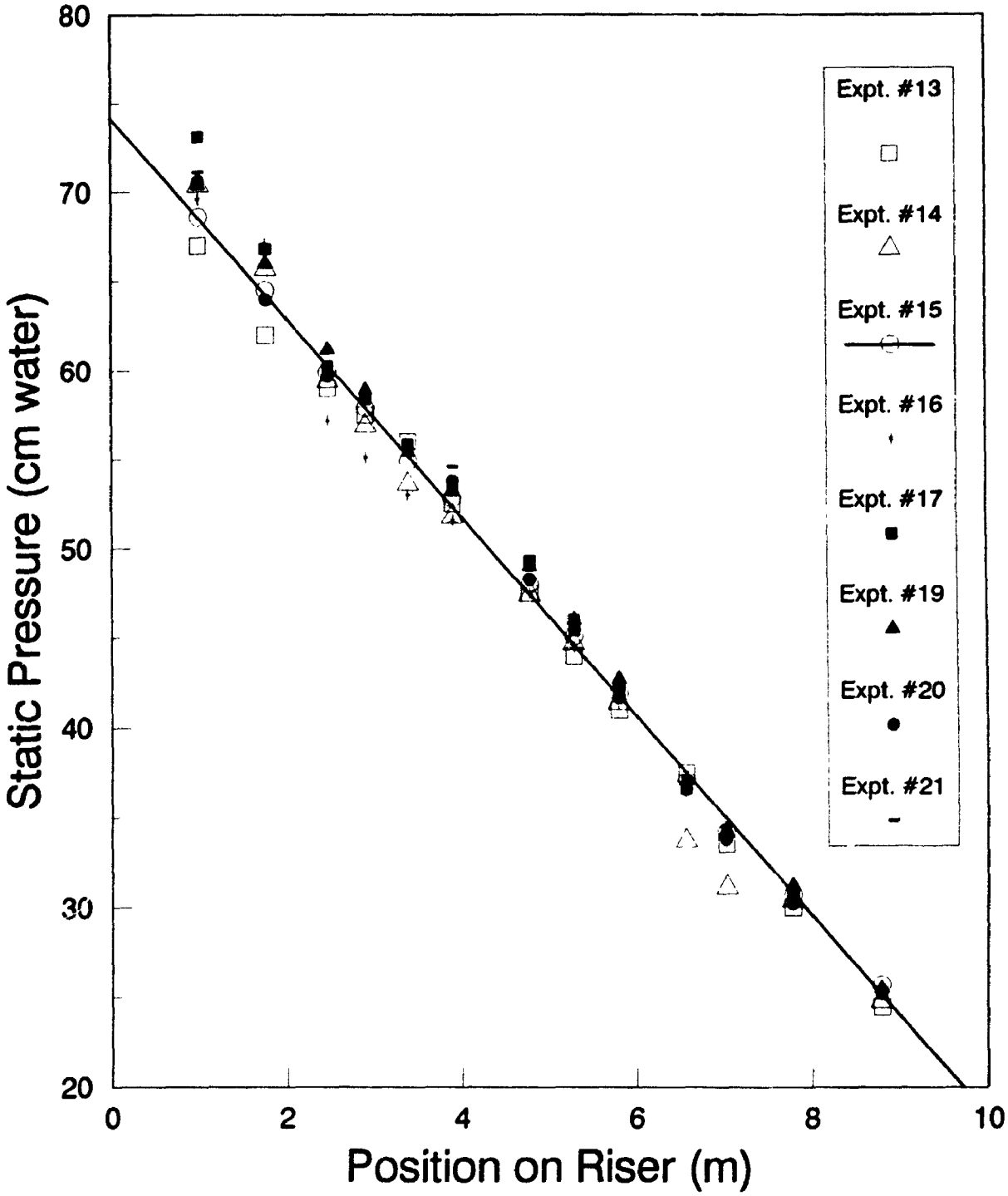

Solids Flux = 196 kg/m²s
Gas Velocity = 6.0 m/s
Solids Holdup = 1.50%

only quantified flows to all parts of the system, but was also a check on the calibration of the various instruments and detection systems. In all cases mass balances on flow were closed to within 6% absolute deviation, which is within the expected margin of experimental error.

It was noted in earlier discussions that pressure taps were systematically placed at 1.5 m intervals along the length of the riser. All except three of those taps were connected to water manometers. The static pressure for each of the taps hooked to manometers was recorded twice during an experiment and averaged. After the completion of a run the static pressure profile was plotted versus the axial coordinate as an additional check (analogous to Fig. 2.8.2) to verify that the test section was in the region of fully developed two-phase pipe flow, and that the transducer calibrations had not drifted.

2.9 PROCESSING OF RAW DATA

Following the completion of an experiment the raw data was analysed to determine the solids volumetric fraction (α), particle velocity (U_p), superficial gas velocity (U_g), solids flux (W_s), and other operational data.

2.9.1 SOLIDS CONCENTRATION AND ERROR ESTIMATION OF α.

The mean solids concentration (by volume) was determined using the mass

of solids recovered following the pinch valve closure. The solids holdup, α, was determined from equation (25a). Here M_s represents the mass of solids collected, A is the cross-sectional area (0.00079 m^2), H is the height of the test section (4.769 m), and ρ_p, is the solids particulate density (2560 kg/m^3 for sand and 2400 kg/m^3 for glass beads from laboratory measurement).

$$\alpha = \frac{M_s}{(\rho_p A H)} \qquad (25a)$$

Hence the mean solids concentration was then given by equation (25b):

$$\alpha = \frac{4 M_s}{\rho_p \pi (0.03175)^2 (4.769)} \qquad (25b)$$

The maximum error associated with the mean solids concentration was estimated based on the following hypotheses: when the lower pinch valve closed first, the solids continued to leave the test section (of length H) at a rate W_{sf} during the time Δt_{pv} , the time elapsed before the upper pinch valve closed. Similarly, when the upper pinch valve was first to close, solids continued to flow into the test section at the rate W_{sf} during Δt_{pv}. The difference between the measured and the real value of the solids

concentration would then be given by equation (25c).

$$\Delta\alpha = \frac{4\, W_{sf}\, \Delta t_{pv}}{\rho_p\, \pi\, D^2\, H} \qquad (25c)$$

The mean solids concentration is related to the mean solids velocity, U_p, by equation (25d).

$$\alpha = \frac{W_{sf}}{\rho_p\, U_p\, A} \qquad (25d)$$

The percentage error can be found by combining equations (25c) and (25d) to give equation (25e).

$$\frac{\Delta\alpha}{\alpha}\,(\%) = \frac{100\, U_p\, \Delta t_{pv}}{H} \qquad (25e)$$

Fig. 2.9.1 shows a plot of the percentage error (computed from equation 25e) versus the solids velocity range used in this thesis research, with Δt_{pv} as a parameter, varying between 1 ms and 15 ms. It is estimated from §2.5.3 that the difference of closure times, Δt_{pv}, varied between 3 and 11 ms for all runs. This boundary of closure times is indicated by the darker oblique lines in Fig. 2.9.1. It is evident that the maximum error would be about 3 % since the maximum particle velocity in this study was about 13 m/s.

Fig. 2.9.1: Maximum Errors of Solids Holdup

Error of α as Function of Valve Closure Time, Δt (ms)

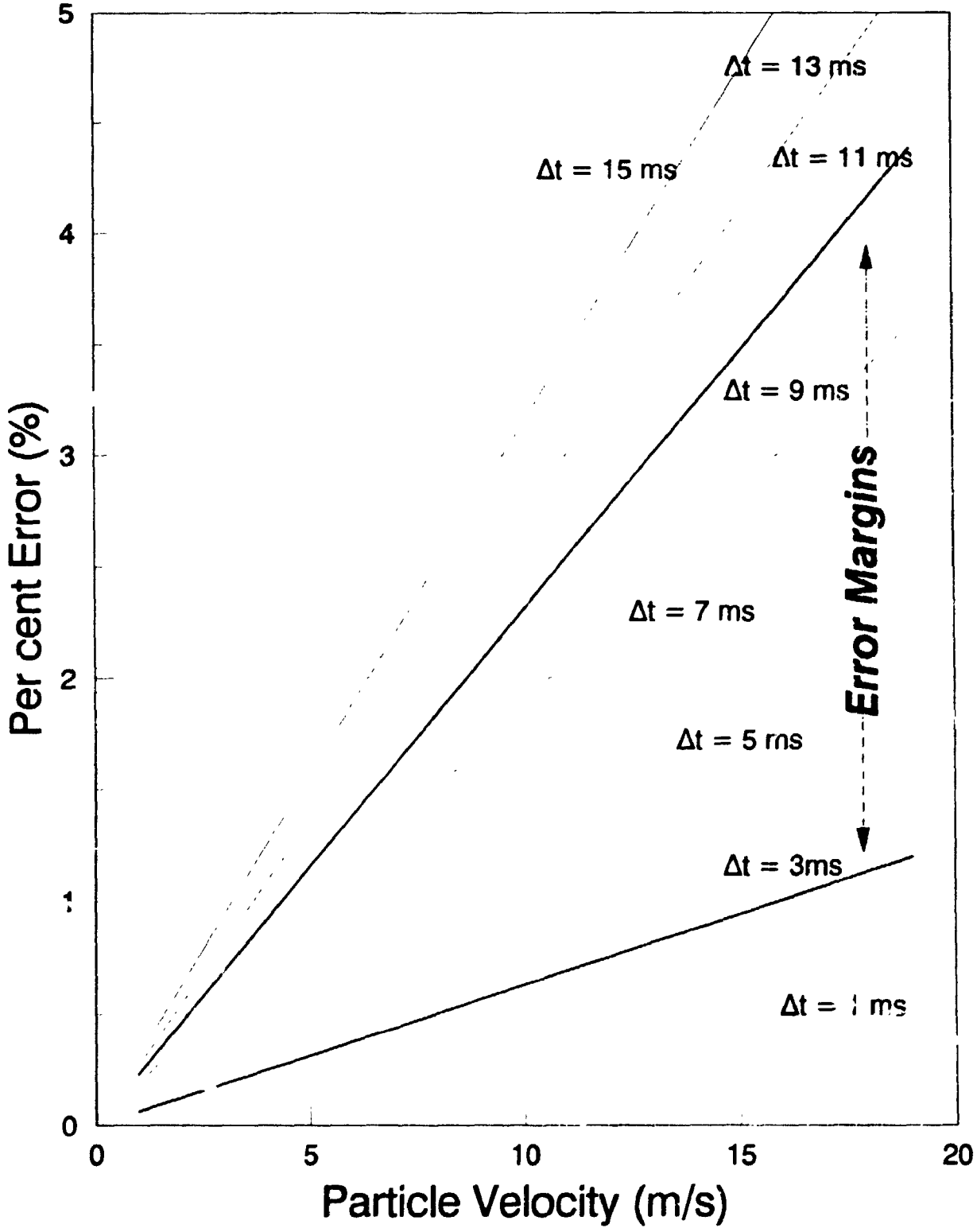

2.9.2 PARTICLE AND SUPERFICIAL GAS VELOCITY ESTIMATION

The particle velocity, U_p, was determined from solids holdup and solids flux rate, W_{sf}, through equation (26), which is an algebraic manipulation of equation (25d). The actual superficial gas velocity, U_g, was corrected for the

$$U_p = \frac{W_{sf}}{(\rho_s A \alpha)} \tag{26}$$

modified cross sectional area available for flow due to solids constriction of the line. This was computed by equation (27).

$$U_g = (U_{gs})(\ldots - \alpha) \tag{27}$$

The actual slip velocity, U_{slip}, was computed from equation (28).

$$U_{slip} = U_g - U_p \tag{28}$$

2.9.3 PRESSURE GRADIENT ESTIMATION

The pressure gradient associated with solids holdup (expressed as a percentage) was computed by equation (29), which is corrected for the inclination angle.

$$\frac{\Delta P_{holdup}}{L} = \frac{\rho_p \alpha (9.81) \cos(\theta)}{100} \tag{29}$$

The pressure gradient associated with gas friction with the wall could be computed from equation (30a).

$$\frac{\Delta P_{gas}}{L} = \frac{2 f_g \rho_g \epsilon U_g^2}{D} \qquad (30a)$$

By measuring the empty pipe pressure gradient (with gas flowing at known superficial velocities through the tube), it is possible to estimate f_g as a function of U_g or Re, the Reynolds number. This was done for gas velocities between 4 and 15 m/s ($10000 < Re < 30000$) in this research, and the results are shown on the Moody Diagram in Fig. 2.9.2. They are compared with the Blasius equation prediction for smooth pipes (Streeter and Wylie, 1979) represented by equation (30b).

$$f_g = 0.0791\ Re^{-0.25} \qquad (30b)$$

It is evident from Fig. 2.9.2 that there is good agreement between the Blasius prediction and the experimental results.

The pressure gradient due to gas alone (equation 30a) is plotted versus the superficial gas velocity range in Fig. 2.9.3. For the gas velocity range used in this research (≈4 to 15 m/s), $\Delta P_{gas}/L$ is less than 100 Pa/m. For most experiments it was less than 40 Pa/m because the gas velocity range of interest was less than 10 m/s for both types of particles. Clearly, the pressure gradient due to gas-wall friction is a minor contribution to the total pressure gradient in this research.

Fig. 2.9.2: Experimental Moody Diagram [1]

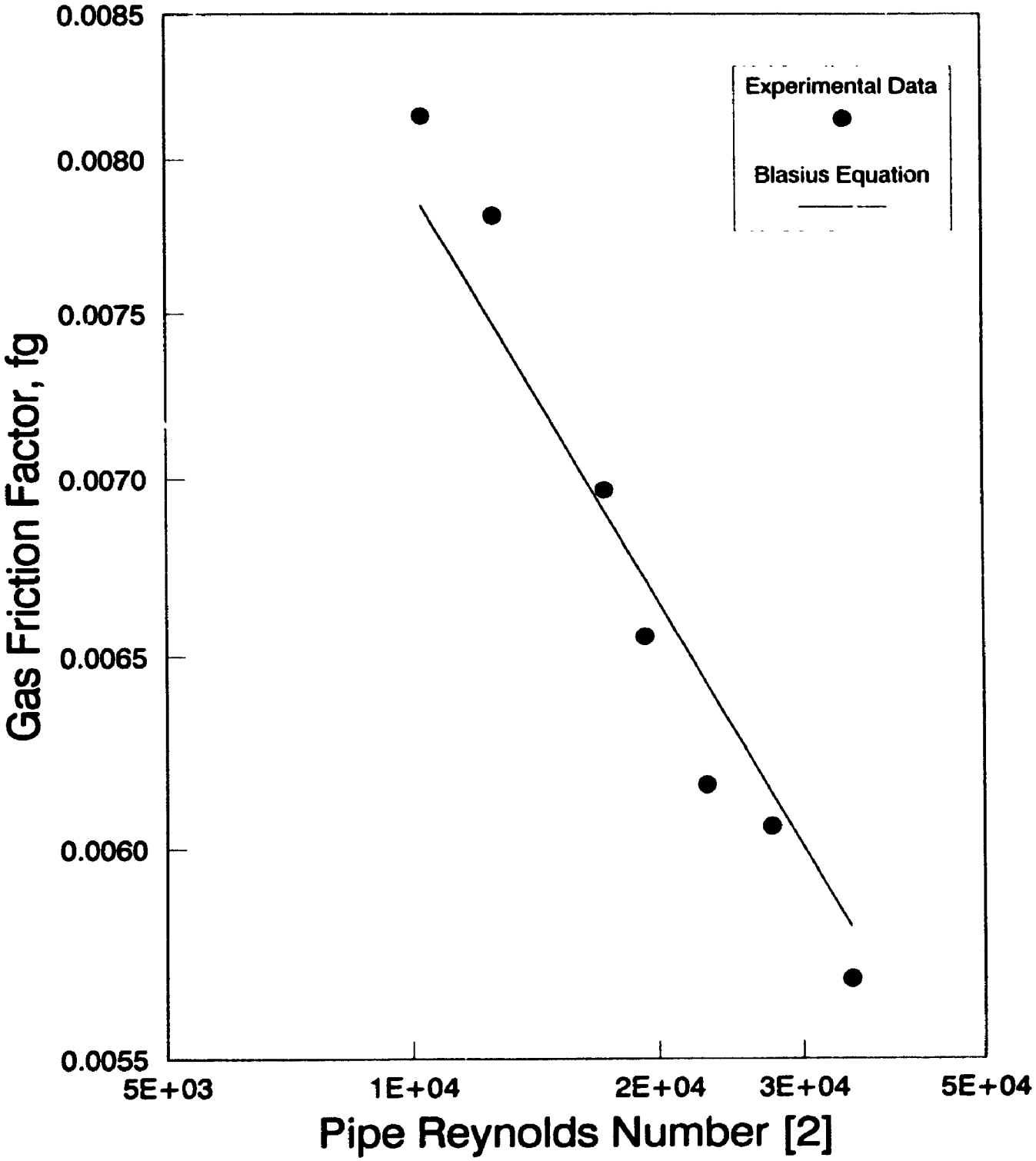

1. Blasius Equation for Smooth Pipe; Solid Line
2. Air velocity Range is 4 - 15 m/s.

Fig. 2.9.3: Empty Tube Pressure Gradient

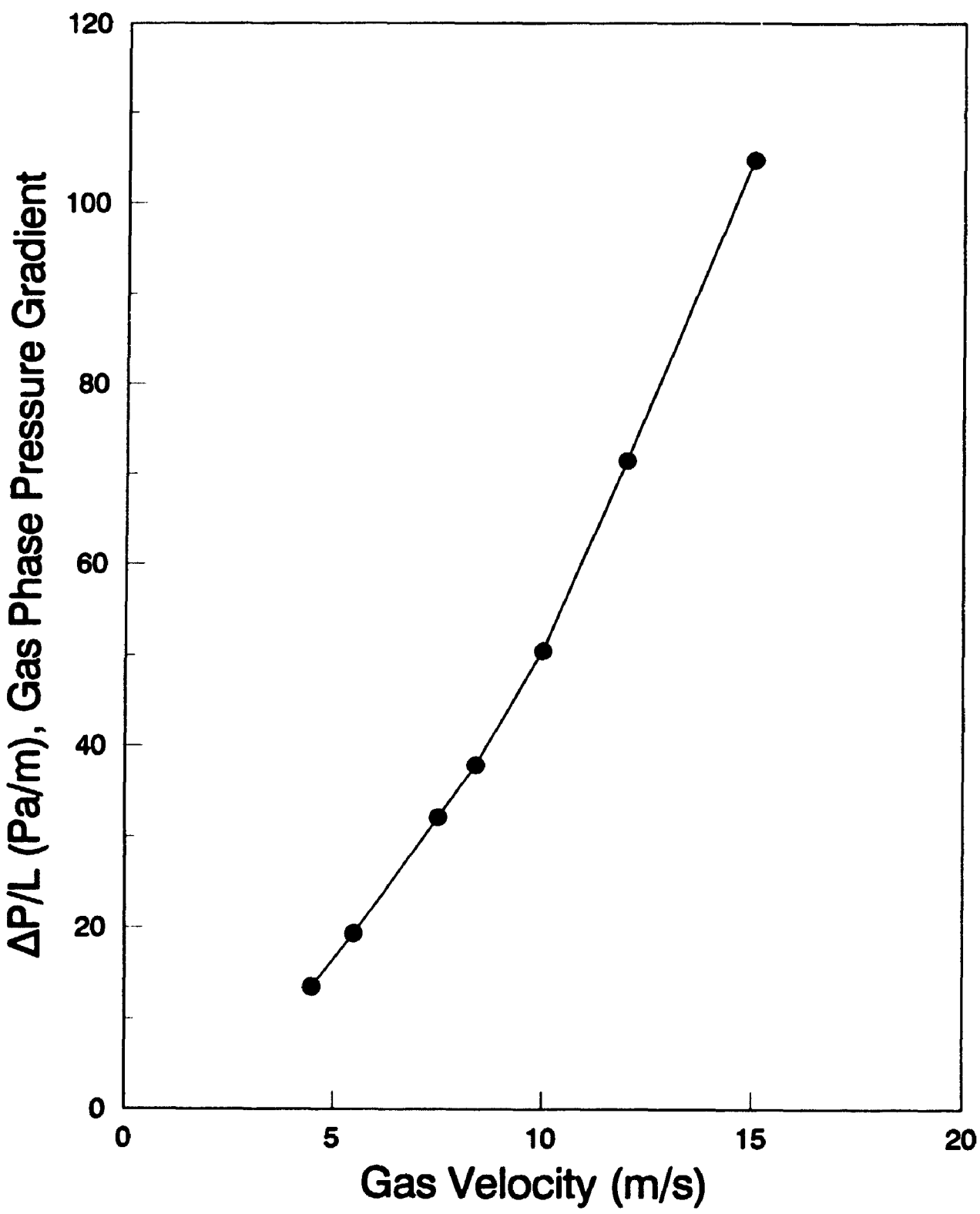

The pressure drop due to solids friction with the tube wall (or residual pressure gradient) was determined as the difference between the total pressure drop and that due to the solids holdup (equation 29) and gas-wall friction components (equation 30a), using equation 31.

$$\Delta P_{fs} = \Delta P_{total} - \Delta P_{holdup} - \Delta P_{gas} \qquad (31)$$

Since the flow was fully developed, there were no acceleration terms (reference equation 8; § 1.6.1) present in the computation. It is also assumed that the gas phase holdup term (equation 9, §1.6.1) is negligible, and this has been verified.

The solids/wall friction factor, f_s, was obtained from ΔP_{fs}, and is defined by equation (32).

$$f_s = \frac{\Delta P_{fs}\, D}{2\, \rho_p\, \alpha\, U_p^2\, (100)\, L} \qquad (32)$$

The basis of this form of relationship is derived from equation 10; § 1.7. Following an experiment the data was analysed by a series of FORTRAN programs written for the PC microcomputers, which are given in Appendix D. Program PDROP computes the pressure gradient associated with gas-wall friction and solids-wall friction using literature correlations. It uses the Capes, Jones, and Yang correlations for solids-wall frictional pressure drop. The program compares experimental results with literature

predictions. Program CORANA compares experimentally observed particle velocities with literature values. These correlations include Konno and Saito, Myler, Matsen, Zaltash, Nakamura, and Yang. Program CORREL computes the model parameters for the Klinzing thermodynamic approach. Program LIFTD2 computes lifting efficiencies for particles in pneumatic transport, whose derivations are given in Appendix E. Finally, the FORTRAN program TRDAT could be used to calculate a variety of derived parameters including velocities and friction factors from experimental data.

2.10 SUMMARY OF EXPERIMENTAL CONDITIONS

A summary of the ranges of experimental conditions are as follows:

$$U_g \approx 4.0 - 15 \text{ m/s}$$

$$W_s \approx 30 - 300 \text{ kg/m}^2\text{s}$$

$$W_{st}/W_g \approx 5 - 40 \text{ kg solids/kg air}$$

$$\alpha \text{ (v/v)} \approx 0.1 - 5 \text{ (\%)}$$

$$0^\circ \leq \theta \leq 18^\circ$$

$$d_p \approx 197 \text{ µm (sand) and } 441 \text{ µm (glass beads)}$$

2.10.1 SAND PARTICLES

A particle size distribution (PSD) for the sand particles is shown in Fig. 2.10.1. The Sauter mean diameter for sand was 197 µm. The sand particles represent Geldart Group B powders, with a particle sphericity of 0.84. Although a range of gas velocities of up to 12 m/s were tested for sand

particles, about 90% of the experiments were conducted at gas velocities between 4.5 and 9 m/s. This gas velocity range corresponds to conditions encountered in the fast fluidization regime (Yerushalmi and Cankurt, 1978). Gas velocities between 5 and 8 m/s (for this tube size) are probably most representative of typical commercial riser flow hydrodynamic conditions, while those below 4.5 m/s are not of commercial significance importance because slugging flow sets in.

About 60% of all experiments for sand particles were conducted at a solids flux of between 90 and 165 kg/m^2s. This range of conditions represents typical circulating fluidized bed operation (Westphalen, 1991). Approximately 80% of all experiments were conducted with a solids holdup of less than 1.5%. Higher solids holdups were found for large inclination angles, usually at the 18° angle of inclination.

2.10.2 GLASS BEADS

The particle size distribution of the glass beads is shown in Fig. 2.10.2. The Sauter mean diameter was determined to be 441 μm with a particle sphericity of about 1.0. The glass beads represent a Geldart Group B powder (Geldart, 1973). For the 441 μm glass beads (terminal velocity ≈ 3.2 m/s) the gas velocity was investigated over a narrow range. About 30% of all experiments were conducted between 7.5 and 8.5 m/s, which was

Fig. 2.10.1 : PSD for Sand

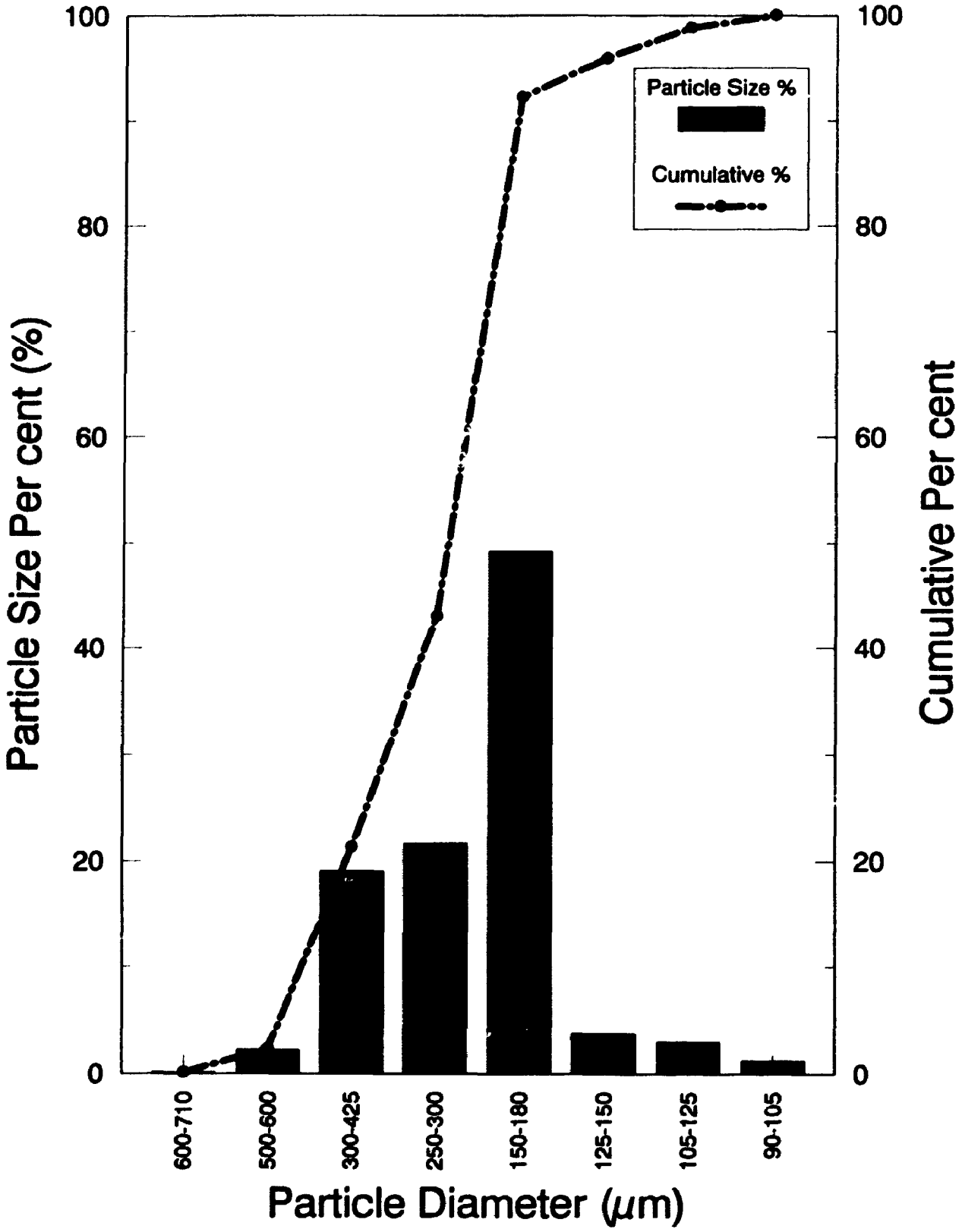

Fig. 2.10.2 : PSD for Glass Beads

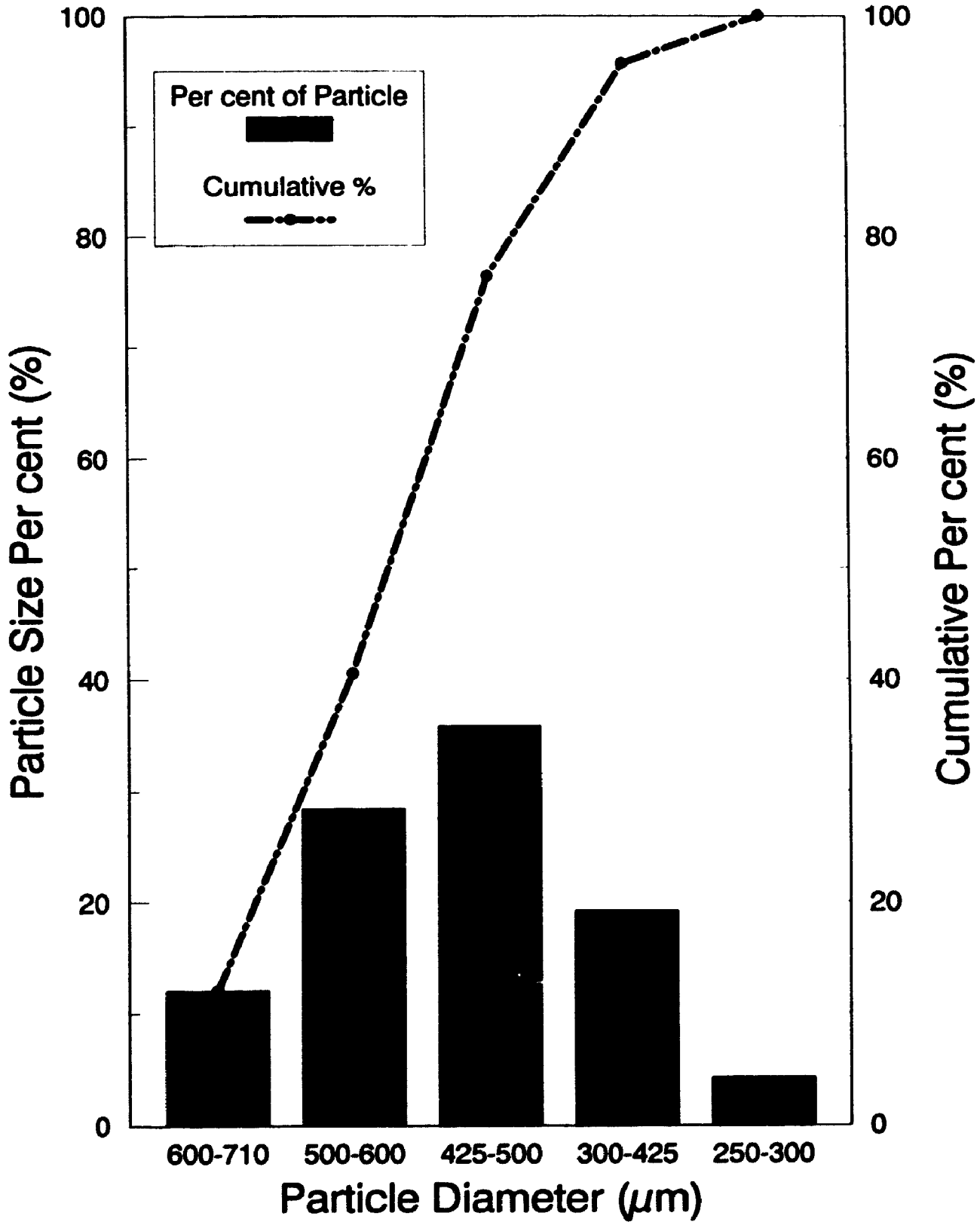

determined experimentally to be a transition gas velocity. It was in this region that changes in the hydrodynamic flow structure of the suspension were visually observed. Some experiments were also done above 10 m/s in the entrained flow regime.

About 95% of all experiments were for a solids flux of less than 250 kg/m^{2}s. The range of solids fluxes was considerably larger than that investigated for sand particles. About 45% of all experiments were performed at riser holdups of between 1.5% and 3.5% solids by volume. The range varied from 0.5% - 6%, but most of the holdups above 3.5% were in inclined lines.

2.11 TIME SERIES ANALYSIS OF DATA

The data collected by pressure transducers and collected in data files on Apple II-formatted diskettes, was converted to IBM PC compatible format using the appropriate computer hardware and software peripherals. It was then analysed by time series methods (§ 4.9, § 4.10) using the commercial software package NCSS (Hintze, 1990). The analysis included determination of the mean, standard deviation, skewness, kurtosis, and probability density function (PDF) of each data set. Power spectral analysis to determine dominant frequency was also performed. Autocorrelations and partial autocorrelations were computed, and a stochastic (ARIMA) model was developed for the prediction of the pressure gradient time series.

3. RESULTS

3.1 QUALITATIVE FLOW OBSERVATIONS

3.1.1 HYDRODYNAMICS OF RISER FLOW

The literature often refers to the phenomenon of core-annulus flow in the non-slugging dense regime, originally documented by Gajdos and Bierl (1978). Grace (1990) indicated that the concept of the dilute core/dense annulus is simplistic, and only valid on a time-averaged basis. In the present research study the core-annulus phenomenon was indeed apparent after time-averaging of the flow patterns, consistent with the observations of Grace (1990). The instantaneous flow resembled long clusters of particles streaming upwards, and weaving around the pipe like a swirling rope. Extensive refluxing of solids was observed at the pipe walls with a central upflow of solids. In corroboration of these results, Mok et al. (1989) found "diffused slugs" accompanied by extensive solids recirculation, especially at lower velocities. Similar to the observations made here, their flow patterns were made up of periods of high concentrations, interrupted by intervals containing lesser amounts of particles.

Further substantiation of the observations made in this research study can be gleaned from Dry and White (1989), who have shown that a radially symmetric core/annulus structure may exist at low gas velocities (about 5 m/s for FCC particles used in their work), but that it disintegrates to a

more random lateral distribution of lean and dense regions at higher gas velocities. Dry and Christensen (1988) observed that the core-annulus model is a time-averaged hydrodynamic configuration which is not necessarily valid for a total time less than the cycling period of the density inversion.

Brereton and Grace (1993) defined an intermittency index for riser transport, which would be zero for ideal core-annulus flow, and 1 for perfect cluster flow. Used to characterise the flow in their riser, it was observed that the flow behaviour was always between these two limits. Although the core-annulus formation was favoured with increasing height, it was noted that there continued to be substantial inhomogeneity in the flow structure. It was concluded on this basis that a pure core-annulus model represents an over simplification of the true flow structure, which was the same conclusion reached in the present work.

3.1.2 DEPOSITION OF SOLIDS AT THE PIPE WALL

Deposited solids (solids held immobile at the wall for an instant of time visible to the naked eye) were observed, before they were either swept upwards, or fell downwards some distance before being reentrained by core gas flow. Ocone et al. (1993) have rationalized this phenomenon by noting that the particles flow downward in the dense layer and drag gas with

them; conversely, in the upper part of the duct, the gas flows upward and drags particles in that direction. Hence, the direction of flow is determined mainly by the gas phase pressure gradient in the upper part of the duct, and also by the axial component of gravity in the lower part.

The amount of solids deposition observed in the current study increased as the gas velocity was lowered, to a maximum at the choking point. Grace (1990) found that particles may make hundreds of circuits because of internal reflux before leaving the system. Depending upon the exit geometry, gas velocity, and reactor height, it was claimed that particles could spend 2 to 20 s in each one of these circuits.

Solids deposition was observed even for the vertical line orientation at gas velocities approaching the choking point. Rhodes (1990) observed that up to 50% of the particles were recirculated for solids fluxes of about 50 kg/m^2s and a gas velocity of 4 m/s, using 64 μm particles in vertical risers. Rhodes et al. (1992b) observed solids refluxing even in the dilute phase regime, a phenomenon not reported in previous dilute phase pneumatic transport literature.

The quantity of deposited solids observed for the sand and glass particles used in this research increased with line inclination. Some of the particles

were partially supported by the underside of the pipe wall at lower gas velocities and line inclinations of 11° and more. Deposition of solids at higher line inclinations allowed for solids holdups exceeding the choking volumetric holdup of about 3% in the line.

Rhodes et al. (1992c) have observed that the particles cluster together in arch-shaped "swarms", which occur as the result of small irregular pulses of gas, assisting wall friction forces in holding up groups of particles against gravity. The pulses of gas are also apparently responsible for the eventual break-up of the swarm. By measuring particle turbulent energies in the core and annulus, Wang et al. (1993) have shown that there is preferential formation of clusters in the annular region relative to the core. These authors found a steady decrease of the turbulent particle energy in the vicinity of the wall.

3.1.3 MECHANISM OF SOLIDS DEPOSITION

Senior and Brereton (1992) stated that there are two possible mechanisms by which upflowing core particles are deposited at the pipe wall: particle turbulent diffusion and particle-particle collisions. Reeks and Hall (1988) have observed that deposition of particles exposed to the mainstream flow is controlled by two processes:

i) initial deposition of solids which is modified by a fraction adhering, due to impact adhesion or particle bouncing;

ii) resuspension, or the subsequent removal from the surface by local turbulence at the surface after time scales greater than the timescale of the turbulence.

Sinclair and Jackson (1989) claim that it is the interaction of the fluctuating part of the particle motion with the mean particle motion. This action generates stresses in the cluster of particles, and results in the lateral segregation of solids causing particle deposition. The deposition of solids in inclined ducts has been modelled mathematically by Ocone et al. (1993) using the methodology of Sinclair and Jackson (1989).

3.2 PRESSURE GRADIENT TIME SERIES CHARACTERISATION

3.2.1 SLOPE OF THE PRESSURE GRADIENT TIME SERIES

The slope of the pressure gradient time series was obtained by performing a linear regression on all 2050 points obtained from data acquisition. An average drift of about 5 Pa/m was observed for the pressure gradient over the duration of an experiment. This represents about 1% of the mean value. A maximum of 3% was allowed before an experiment was replicated.

3.2.2 VERIFICATION OF THE ASSUMPTION OF GAUSSIAN (NORMALIZED) PRESSURE GRADIENT DISTRIBUTIONS

In this work the mean pressure gradient ($\mu_{\Delta P/L}$), and its standard deviation ($\sigma_{\Delta P/L}$), obtained from the 2050 pressure transducer signals for each experiment, are used to characterise the hydrodynamic flow conditions in the test section. The assumption made is that the probability density function (PDF) of the time series is normal or Gaussian, and hence, can uniquely be characterised by μ and σ alone. This hypothesis will be verified in this section, as a preface to all subsequent data presentation and interpretation.

All pressure gradient time series signals were analysed statistically for the first four moments of the distribution to verify the validity of the assumption of a normal distribution. The first four moments are : mean (μ), standard deviation (σ), skewness (ψ), and kurtosis (κ) respectively.

3.2.3 STANDARD DEVIATION AND COEFFICIENT OF DEVIATION

The mean pressure gradient can be defined by equation (33), where P_i represents the sequence of pressure gradient signals measured. It estimates the value around which clustering occurs.

$$\mu = \sum_{i=1}^{N} \frac{P_i}{N} \qquad (33)$$

A parameter that can be used to characterise the fluctuations of the pressure gradient around the mean is the standard deviation of the time series. The standard deviation is given by equation (34):

$$\sigma = \left(\sum_{i=1}^{N} \frac{(P_i - \overline{P})^2}{(N - 1)} \right)^{\frac{1}{2}} \qquad (34)$$

Equation (34) estimates the mean squared deviation of P_i from its mean value. The standard deviation can be normalised after dividing it by the mean (equation 33) to give the coefficient of deviation ($\overline{\sigma}$), defined by equation (35):

$$\overline{\sigma} = \frac{\sigma}{\mu} \qquad (35)$$

3.2.4 SKEWNESS AND KURTOSIS OF TIME SERIES DISTRIBUTIONS

The skewness characterises the degree of asymmetry of the distribution around its mean, and is a nondimensional quantity. A normal (Gaussian) PDF should have a skewness of zero. A positive value of skewness indicates a distribution with an asymmetric tail extending outwards toward more positive values; conversely a negative skewness signifies a distribution extending toward more negative values. The skewness is defined by

$$\Psi = \frac{1}{N} \sum_{i=1}^{N} \left(\frac{(P_i - \mu)}{\sigma} \right)^3 \qquad (36)$$

equation (36).

The kurtosis is also a nondimensional quantity. It measures the relative peakedness or flatness of a distribution relative to a Gaussian distribution (Press et al., 1986). The kurtosis of the distribution is given by equation (37) where the -3 term makes the value zero for a normal distribution:

$$\kappa = \left(\frac{1}{N} \sum_{i=1}^{N} \left(\frac{(P_i - \mu)}{\sigma} \right)^4 \right) - 3 \qquad (37)$$

3.2.5 NORMALITY OF PRESSURE GRADIENT TIME SERIES

Fig. 3.2.1 shows a probability density function (PDF) for the variable $\bar{\sigma}$-, (the coefficient of deviation), for the pressure gradient time series with experiments at all four line inclinations. The average value of $\bar{\sigma}$- is 0.099 with a standard deviation of 0.033. It is greater than 0.10 of the signal intensity for 40% of the experiments performed. In comparison, Matsumoto and Harakawa (1987) have found that the coefficient of variation for pressure fluctuations was 0.2 in the dilute phase, but increased to 1.0 in the fast fluidization regime.

Linear correlations between $\bar{\sigma}$- and independent variables were estimated using the statistical program NCSS. For the vertical line it was found that $\bar{\sigma}$- is strongly correlated with both solids flux (0.68) and solids holdup

Fig. 3.2.1 : Deviation Coefficient PDF for ΔP/L Sand Particles All Inclinations

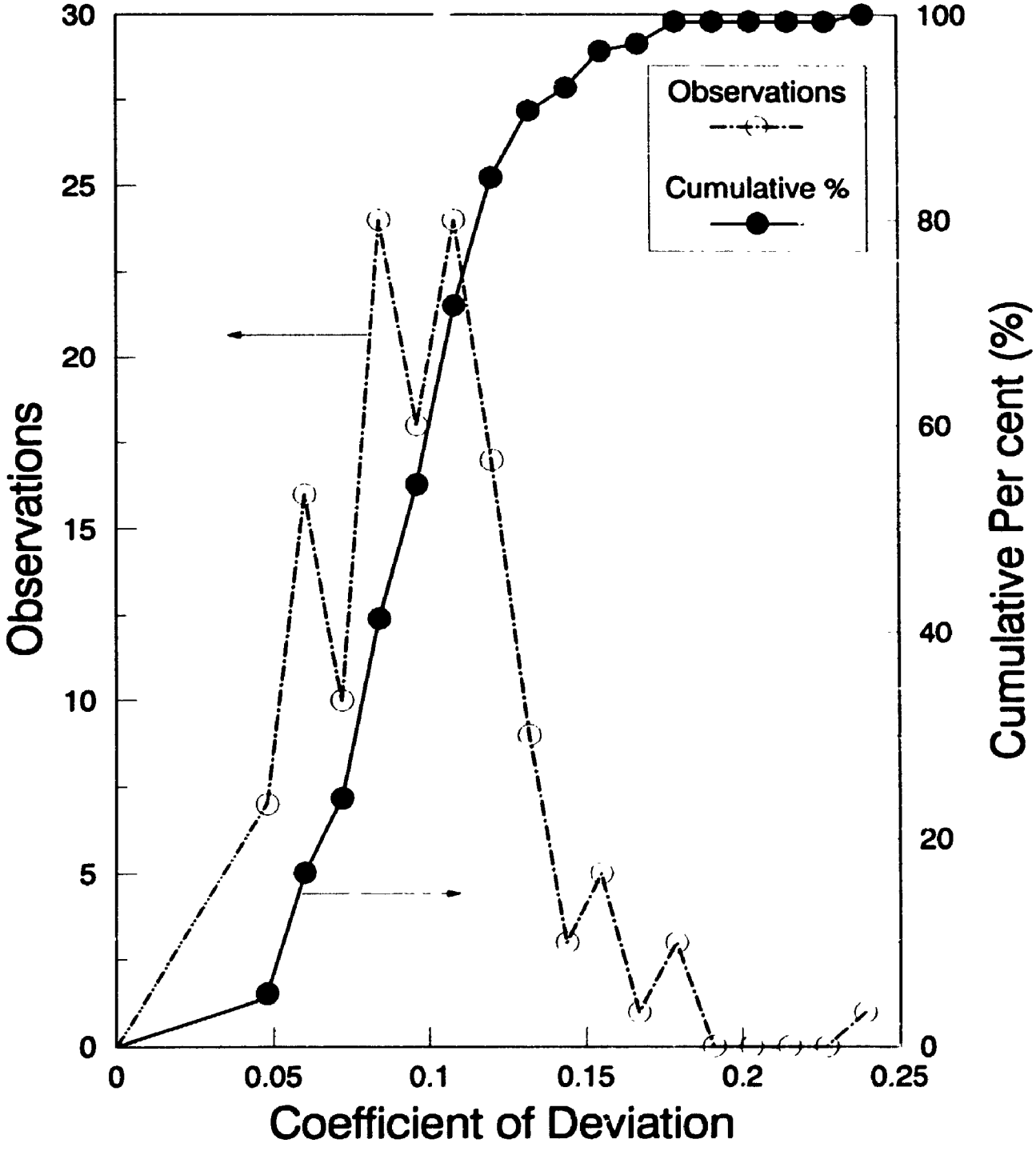

μ = 0.099
σ = 0.033

(0.87), and is slightly correlated with the gas velocity (-0.23). At 18° the correlation of $\bar{\sigma}$- with all three variables decreases.

A PDF of ψ (skewness) is shown in Fig. 3.2.2. The narrow distribution for skewness indicates that the PDFs of the pressure gradient series taken were symmetric about the mean. About 80% of the pressure gradient time series investigated had a skewness of between -0.62 and 0.40, which demonstrates the validity of the normality assumption. The average skewness is -0.081 (standard deviation of 0.040), and was not significantly correlated with any of the controlled parameters.

A PDF of the kurtosis function, κ, is shown in Fig. 3.2.3. Approximately 80% of the pressure gradient distributions for sand have a kurtosis of between -0.55 and 0.71. The remaining 20% have a kurtosis greater than 1; this indicates a flat distribution with a large number of extreme values for those experiments. The average kurtosis is 0.439 with a standard deviation of 0.061. Although the PDF of the pressure gradient distribution is slightly flat based on the mean value of 0.439 at 95% confidence, the assumption of normality would be appear to be a reasonable one. Hence, the mean and standard deviation of the PDF for the pressure gradient time series can be used to characterise the pressure gradient time series completely for all line inclinations.

Fig. 3.2.2: Skewness PDF of ΔP/L
Sand Particles all Inclinations

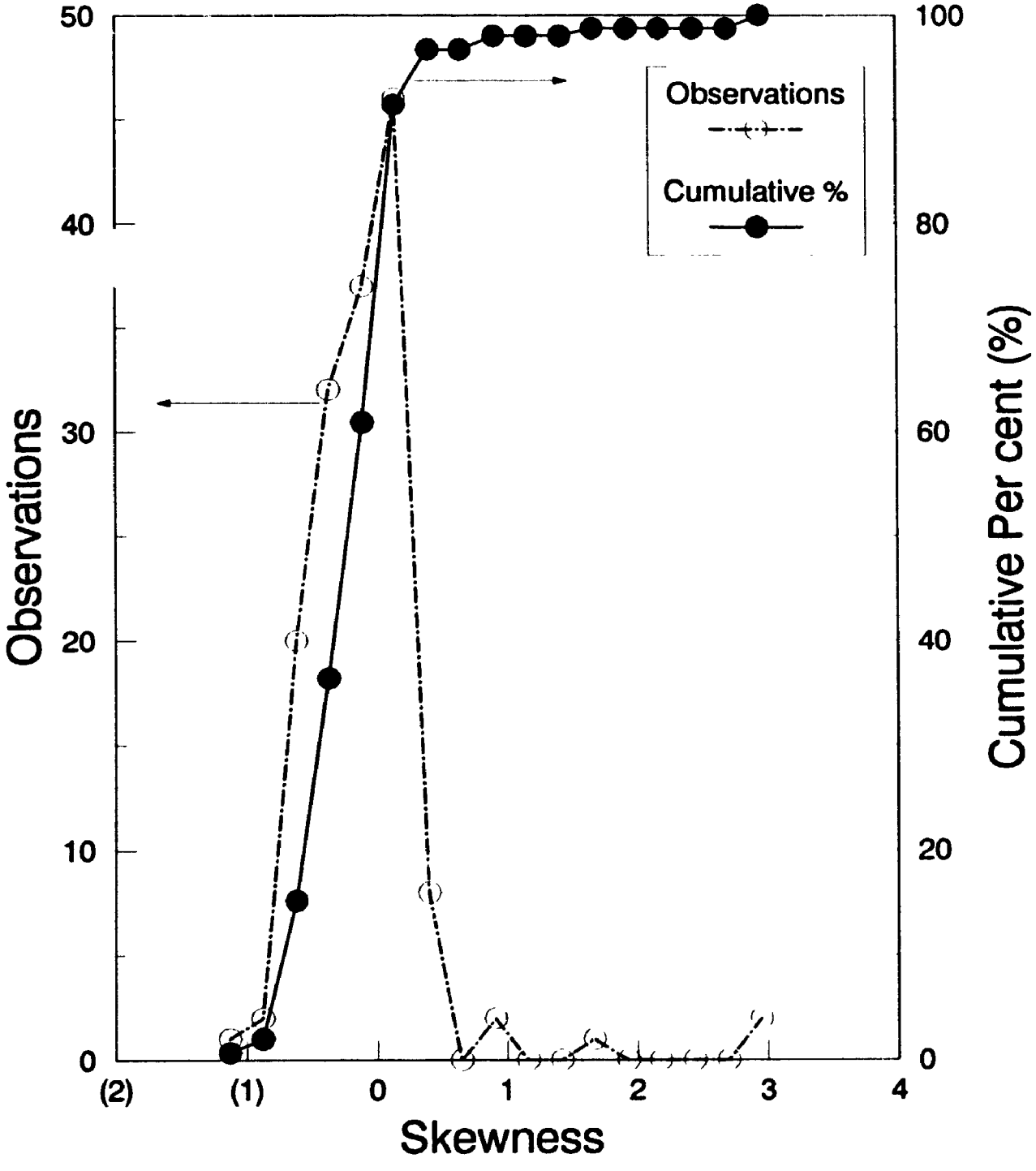

μ = -0.081
σ = 0.040

Fig. 3.2.3: Kurtosis PDF of ΔP/L [1]
Sand Particles all Line Inclinations

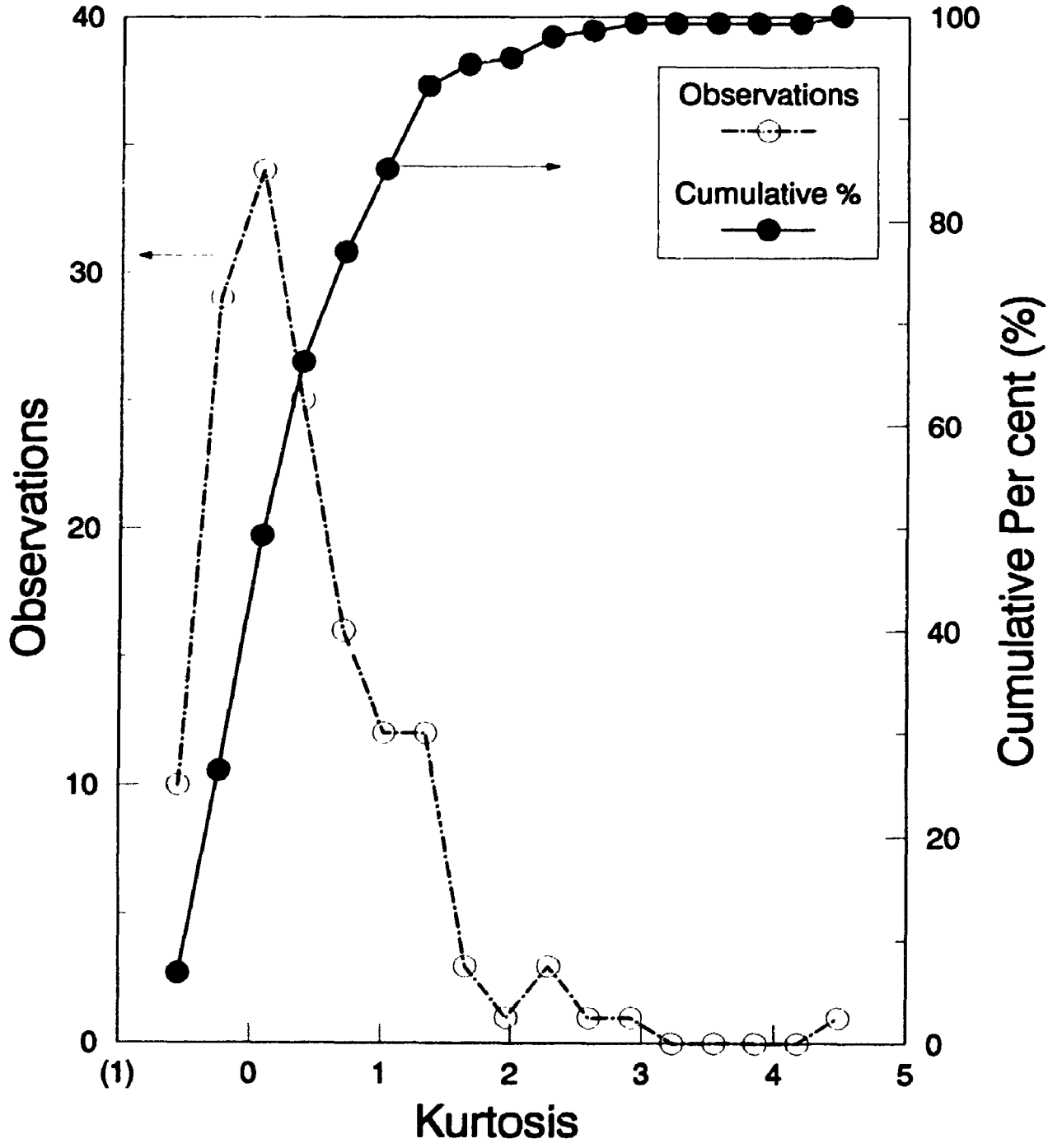

μ = 0.439
σ = 0.061
1. Kurtosis or Flatness Factor

The skewness and kurtosis of a PDF can sometimes provide useful information about the process (Tsuji and Morikawa, 1982), but this was not the case here. They were both random variables with values close to zero, and were not enlightening of the process characteristics in any way. However, the analysis of these third and fourth order moments was significant in this research for demonstrating that the assumption of normality for the pressure gradient time series is a valid one.

3.3 EFFECT OF SOLIDS FLUX ON PRESSURE GRADIENT

One of the principal objectives of this study was to elucidate the fast fluidization (or riser) hydrodynamics of the 2-phase mixture for inclined lines. The effects of inclination angle, θ, on $\Delta P/L$ will be examined in the ensuing section.

3.3.1 EFFECT OF LINE ORIENTATION WITH SAND PARTICLES

For the vertical riser the effect of sand flux (in kg/m^2s) on pressure gradient is shown in Fig. 3.3.1. The linear least squares regression lines are not extrapolated to the origin because it is known from related studies (Ginestet et al., 1993; Mok et al., 1989) that there is a transition between the dilute and dense phases in the low solids flux regime. For the current study the dilute phase regime was not considered. Rather, the gas velocity was varied between 4.5 m/s and 9.5 m/s, representing non-slugging dense transport.

Fig. 3.3.1 : Pressure Gradient vs. Sand Flux
Vertical Line Orientation

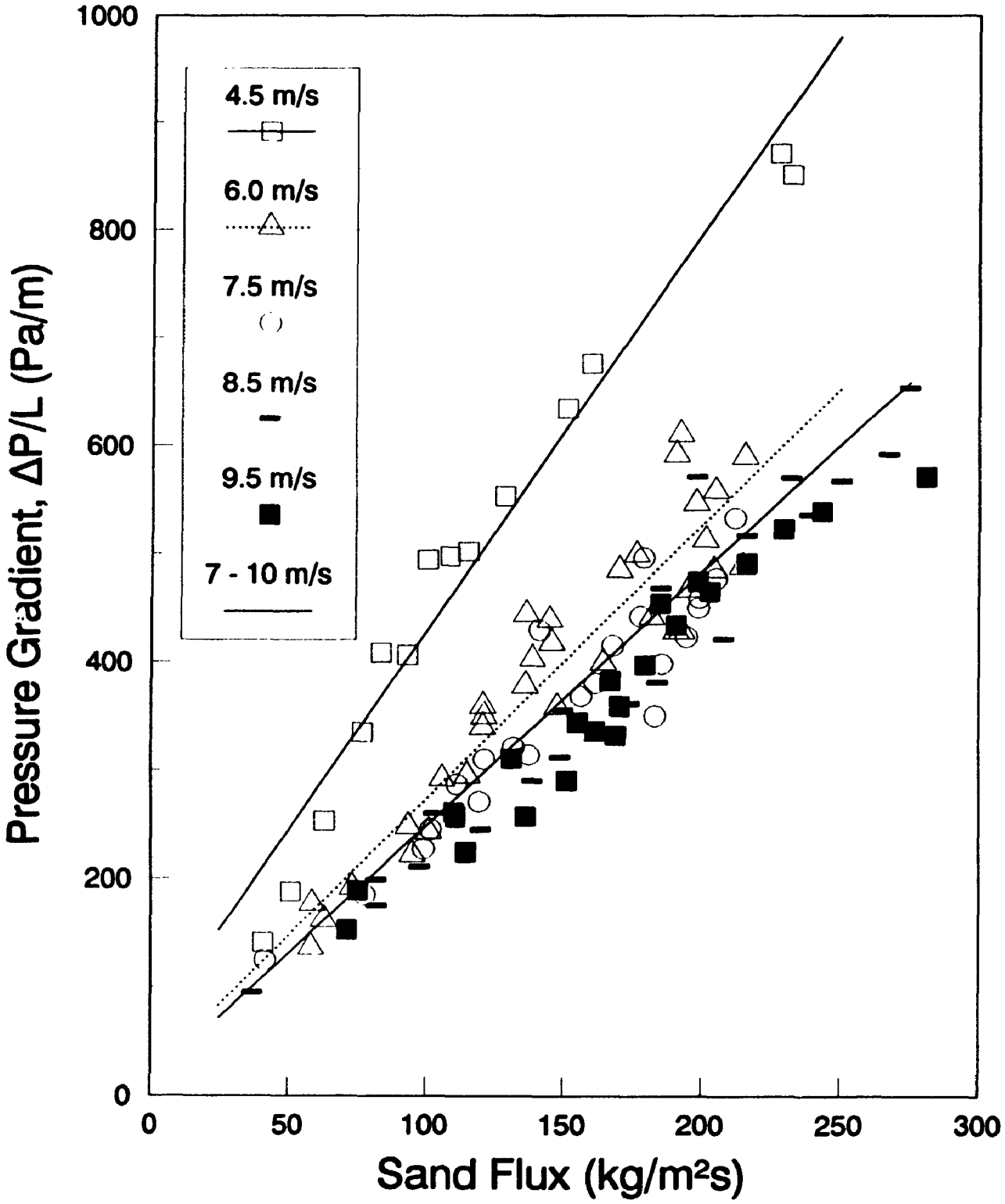

For gas velocities greater than 7.5 m/s, the pressure gradient increases linearly (slope = 2.35 s^{-1}) with solids flux. There is no significant effect of gas velocity in this fully entrained range, so a single least squares line was fitted through all the points.

At a gas velocity of 4.5 m/s (indicated by open squares in Fig. 3.3.1), the linear slope is 3.64 s^{-1}. The line does not intersect exactly at the origin because of the small contribution of gas frictional pressure drop losses with the wall, and because of the change of slope in the dilute phase regime (Ginestet et al., 1993). Visual observations indicated that the particles were undergoing extensive particle reflux at 4.5 m/s. Throngs of particles, momentarily deposited at the walls, drifted downwards briefly, before being reentrained by the gas. Although there was some evidence of this type of flow behaviour above 6.5 m/s, the particles were carried upwards in rope-like clusters most of the way through the test section as described in § 3.1.

Fig. 3.3.2 shows the effect of solids flux on the pressure gradient for a line inclination of 4°. The minimum gas velocity that could be achieved before slugging flow set in was 5.5 m/s. The pressure gradient is 1000 Pa/m at a solids flux of about 220 kg/m^2s. This result is similar to the results for the vertical line (Fig. 3.3.1), with the exception that the gas velocity is 1 m/s higher at choking. The effect of gas velocity on pressure gradient is more

Fig. 3.3.2 : Pressure Gradient vs. Sand Flux

4° Inclined Line

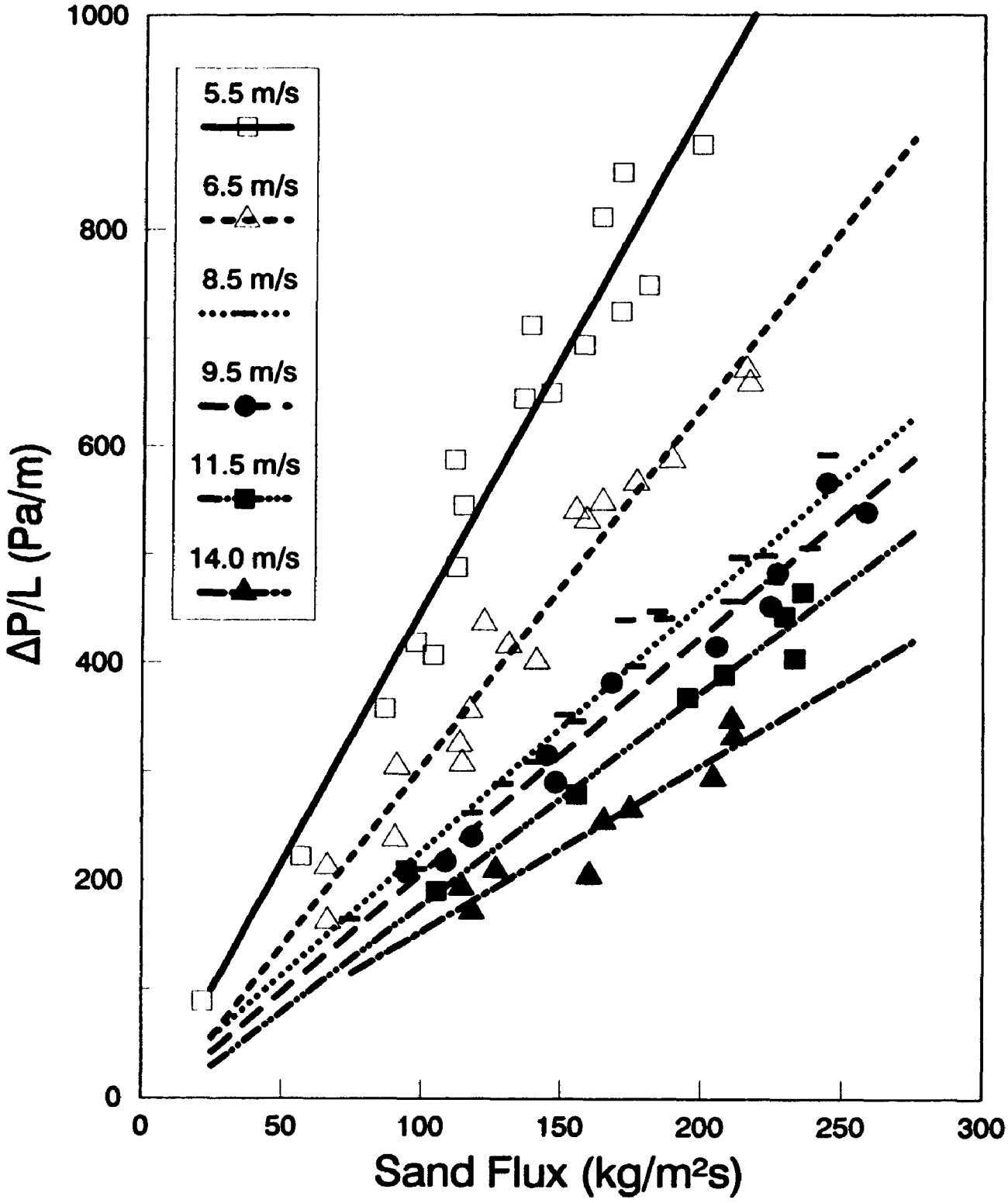

prominent at 4°; the slope decreases continuously with each successive increase of gas velocity from : 4.66 s^{-1} at a gas velocity of 5.5 m/s, to 3.31 s^{-1} at 6.5 m/s, 2.28s^{-1} at 8.5 m/s, and 1.52 s^{-1} at 14.0 m/s. In all cases the pressure gradient increases linearly with solids flux.

Fig. 3.3.3 shows the effect of solids flux on the pressure gradient at 11° from the vertical. The slope of the least squares lines decreases continuously from 8.58 s^{-1} at 4.5 m/s to 3.37 s^{-1} at 7.5 m/s.

Fig. 3.3.4 shows the effect of solids flux on the pressure gradient for gas velocities between 5 and 12 m/s for the 18° line orientation. Between 50 and 150 kg/m^2s the slope decreases from 8.52 s^{-1} (at a gas velocity of 5.0 m/s), to 5.11 s^{-1} (at 7.5 m/s), and 1.81 s^{-1} (at 9.5 m/s), beyond which there is no significant change. Based on the results from Figs. 3.3.1 to 3.3.4, it is evident that the pressure gradient increases with line inclination. The pressure gradient is more sensitive to slight decreases of gas velocity as the line inclination is increased.

3.3.2 EFFECT OF LINE INCLINATION WITH GLASS BEADS

This section examines the effect of solids flux on pressure gradient for the glass beads. Fig. 3.3.5 shows the plot of pressure gradient versus glass flux for the vertical line at gas velocities ranging from 7.5 to 16.0 m/s. Below a

Fig. 3.3.3 : Pressure Gradient vs. Sand Flux
11° Inclined Line Orientation

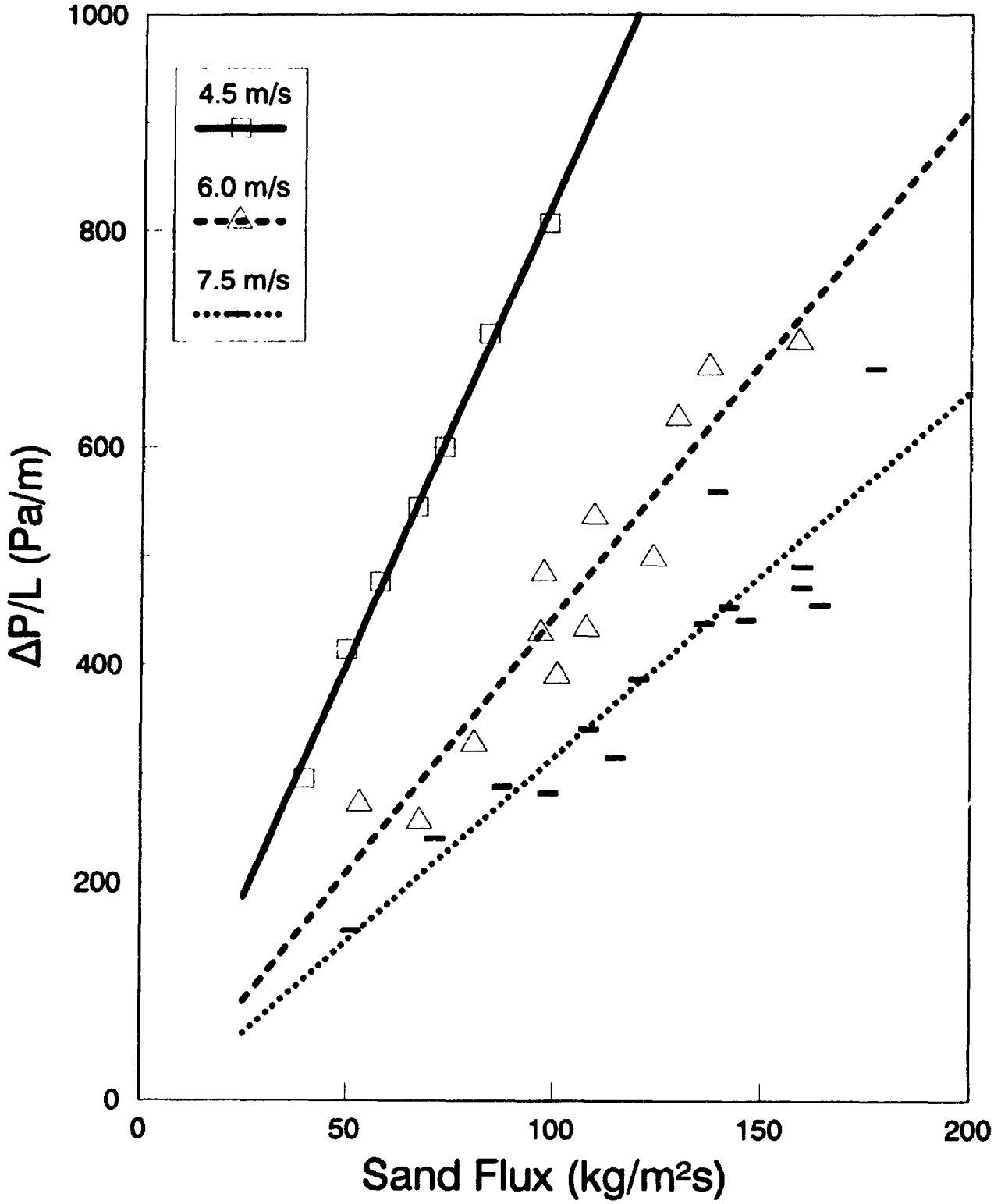

Fig. 3.3.4 : Pressure Gradient vs. Sand Flux 18° Inclined Line Orientation

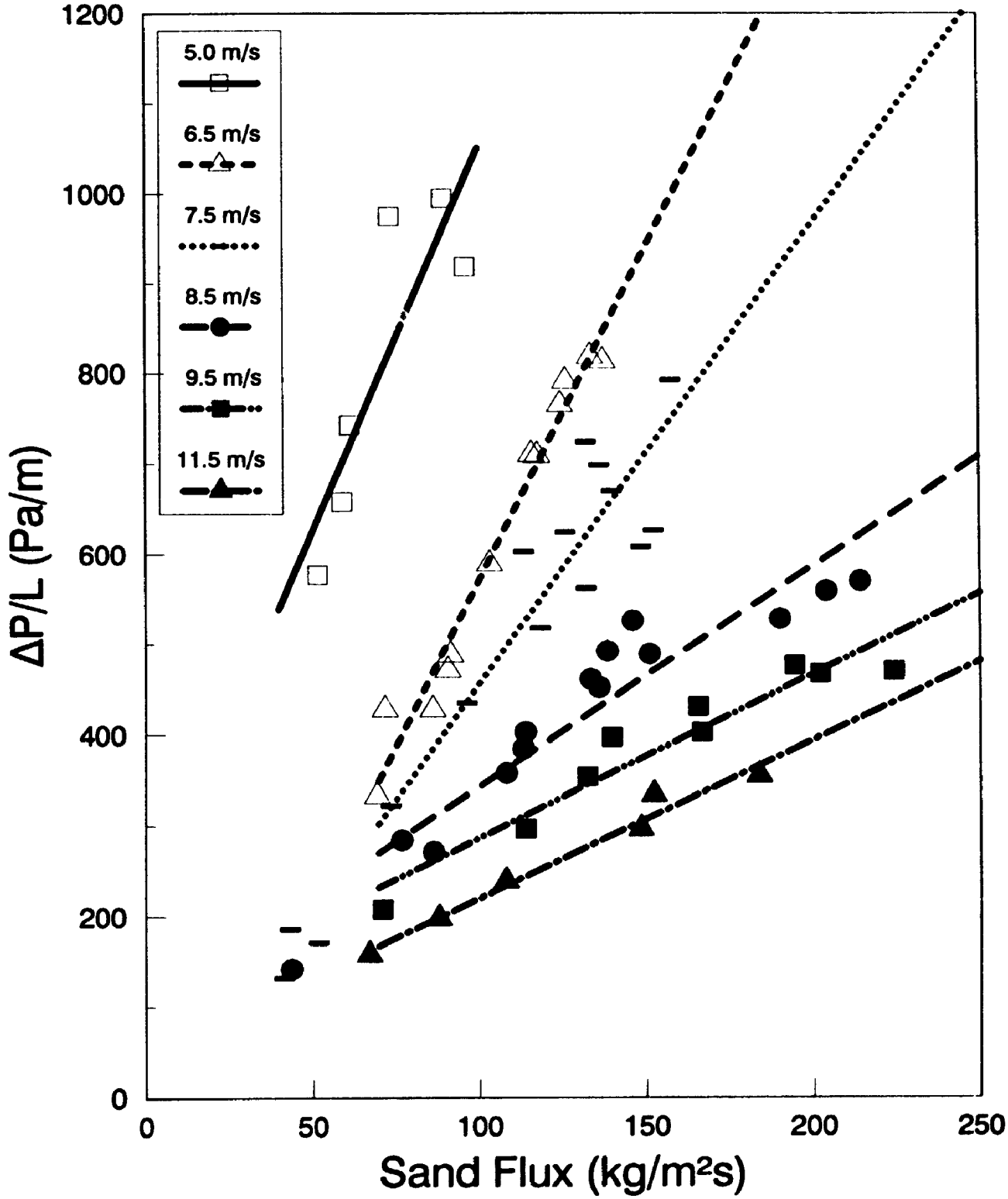

Fig. 3.3.5 : Pressure Gradient vs. Glass Flux
Vertical Line Orientation

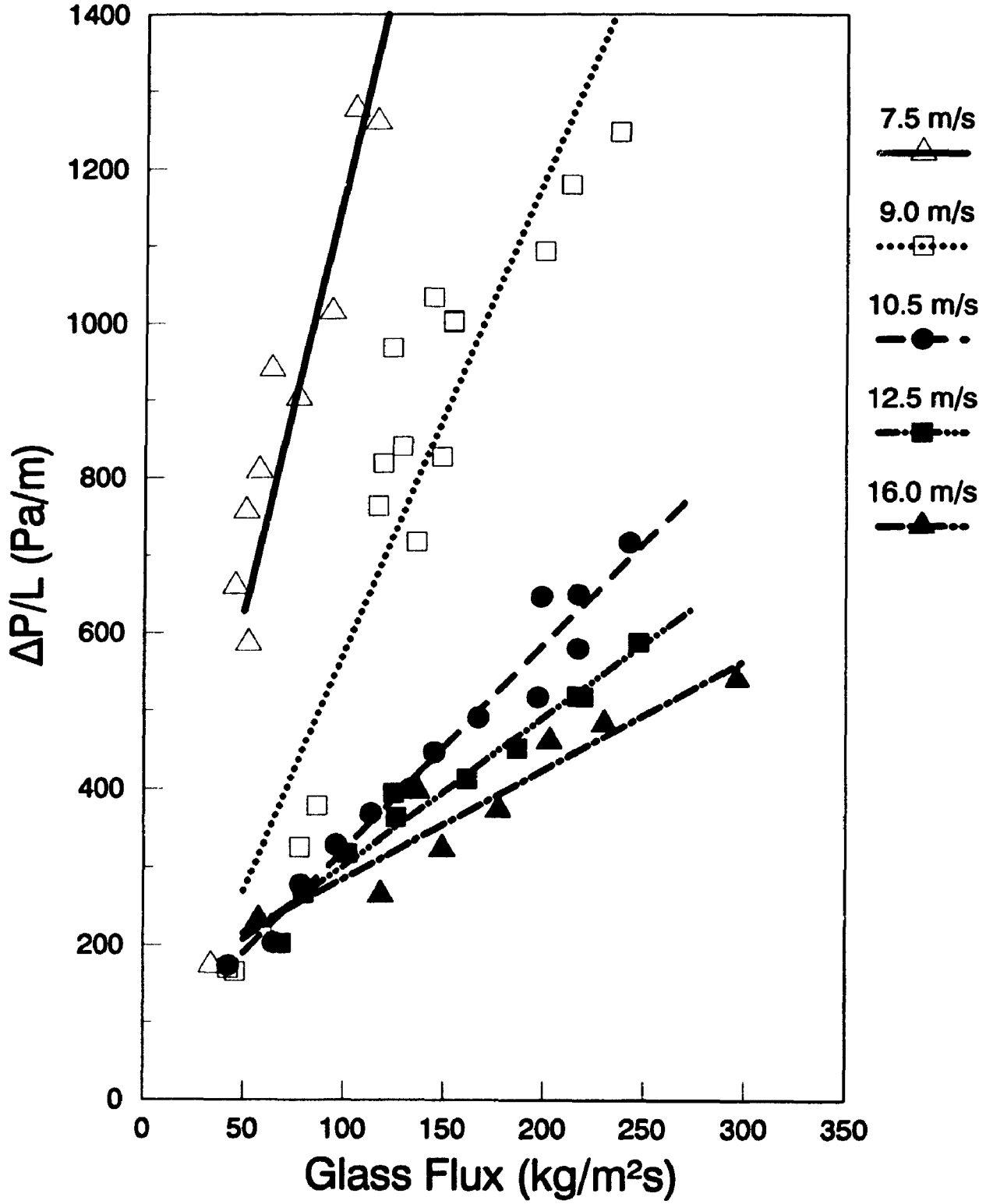

gas velocity of 10.5 m/s the pressure gradient increases sharply with gas velocity. In the linear region between 50 and 150 kg/m^{2}s, the slope increases from 2.63 s^{-1} at 10.5 m/s to 11.0 s^{-1} at 7.5 m/s.

Fig. 3.3.6 shows the pressure gradient versus glass flux data at a line inclination of 7°. The slope increases progressively from 2.43 s^{-1} to 4.26 s^{-1} as the gas velocity decreases from 12.5 m/s to 7.5 m/s. With limited data at 17° (Fig. 3.3.7), the slope decreases from 8.34 s^{-1} at a gas velocity of 9.5 m/s to 3.66 s^{-1} at a gas velocity of 12.0 m/s.

3.4 ZENZ PLOT

The definition of a "Zenz plot" is discussed in § 1.2 and is shown schematically in Fig. 1.2.1. It is a plot of the pressure gradient (in pneumatic transport) versus the gas velocity at constant solids flux. It has commonly been used in the literature to report dilute phase pneumatic transport data.

In most studies in the fast fluidization regime (non-slugging dense phase regime) the pressure gradient is studied as a function of solids flux, at constant gas velocity, similar to the representation of data in Figs. 3.3.1 to 3.3.7 (Yerushalmi et al., 1976). The Zenz format makes it easy to conceptualize the flow regime, however. Flows to the left of the Zenz

Fig. 3.3.6 : Pressure Gradient vs. Glass Flux
7° Inclined Line Orientation

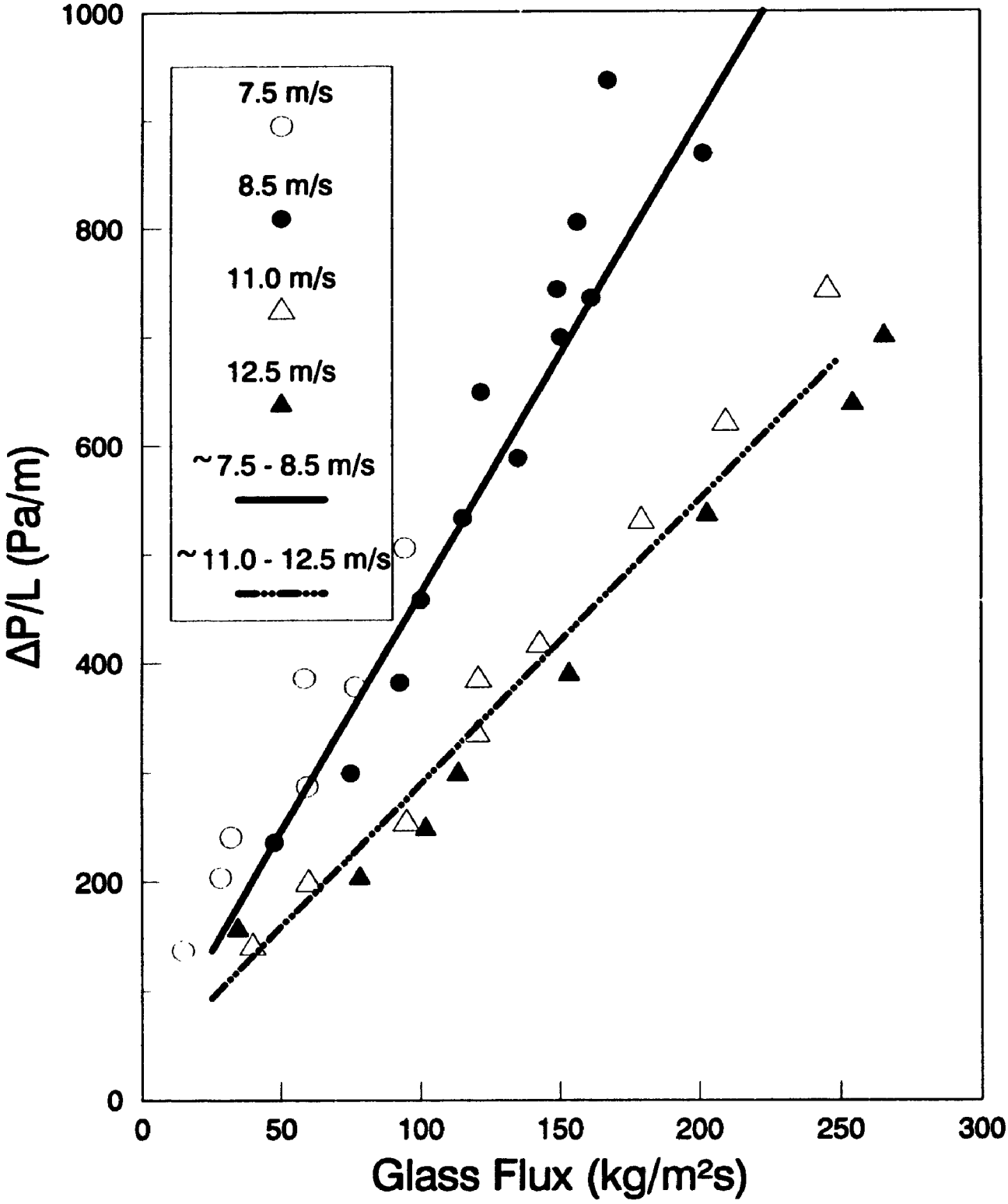

Fig. 3.3.7 : Pressure Gradient vs. Glass Flux
17° Inclined Line Orientation

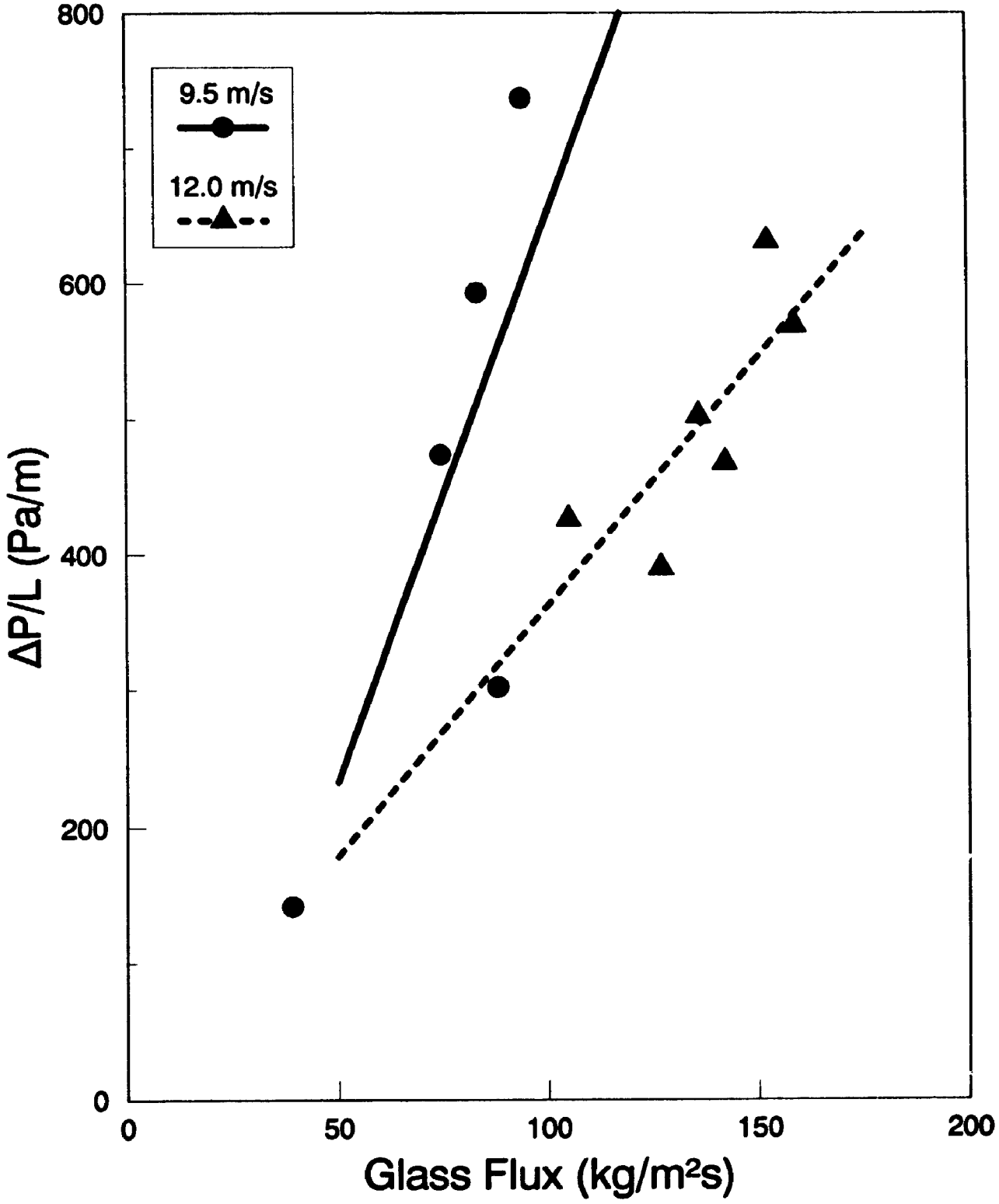

minimum (Fig. 1.2.1), where $[\partial(\partial P/\partial z)]/\partial U_g < 0$, are associated with dense and non-slugging dense phase transport.

3.4.1 DERIVATION OF ZENZ PLOT FROM RAW DATA

To show the experimental data in Zenz Plot format, least squares linear regression lines were obtained from the pressure gradient data at all line inclinations presented in § 3.3. The slope, intercept, and R^2 (goodness of fit) for all least squares regressions are summarised in Table 3.3. These regression fits were used to obtain pressure gradient data at constant solids flux for the range of gas velocities investigated. Since the R^2 statistic for all least squares curves was greater than 0.9, the reconstructed plots are considered as accurate representations of the original data. Solids flux values between 50 and 300 kg/m^{2}s were selected, in 50 kg/m^{2}s intervals, representing the scope of the experimental conditions. All reconstructed plots are shown on the same scales, so that comparisons between different line inclinations is facilitated.

3.4.2 ZENZ PLOT FOR SAND

The representation of the data in Zenz plot format is shown in Fig. 3.4.1 in nomograph style for the vertical line, using sand particles. The results show that the flow regime investigated is on the left side of the Zenz minimum (Fig. 1.2.1 Section CD), confirming that experiments were

Table 3.3: Linear Regression Summary

Pressure Gradient vs. Solids Flux Data

	THETA	VELOCITY (m/s)	R2	SLOPE (1/s)	INTERCEPT (Pa/m)	# POINTS
SAND	0	4.5	0.96	3.64	60.00	15
SAND	0	6.0	0.88	2.53	20.00	33
SAND	0	7.5	0.88	2.19	31.00	22
SAND	0	8.5	0.94	2.34	-8.00	21
SAND	0	9.5	0.95	2.17	6.00	23
SAND	0	8.5	0.82	2.35	13.00	100
SAND	4	5.5	0.95	4.66	-16.10	17
SAND	4	6.5	0.96	3.31	-26.80	17
SAND	4	8.5	0.97	2.28	-1.61	18
SAND	4	9.5	0.97	2.18	-11.80	11
SAND	4	11.5	0.97	1.96	-19.00	7
SAND	4	14.0	0.89	1.52	0.61	9
SAND	11	4.5	0.99	8.58	-26.00	7
SAND	11	6.0	0.90	4.69	-25.00	12
SAND	11	7.5	0.86	3.37	-22.00	15
SAND	18	5.0	0.74	8.52	198.00	6
SAND	18	6.5	0.96	7.36	-166.00	12
SAND	18	7.5	0.92	5.11	-56.00	15
SAND	18	8.5	0.89	2.44	99.00	14
SAND	18	9.5	0.92	1.81	105.00	9
SAND	18	11.5	0.97	1.74	46.00	6
GLASS	0	7.5	0.83	11.00	80.00	10
GLASS	0	9.0	0.88	6.12	-36.00	17
GLASS	0	10.5	0.97	2.63	58.00	13
GLASS	0	12.5	0.97	1.90	112.00	10
GLASS	0	16.0	0.89	1.39	145.00	8
GLASS	7	7.5	0.92	4.26	84.00	7
GLASS	7	8.5	0.92	4.94	-26.00	13
GLASS	7	11.0	0.99	2.92	7.00	9
GLASS	7	12.5	0.99	2.43	29.00	8
GLASS	17	9.5	0.60	8.34	-184.00	5
GLASS	17	12.0	0.61	3.66	-4.00	6

Fig. 3.4.1: Derived Zenz Plot for Sand Particles Vertical Line Orientation

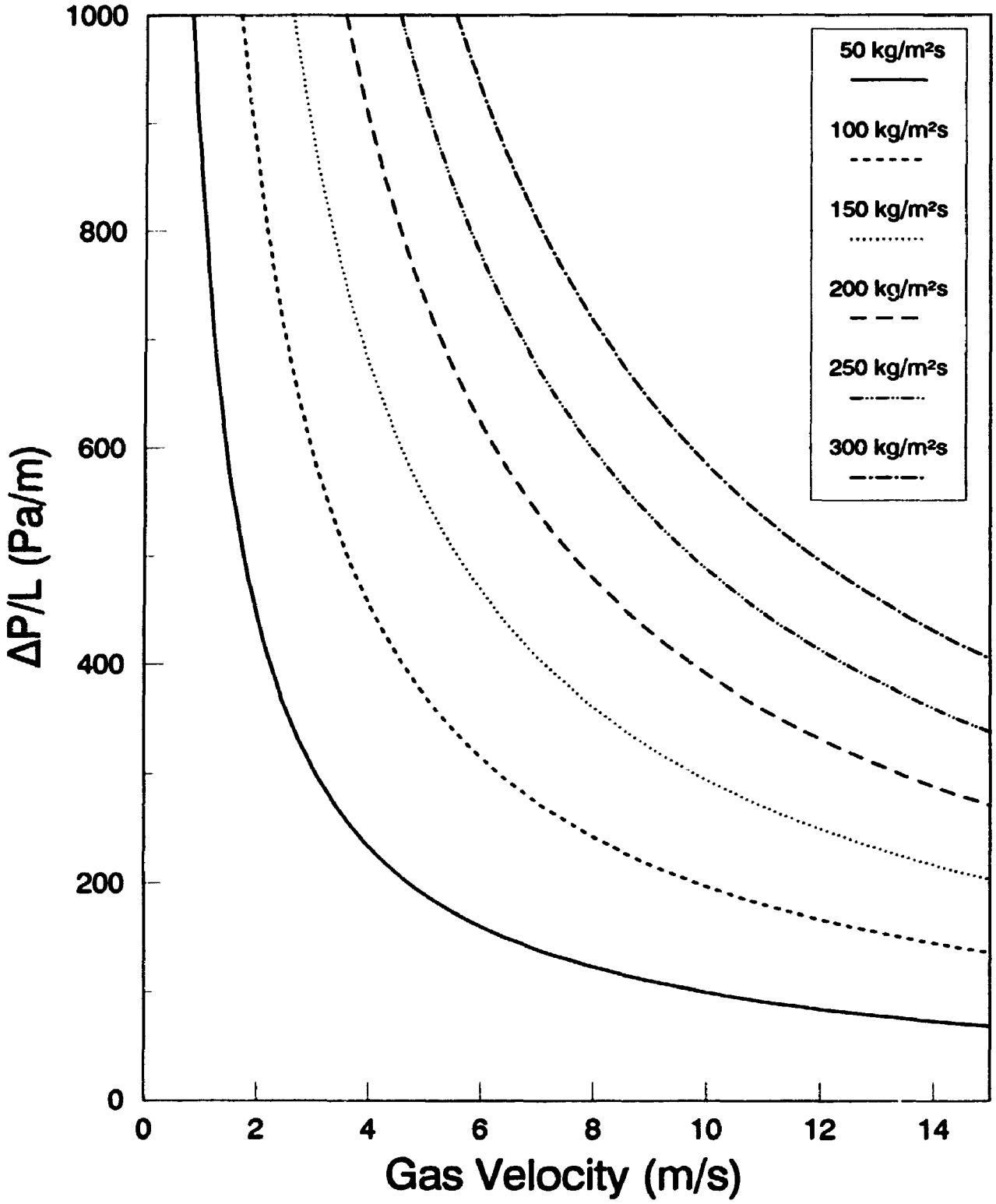

conducted in the non-slugging dense phase or fast fluidization flow regime. For gas velocities greater than 7 m/s the slopes of the curves are virtually nil. At 4° with sand particles (Fig. 3.4.2), $[\partial(\partial P/\partial z)]/\partial U_g$ is significantly higher than for the vertical line (Fig. 3.4.1). The rate of the slope increases further with line inclinations of 11° (Fig. 3.4.3) and 18° (Fig. 3.4.4). The effect of line inclination would seem to be to accelerate the approach to choking (point D, Fig. 1.2.1).

3.4.3 ZENZ PLOT FOR GLASS

Zenz plots were also constructed for experiments conducted with glass beads at all line inclinations. Pressure gradients increase sharply with gas velocities below 8 m/s in the vertical riser (Fig. 3.4.5), in a manner not observed for the sand particles at the same orientation (Fig. 3.4.1). A reconstructed Zenz plot of the data at 7° is shown in Fig. 3.4.6. Below a solids flux of 100 kg/m^{2}s the approach to choking is rapid, as the gas velocity is reduced below 8 m/s. Insufficient data at a line inclination of 17° prevented reconstruction of a Zenz plot at this line orientation.

One of the objectives of this research was to expand the small database of experimental data which currently exists for non-slugging dense phase riser transport. The data presented in Figs. 3.4.1 to 3.4.6 can be used for the estimation of the choking velocity under the hydrodynamic conditions that

Fig. 3.4.2: Derived Zenz Plot for Sand Particles
4° Inclined Line Orientation

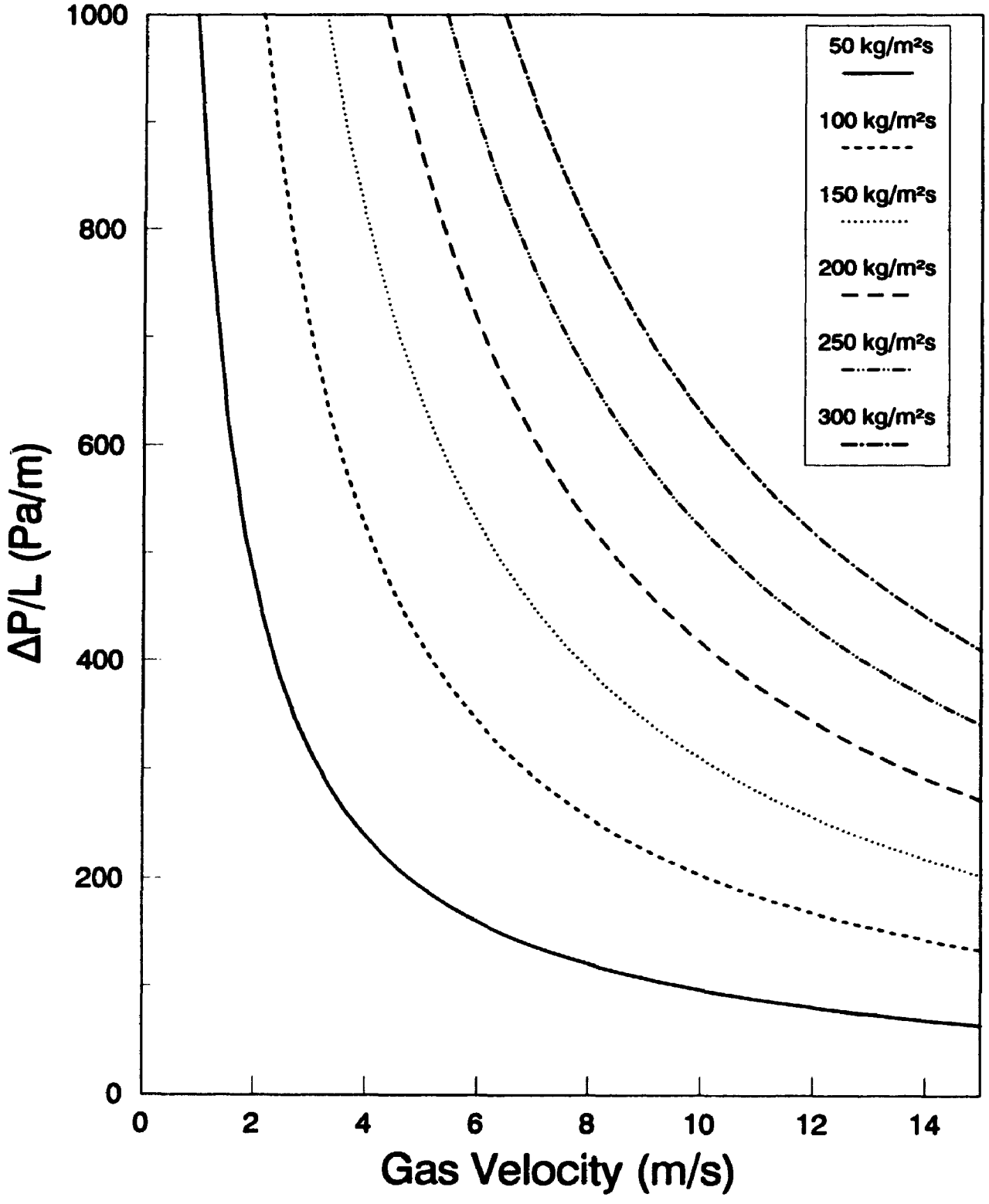

Fig. 3.4.3: Derived Zenz Plot for Sand Particles 11° Line Orientation

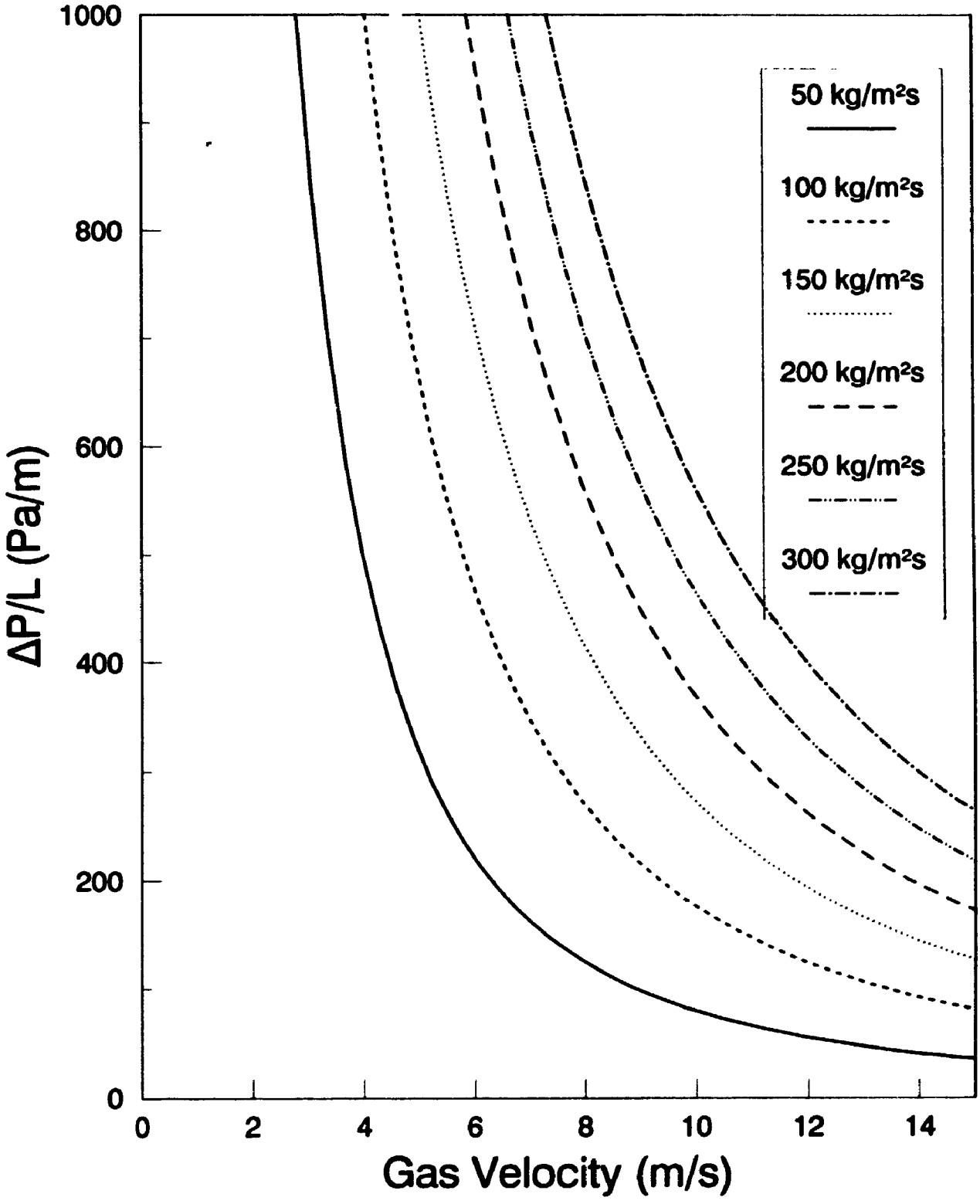

Fig. 3.4.4: Derived Zenz Plot for Sand Particles 18° Inclined Line Orientation

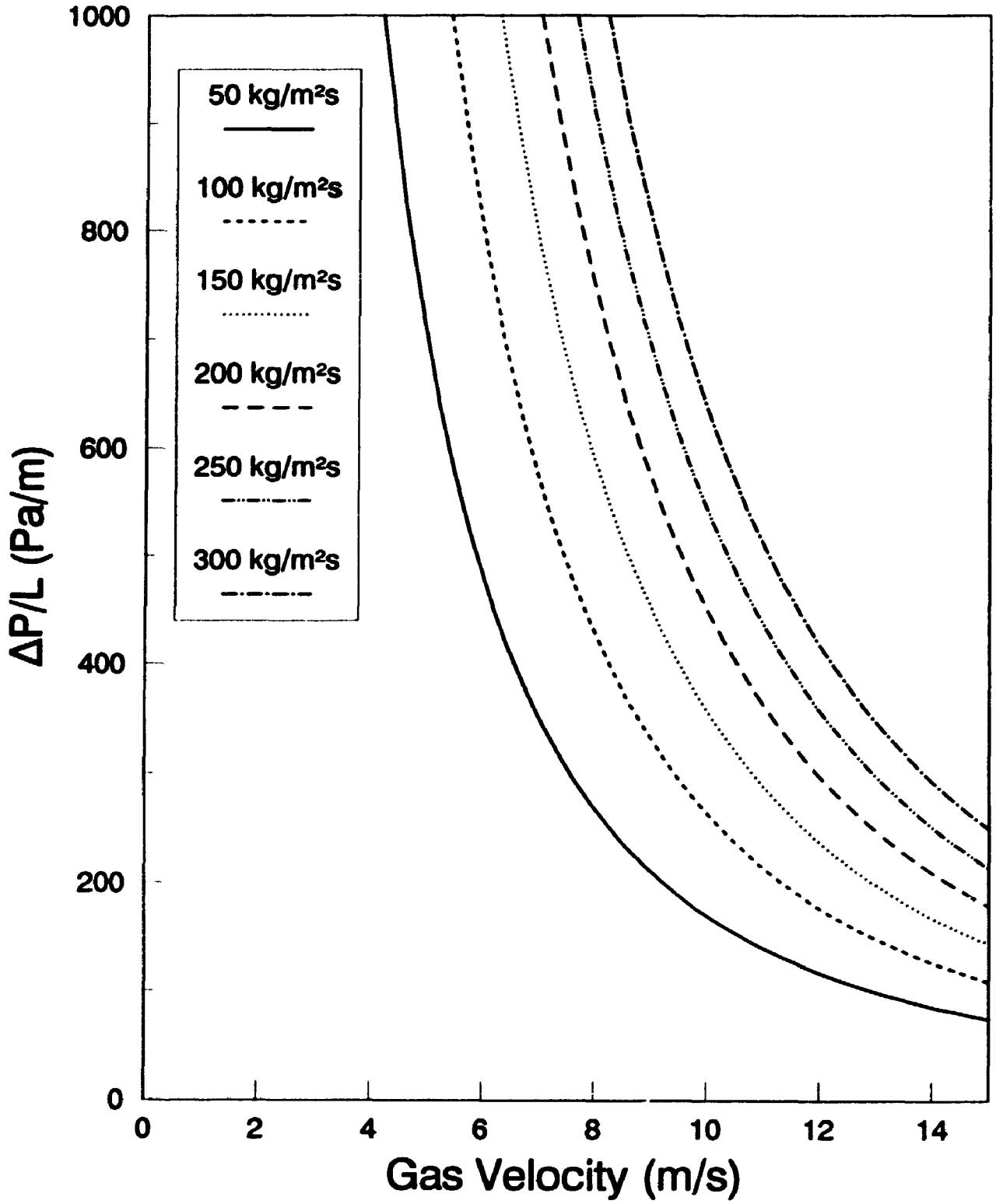

Fig. 3.4.5: Derived Zenz Plot for Glass Vertical Line Orientation

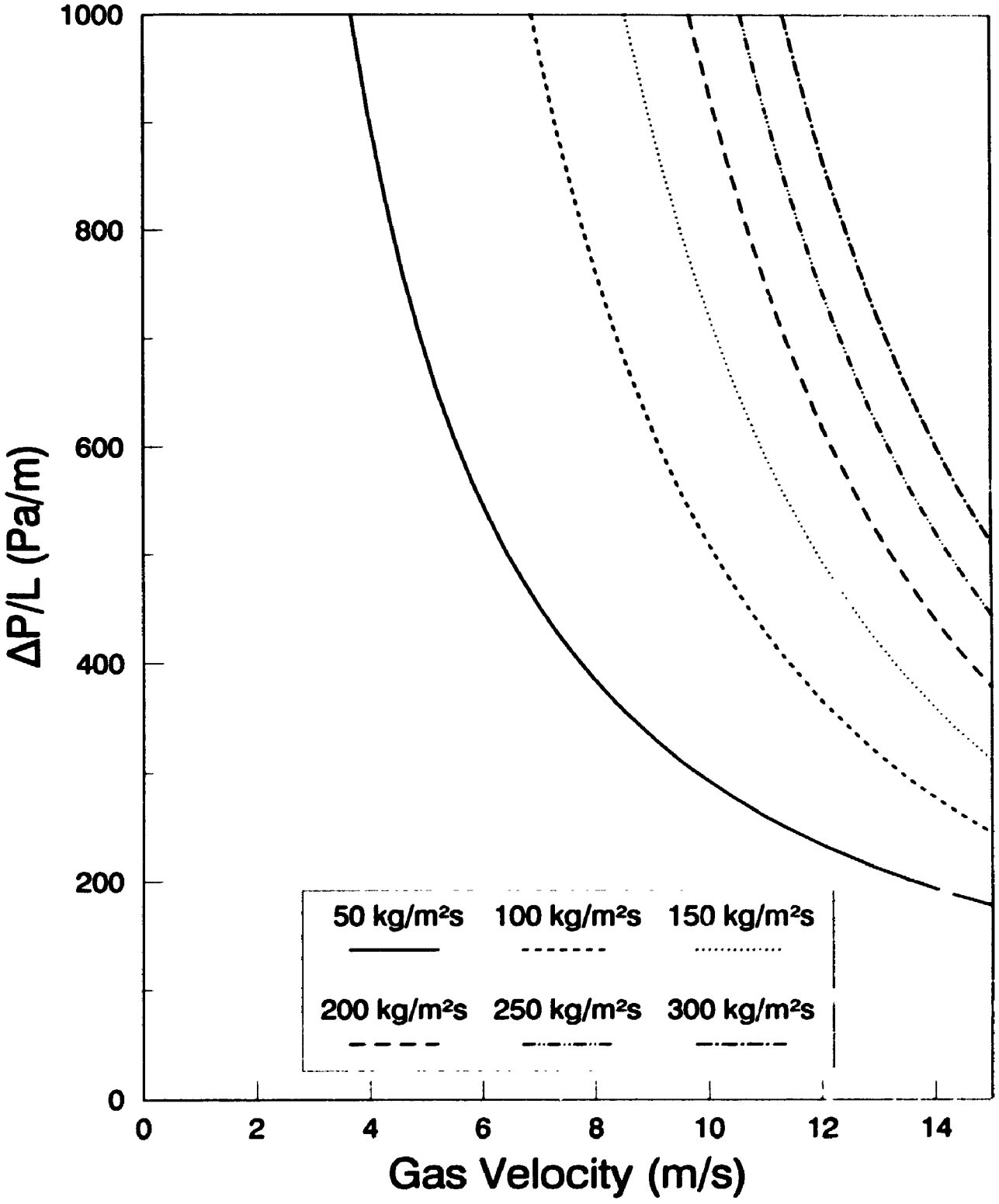

Fig. 3.4.6: Derived Zenz Plot for Glass
7° Line Orientation

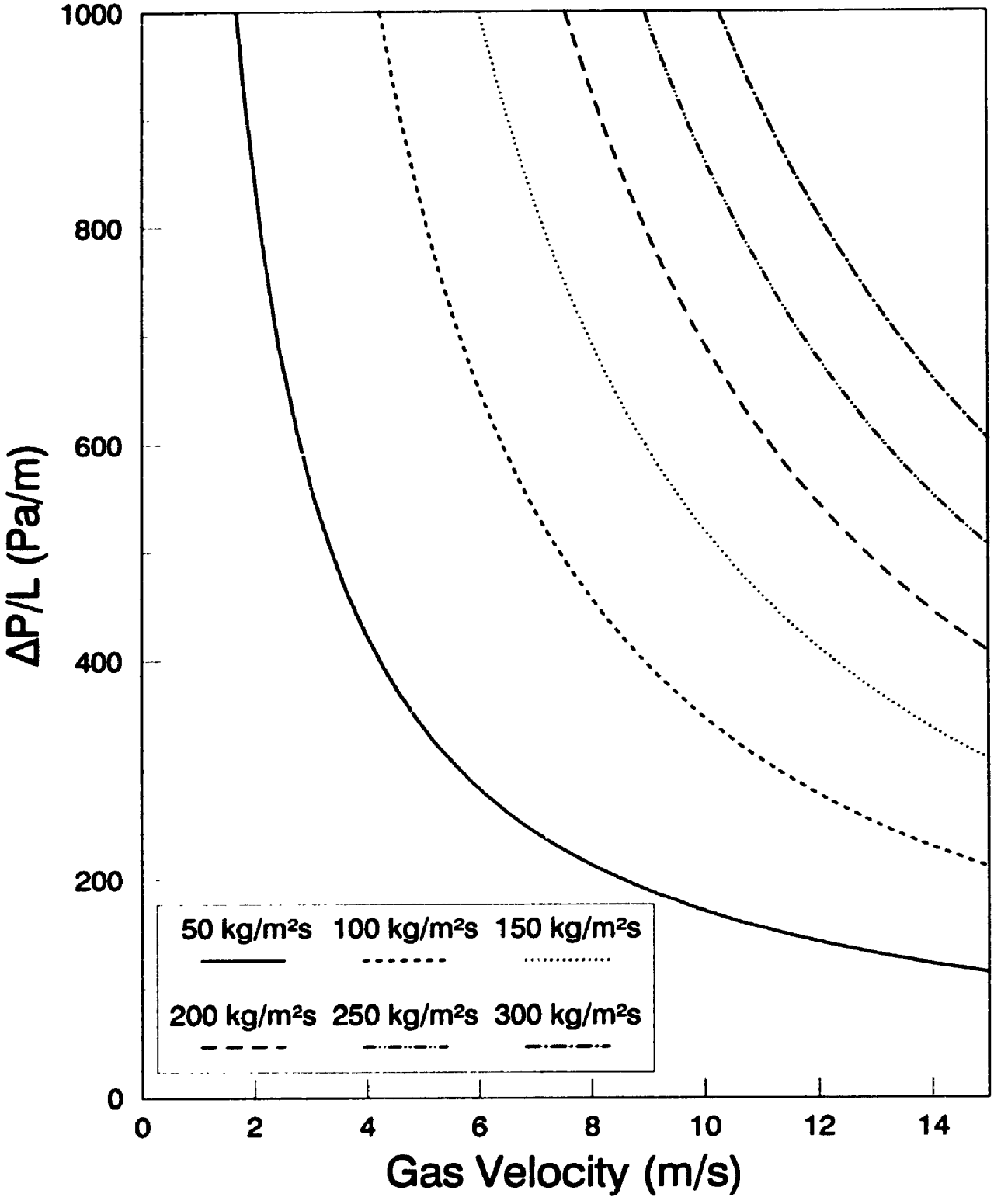

can be expected in riser flow.

Based on the results of Figs. 3.4.1 to 3.4.6 there are several constraints involved in the selection of a design gas velocity in oblique risers. It must be high enough to ensure that a large fraction of pressure energy is not lost in reaccelerating refluxing particles at the wall. (Efficiency of riser transport, under conditions of increased refluxing tendencies with line inclination, is discussed in § 4.3). The gas velocity should also be the minimum practically achievable to prevent unnecessary power consumption and attrition problems. The attrition in commercial pipes is proportional to the cube or fourth power of the conveying velocity, so that a reduction of gas velocity by 20% decreases wear and attrition by 50% (Wirth, 1986).

3.5 EFFECT OF SOLIDS FLUX ON SOLIDS HOLDUP

The solids holdup was measured between two pinch valves (Fig. 2.5) which closed within 3 to 10 ms of each other. The maximum absolute error of the measurement was 3%. The solids holdup was collected during an experiment for all experimental conditions. Since the data in this thesis was obtained to the left of the Zenz minimum (Figs. 3.4.1 - 3.4.6), the most important contribution to the total pressure gradient (equation 9, § 1.6) is that due to solids holdup in the line. For this reason plots were constructed to specifically illustrate the effect of operating parameters on the solids

holdup.

3.5.1 SAND HOLDUP

Fig. 3.5.1 shows the results for the vertical riser transport of sand particles at gas velocities between 4.5 and 9.5 m/s. In the dilute phase there would be a change of slope detected in the solids flux regime between 0 - 50 kg/m^{2}s (Ginestet et al , 1993). Based on the observations of Ginestet et al. there is a slope increase after this initial dilute phase region, and it is the intermediate region which represents the scope of the present experimental work.

In accordance with the results obtained for the pressure gradient (Fig. 3.3.1) for the same conditions, the solids holdup increases linearly with solids flux, but decreases with gas velocity. There is also more resolution of solids holdup data at higher gas velocities (Fig. 3.5.1), in comparison with the pressure gradient data for the same conditions (Fig. 3.3.1). The slope of the holdup versus solids flux curve decreases from 1.28×10^{-4} m^{2}s/kg to 0.9×10^{-4} m^{2}s/kg, as the gas velocity increases from 4.5 to 6.5 m/s. From visual observations the increase of solids holdup at lower gas velocities was also apparent. Extensive solids refluxing at 4.5 m/s led to large wall deposits of solids. The line was approaching choking conditions for a solids flux exceeding about 150 kg/m^{2}s. At 210 kg/m^{2}s the volume fraction is 3% at a

Fig. 3.5.1 : Solids Holdup vs. Sand Flux Vertical Line Orientation

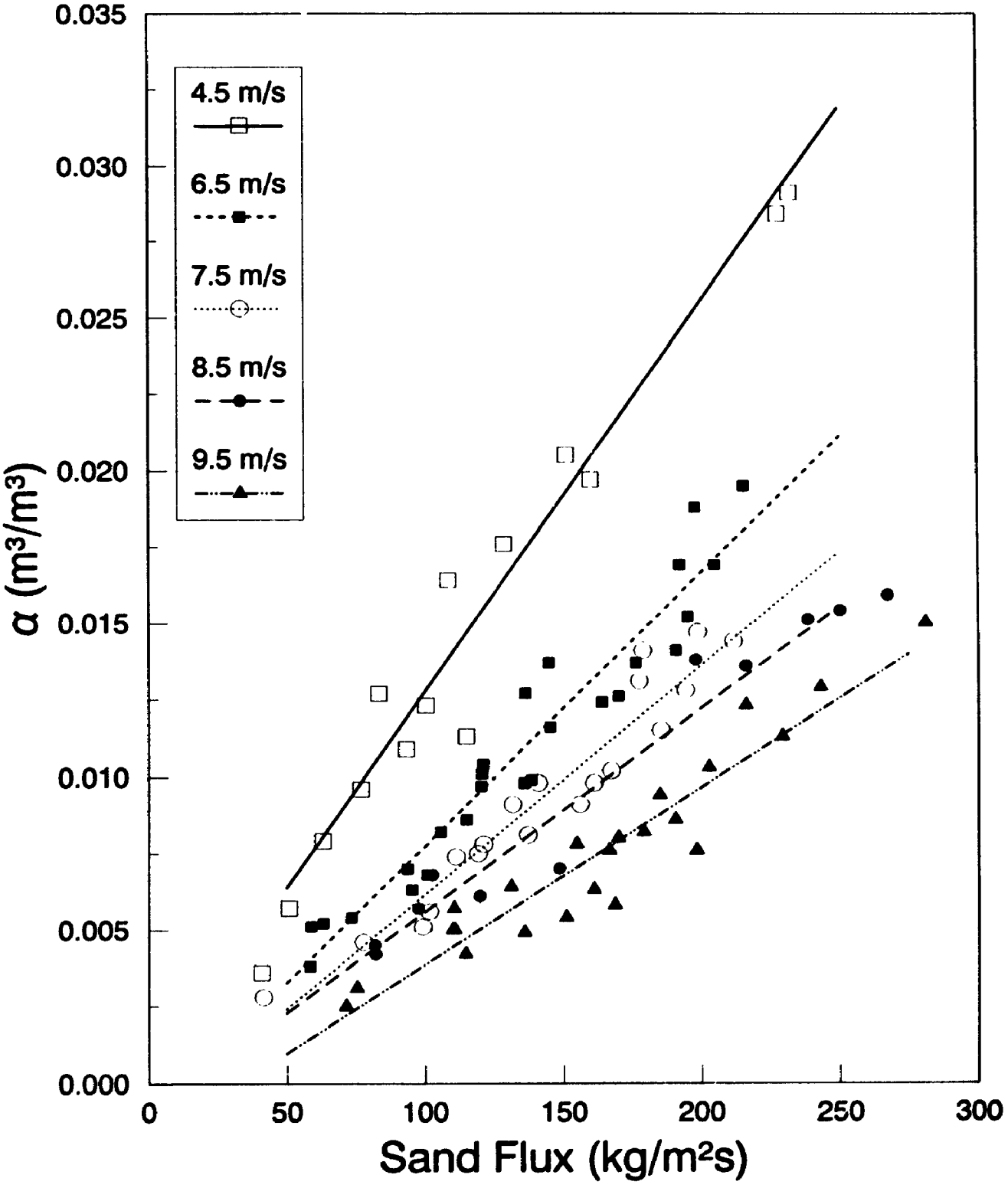

gas velocity of 4.5 m/s (Fig. 3.5.1), and the line was choked based upon visual observations.

The effect of sand flux on solids holdup at a line inclination of 4° is examined in Fig. 3.5.2. At a gas velocity of 5.5 m/s a choking solids holdup of 3% is observed at 180 kg/m^{2}s. This observation would suggest that the solids flux for which choking occurs decreases with line inclination. The slope increases from 0.6x10^{-4} m^{2}s/kg to 1.6x10^{-4} m^{2}s/kg as the gas velocity decreases from 9.5 to 5.5 m/s.

The effect of gas velocity on solids holdup is evident at a line inclination of 11° (Fig. 3.5.3). The slope increases from 0.6x10^{-4} m^{2}s/kg to 4.7x10^{-4} m^{2}s/kg, as the gas velocity decreases from 7.5 to 4.5 m/s.

At 18° (Fig. 3.5.4) the average slope of the curve increases from 0.6x10^{-4} m^{2}s/kg at 8.5 m/s, to 10.0x10^{-4} m^{2}s/kg at 5.0 m/s. At a gas velocity of 5.0 m/s the line is choked at a solids flux less than 75 kg/m^{2}s. The values of the slope, intercept, and R^2 statistic are shown in Table 3.5 for all line inclinations investigated.

The results given in Figs. 3.5.1 to 3.5.4 for sand particles indicate that the choking solids flux in the riser is sensitive to line inclination. Visual

Fig. 3.5.2 : Solids Holdup vs. Sand Flux
4° Inclined Line Orientation

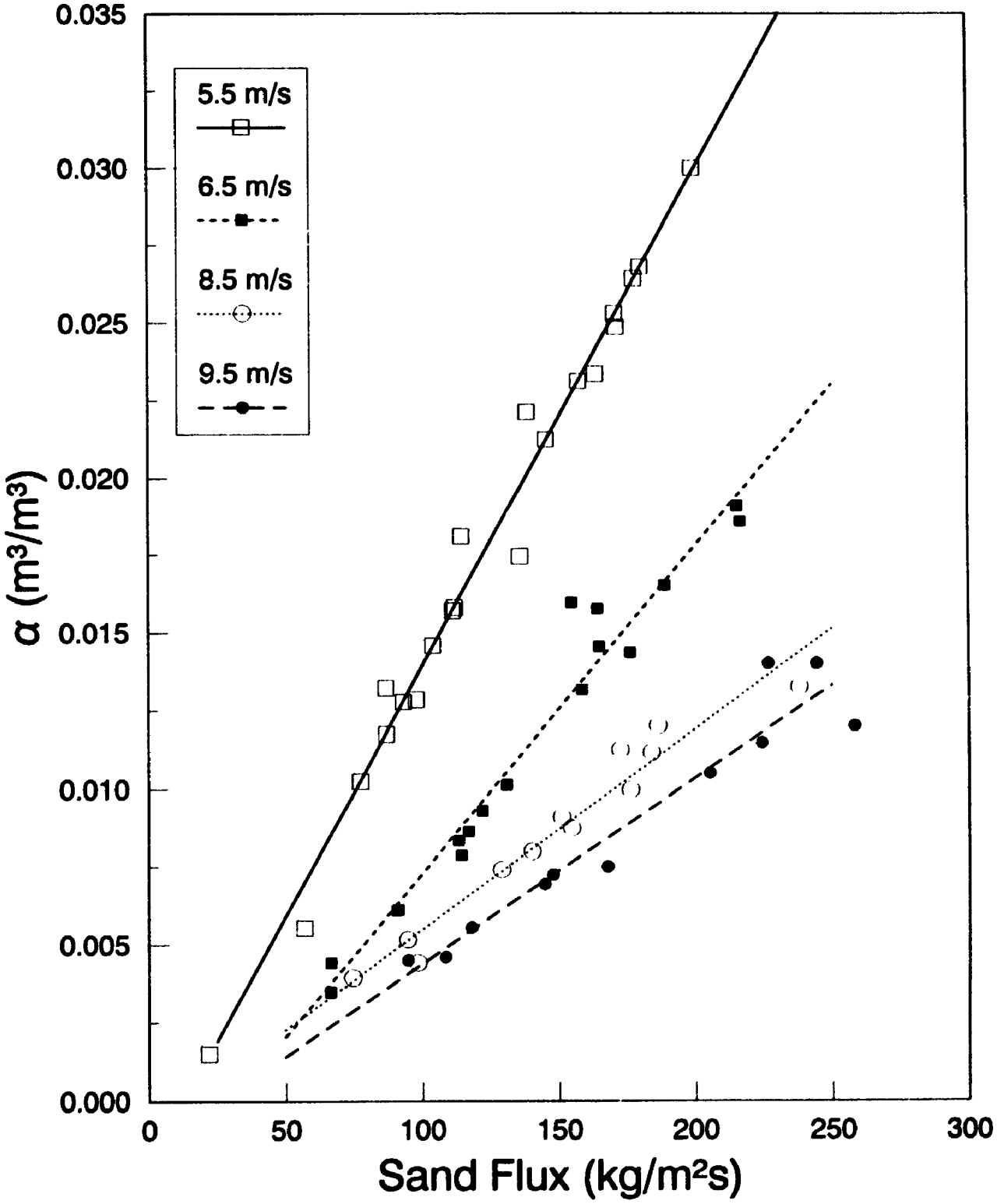

Fig. 3.5.3 : Solids Holdup vs. Sand Flux
11 Degree Inclined Line Orientation

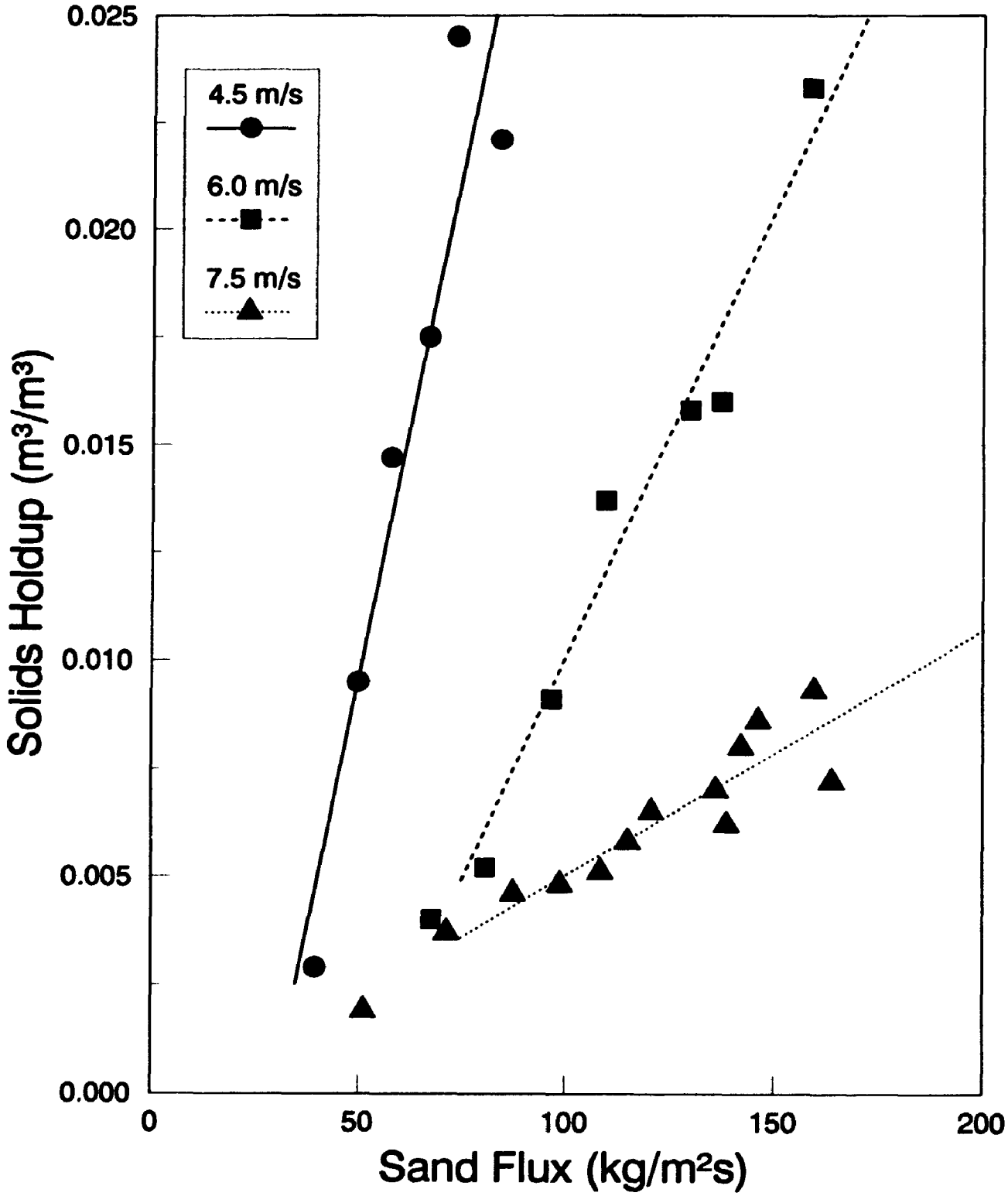

Fig. 3.5.4 : Solids Holdup vs. Sand Flux 18° Inclined Line Orientation

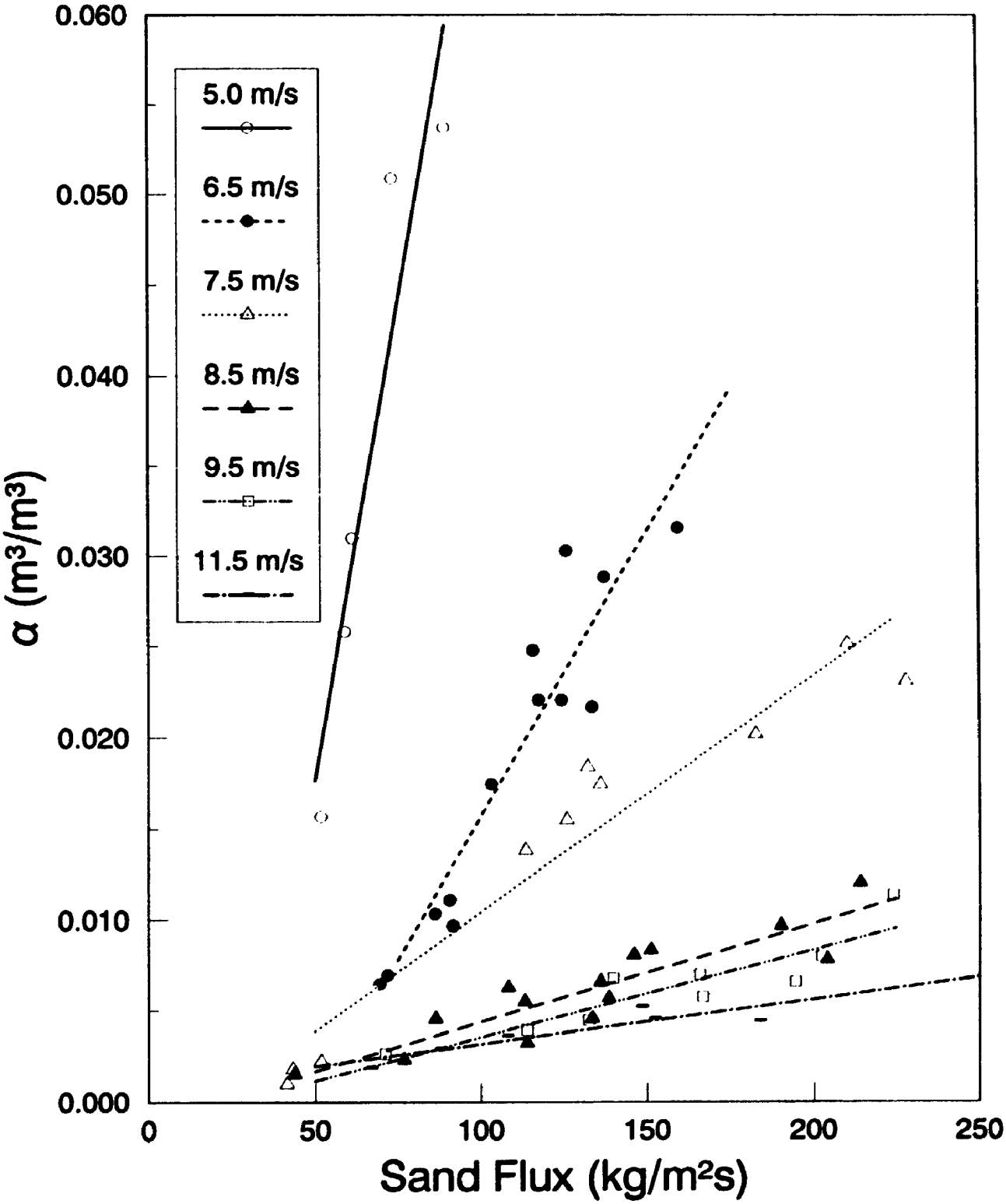

Table 3.5: Linear Regression Summary

Solids Holdup vs. Solids Flux Data

	THETA	VELOCITY (m/s)	R2	SLOPE (m2s/kg)	INTERCEPT (Pa/m)	# POINTS
SAND	0	4.5	0.95	1.28E-04	-3.00E-06	15
SAND	0	6.5	0.94	8.91E-05	-1.20E-03	26
SAND	0	7.5	0.93	7.45E-05	-1.30E-03	19
SAND	0	8.5	0.96	6.10E-05	-1.00E-03	11
SAND	0	9.5	0.91	5.80E-05	-1.90E-03	23
SAND	4	5.5	0.98	1.60E-04	-2.10E-03	21
SAND	4	6.5	0.96	1.00E-03	-3.20E-03	17
SAND	4	8.5	0.95	6.40E-04	-9.20E-04	12
SAND	4	9.5	0.92	5.90E-05	-1.50E-03	11
SAND	11	4.5	0.90	4.71E-04	-1.40E-02	6
SAND	11	6.0	0.97	2.06E-04	-1.10E-02	7
SAND	11	7.5	0.89	5.67E-05	-7.00E-04	13
SAND	18	5.0	0.89	1.04E-03	-3.45E-02	5
SAND	18	6.5	0.89	3.14E-04	-1.58E-02	13
SAND	18	7.5	0.93	1.30E-04	-2.60E-03	10
SAND	18	8.5	0.81	5.70E-05	-1.00E-03	14
SAND	18	9.5	0.81	4.80E-05	-1.30E-03	9
SAND	18	11.5	0.78	2.40E-05	7.40E-04	6
GLASS	0	6.5	0.18	5.30E-04	1.78E-02	6
GLASS	0	7.5	0.85	5.60E-04	1.40E-03	10
GLASS	0	9.0	0.84	2.00E-04	-5.50E-03	20
GLASS	0	10.5	0.93	1.10E-04	2.10E-03	13
GLASS	0	12.5	0.98	1.10E-04	-1.10E-03	9
GLASS	0	16.0	0.94	6.00E-05	-1.50E-03	7
GLASS	7	7.5	0.95	1.86E-04	2.46E-03	7
GLASS	7	8.5	0.92	2.09E-04	-3.20E-03	13
GLASS	7	11.0	0.96	1.30E-04	-2.50E-03	9
GLASS	7	12.5	0.97	9.90E-05	-1.80E-03	8
GLASS	17	9.5	0.86	4.10E-04	-1.13E-02	5
GLASS	17	12.0	0.21	1.12E-04	1.60E-03	6

observations indicated that the flow would not necessarily collapse into a slugging dense flow at a solids holdup of 3%. With increasing line inclination the solids holdup that could be held in the line increased, because not all of the particles were supported by the gas (Ocone et al., 1993). Massive quantities of solids were observed to be deposited at the pipe walls, particularly at higher line inclinations near the choking velocity. The solids refluxed on several occasions at different points through the test section on their flight through the riser.

3.5.2 GLASS HOLDUP

The effect of glass flux on the solids holdup for vertical riser transport is shown in Fig. 3.5.5, for gas velocities between 6.5 and 16.0 m/s. The solids holdup increases linearly with the solids flux, and increases rapidly for a gas velocity below 10.5 m/s. The slope increases from 0.6×10^{-4} m^2s/kg at 16 m/s to 5.6×10^{-4} m^2s/kg at 7.5 m/s. Solids holdups exceeding 5% were obtained without the onset of incipient slugging flow. However, extreme refluxing of particles at the walls was observed for the beads, and the flow patterns were often erratic and unpredictable. Pressure drop fluctuations were very high.

Fig. 3.5.6 shows the linear dependence between solids holdup and glass flux at a line inclination of 7°. The slope increases progressively from 1.0×10^{-4}

Fig. 3.5.5 : Solids Holdup vs. Glass Flux
Vertical Line Orientation

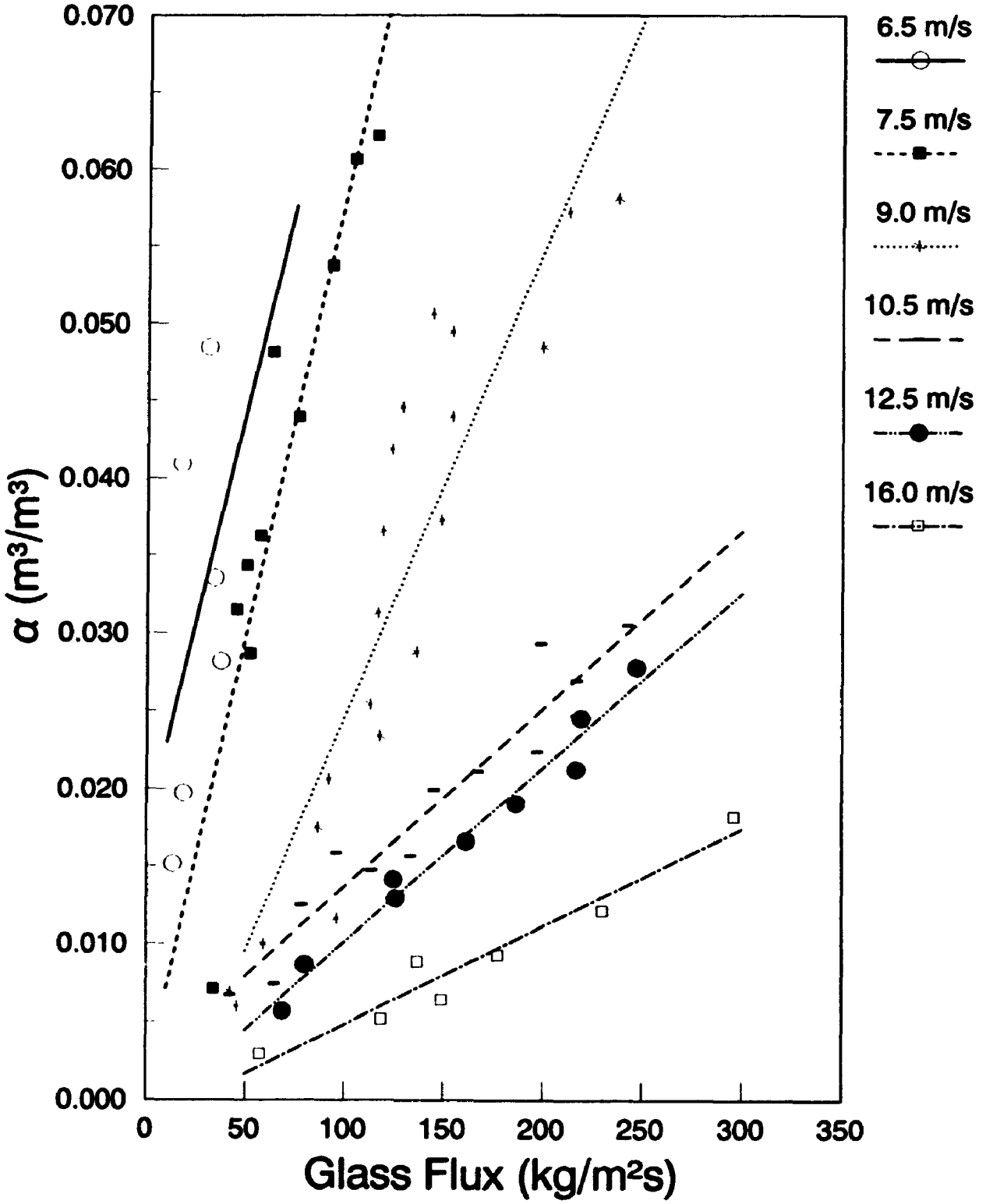

Fig. 3.5.6 : Solids Holdup vs. Glass Flux
7° Inclined Line Orientation

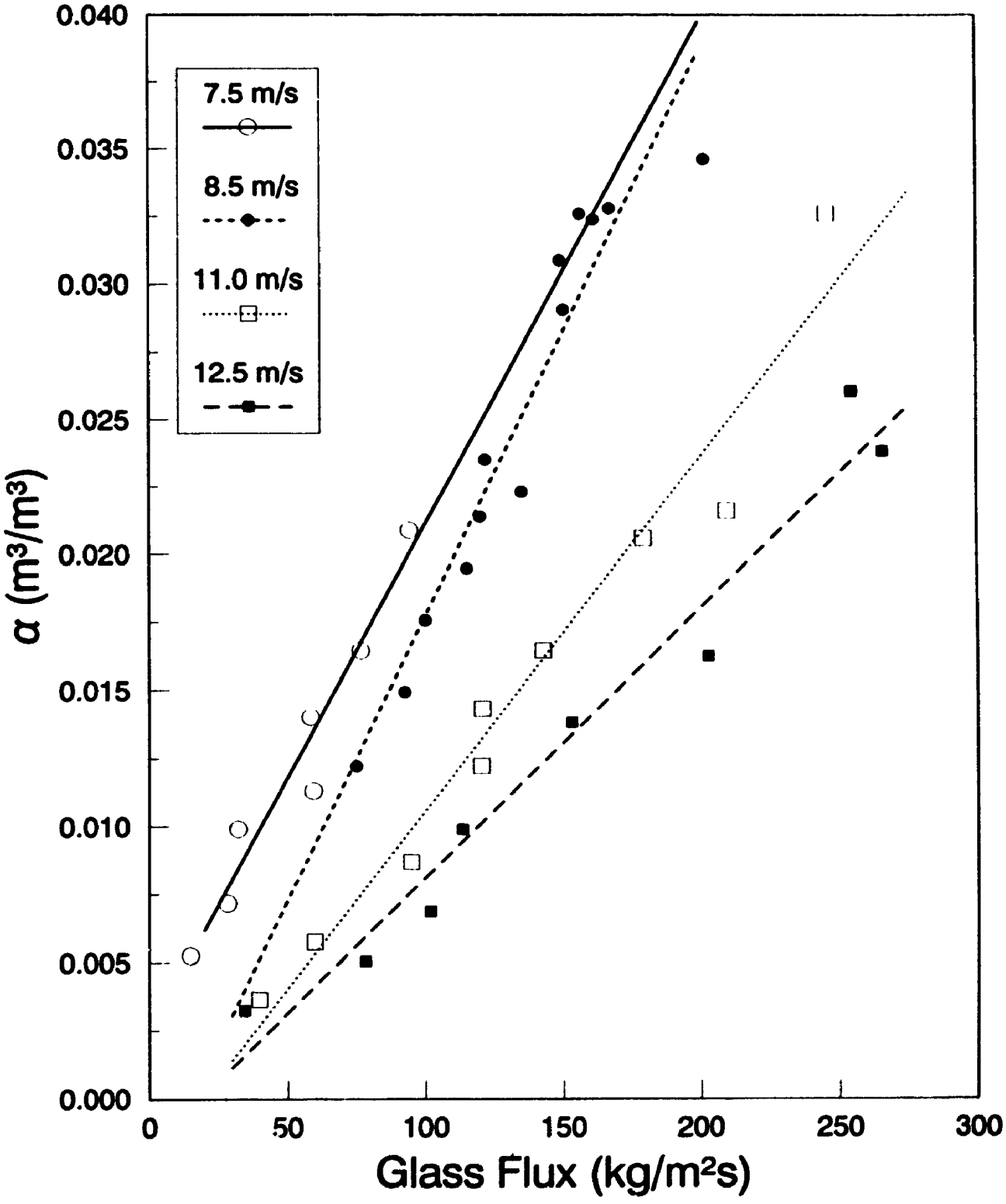

m^2s/kg to $1.9x10^{-4}$ m^2s/kg, as the gas velocity decreases from 12.5 to 7.5 m/s. Fig. 3.5.7 shows the effect of solids flux on the holdup at a line inclination of 17°. A choking holdup of 3% is observed at a gas velocity of 9.5 m/s and a solids flux of 80 kg/m^2s.

The solids flux range studied at 17° for glass beads was limited to below 150 kg/m^2s. At higher values it was not possible to perform experiments for line inclinations exceeding 7° and gas velocities below 10 m/s. Although there was some transport of particles, the fluctuations were so large that reliable replicate data could not be obtained.

3.6 EFFECT OF SOLIDS MASS LOADING ON PRESSURE GRADIENT

The solids mass loading, m^*, is the ratio of the solids to gas mass flowrates. It has traditionally been used in the literature to characterise pneumatic transport flows.

The loading in this research was varied between 5 to 30. Loads less than 10 are considered to be in the dilute phase, while those greater than 10 but less than 80 are in the non-slugging dense phase (Konrad, 1986). This is clearly an approximate definition, since it is known that the entire range of experimental work covered here is in the non-slugging dense phase, which includes those experiments at a solids loading of 5 to 10.

Fig. 3.5.7 : Solids Holdup vs. Glass Flux
17° Inclined Line Orientation

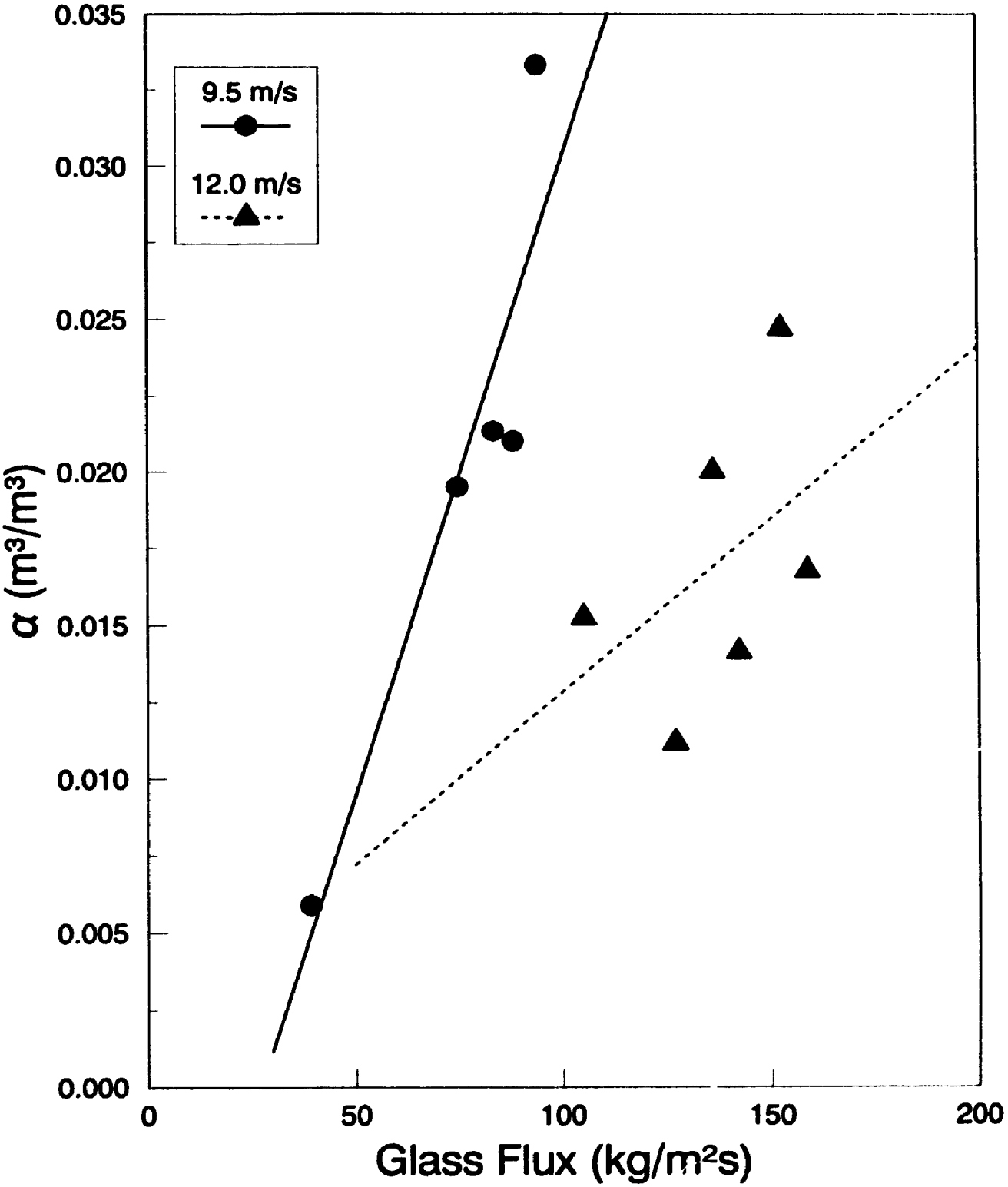

3.6.1 EFFECT OF SAND LOADING ON PRESSURE GRADIENT

For the vertical line (Fig. 3.6.1) the pressure gradient increases linearly with m^* between 5 and 40. The same is true at 4° (Fig. 3.6.2). The slopes of the two data sets are 22 and 24 Pa/m respectively, and there is no significant effect of gas velocity for either case. Some deviation from the least squares regression line is expected because the experimental conditions at the same solids loading can be quite different, particularly near the choking gas velocity.

At 11° (Fig. 3.6.3), the pressure gradient increases linearly with m^* (slope = 32 Pa/m) for gas velocities greater than 6 m/s. At a gas velocity of 4.5 m/s, however, the pressure gradient is higher than the least squares linear regression curve (for gas velocities above 6 m/s). This is thought to be due to refluxing of solids near the choking velocity, resulting in larger pressure gradients.

The effect of gas velocity on the plot of $\Delta P/L$ versus m^* is stronger at a line inclination of 18° (Fig. 3.6.4). The sensitivity of the flow to gas velocity, which was visually apparent in § 3.1, is graphically observed in Fig. 3.6.4. Distinct least squares lines could be generated for each gas velocity in Fig. 3.6.4. At 18° the hydrodynamic flow conditions were observed to vary significantly as the gas velocity was reduced to choking conditions. The

Fig. 3.6.1 : Pressure Gradient vs. Sand Loading Vertical Line Orientation

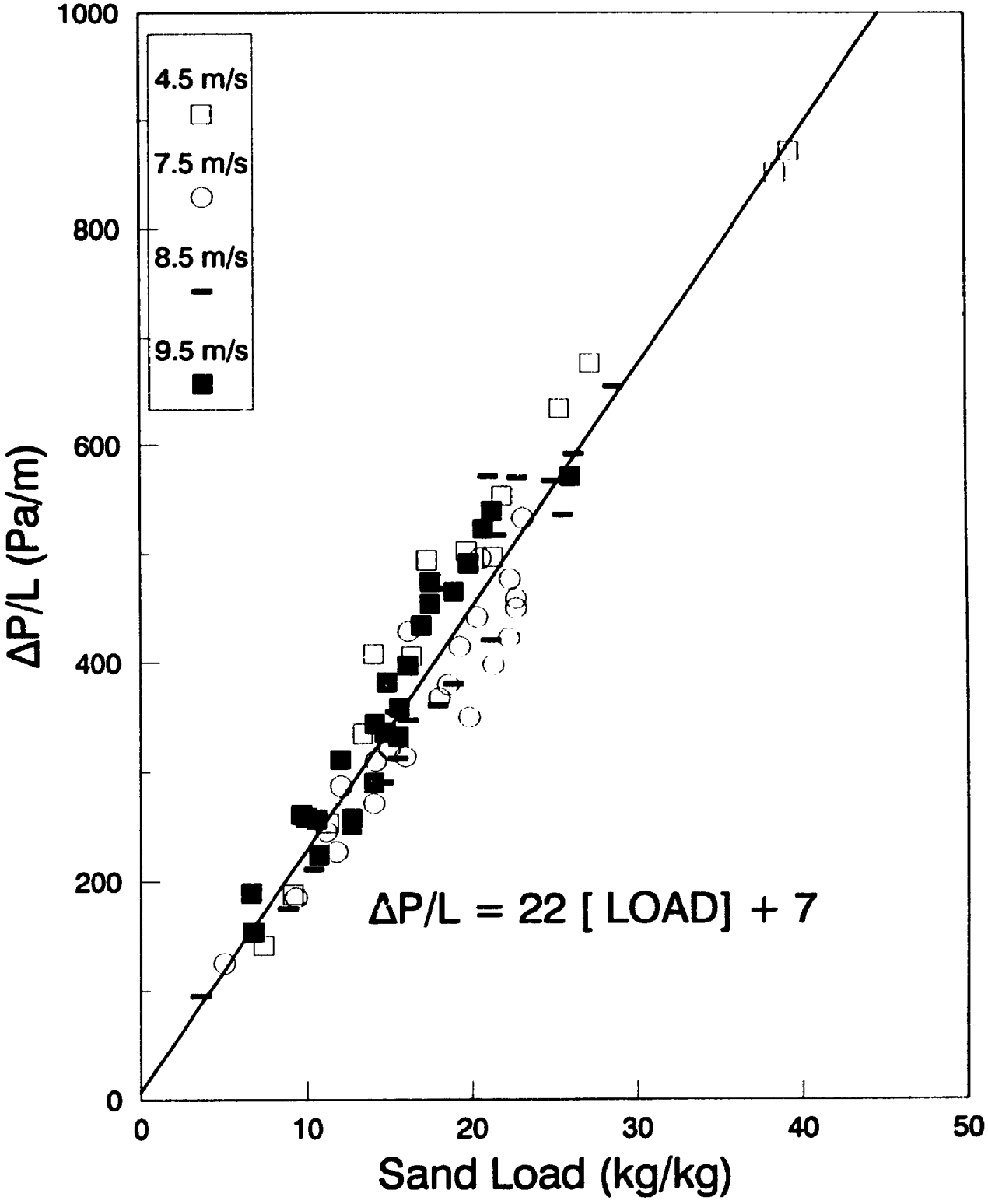

Fig. 3.6.2 : Pressure Gradient vs. Sand Loading
4° Inclined Line Orientation

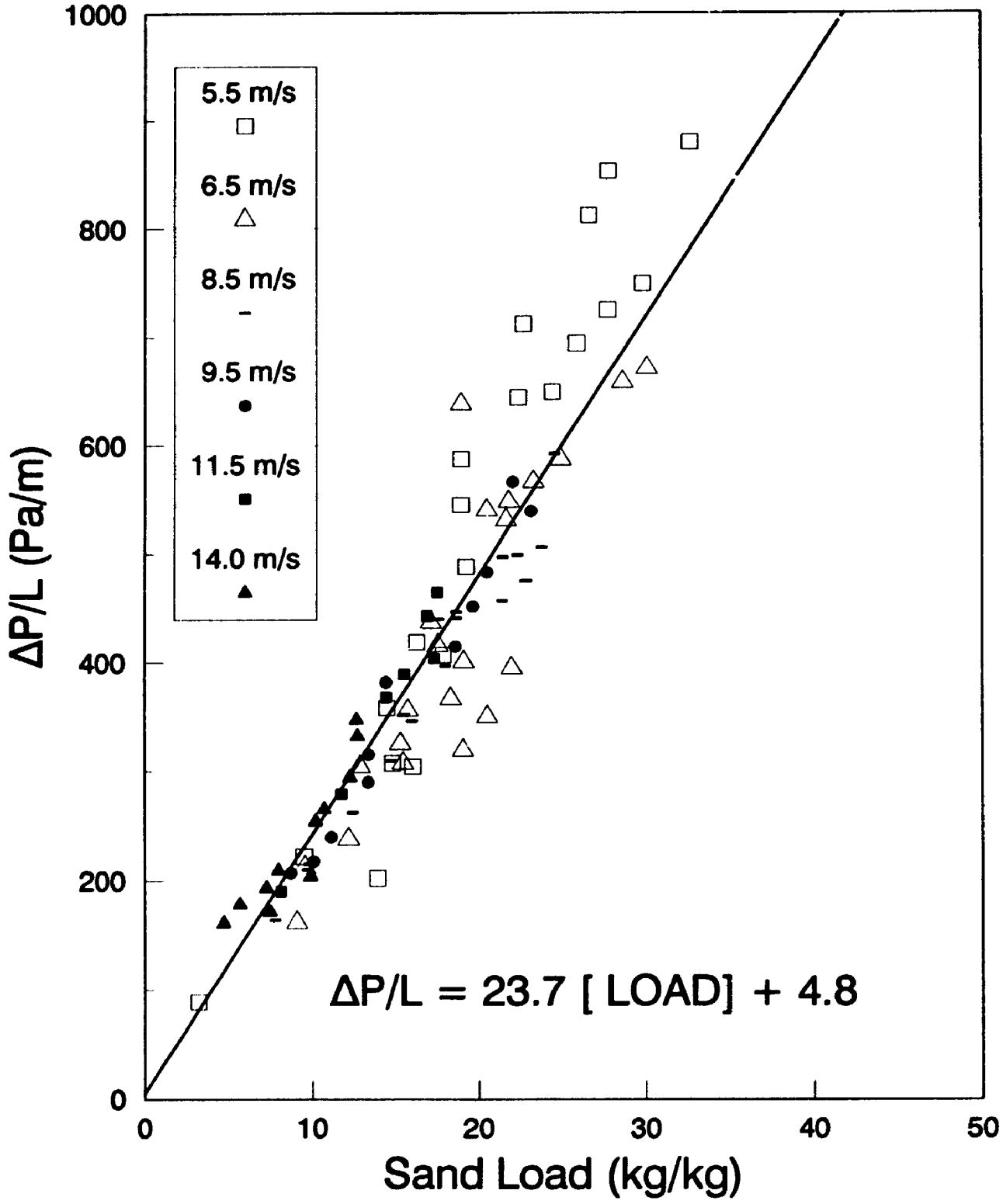

Fig. 3.6.3 : Pressure Gradient vs. Sand Loading
11° Inclined Line Orientation

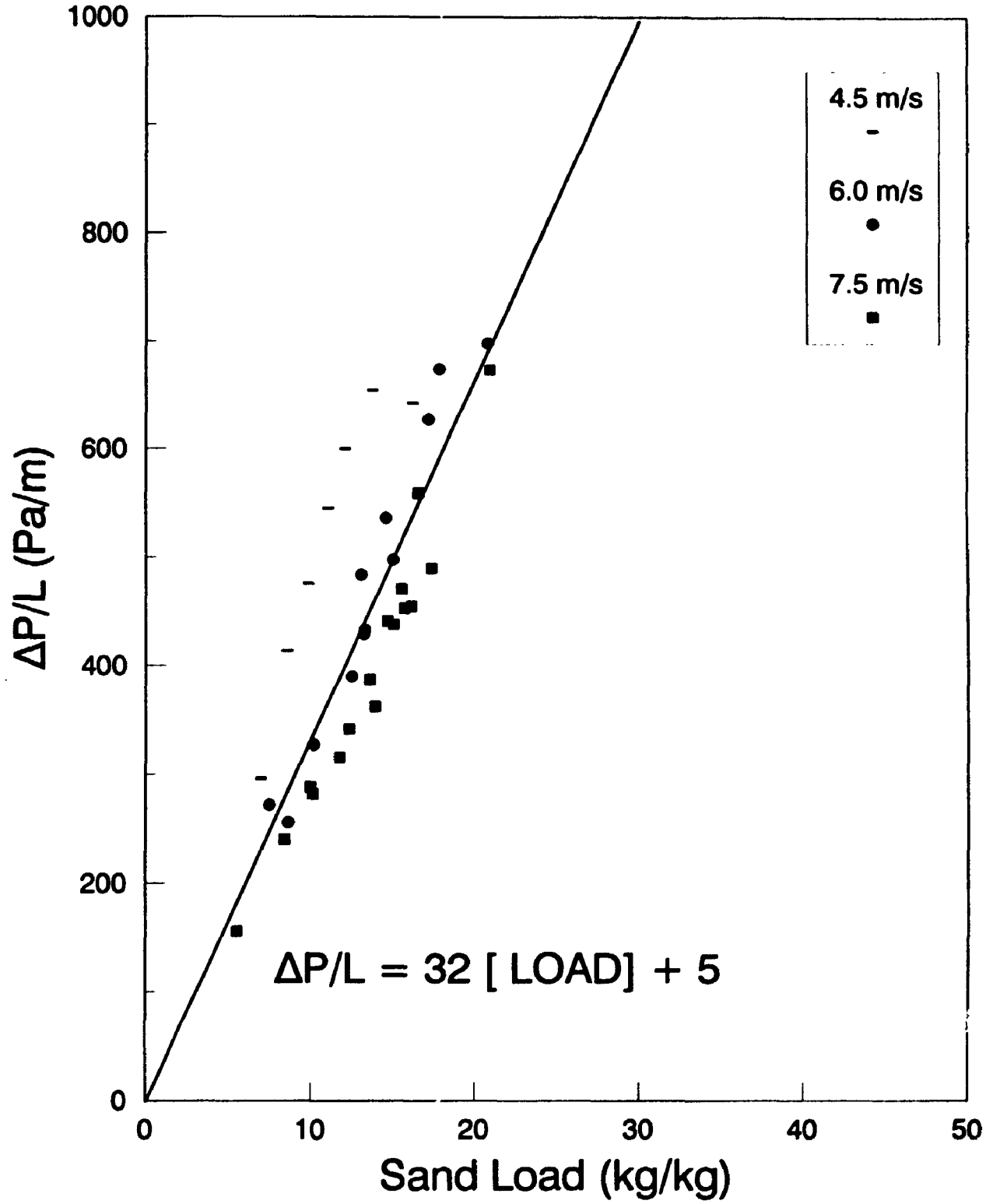

Fig. 3.6.4 : Pressure Gradient vs. Sand Loading
18° Inclined Line Orientation

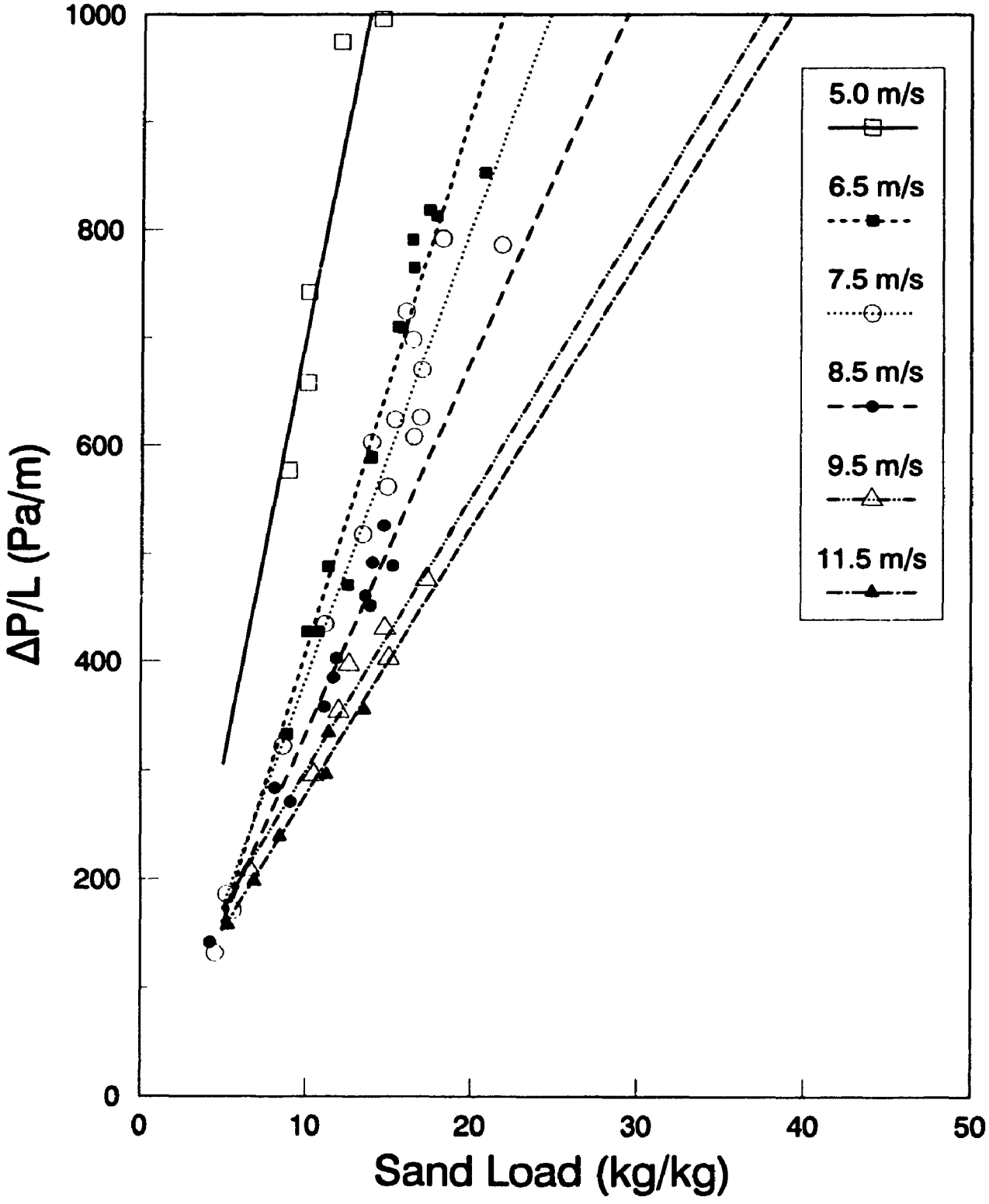

lines converge towards the origin (Fig. 3.6.4) at a solids loading of less than 5 where the flow is dilute.

3.6.2 EFFECT OF GLASS LOADING ON PRESSURE GRADIENT

Fig. 3.6.5 shows the effect of m^* on the pressure gradient for glass beads in vertical riser transport for a range of gas velocities between 6 - 16 m/s. The slope of the linear fit for gas velocities above 10.5 m/s is 19 Pa/m. This is close to the value of 22 Pa/m observed for sand particles at the same line orientation. The slope of $\Delta P/L$ with m^* in the vertical riser increases to 55 Pa/m as the gas velocity decreases to 7.5 m/s.

There is apparently a flow transition at a gas velocity of about 7.5 m/s in the vertical riser transport of glass (Fig. 3.6.5). It was very difficult to obtain data for the glass beads at gas velocities below 8 m/s because of extensive solids refluxing. The suspension often collapsed into a slugging erratic flow ("fuzzy" transition in left branch of Fig. 1.3), and was sensitive to minor perturbations of the solids holdup. The erratic flow conditions caused fluctuations of the pressure gradient, and the line was rapidly approaching choking conditions below 8 m/s.

The erratic flow characteristics of the glass beads could be related to the different coefficient of restitution for these particles in comparison with

Fig. 3.6.5 : Pressure Gradient vs. Glass Loading Vertical Line Orientation

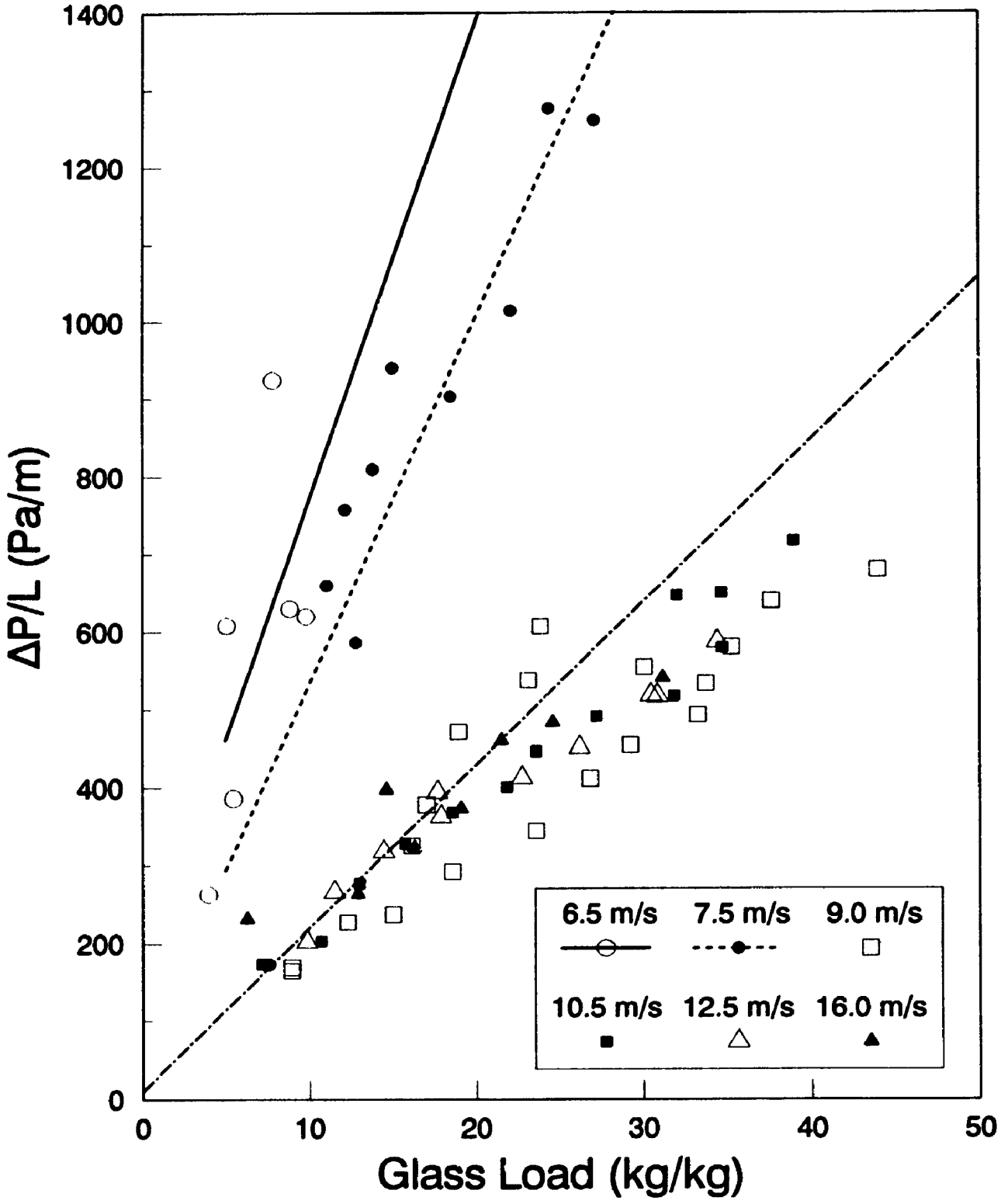

sand. Ocone et al. (1993) have noted that the transition from the deposited layer of solids at the wall to the flowing suspension adjacent to it, is extremely sensitive to the specific coefficient of restitution of the particles.

At line inclinations of 7° (Fig. 3.6.6) and 17° (Fig. 3.6.7) the pressure gradient increases linearly with the mass loading of glass beads in the line. The slope of the curve at 7° (Fig. 3.6.6) is about 20.6 Pa/m, which is close to the value of 24 Pa/m observed for sand particles in the 4° inclined line (Fig. 3.6.2). This result would imply that the impact of line inclination is minimal below a line inclination of about 7°, in agreement with the observations of Zenz (1957), providing that the gas velocity is sufficient to maintain a net upflow of solids.

At 7°, based on visual observations, the slight line incline made it easier to control the flow. Particles slid gently along the underside of the tube, instead of falling long distances in the vertical riser, before being reentrained. Large pressure gradient fluctuations and a loss of pressure energy which were recorded in the vertical risers, were not as prominent in the inclined lines for the glass beads. This more stable hydrodynamic configuration manifested itself in a reduction of the pressure gradient fluctuations as characterised by the standard deviation.

Fig. 3.6.6 : Pressure Gradient vs. Glass Loading
7° Inclined Line Orientation

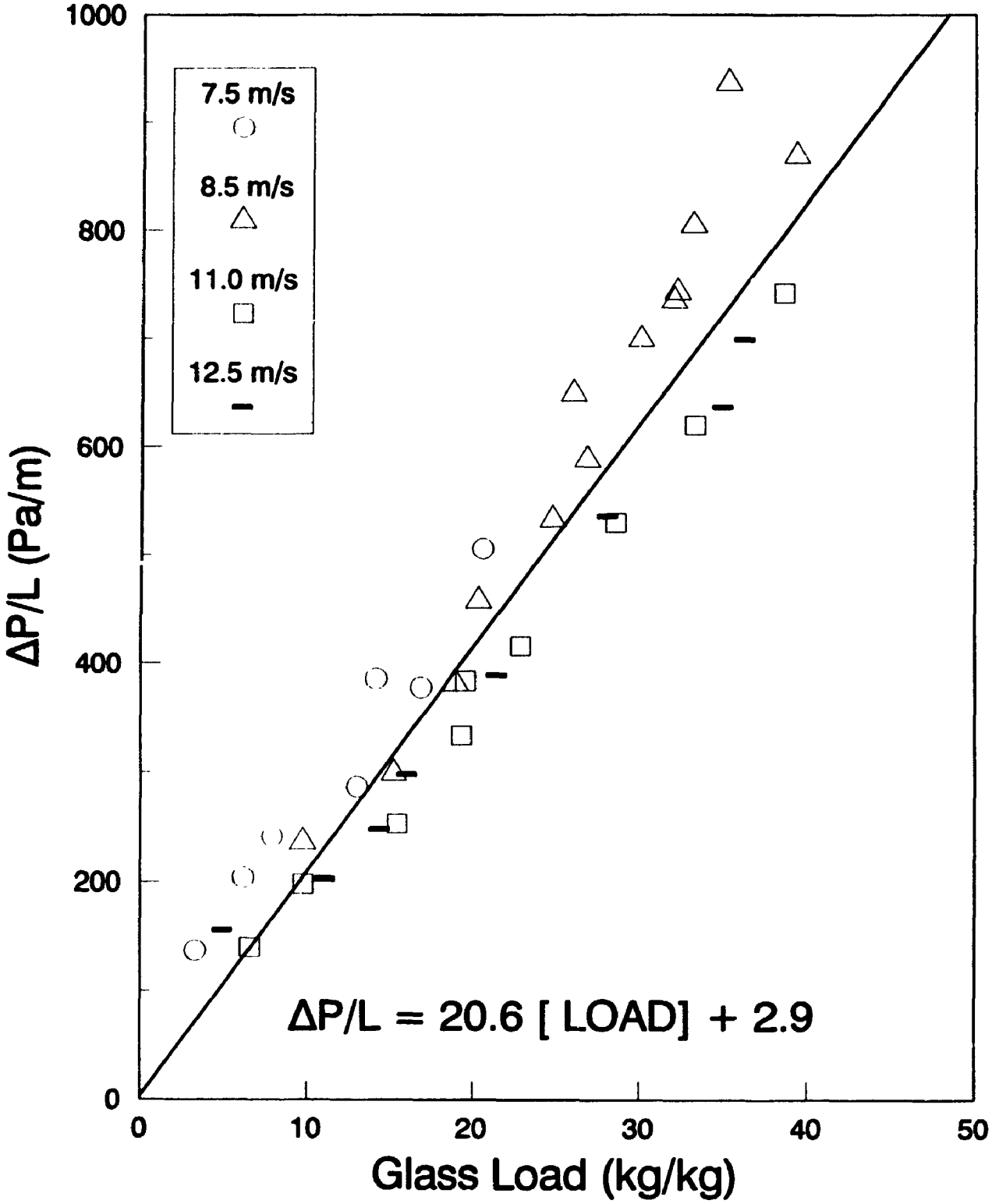

Fig. 3.6.7 : Pressure Gradient vs. Glass Loading 17° Inclined Line Orientation

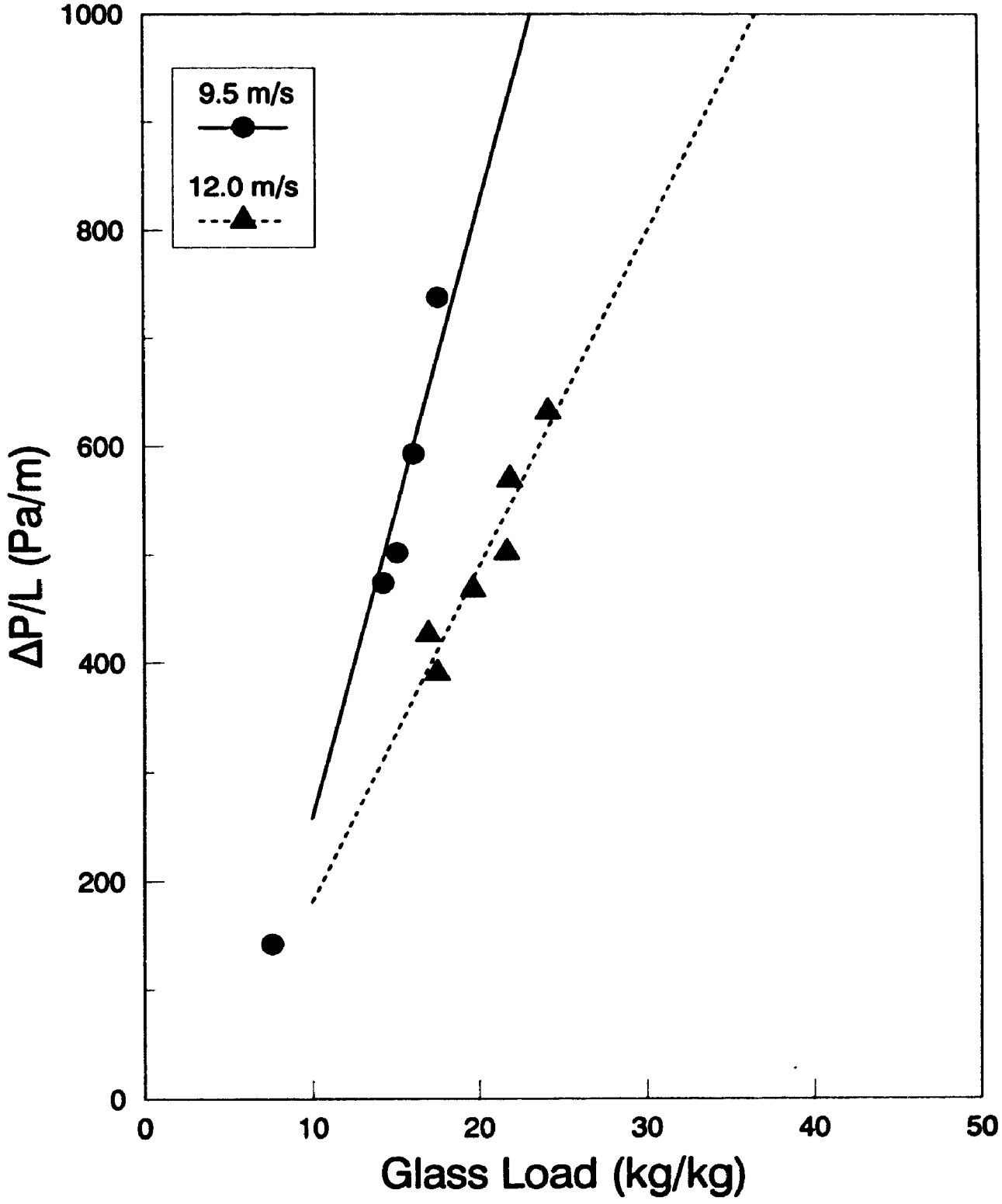

3.7 STANDARD DEVIATION OF PRESSURE GRADIENT FLUCTUATIONS

Matsui (1984) has found that the standard deviation of the pressure drop fluctuations is proportional to the void fraction fluctuations in the vertical riser. This result implies that there may be a dependence of the standard deviation with the specific solids holdup in the riser. To further investigate this relationship for the current study, the standard deviation of the pressure gradient fluctuations was plotted versus the sand and glass holdups in the inclined risers.

3.7.1 EFFECT OF SAND HOLDUP ON STANDARD DEVIATION

Fig. 3.7.1 shows that the standard deviation of the pressure gradient time series is linearly dependent upon the solids holdup for the vertical transport of sand particles. It increases to 45 Pa/m at a solids holdup of 2.5%, and the slope of the least squares line is 22 Pa/m/%. The effect of gas velocity is not significant. At a line inclination of 4° the slope of the least squares line is 27 Pa/m/% (Fig. 3.7.2). No effect of gas velocity is observed at 4°. At 11° (Fig. 3.7.3), σ increases with a linear slope of 25 Pa/m/%, and there appears to be a transition solids holdup at about 0.2%, below which the slope increases dramatically. At 18° (Fig. 3.7.4), there also appears to be a similar break in the profile for $\alpha \approx 0.2\%$. No significant effect of gas velocity is apparent, and the slope of the least squares line is 22 Pa/m/%. It seems

Fig. 3.7.1: Standard Deviation vs. Sand Holdup
Vertical Line Orientation

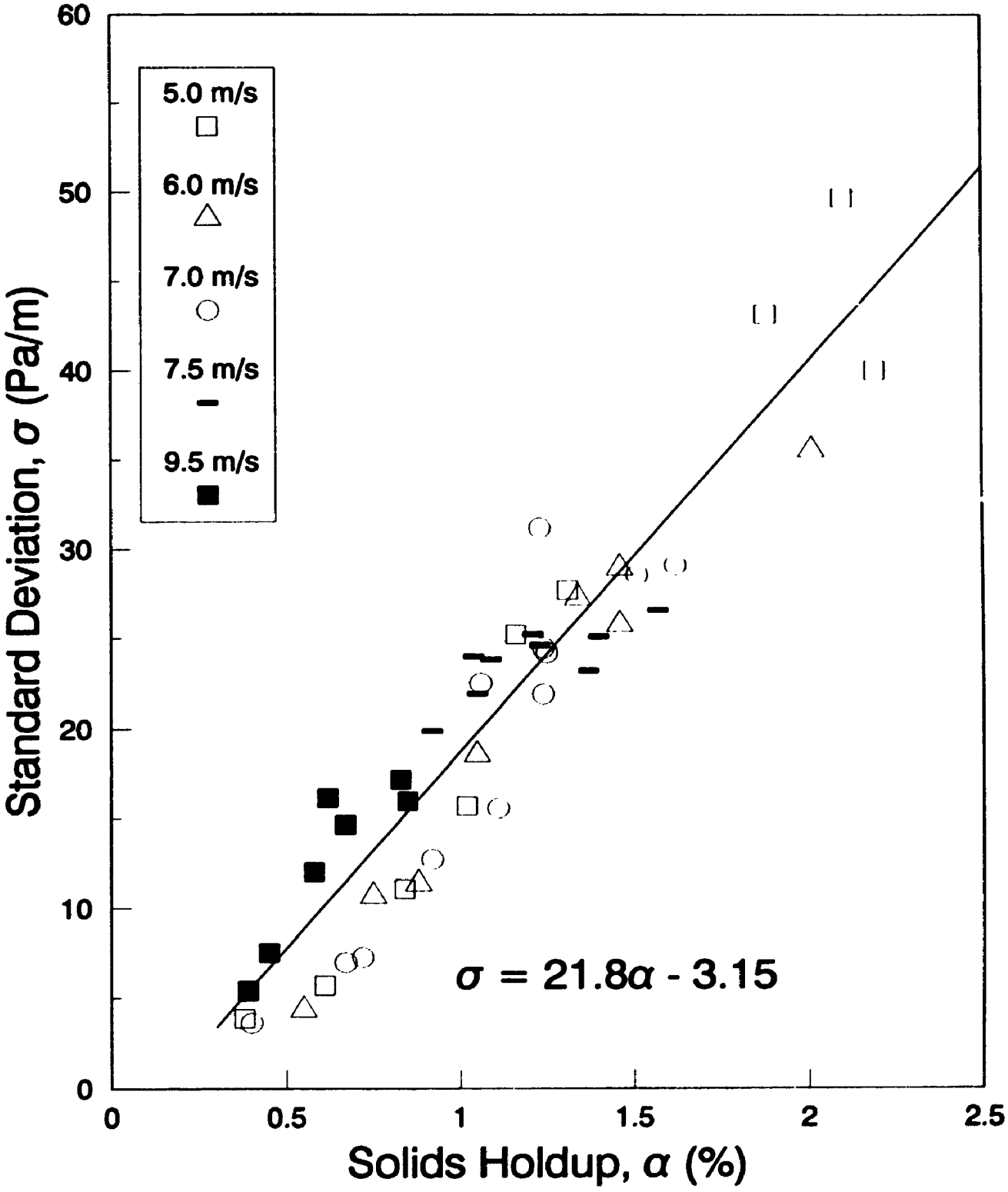

Fig. 3.7.2 : Standard Deviation vs. Sand Holdup
4° Inclined Line Orientation

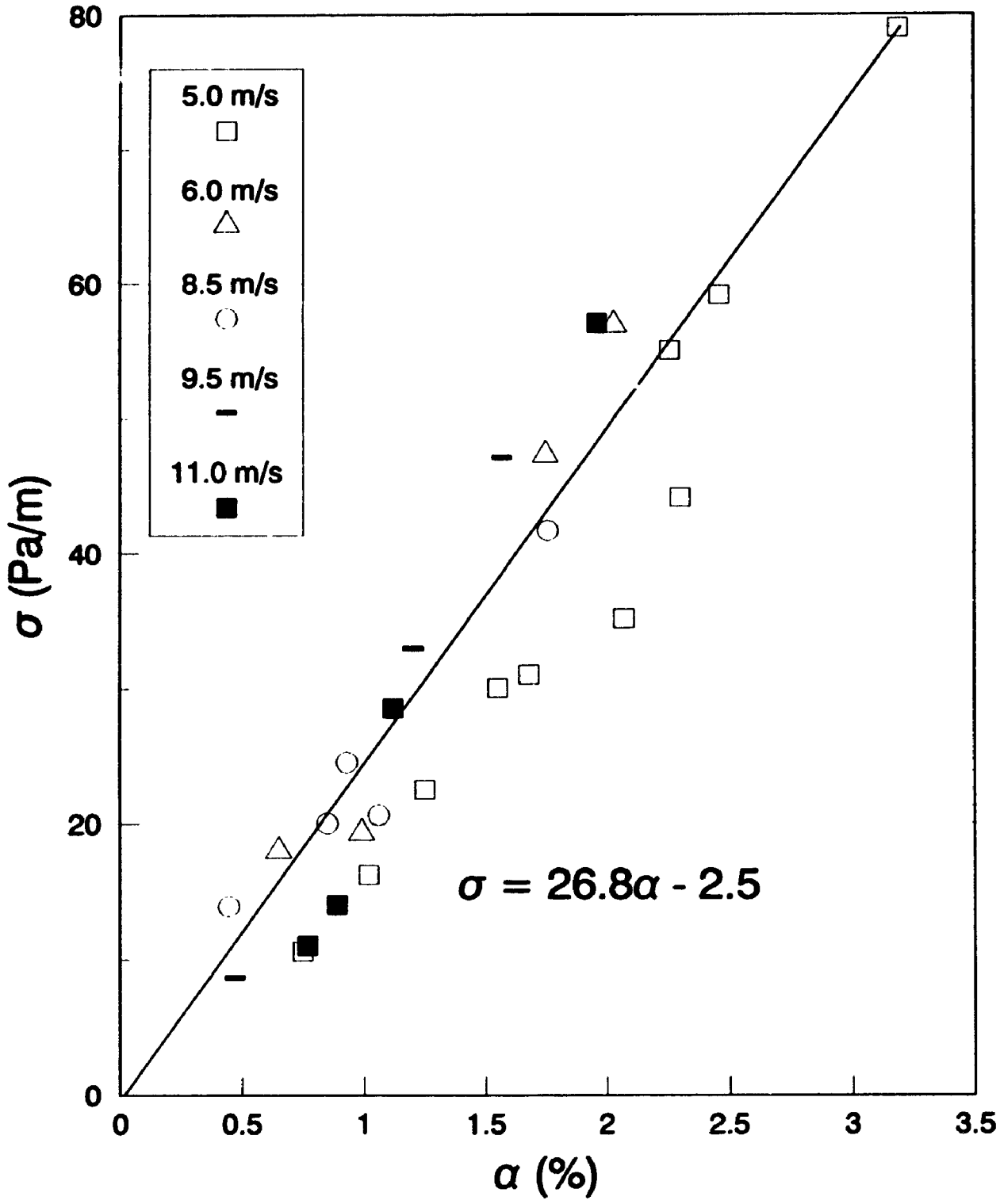

Fig. 3.7.3 : Standard Deviation vs. Sand Holdup
11° Inclined Line Orientation

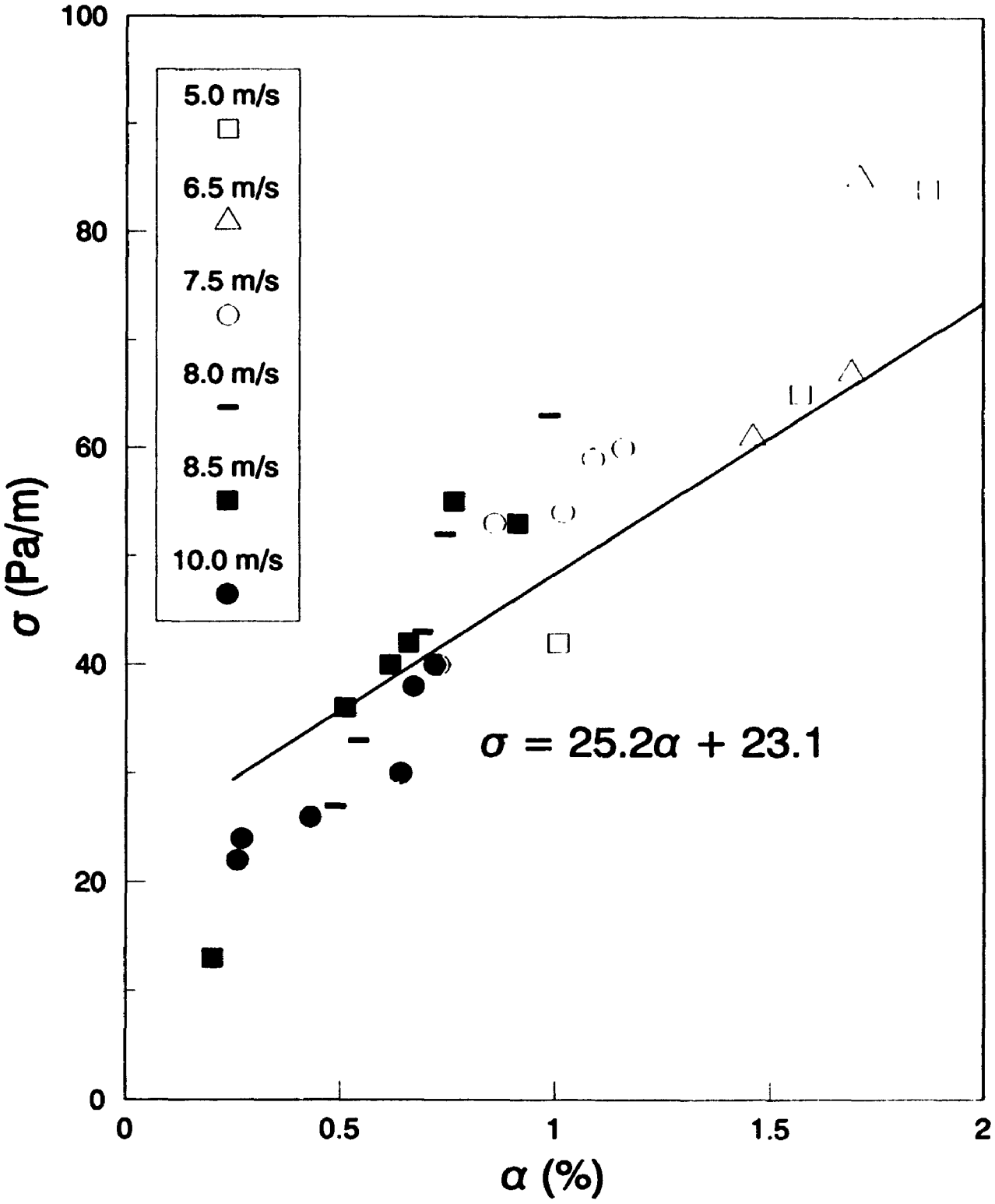

Fig. 3.7.4 : Standard Deviation vs. Sand Holdup
18° Inclined Line Orientation

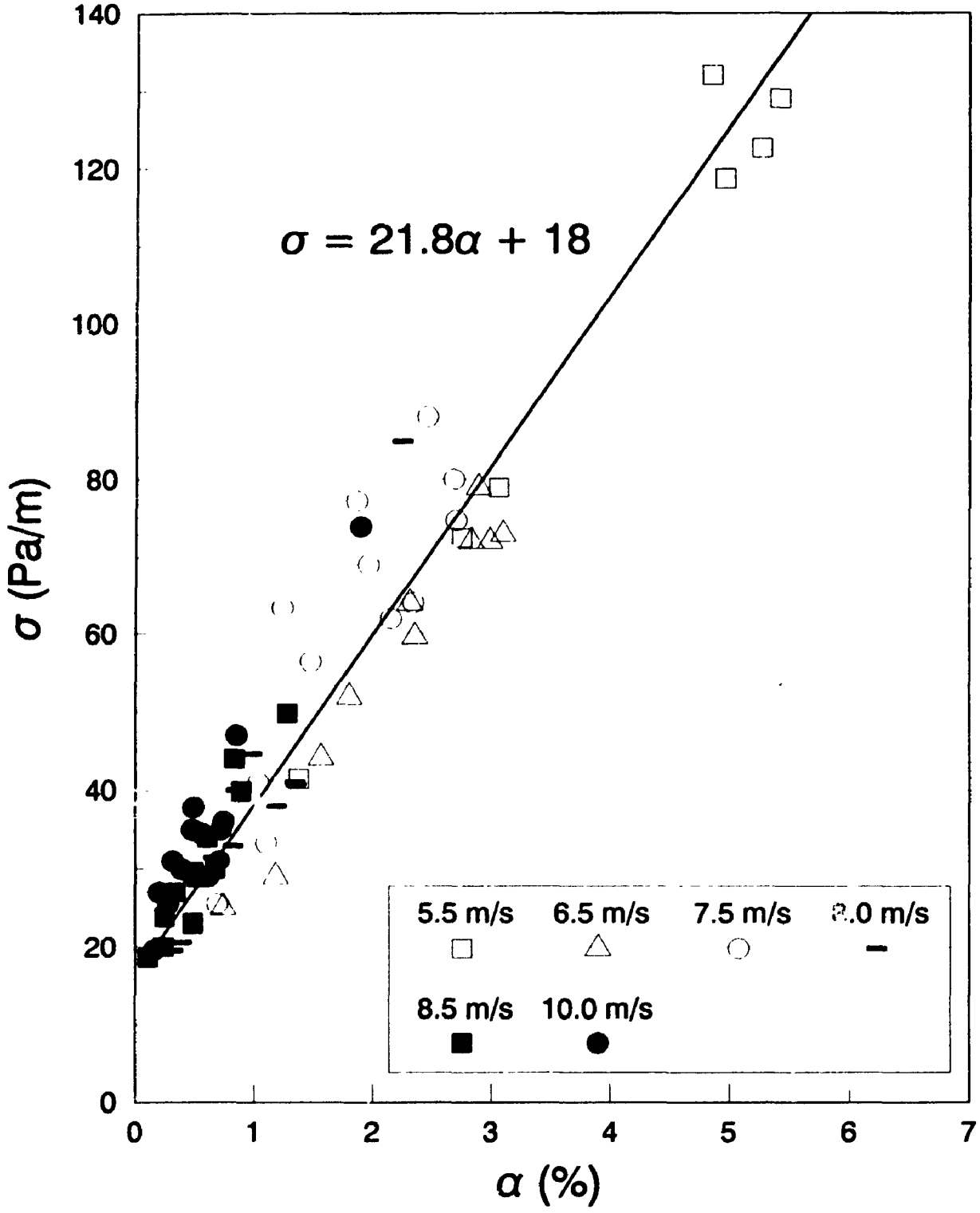

that the slope of the least squares regression linear fit is not significantly affected by θ, as observed from the results of Figs. 3.7.1 to 3.7.4 for sand particles.

3.7.2 EFFECT OF GLASS HOLDUP ON STANDARD DEVIATION

The effect of α on σ for glass beads transport is shown in Fig. 3.7.5 for the vertical line. The standard deviation increases at a rate of 8.7 Pa/m/%. At 7° (Fig. 3.7.6) a break in the profile is also observed for $\alpha \approx 1.2\%$. The slope increases from 3 to 7 Pa/m/% after the transition at 1.2%. The cause of the transition point observed for the glass beads is inconclusive based on the available information. There was insufficient data available at 17° to derive conclusions at the 17^0 orientation, shown in Fig. 3.7.7. The slope of the line is 6.5 Pa/m/% and no break was observed.

The change of slope observed at low solids volumetric holdups of glass beads has also been shown elsewhere by Ginestet et al. (1993). The abrupt change of slope could be due to changing hydrodynamic flow conditions, representing a transition to choking flow. Solids holdups below 2% were associated with fully entrained flow conditions, where the gas velocity was above 9 m/s.

Fig. 3.7.5 : Standard Deviation vs. Glass Holdup Vertical Line Orientation

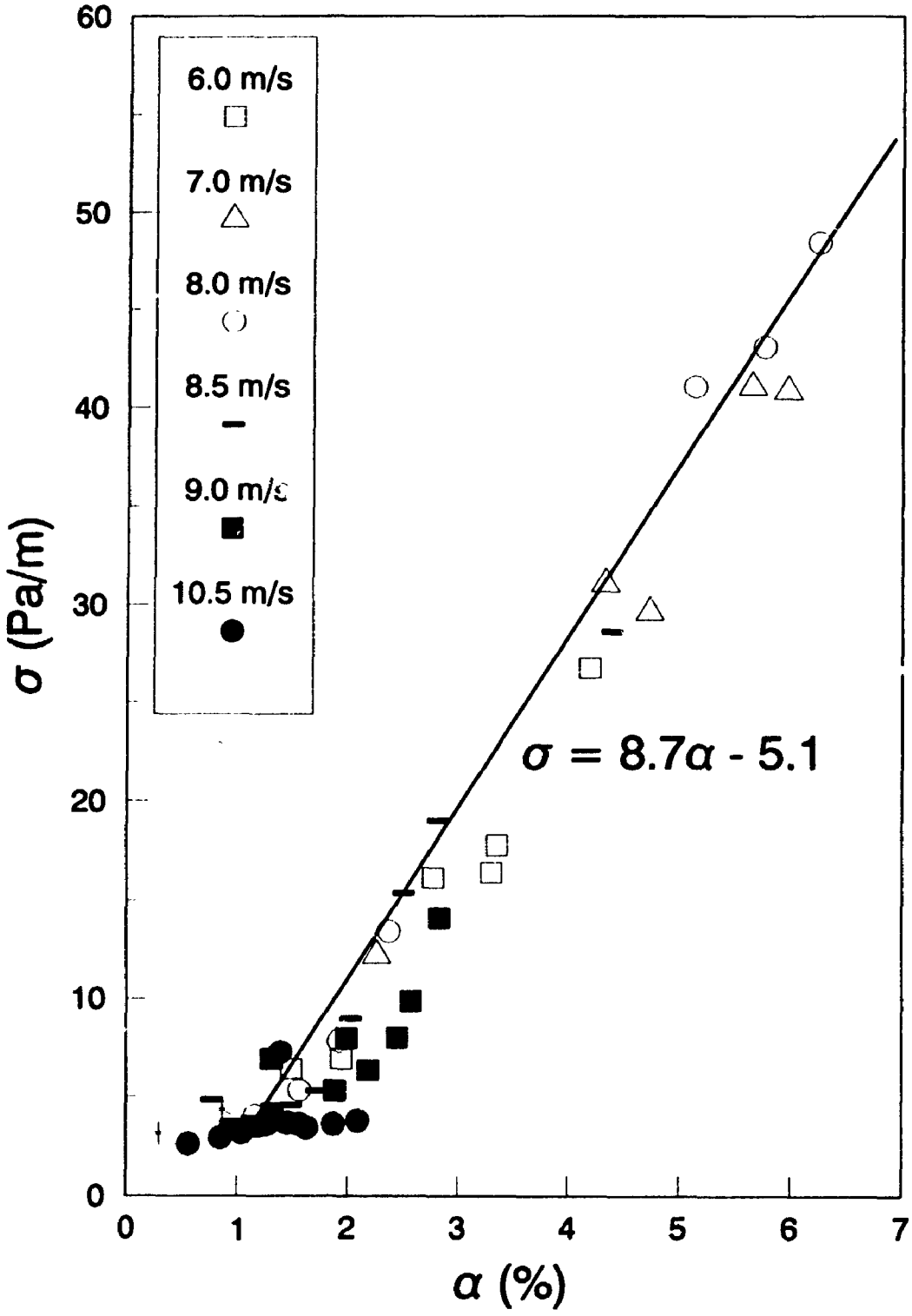

Fig. 3.7.6 : Standard Deviation vs. Glass Holdup 7° Inclined Line Orientation

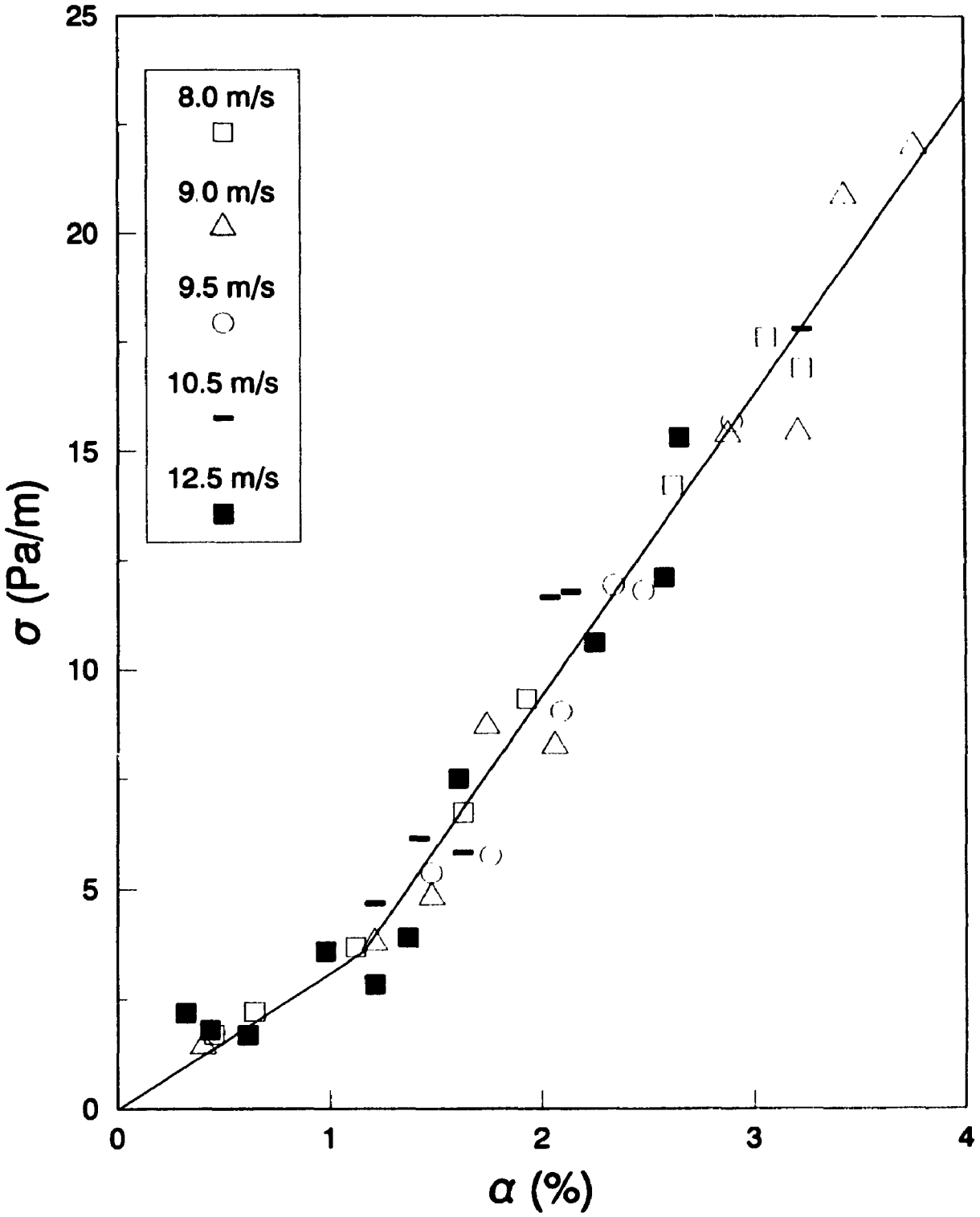

Fig. 3.7.7 : Standard Deviation vs. Glass Holdup
17° Inclined Line Orientation

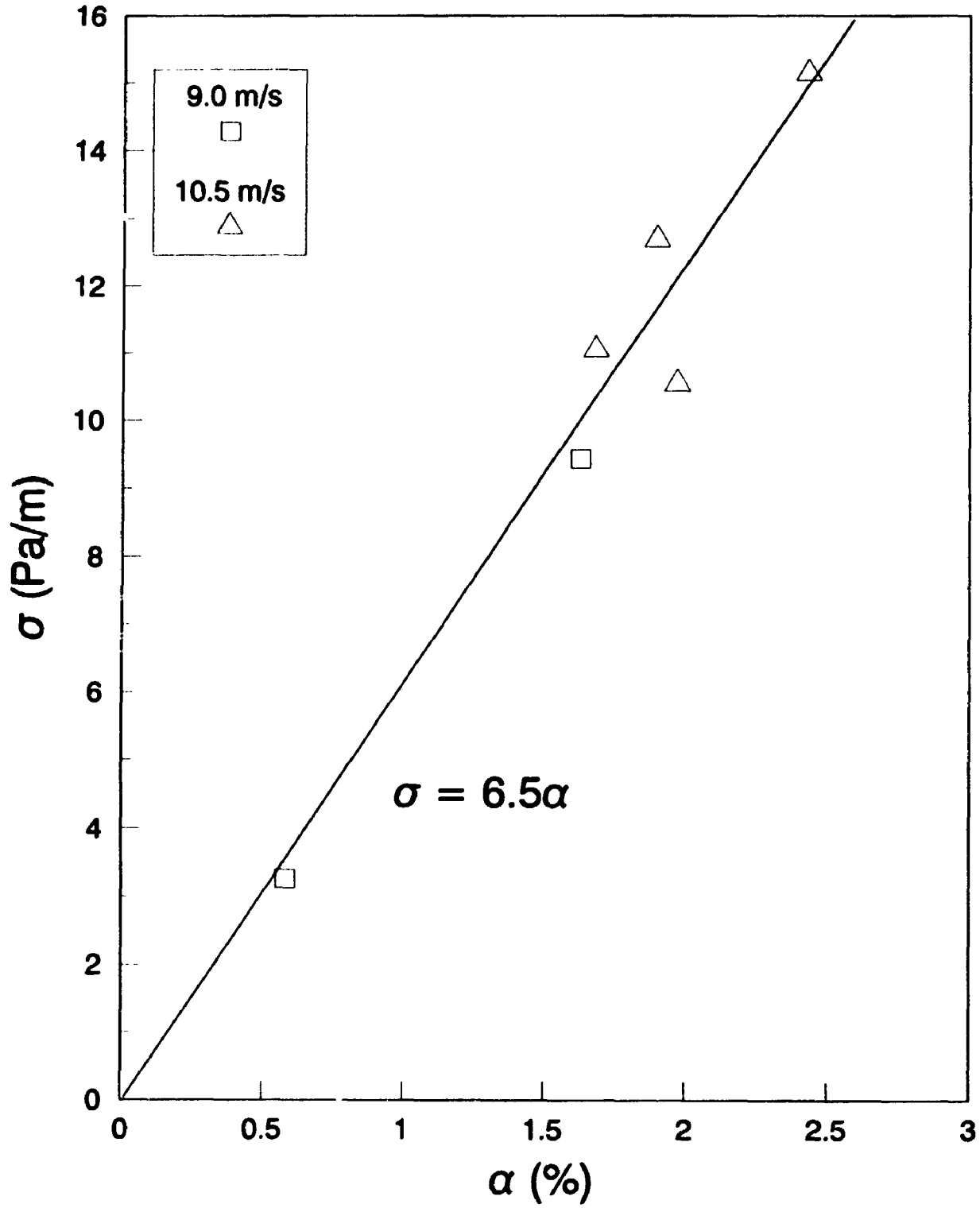

4. ANALYSIS OF RESULTS

4.1 PARTICLE VELOCITY AND CHOKING POINT

The mean particle velocity was computed for each experiment using equation 14 in § 1.9. The experimental data was compared with literature correlations including Konno and Saito (1969), Matsen (1982), Myler (1987), Zaltash (1987), and Hinkle-IGT (Institute of Gas Tech., 1978). These correlations are given in § 1.9 and the FORTRAN program CORANA, which was used to compute these quantities, is given in Appendix D.

4.1.1 PARTICLE VELOCITY CORRELATIONS FOR SAND AND GLASS

Table 4.1.1 summarizes the results of the particle velocity correlation study for both the sand and glass particles. An absolute average deviation, ξ, (comparing the correlation with the experimental results), was computed for each of the experimental runs, and is tabulated as a percentage. Only the Zaltash correlation is defined for inclined lines.

From Table 4.1.1, for sand particles using a line inclination of less than 4°, it was found that the Konno, Myler, and Zaltash correlations could fit the data with ξ of about 10%. The Matsen and Hinkle correlations both gave avalue of ξ of between 22% and 66% for line inclinations of up to 4°. None of the correlations, including Zaltash, were reliable for estimation of the particle velocity for line inclinations above 4°. Moreover, these correlations

were developed from dilute phase pneumatic transport data where solids refluxing and radial dependence of particle velocity is much less significant.

TABLE 4.1.1 : COMPARISON OF CORRELATIONS FOR PARTICLE VELOCITY[1]

CORR.[2]	ξ (%)						
	⌊, Θ (SAND) (GLASS)				⌊, Θ		
	0°	4°	11°	18°	0°	7°	17°
KONNO	4.6	10.3	52.1	96.8	2.4	1.0	1.7
MATSEN	51.6	65.6	61.7	83.2	591	201	203
MYLER	0.9	6.9	47.7	90.9	303	126	193
ZALTASH	7.4	2.3	34.9	72.2	234	94	153
HINKLE	22.8	34.1	87.4	141	486	210	286

For glass beads it is evident from Table 4.1.1 that the Konno correlation is most robust. It provided reliable estimates of the particle velocity for all line inclinations. All of the others are inadequate for the glass particles at all line inclinations. The Zaltash correlation does not provide a good

[1] Correlation equations given in Section 1.9 of thesis.

[2] Particle velocity correlation.

estimation of the data, even though it was originally developed for inclined lines. This is probably because it was derived for the dilute phase transport of solids.

4.1.2 INSTABILITY OF SUSPENSION NEAR CHOKING

The choking velocity, or the classical 'Type C' system (Bi et al, 1993), is the most difficult experimental parameter to measure with confidence. In some cases the system does not choke, but the suspension collapses directly from dilute phase flow to slugging flow, as the gas velocity is reduced beyond a critical minimum (Fig. 1.3). Extensive solids refluxing accompanying the transition to choking, and subsequent slug flow often makes it troublesome to control the operating conditions precisely.

In this study the system at the choking point was sensitive to minor gas and solids flow perturbations, and to slight changes of the pressure in the fluidized bed feeder. Because of these problems it was difficult to obtain more low velocity (< 6 m/s) and high solids flux (> 165 kg/m^{2}s) data, especially for glass beads transport.

Experiments with glass beads were particularly difficult due to the instability of the suspension near choking velocities. The suspension often collapsed in on itself resulting in an erratic slugging flow. At other times,

under identical conditions, the suspension could be maintained as a non-slugging dense phase flow. The tendency towards slugging or annular nonuniform flow was not always predictable. Model simulation done by Bi and Zhu (1993) has shown that the operating instability and the maximum solids circulation rate attainable are strongly influenced by the total solids inventory in the system, and the unit geometry such as standpipe size and solids feeding device. They claim that sufficient back pressure needs to be provided at the bottom of the riser, by increasing the pressure buildup in the standpipe, or by lowering the resistance through the solids control valve.

The instability of pneumatic transport in the non-slugging dense phase regime for vertical and inclined lines may have potential implications for commercial scale oblique risers. The operating gas velocity in such systems should be maintained at least 2-3 m/s above the measured choking velocity to minimize transitions to the choking regime via flow instabilities. Another possibility would be to implement baffles at the pipe wall to break up the solids down-flow layer. Jiang et al. (1991), for instance, have found that doughnut baffles mounted at suitable intervals in the riser can be used to break up the solids layer by withstanding the downward particle motion. Pita and Sundaresan (1993) observed that circumferential injection of the solids could decrease the extent of internal recirculation in large commercial

risers.

4.1.3 CHOKING HOLDUP FOR SAND AND GLASS

Leung et al. (1971) found that choking in vertical pneumatic transport usually occurred at a voidage of 0.97. This has been verified by Ocone et al. (1993) who concluded from their mathematical model, that the upper half of an inclined duct nowhere contains more than 3% by volume of solids. Their conclusions are corroborated by the results shown in Table 4.1.2 for all line inclinations in this study. The measured choking velocity varies from 4.5 to 5.5 m/s for sand particles, and 7.5 to 9.5 m/s for glass beads. Based on the Yang (1988) correlation, the choking velocity for sand should be 4.6 m/s for vertical lines, which yields a deviation of just 2.2% with the observed result. This result is corroborated by Horio et al. (1992) who observed a choking velocity of 4.5 m/s for silica sand particles. For glass beads the experimentally observed choking velocity was 7.5 m/s, compared with Yang's value of 6.3 m/s. The solids volumetric holdup for which choking was observed was approximately 0.03. The correlations are not applicable for inclined lines, so comparisons were not possible for the oblique risers.

Although it is conceivable that the line could choke at higher gas velocities, providing that the solids flux could be maintained sufficiently high (§ 4.1),

such conditions could not be achieved with the present equipment. Whether the solids holdup would exceed 3% at gas velocities above 5 m/s for silica sand is not known from this database, because the maximum solids flux that could be achieved with this equipment was about 300 kg/m^{2}s. For a solids flux of up to 300 kg/m^{2}s the solids holdup was less than 2% at gas velocities above 7 m/s.

TABLE 4.1.2 : CHOKING VELOCITY FOR SAND AND GLASS

PARTICLE	$\Delta\Theta$	SOLIDS FLUX	SOLIDS HOLDUP			ξ[1]
		W_s (kg/m^{2}s)	α (v/v)	U_{gc}[2] (m/s)	U_{gc}[2]	(%)
SAND	0	230	0.029	4.5	4.6	2.2
SAND	4	200	0.030	5.5		
SAND	11	75	0.027	4.5		
SAND	18	65	0.034	5.0		
GLASS	0	145	0.032	7.5	6.3	19
GLASS	7	150	0.028	8.5		
GLASS	17	90	0.033	9.5		

[1] ξ is the absolute deviation between the two quantities expressed as %.

[2] Experimentally measured choking velocity at conditions specified.

Wong et al. (1992) have demonstrated that the solids concentration at the injection point for similar conditions (277 μm sand particles at 200 kg/m^{2}s and 6 m/s) in their rig is about 25%, but decreases to 3% in the test section. It would seem, therefore, that the transition to choking may be influenced by the concentration of solids at the injection point to the riser, as much as by the concentration of solids in the fully developed section of the riser.

The solids flux at choking decreased with line inclination for both types of particles. For the sand particles the solids flux decreased from 230 to 65 kg/m^{2}s (Table 4.1.2) as the line was inclined from the vertical to 18°. For glass beads no effect of solids flux was observed for the 7° inclined line. At 17° the flux decreased from 150 kg/m^{2}s (for 7° line) to 90 kg/m^{2}s.

The fluidized bed feeder/dipleg return system could not sustain a solids flux in excess of 300 kg/m^{2}s. The pressure in the bed needed to be maintained so high that solids could not be returned back into the bed from the dipleg connecting the disengaging chamber to the fluidized bed feeder (Fig. 2.1). the phenomenon is similar to the Type B choking system as described by Bi et al. (1993).

4.1.4 CHOKING VELOCITY FROM ASSUMED CHOKING VOIDAGE

In the literature the choking point is usually defined as that velocity for

which the pressure gradient increases rapidly with the gas velocity at constant solids flux. However, there is no criterion to identify precisely what value of slope can be considered as high enough to be called the choking point. Satija et al. (1985) observed that all of the correlations in the literature to characterise choking transitions are based upon stable slugging flow. They are not usually applicable to the non-slugging transition (left branch of Fig. 1.3) such as that observed in this research. Hence, alternative methods of choking velocity estimation were sought in this research which could be used in process applications, when operation near choking conditions cannot be tolerated for any length of time.

From the plots of solids holdup with solids flux (Figs. 3.5.1 to 3.5.7), the solids flux corresponding to a given gas velocity at a solids holdup of 3% (choking holdup from Table 4.1.2), was interpolated from the least squares regression curves. Since the R^2 statistic was greater than 0.9 for all regressions considered, the interpolation of the choking solids flux for a given gas velocity could be extracted from the curve fit with confidence. Knowledge of the solids flux for a given gas velocity at 3% solids holdup, allowed the particle velocity to be determined using equation 14 in § 1.9. The gas velocity at a solids holdup of 3% represents a choking velocity based upon Table 4.1.2, and is substantiated by the work of Ocone et al. (1993). This choking velocity was plotted versus the particle velocity,

obtained by interpolation, and is plotted in Fig. 4.1.1. The choking velocity, U_{gc}, could be correlated with the sand particle velocity using equation (38).

$$U_{gc,\,sand} = 4.15 + 0.633\ U_{sand} \qquad (38)$$

The glass beads choking velocity was correlated using equation (39).

$$U_{gc,\,glass} = 5.22 + 1.80\ U_{glass} \qquad (39)$$

Equations (38) and (39) provide a method of predicting the gas velocity at choking if the particle velocity is known, or can be calculated.

4.1.5 USE OF STANDARD DEVIATION, σ, TO IDENTIFY CHOKING POINT FOR SAND PARTICLES

The use of the standard deviation of the pressure gradient fluctuations, σ, to classify and characterise various hydrodynamic flow regimes has been studied by Dhodapkar and Klinzing (1993). Satija et al. (1985) have attempted to use σ to identify the choking point in their vertical riser. In this research σ was plotted versus the solids flux and gas velocity to determine if it could be used to characterise the choking point in vertical and inclined risers operated in the non-slugging dense flow regime. A large increase of σ with one or both of these variables at certain conditions could represent the transition to the choking point.

Fig. 4.1.1: Choking Gas Velocity Correlations [1]

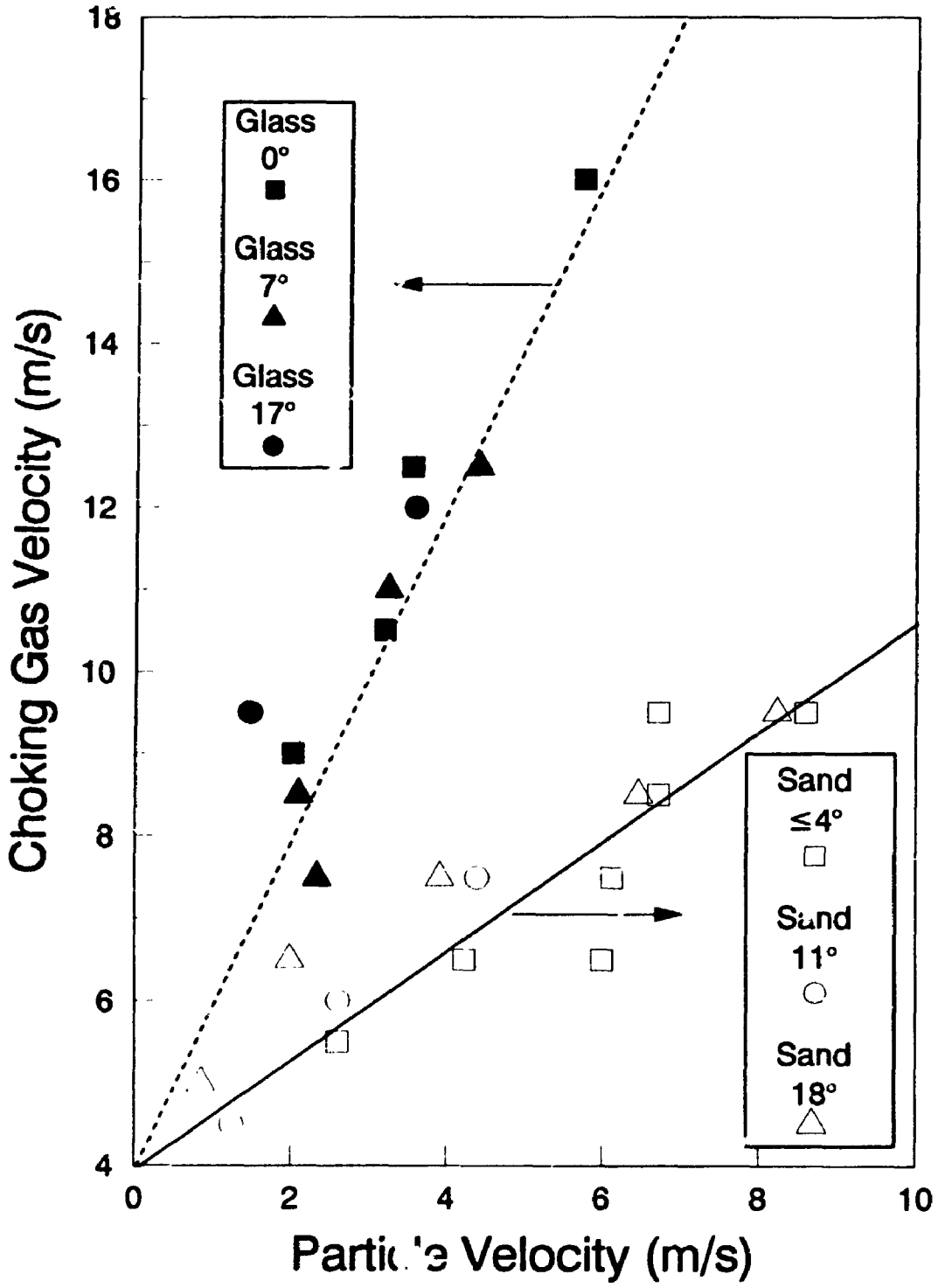

1. Choking Gas Velocity Assumed at 3% Solids Holdup

Fig. 4.1.2 shows a plot of σ (calculated from equation 32, § 3.2.2) versus the solids flux, W_s and the gas velocity U_g for the vertical transport of sand particles using the 3-D graphics software AXUM (Trimetrix, 1993). The data points are connected by line segments to the W_s-U_g plane to clearly indicate the magnitude of each of the observations.

It is evident from Fig. 4.1.2 that σ increases rapidly for a solids flux exceeding 100 kg/m^{2}s. This increase of σ with W_s is steep for gas velocities below about 7 m/s. At the lowest gas velocity of 4.5 m/s used in this study, the increase of σ with both variables is immediate, even at a solids flux of less than 50 kg/m^{2}s. It would seem that there is a gradual approach to choking as the gas velocity decreases below 7 m/s, which is dependent upon the solids flux. For gas velocities less than 6 m/s and for a solids flux in excess of 150 kg/m^{2}s, the system stability is sensitive to minor perturbations of either variable.

Fig. 4.1.3 shows the relationship of σ with W_s and U_g for a line inclination of 11° with sand particles. Based on laboratory experience it was not possible to operate at a solids flux exceeding 150 kg/m^{2}s at this line inclination. Extensive refluxing with transition to slug flow was possible, which led to erratic and chaotic type flows. The standard deviation increases from about 50 Pa/m at 100 kg/m^{2}s to about 100 Pa/m at 150

Fig. 4.1.2: Standard Devlation, σ, of Pressure Gradient Fluctuations
Sand Particles In Vertical Orientation

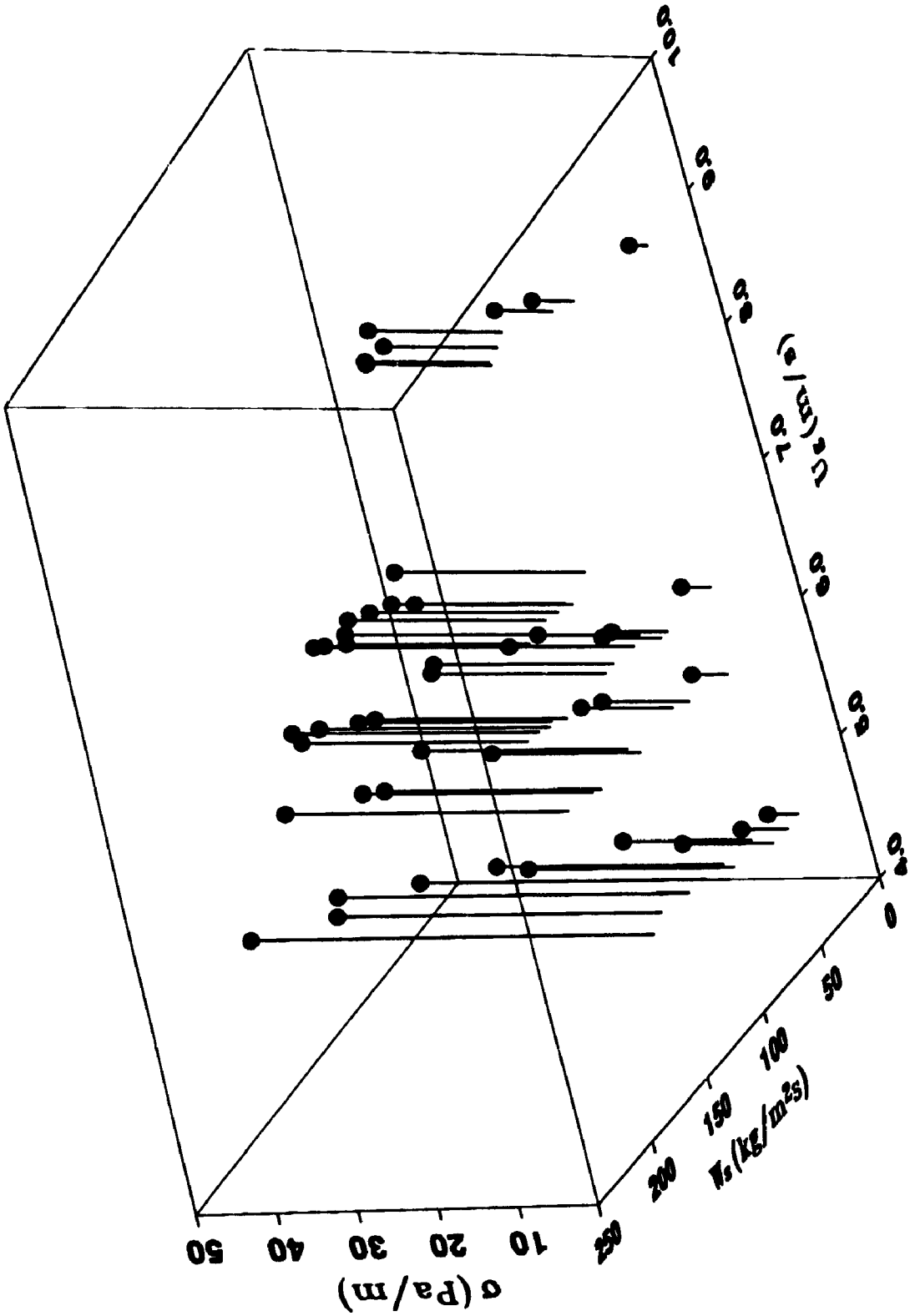

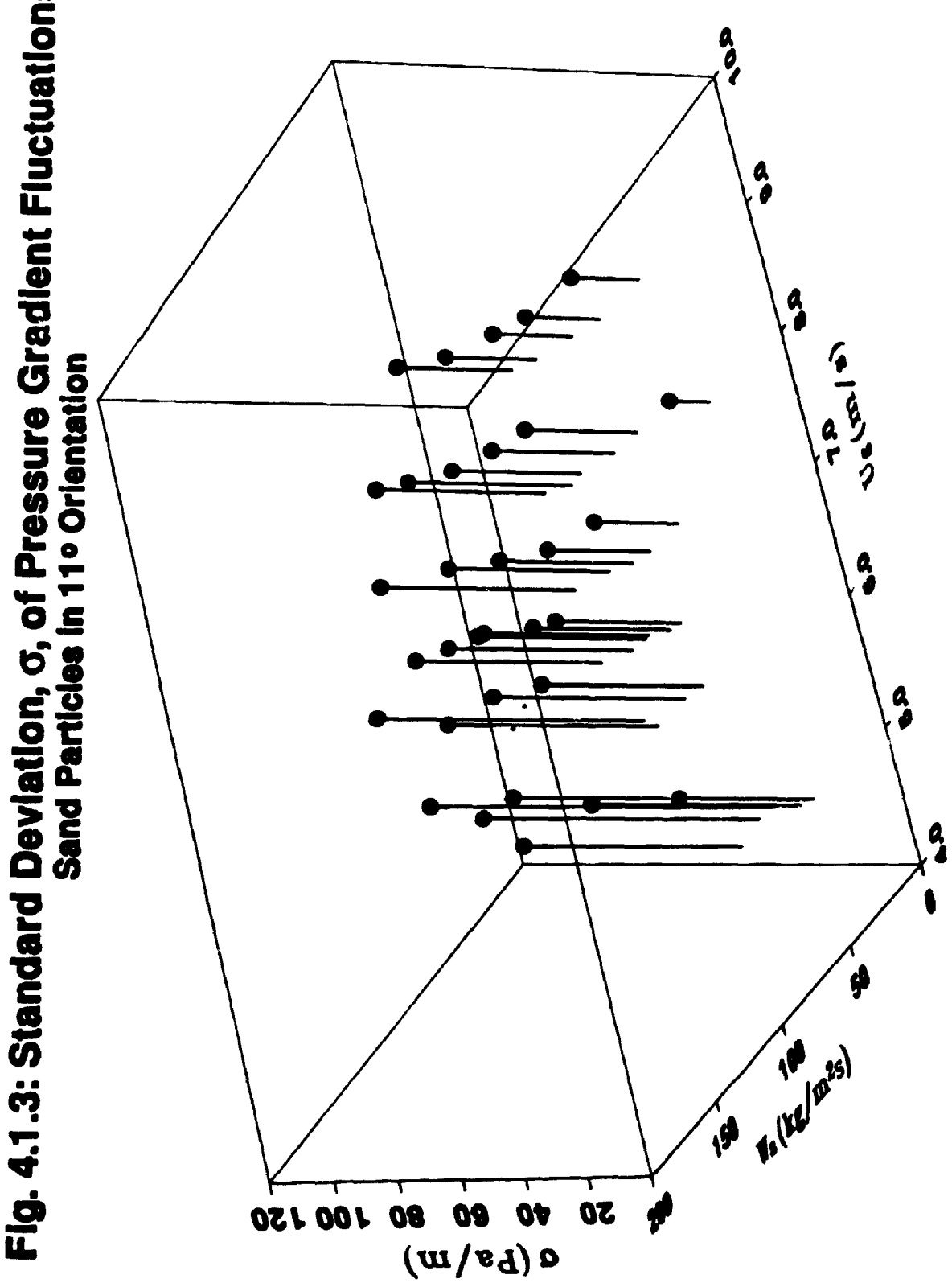

Fig. 4.1.3: Standard Deviation, σ, of Pressure Gradient Fluctuations Sand Particles in 11° Orientation

kg/m^{2}s (Fig. 4.1.3) for a gas velocity of 4.8 m/s. The line could approach choking at all gas velocities for a solids flux exceeding about 125 kg/m^{2}s. There was also a slight increase of σ with decreasing gas velocity.

At a line orientation of 18° (Fig. 4.1.4), choking is approached rapidly as the solids flux increases beyond 100 kg/m^{2}s. There is a sharp increase of σ at all gas velocities for this solids flux. As W_s increases from 100 to 250 kg/m^{2}s in Fig. 4.1.4, σ increases from 50 to over 150 Pa/m at a gas velocity of 5 m/s. Visually, this increase of σ was observed as long streamers of refluxing particles, which occasionally collapsed into slugging flow at gas velocities close to 4.5 m/s.

These results (Figs. 4.1.2 to 4.1.4) suggest that the choking velocity is strongly influenced by the sand flux and gas velocity. The increase of σ with W_s at constant U_g is accelerated with progressive increments of θ. This would indicate that a plot of σ with W_s and U_g may be appropriate for identification of the choking at all line inclinations, including the vertical orientation. The choking point would correspond to those values of W_s and U_g for which the rate of change of σ with either variable increased significantly.

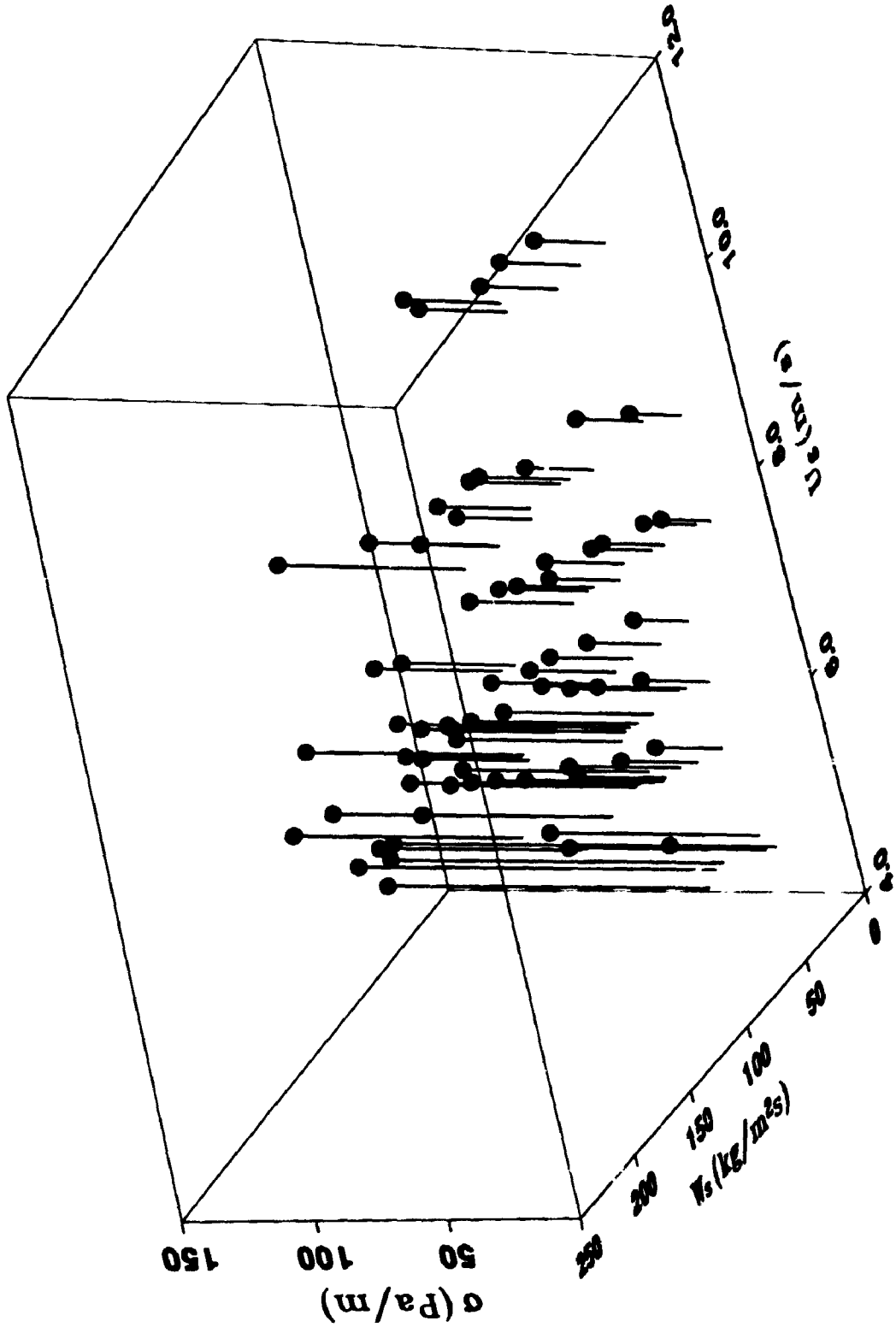

Fig. 4.1.4: Standard Deviation, σ, of Pressure Gradient Fluctuations
Sand Particles in 18° Orientation

4.1.6 USE OF STANDARD DEVIATION, σ, TO IDENTIFY CHOKING POINT FOR GLASS BEADS

In § 3.6.2 it was noted that it was difficult to perform experiments at high solids flowrates near the choking velocity for glass beads. The suspension would often collapse in on itself, and this tendency was not always a priori predictable. A 3-D scatter plot of σ versus W_s and U_g for the vertical transport of glass beads (Fig. 4.1.5), shows the experimental data. The increase of σ is a function of both the solids flux and gas velocity. There is a sharp increase of σ for a solids flux greater than 100 kg/m^{2}s, and a gas velocity of less than 9 m/s. From visual observations those experiments at a gas velocity of 8 m/s were sensitive to slight perturbations of W_s.

The flow of glass beads in a slightly inclined line seemed more stable in comparison with the vertical riser. The particles apparently formed tighter clusters and would move as a unit through the pipe in the inclined line. Long ropes of solids were transported along the tube wall without the extensive refluxing characteristic of the vertical line. For the vertical transport of glass beads, long streamers of particles were observed to drop long distances through the tube before being reentrained by the gas. This is thought to have led to the erratic flow conditions at gas velocities below 9 m/s which were encountered in the lab.

Fig. 4.1.5: Standard Deviation, σ, of Pressure Gradient Fluctuations
Glass Beads in Vertical Orientation

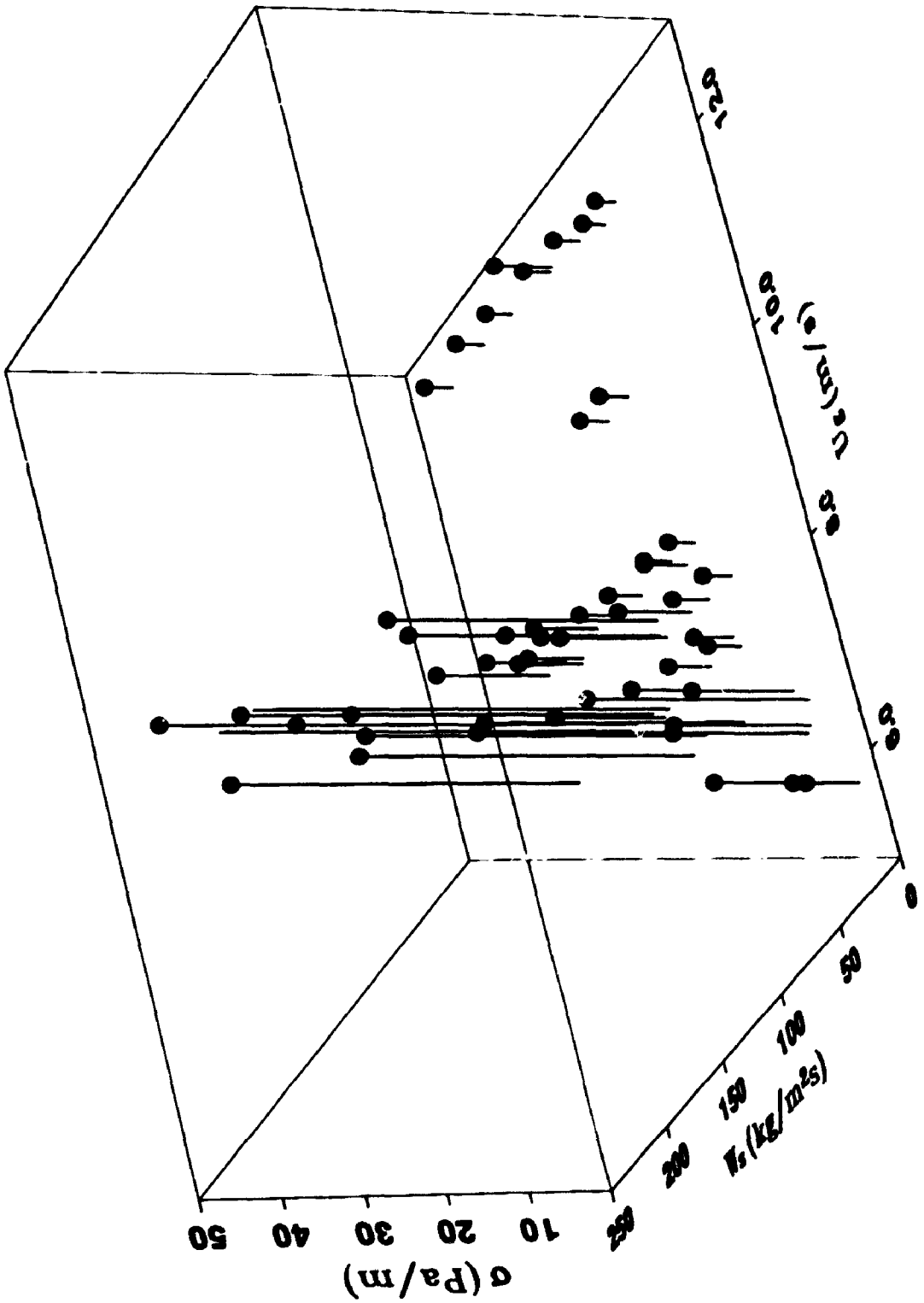

Fig. 4.1.6 shows that under the same conditions, the magnitude of σ is significantly less than that observed for the vertical line in Fig. 4.1.5. An increase of σ with W_s is apparent as the solids flux exceeds 200 kg/m^{2}s, but its rate of increase (from 10 to 50 Pa/m as the solids flux increases from 200 to 300 kg/m^{2}s), is comparatively small. In accordance with the other pressure gradient fluctuation data obtained (Figs. 4.1.2 to 4.1.5), there is an increase of σ with W_s, and a small but detectable increase of σ with U_g at constant W_s.

Some experimental data was collected at a line inclination of 17° for the glass beads. Preliminary trends observed were similar to those for 7°, but there was insufficient data available to make clear conclusions.

It seems that a plot of σ with W_s and U_g may be a suitable alternative for on-line estimation of the choking transition. The method seems to be generally applicable to all line orientations, and to different particle diameters. This graphical technique may be appropriate to non-slugging systems (such as the two described), which do not exhibit sharp transitions to choking at a unique gas velocity for all solids fluxes.

4.2 EFFECT OF SOLIDS HOLDUP ON SLIP VELOCITY

Theoretical analyses disclaiming the single particle terminal velocity slip

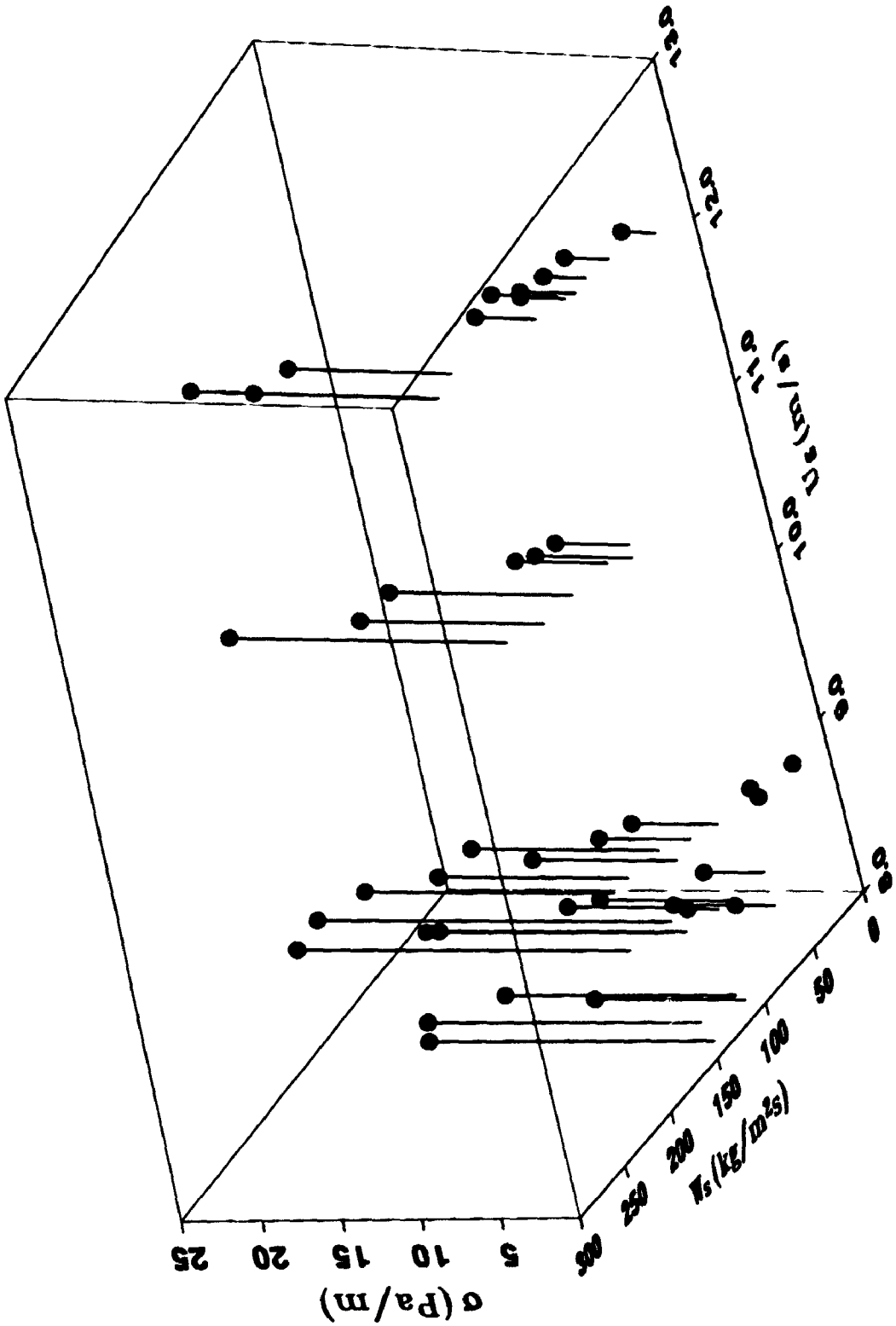

Fig. 4.1.6: Standard Deviation, σ, of Pressure Gradient Fluctuations
Glass Beads in 7° Orientation

velocity -in lieu of the cluster concept- have been put forth by Yang (1983) and Matsen (1982). High-speed video evidence has confirmed the presence of clusters (Li et al., 1990; Takeuchi and Hirama, 1991; Arena et al., 1992).

In a recent study (Yang et al., 1993), it has been shown that the slip velocity based on the simple definition of equation 28 (Section 2.9) grossly over estimates the actual slip velocity in a CFB. Based on their research it is now known that the slip velocity profile is flat through the core of the tube, but increases rapidly near the pipe wall, where there is a solids annulus. Yang et al. (1993) also noted that although the difference between the apparent slip velocity and the actual slip velocity is very high, most of the difference is attributed to radial segregation, and only a small fraction is related to cluster formation.

Based on the work of Yang et al. (1993) and others, it is now known that single small particles have no identity except in cases of very dilute transport where the solids loading would be less than 1.

4.2.1 APPARENT SLIP VELOCITY FOR SAND PARTICLES

The apparent slip velocity was computed using equation (28), §2.9.2. For the sand particles used in this work the terminal velocity is 1.5 m/s, while for glass beads it is 3.4 m/s. Fig. 4.2.1 shows the slip velocity versus solid

Fig. 4.2.1 : Slip Velocity vs. Sand Holdup
Vertical Line Orientation

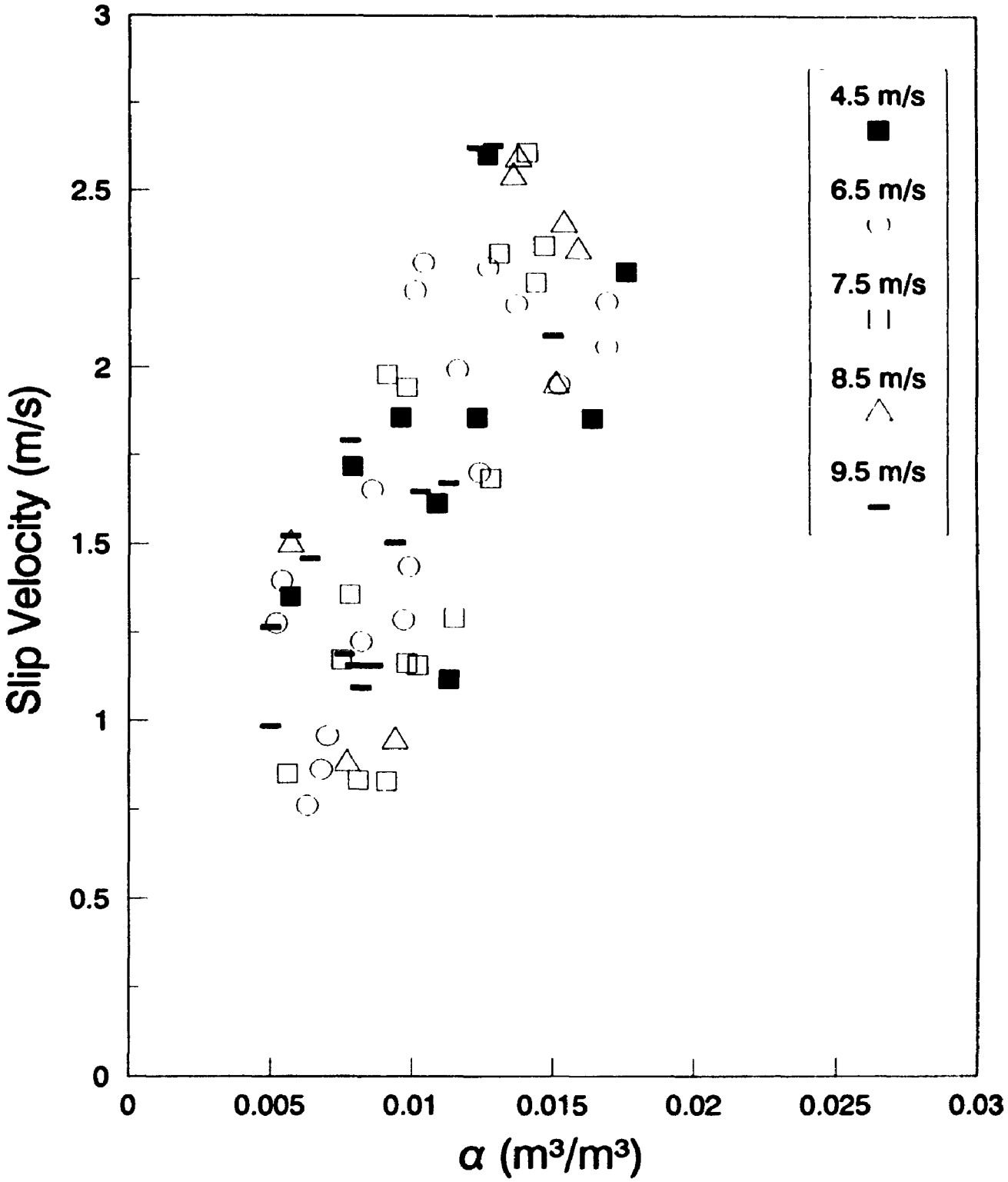

holdup for sand particles in the vertical riser. The slip velocity increases linearly with a solids volumetric holdup of up to 0.02, and is not affected by gas velocity. There is some scatter of the data, but this is expected due to the multiple sources of experimental error that can be attributed to U_{slip} and U_p (equation 26).

In some cases the slip velocity is less than 1.5 m/s, (the terminal velocity), which is not surprising because the terminal velocity is based on the average particle size. From Fig. 2.10.1, it is obvious that there is a large distribution of particles, of which about 5% were less than the Sauter mean diameter.

Fig. 4.2.2 shows the effect of α on the slip velocity of sand particles for a line inclination of 4°. The slip velocity increases linearly for $\alpha < 0.015$. The decreased rate of slip velocity rise (at a slip velocity of 2.5 m/s and a solids holdup of 0.02), may represent a change of hydrodynamic flow conditions as choking is approached. Particles move closer together, and the more aerodynamic configuration of the particle clusters reduces drag, and decreases the rate of increase of slip velocity with solids holdup (Rhodes et al., 1992c). Yang et al. (1993) also found that the local slip velocity increase with the solids holdup is nonlinear, and that it levels off above a solids holdup of about 0.02.

Fig. 4.2.2 : Slip Velocity vs. Sand Holdup
4° Inclined Line Orientation

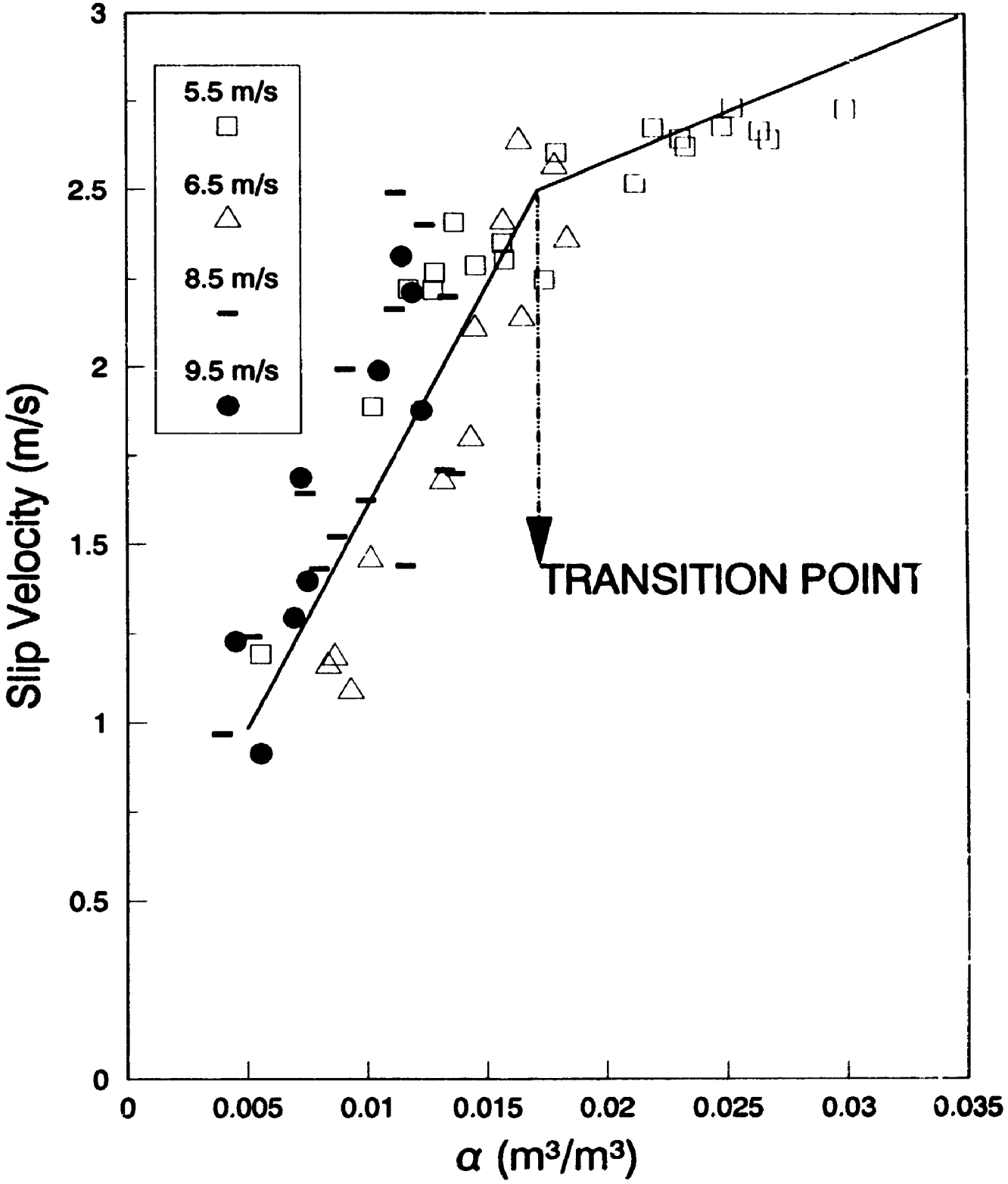

Fig. 4.2.3 shows the slip velocity versus solids holdup on the slip velocity at 11° for sand particles. A transition point, similar to that observed at 4°, is observed at a slip velocity of 3 m/s and at a solids volumetric holdup of 0.012. The transition occurs at a lower solids holdup and at a higher slip velocity than that observed for 4°. The rate of increase of slip velocity with solids holdup is 1.5 times that observed in Fig. 4.2.2 (for the 4° line) before the transition. The slip velocity increases further to about 5 m/s at a solids holdup of 0.03 after the transition point. The data agrees with the prediction of Al Taweel et al. (1989), who found that the ratio of aggregate terminal settling velocity to particle terminal velocity (for the types of particles used in this study) was about 2 to 3. Patience et al. (1992) observed a ratio of 2 for riser flow under a wide variety of operating conditions.

Fig. 4.2.4 shows the effect of solids holdup on the computed slip velocity at a line inclination of 18°. The initial increase of slip velocity to the transition point is 2.3 times faster than that observed in Fig. 4.2.2 (at 4°). A slip velocity of 4 m/s is observed at a solids volumetric holdup of about 0.011 for the 18° line. The slip velocity increases to a maximum of about 4.7 m/s for solids holdups exceeding 0.02. Slip velocities above 2.5 m/s are observed for the low gas velocity range below 7.5 m/s, where there is annulus formation with refluxing visually observed.

Fig. 4.2.3 : Slip Velocity vs. Sand Holdup
11° Inclined Line Orientation

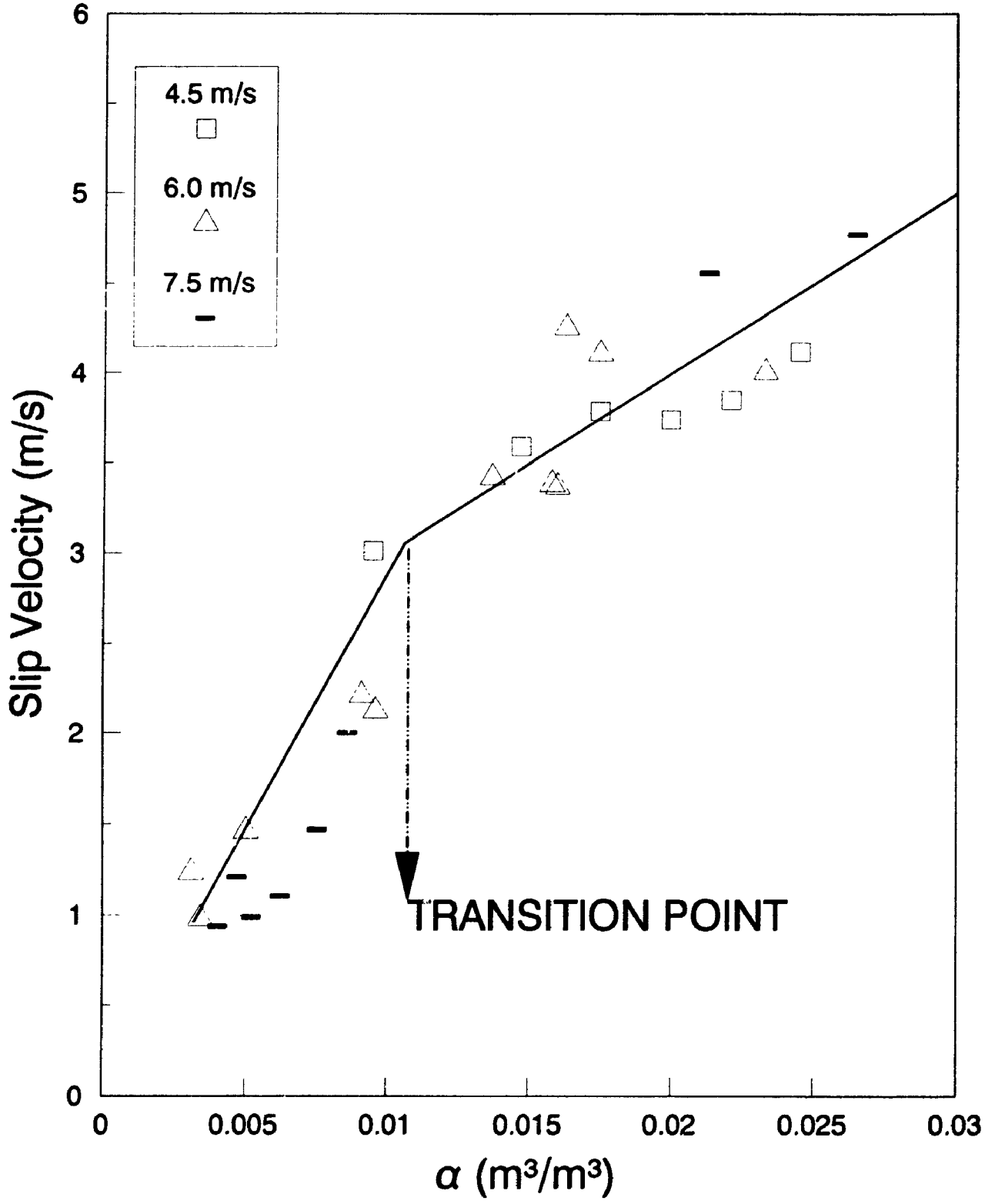

Fig. 4.2.4 : Slip Velocity vs. Sand Holdup 18° Inclined Line Orientation

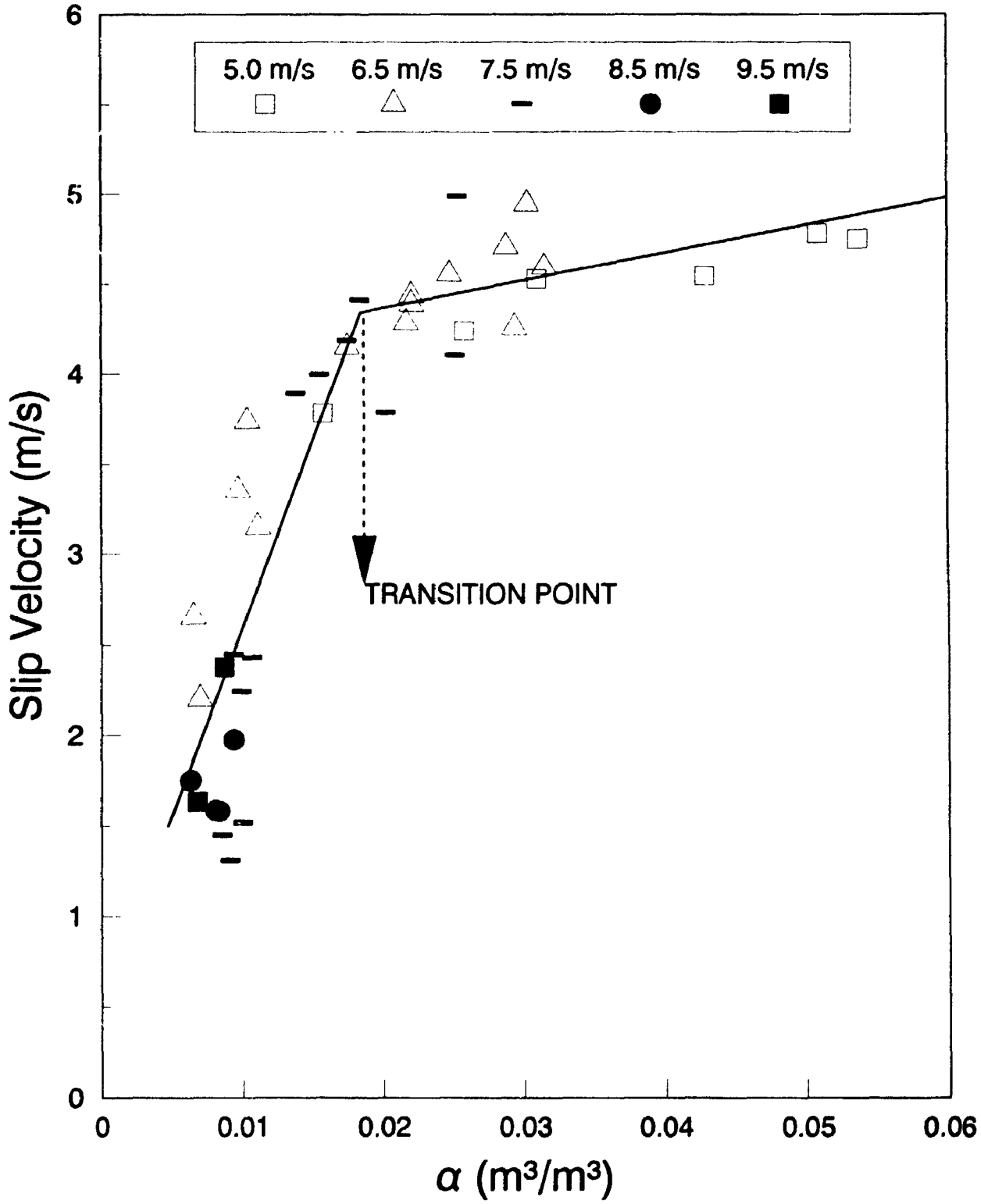

4.2.2 SPECULATION ON THE NATURE OF THE TRANSITION POINT

The transition point detected in Figs. 4.2.2 to 4.2.4 is thought to represent the change of hydrodynamic flow conditions from dilute dispersed flow, to cluster flow with solids deposition and refluxing. The solids deposition can be attributed to stable clusters of particles which migrate to the pipe wall. The clusters are thought to form as a result of the tendency of multiphase systems to reorganize themselves in order to minimize energy dissipation and maximize entropy generation (Al Taweel et al., 1989). In comparison to the aggregates formed by chemical and/or electrostatic forces which are quite strong, the forces holding a hydrodynamic aggregate together are quite small.

The initial increase of slip velocity is due to clustering as the density of the suspension increases. Eventually, at a solids holdup of about 0.01 (depending upon the line inclination), the clusters of particles migrate to the wall. Finer particles remain in the core of the pipe, with some of them travelling up to twice the average gas superficial velocity (Yang et al., 1993). For those particles deposited at the wall, the velocity is temporarily zero. Refluxing particles would actually subtract from the net upwards velocity vector. The combination of some particles moving faster than the gas, and some refluxing down, eventually reaches a stable equilibrium.

Rhodes et al. (1991) have found that the deposited particles at the wall descend in the form of swarms with voidages in the range of 0.8 to 0.93, with a downwards velocity of about 0.3 to 1.0 m/s. This phenomenon would lower the apparent computed particle velocity, thereby increasing the computed slip velocity. The number of these quasi-stationary particles is expected to increase with line inclination because the under side of the pipe wall is capable of sustaining more deposited particles at higher line inclinations. This, in turn, would lead to more refluxing and a lower net average upwards particle velocity component. The number of deposited particles could be expected to rise with a decreasing gas velocity at constant solids holdup, since solids refluxing is more severe at lower gas velocities.

4.2.3 SLIP VELOCITY FOR GLASS PARTICLES

Fig. 4.2.5 shows the effect of slip velocity versus solids holdup for glass beads in the vertical orientation. Unlike sand particles in the vertical orientation (Fig. 4.2.1), the slip velocity is affected by the gas velocity. For the range of gas velocities below 9 m/s, the slip velocity increases linearly for $\alpha < 0.02$. For gas velocities above 9 m/s, the slip velocity continues to increase with the solids holdup. A maximum slip velocity of about 9 m/s is observed for a gas velocity of 12.5 m/s; no maximum is observed for the 16 m/s gas velocity data.

Fig. 4.2.5 : Slip Velocity vs. Glass Holdup Vertical Line Orientation

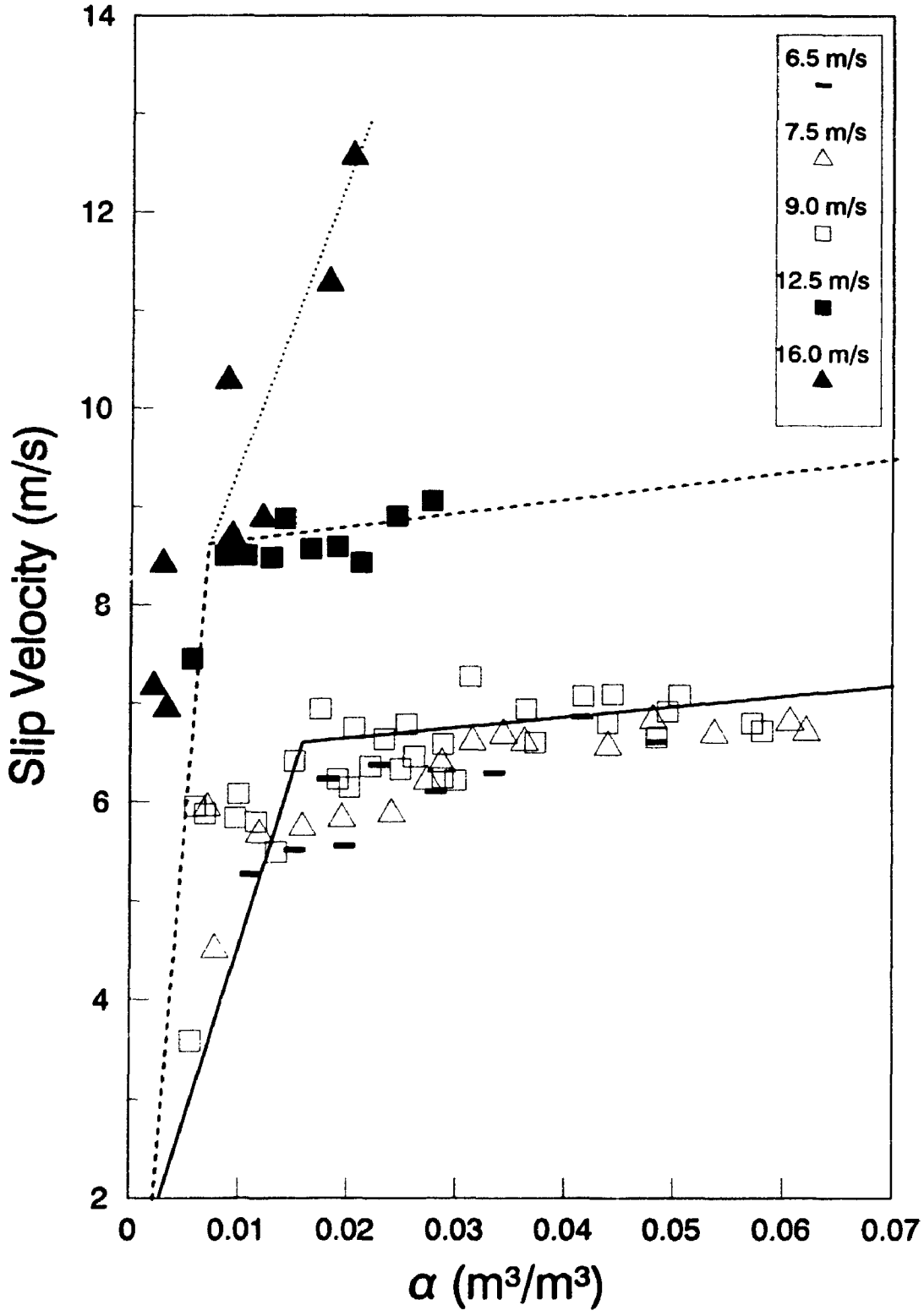

Unlike the case for sand, a transition point is observed for the glass beads in the vertical orientation (Fig. 4.2.5). The cause of the transition point is thought to be linked to annulus formation and refluxing at the wall. The deposition of particles in the vertical line orientation can be better understood if it is considered that the dominant forces which govern the transverse transport of particles are the turbulent diffusion force (pushing the particles to the wall) and the drag force, which opposes the particle motion (Lee, 1991). If the particle is pushed radially outward by the diffusion force, while being resisted by the drag, it will bounce off the wall. On its way back into the fluid it is further slowed by the drag, and its longitudinal momentum decreases to zero, because of the slow-moving fluid at the wall.

Similar characteristics are observed for a line inclination of 7° (Fig. 4.2.6). A slip velocity of 6 m/s is observed (for gas velocities below 9 m/s), which increases to 9 m/s for gas velocities above 11 m/s. For both the sand and glass particles the transition point occurs at about 1% solids holdup. The effect of solids holdup on the slip velocity for a line inclination of 17° is shown in Fig. 4.2.7. Because of the limited pool of data for this line inclination, no transition point was observed.

Although the computed slip velocity data shown in Figs. 4.2.1 through 4.2.7

Fig. 4.2.6 : Slip Velocity vs. Glass holdup
7° Inclined Line Orientation

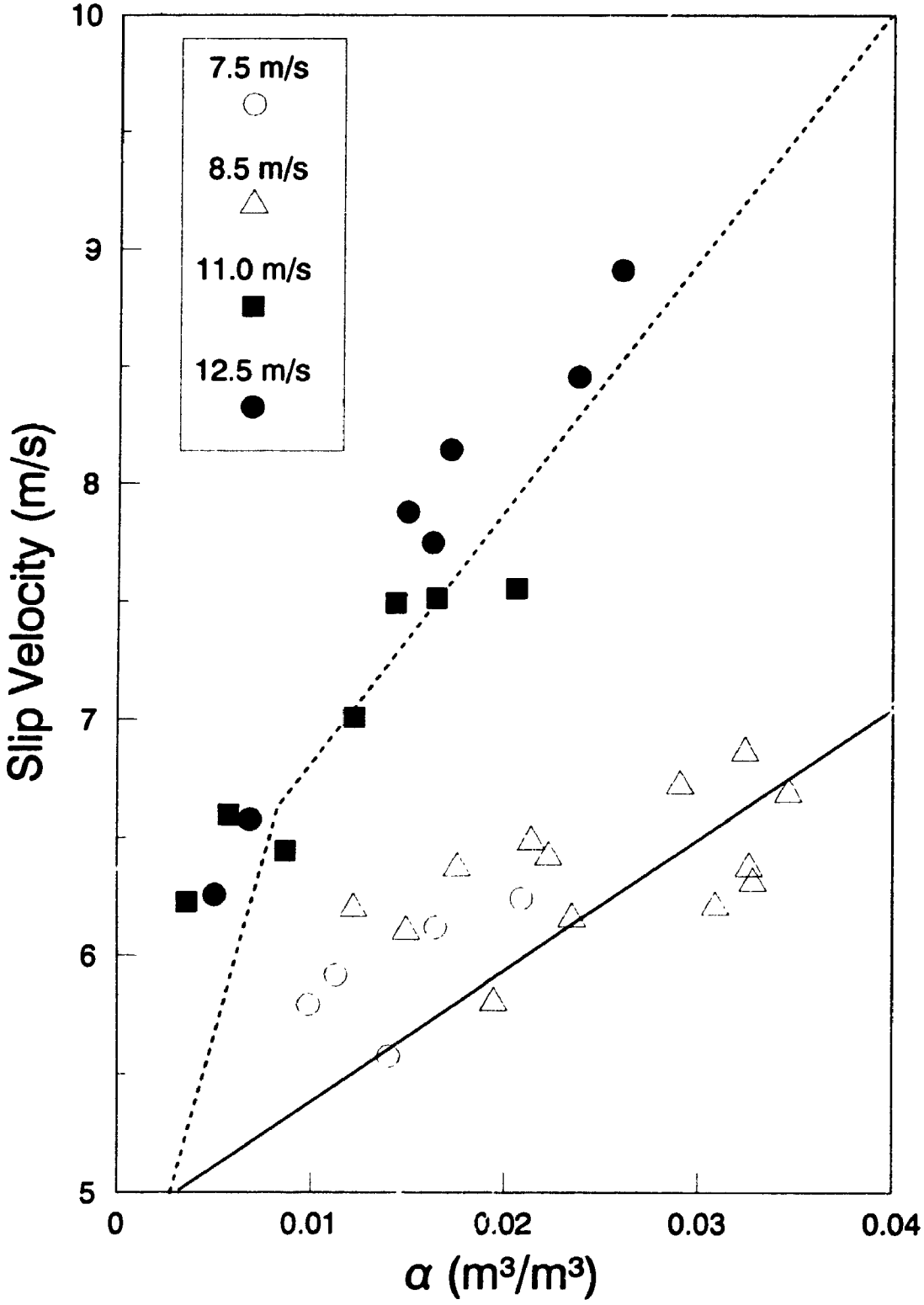

Fig. 4.2.7 : Slip Velocity vs. Glass Holdup
17° Inclined Line Orientation

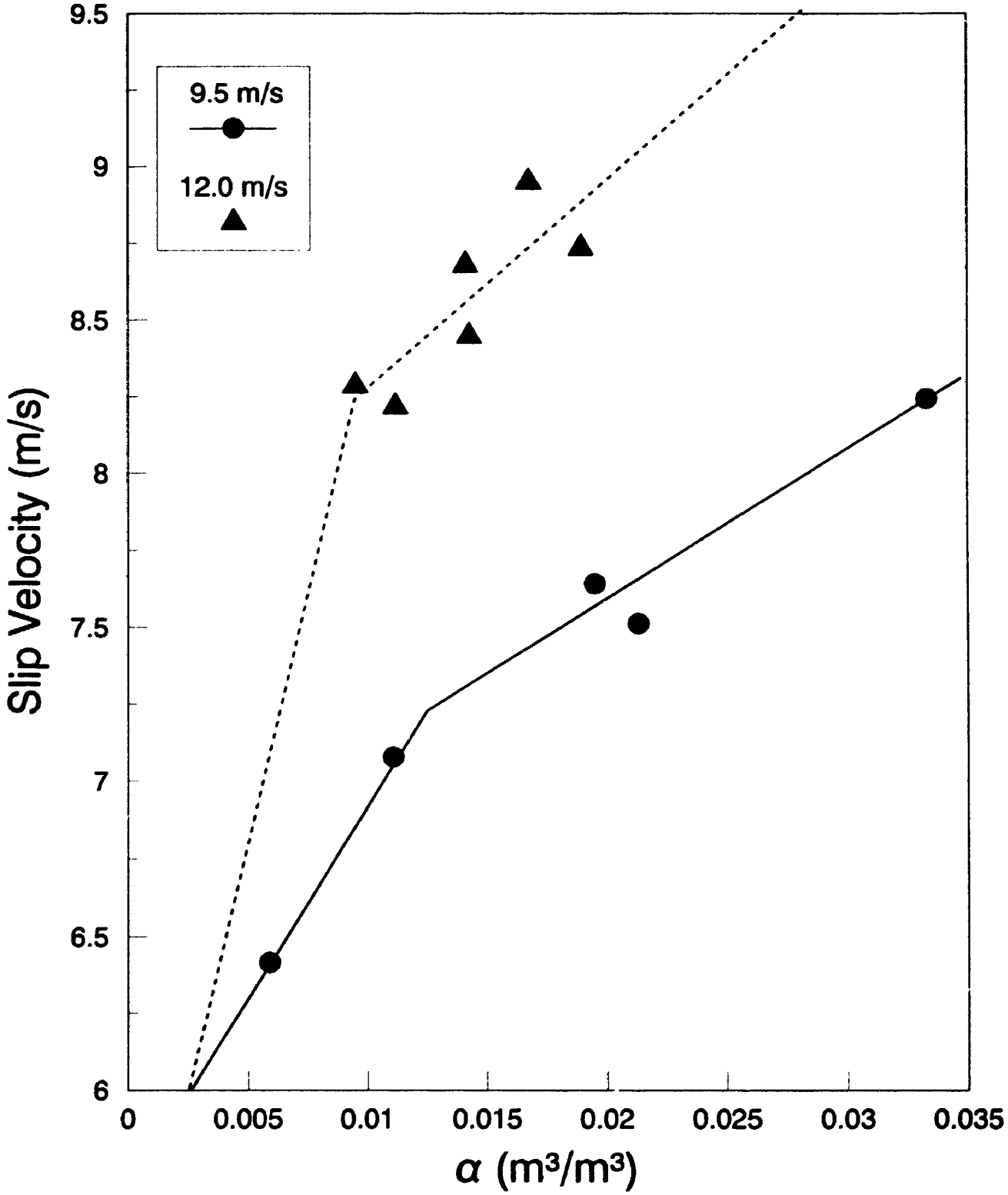

are based on equation (28), which is known to over estimate the actual slip velocity (Yang et al., 1993), it does show that the effects of line inclination and particle diameter on the slip velocity are significant.

4.3 LIFTING EFFICIENCY

Previous work in both the dilute and dense phase flows of pneumatic transport has not investigated the impact of operating conditions on the lifting efficiency of the particles being transported. The importance of lifting efficiency can not be under estimated in engineering applications, where the economic ramifications of scale-up must carefully be considered. In this research a variety of different forms of lifting efficiency were derived (Appendix E), which were subsequently used to characterise the flow regime investigated. The concept of lifting efficiency was then applied for comparison between the non-slugging dense phase transport data (this research) with dilute phase transport in inclined lines (Zaltash, 1987) in § 4.3.5.

4.3.1 DEFINITIONS OF LIFTING EFFICIENCY

A gross lifting efficiency, η_{gross} (derivation in Appendix E), can be defined by equation (40a).

$$\eta_{gross} = \frac{\left(m^{*}\rho_g \, g\cos\theta \right)}{\left(- \frac{\partial P}{\partial Z} \right)} \qquad \textbf{(40a)}$$

A single particle lifting efficiency, η_p, (whose derivation is given in Appendix E), can be defined in equation (40b).

$$\eta_p = \left(1 - \frac{U_t}{U_g} \right) \qquad \textbf{(40b)}$$

A net lifting efficiency, η_{net} (derivation in Appendix E), can be defined by equation (40c).

$$\eta_{net} = \frac{\left(m^{*}\rho_g \, g\cos\theta \right)}{\left(- \frac{\partial P}{\partial Z} \right) - \left(- \frac{\partial P_g}{\partial Z} \right)} \qquad \textbf{(40c)}$$

Equation (40a), which computes the gross lifting efficiency, η_{gross} , represents the gain of potential energy of solids divided by the rate of energy expenditure of the gas. This is the form used for comparison of the various flow regimes in this research. The net lifting efficiency (η_{net} ,equation 40c) corrects the denominator of the gross efficiency term by subtracting the gas-wall friction term. The various line inclinations given here were computed using the FORTRAN program LIFTD2 in Appendix D.

4.3.2 ENERGY DISSIPATED

The energy dissipated in the pneumatic transport of particles was computed by dividing the net lifting efficiency by the particle lifting efficiency, and subtracting this fraction from 1 (equation 40d). When expressed as a percentage, the expression represents the percentage of energy that was dissipated as frictional energy losses.

$$E_{DISS\%} = \left(1 - \frac{\eta_{NET}}{\eta_{PARTICLE}} \right) * 100\% \qquad (40d)$$

4.3.3 MEAN AND STANDARD DEVIATION OF GROSS LIFTING EFFICIENCY

It was found from extensive statistical correlation analyses (Appendices F1 to F3) that the (net) lifting efficiency (equation 40c) was not significantly correlated with either the solids flux or the gas velocity for the sand particles. As a result of this noncorrelation, the mean lifting efficiency (with standard deviation, $\sigma[\eta_p]$) was subsequently calculated. Table 4.3.1 shows the data for both the sand and glass particles. For sand, it is apparent that η_{gross} decreases with line inclination from 53.5 ± 7.6% (vertical) to 32.2 ± 7.3% at 18°. For glass, however, the same trend with θ was not apparent. The mean value of η_{gross} remained constant at about 25 to 30%, and was invariant with θ within the range of uncertainty.

Table 4.3.1: Mean and Standard Deviation of Gross Lifting Efficiency, η_{gross} and Particle Lifting Efficiency, $\eta_{particles}$

PARTICLE	θ (°)	η_{gross} (%)[1]	$\sigma(\eta_{gross})$%[2]	$\eta_{particle}$(%)[3]	$\sigma(\eta_{p})$%[4]
SAND	0	53.5	7.6	79.1	4.9
SAND	4	49.7	8.5	80.4	6.1
SAND	11	35.3	6.2	78.5	3.8
SAND	18	32.2	7.3	80.8	3.7
GLASS	0	25.2	9.3	60.5	9.3
GLASS	7	30.2	14.9	60.6	6.8
GLASS	17	24.2	7.3	65.3	4.5

The value of η_{gross} can be compared with the particle lifting efficiency, $\eta_{particle}$ in Table 4.3.1. For sand particles $\eta_{particle}$ is about 80% at all line inclinations, while for glass, $\eta_{particle}$ is approximately 60%. Hence, the gross lifting efficiency is significantly lower than $\eta_{particle}$.

---

[1] Gross lifting efficiency, from equation (40a).

[2] Standard deviation of gross lifting efficiency.

[3] Particle lifting efficiency, from equation (40b).

[4] Standard deviation of particle lifting efficiency.

Fig. 4.3.1 shows a PDF of η_{gross} for sand particles at all line inclinations. The ordinate represents the percentage of experiments at a given value of η_{gross}. As θ increases it is apparent that the PDF progressively shifts toward the lower values.

Fig. 4.3.2 shows the equivalent PDF for glass beads. In this case, however, there is a less significant trend of η_{gross} with θ, which is corroborated by the results of Table 4.3.1.

Fig. 4.3.3 compares the value of η_{gross} for both the non-slugging dense phase (this thesis) with dilute phase data compiled from the raw pressure gradient data given by Zaltash (1987). For both cases (Fig. 4.3.3), the particle diameter was a nominal 450 μm in diameter and had a density of about 2400 kg/m^3. The only other difference between the two sets of data was that the non-slugging data was obtained in a 0.03175 m tube, while the dilute phase data (Zaltash, 1987) was gathered from a 0.0504 m tube. The PDF of gross lifting efficiency for dilute phase data is lower than that for non-slugging dense data. The average of the distribution for dilute phase data is 11.8 ± 6.3% (Table 4.3.2); in comparison, η_{gross} for the non-slugging phase (Table 4.3.1) is 25.2 ± 9.3%. Clearly, the efficiency of lifting for vertical pneumatic transport is higher in the non-slugging dense phase.

Fig. 4.3.1: PDF of Gross Lifting Efficiency

Sand Particles at All Line Inclinations

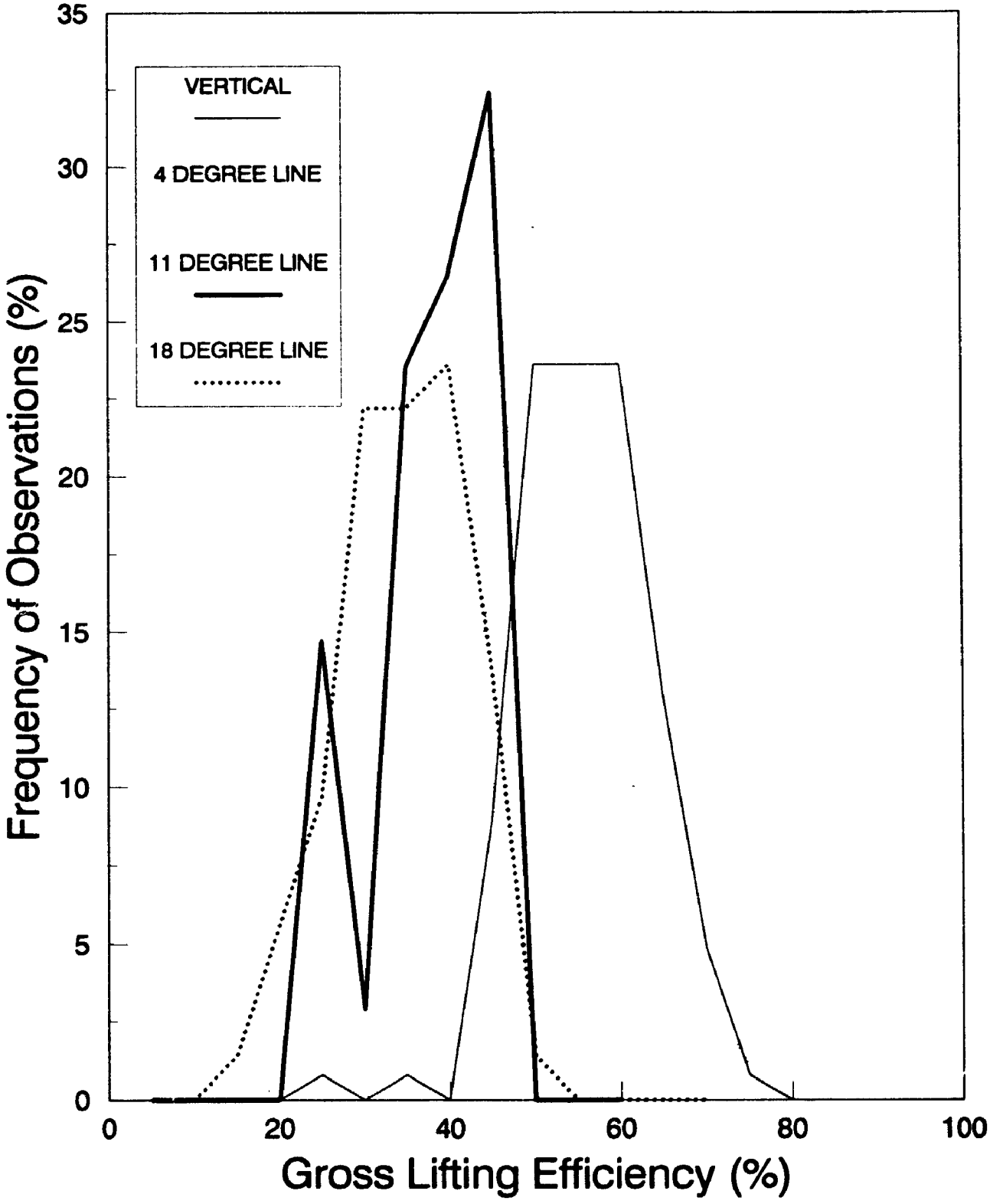

Fig. 4.3.2: PDF of Gross Lifting Efficiency

Glass Beads at All Line Inclinations

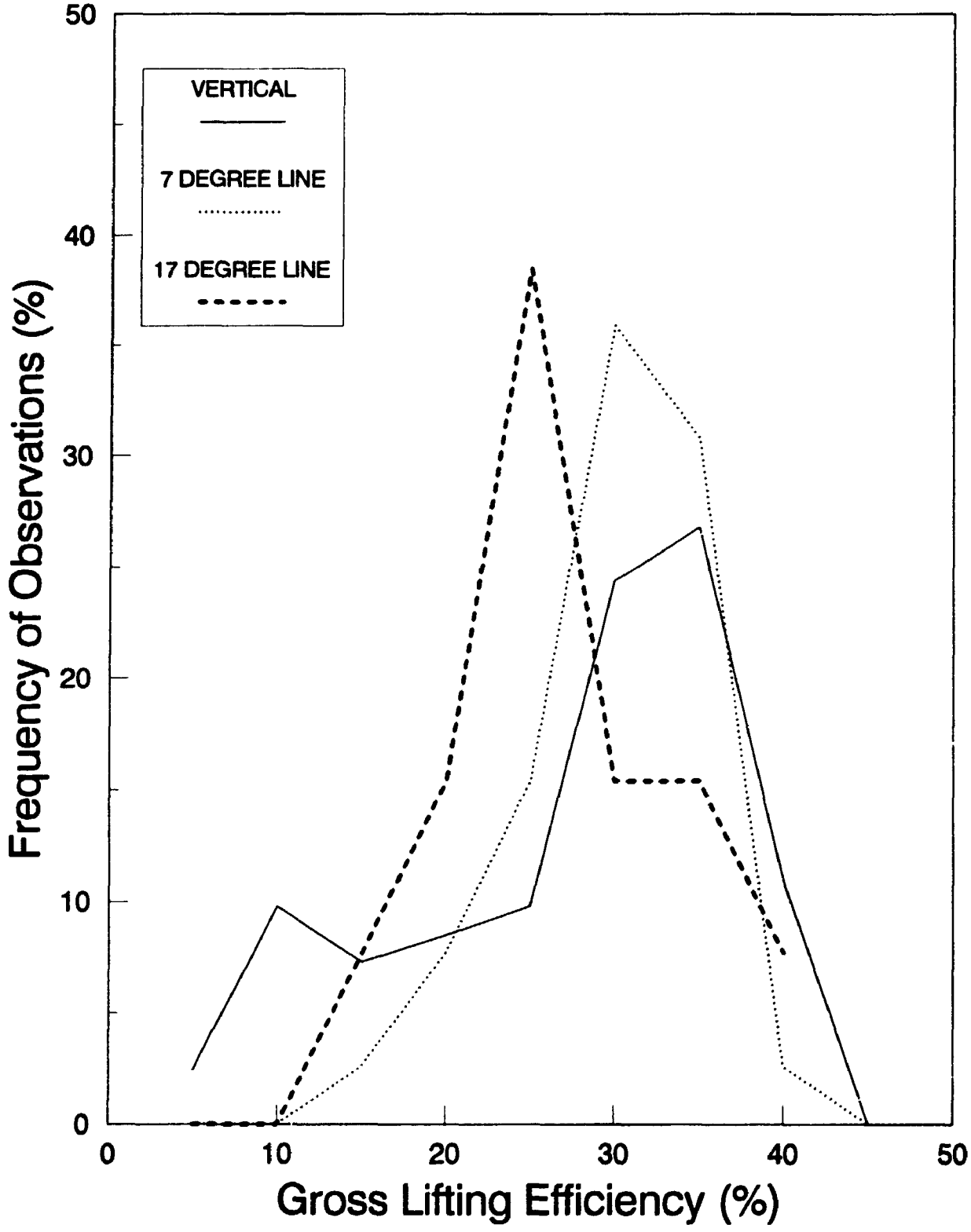

Fig. 4.3.3: Gross Lifting Efficiency Comparison

Dilute Phase vs. Non-Slugging Dense Phase, Vertical Transport

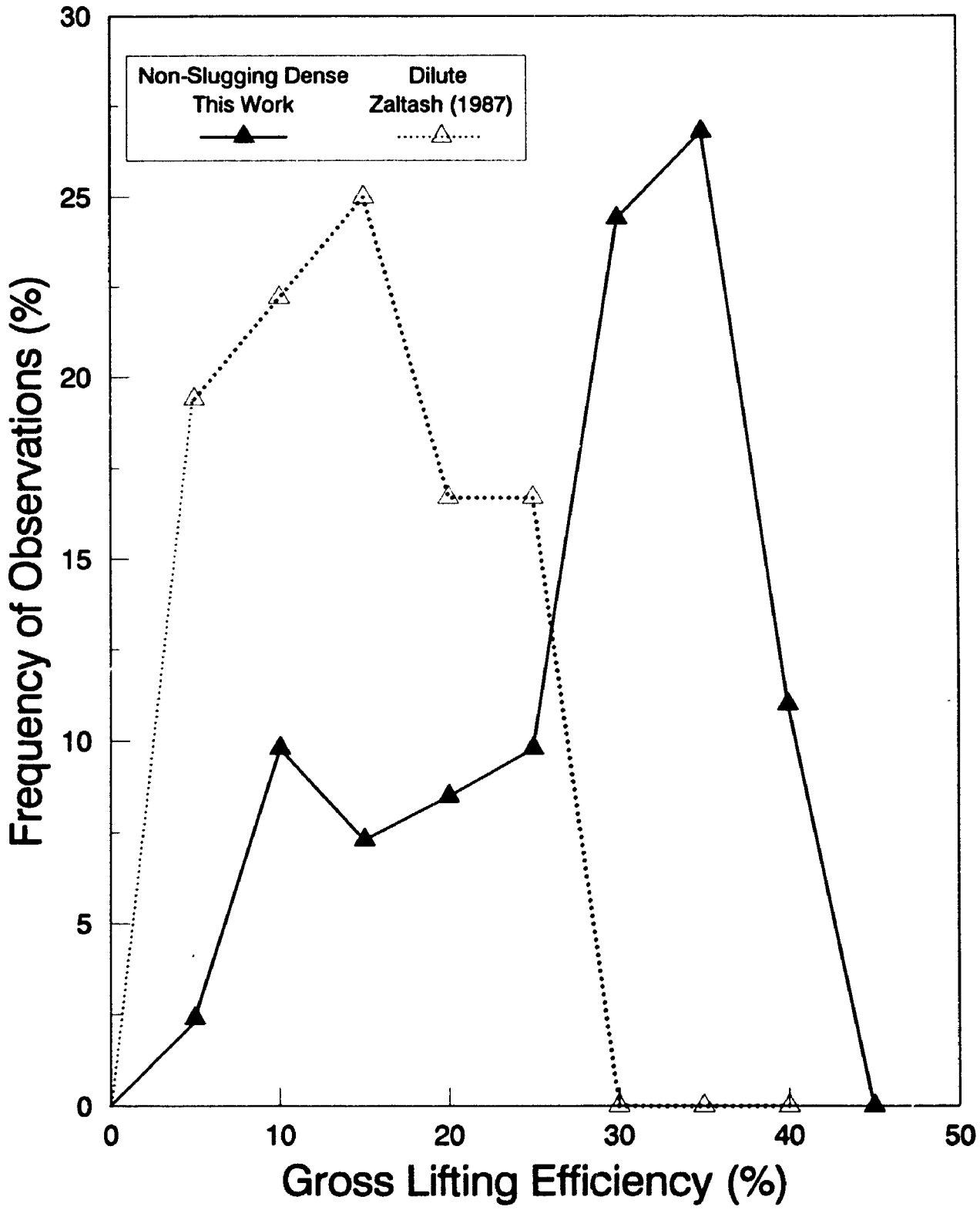

The correlation of dilute phase gross lifting efficiency (η_{gross}) with the controlled variables (used by Zaltash) is shown in Appendix F4. The gross lifting efficiency is shown for the upper hemisphere of the pipe ($\eta_{gross,\,U}$) and the lower hemisphere ($\eta_{gross,\,L}$). In the lower hemisphere of the pipe, $\eta_{gross,\,L}$ was correlated significantly (-0.31) with line inclination (from the horizontal), gas velocity, U_g (-0.37), and the particle velocity, $U_{P,L}$ (-0.32). For the upper hemisphere of the pipe, $\eta_{gross,\,U}$ was correlated with line inclination (0.65) and solids flux, $W_{S,U}$ (0.70).

4.3.4 DILUTE PHASE LIFTING EFFICIENCY COMPARISON

Table 4.3.2 compares the average gross lifting efficiency for various conditions used for dilute phase transport by Zaltash (1987). The gross lifting efficiency was computed using equation (40a) for all of the experimental conditions covered by Zaltash (1987) for dilute phase transport. For the purposes of this table, the line inclination, θ, is measured from the *horizontal*.

The gross lifting efficiency, $\bar{\eta}_{gross}$, is less than 10% for most of the conditions where the line is not vertical (90°). The exception is at 30°, and for a particle diameter of 67 μm, where $\bar{\eta}_{gross} = 13.3 \pm 10.8\%$. However, based on the large magnitude of the standard deviation it seems likely that this may be a spurious result. For comparison, at 45° the value of $\bar{\eta}_{gross} = 6.9 \pm 5.0\%$

for the same 67 μm particles.

Table 4.3.2: Comparison of Gross Lifting Efficiency for Dilute Phase Transport Data, Computed from Zaltash (1987)

θ (°)	d_p (μm)	D (m)	ρ_p (kg/m^3)	η (%)	σ (η_{gross} %)
30	900	0.0504	2464	6.6	4.3
30	900	0.0266	2464	5.3	3.6
30	450	0.0504	2395	6.8	3.9
30	450	0.0266	2395	6.1	3.9
30	400	0.0504	5004	6.1	4.6
30	400	0.0266	5004	5.9	3.7
30	67	0.0504	2470	13.3	10.8
30	67	0.0266	2470	8.7	8.9
45	900	0.0266	2464	6.3	3.9
45	450	0.0266	2395	6.3	4.3
45	400	0.0266	5004	5.7	3.4
45	67	0.0266	2470	6.9	5.0
60	900	0.0504	2464	1.3	0.8
60	450	0.0504	2395	1.5	0.9
60	400	0.0504	5004	1.2	1.8
60	67	0.0504	2470	2.3	1.1
90	900	0.0504	2464	15.0	7.5
90	450	0.0504	2395	11.8	6.3
90	400	0.0504	5004	38.2	13.8
90	67	0.0504	2470	24.4	10.4

For the vertical line the efficiency increases to 38.2 ± 13.8 % for 400 μm

particles, with a density of 5004 kg/m^3. It is evident that η_{gross} decreases as the line is inclined from the vertical position. Moreover, it seems that there is a local minimum of lifting efficiency at 60° from the horizontal orientation. There is no significant effect of tube diameter or particle diameter. It seems, therefore, that the lifting efficiency is primarily influenced by the line inclination and the gas velocity.

4.3.5 NET LIFTINC EFFICIENCY IN NON-SLUGGING DENSE PHASE

The net lifting efficiency, η_{net}, was computed for all of the data in this research using equation (40c). The variation of η_{net} with line inclination (from the vertical), and solids loading (kg solid/kg air) is shown in Fig. 4.3.4 for the sand particles. The graph shows a 3-dimensional representation of η_{net} with solids loading and line inclination, θ. A linear least squares regression plane has been drawn through the experimental data points. The deviation of the least squares estimate with the data is indicated by vertical lines connecting the data to the plane. The value of η_{net} decreases continuously with θ, and is mildly affected by the solids (sand) loading. The decrease of η_{net} with θ ($\leq 18^0$) is in agreement with the results of Zaltash (1987) for the dilute phase transport conditions.

Fig. 4.3.5 shows the effect of θ and solids loading on η_{net} for the glass beads in non-slugging dense phase transport conditions studied in this research.

Fig. 4.3.4: Lifting Efficiency, η_{net}, for Sand Particles
Effects of Line Inclination, θ, and Solids Loading, Γ

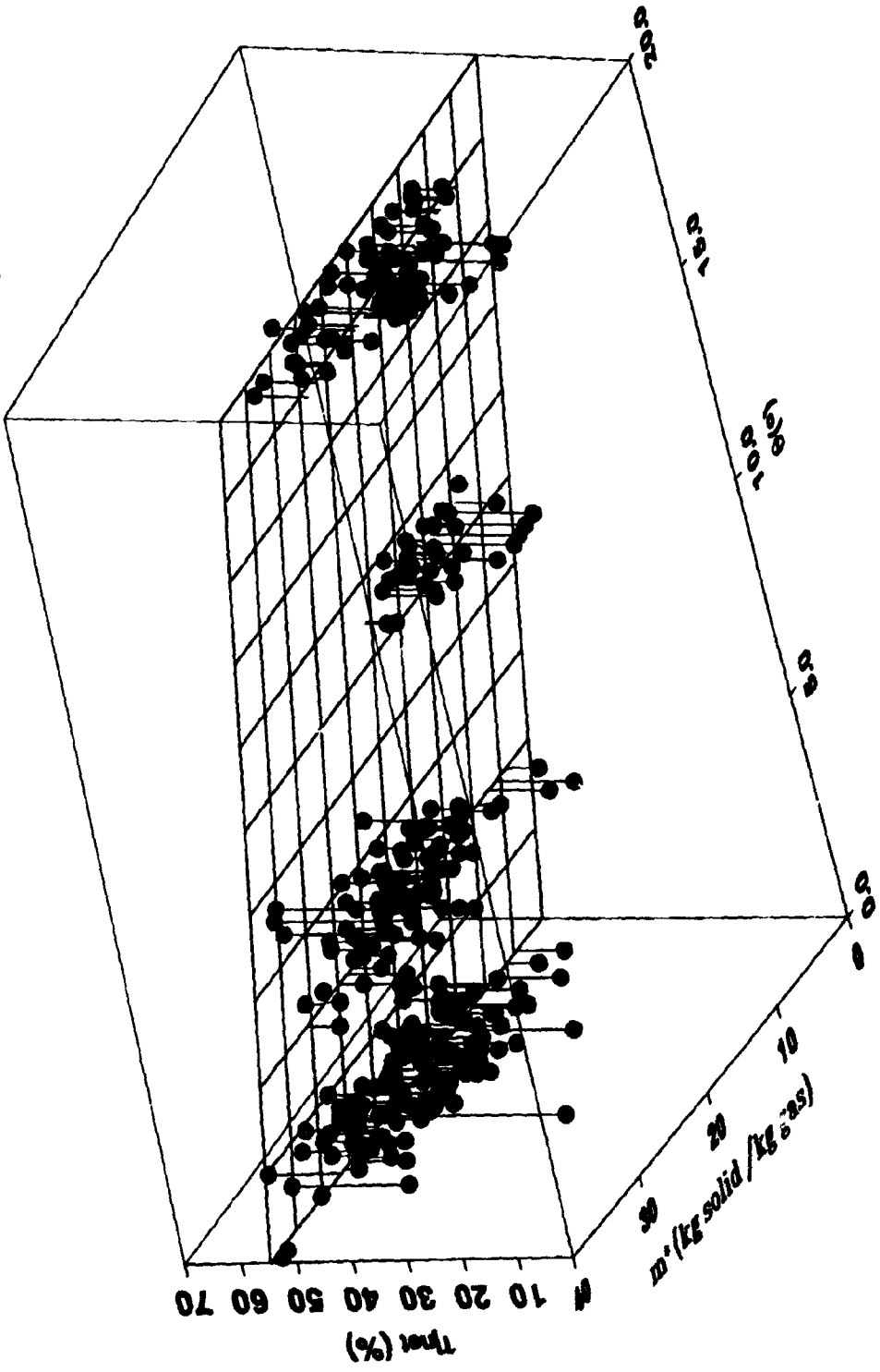

Fig. 4.3.5: Lifting Efficiency, η_{net}, for Glass Particles
Effects of Line Inclination, θ, and Solids Loading, m'

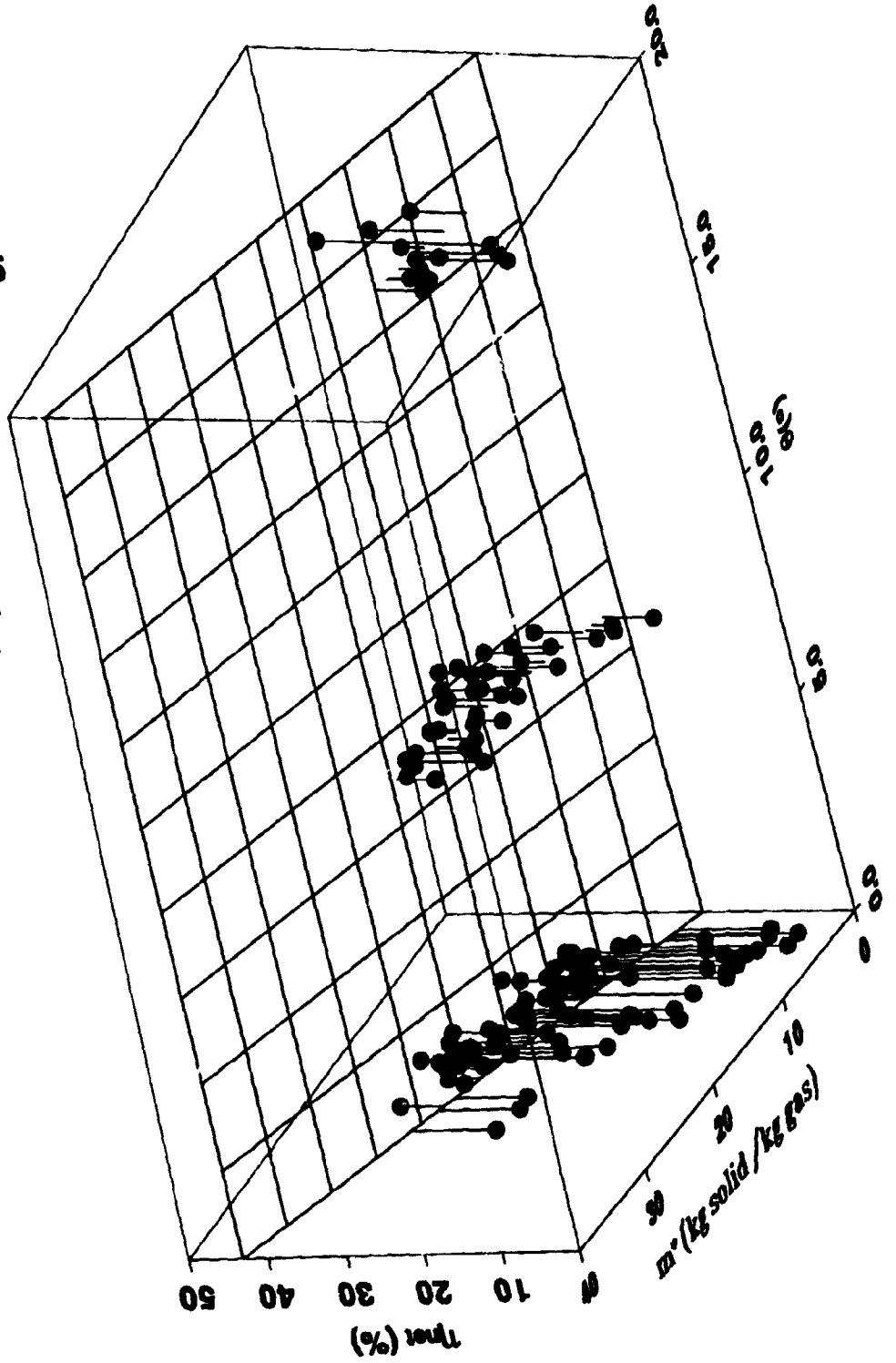

The variation of η_{net} with θ is minimal, but the effect of solids loading is much more prominent than that observed for sand. The value of η_{net} decreases from about 35% to less than 10% as the solids loading decreases from 25 to 5. The lifting efficiency increases as the suspension becomes denser at higher mass loadings.

Line inclination may not be a factor for the lifting efficiency of glass beads (Fig. 4.3.5) because there is massive amounts of solids refluxing at all line inclinations. In comparison, large refluxing tendencies were observed at 18° for the sand particles, but this phenomenon was not significant for line inclinations of less than 11°.

4.4 RESIDUAL PRESSURE GRADIENT

The total pressure drop in fully-developed 2-phase pipe flow is usually expressed as the sum of three components as defined by equation (41).

$$\Delta P_{total} = \Delta P_{HOLDUP} + \Delta P_{GAS|WALL} + \Delta P_{SOLIDS|WALL} \qquad (41)$$

$$\left(\frac{\Delta P}{L}\right)_{TOT} = \left(\frac{\Delta P}{L}\right)_{HOLDUP} + \left(\frac{\Delta P}{L}\right)_{GAS|WALL} + \left(\frac{\Delta P}{L}\right)_{SOLIDS|WALL} \qquad (42)$$

(i) *(ii)* *(iii)*

These terms are:

i) that due to solids holdup per unit length in the pipe;

ii) gas frictional unit pressure drop and;

iii) solids-wall pressure gradient or residual pressure gradient.

The residual pressure gradient, which is normally associated with solids-wall frictional forces, is used to define the solids friction factor, as given by equation (31b) in § 2.9.

4.4.1 ESTIMATION OF RESIDUAL PRESSURE GRADIENT

In the dense annular phase close to the choking velocity, the largest contribution of pressure gradient is from the solids holdup, component i (Rhodes et al., 1992a). Experiments in the current study indicate that the total fraction of pressure gradient that can be attributed to solids holdup increases with line inclination for $\theta > 4°$. Gas frictional pressure drop with the wall (ii) is a minor component of the total gradient, accounting for less than 10% in dense phase transport. It is computed by assuming single-phase empty pipe flow (Fig. 2.9.3).

The component of pressure gradient associated with solids-wall friction (or residual pressure gradient) is usually computed as the difference between the total gradient (which is known from experiment), and the sum of gas

frictional pressure drop (by correlation or experimentally measured for the gas velocity being considered), and solids holdup which is determined experimentally. Because of the solids deposition in inclined lines, the pressure gradient from solids holdup is over estimated in oblique risers, and the residual pressure gradient computed by difference has no physical meaning. Thus, the residual pressure gradient is relevant for the vertical riser orientation only.

4.4.2 RESIDUAL GRADIENT FOR SAND IN VERTICAL LINE

Fig. 4.4.1 shows a plot of the residual pressure gradient with solids flux for the vertical transport of sand particles. The residual gradient decreases from about 1000 Pa/m at a solids flux of 50 kg/m^{2}s, to -200 Pa/m at a solids flux of 250 kg/m^{2}s. When the residual gradient is divided by the total pressure gradient a "residual gradient per cent" is obtained. The average value of the residual gradient per cent for the sand particles was computed to be about 22%.

Van Swaiij et al. (1970) have found that the residual pressure drop is negative for suspension densities exceeding 50 kg/m^3, which is the range of mixture densities studied in this thesis. Boothroyd (1966) has shown that the sum of the solids phase pressure drop and gas phase pressure drop is lower than the estimated gas phase pressure drop alone. Miller and

Fig. 4.4.1: Residual Pressure Gradient for Sand Vertical Line Orientation

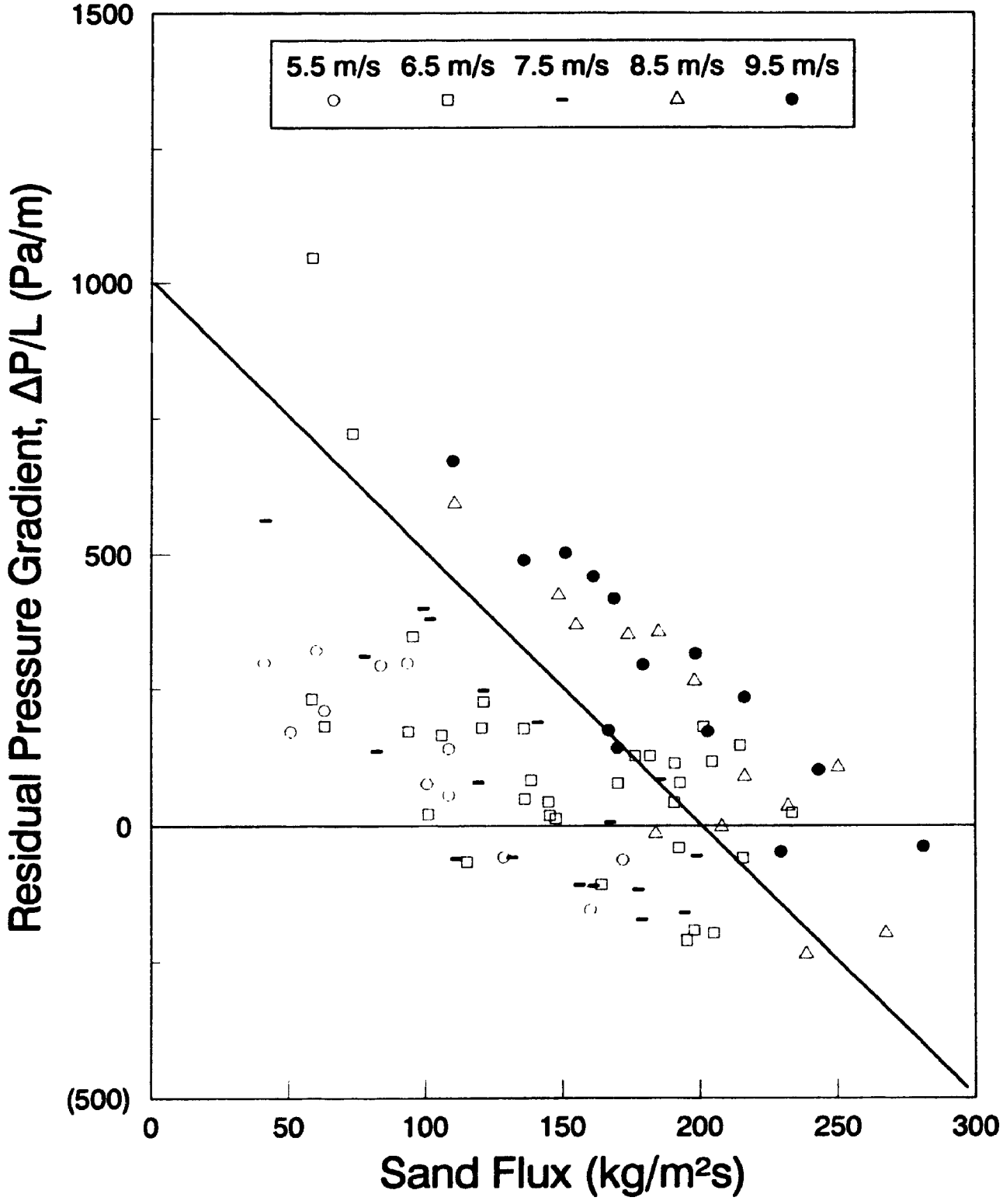

Gidaspow (1992) have found experimentally that the shear at the wall is always negative when there exists a down flowing annulus, as it must be for consistency with a no-slip or partial-slip wall boundary condition. Their experimental results confirmed the negative shear stress at the wall under conditions of solids reflux.

At higher flux the extent of solids reversal increases. The reversal of solids for fluxes above 100 kg/m^{2}s and holdups above 1%, leads to the negative residual pressure gradient and a negative solids-wall friction factor. A negative friction factor is reasonable under conditions of solids reversal since the solids at the wall are flowing opposite to the flow of the gas through the core of the tube. The direction of flow is determined primarily by the gas phase pressure gradient in the upper part of the duct, and by the axial component of gravity in the lower part (Ocone et al., 1993). The particle velocity decreases continuously from the core to the annular region at the wall (Wang et al., 1993).

Capes and Nakamura (1973) have found that negative pressure drops for solids-wall loss occurred for about 20% of the cases they studied, and these were concentrated near the choking velocity where there is extensive solids reflux. They showed the annular flow regime of gas-solids transport led to a lower line pressure drop because of solids down flow, and the resulting

negative pressure loss associated with that phenomenon.

The variation of data observed from Fig. 4.4.1 is not surprising since the residual is computed from three sources, all of which have errors associated with them. A slight error in the solids holdup can have a major impact upon the residual gradient, since the pressure gradient due to holdup is close in magnitude to the total pressure gradient. Miller and Gidaspow (1992) reported that there was up to 100% deviation observed in their study, between the observed residual pressure gradient and that calculated, based on the contributions from the solids holdup and gas-friction pressure drops in the test section of the vertical riser.

4.4.3 RESIDUAL GRADIENT FOR GLASS IN VERTICAL LINE

For glass beads the solids holdup collected between pinch valves represents a pressure gradient higher than the total pressure gradient due to extreme lateral segregation of particles with deposition. Because of the over estimation of the solids holdup contribution to the overall pressure gradient, the residual pressure gradient is under estimated, and is negative for all range of conditions studied for glass beads. Miller and Gidaspow (1992) have noted that although the pressure drop minus the weight of the bed can be negative, their results showed that the pressure drop minus the weight of the upflowing core was always positive, a necessary condition for upward

motion.

Fig. 4.4.2 shows a plot of the computed residual gradient versus the glass flux. Three sets of regression lines are represented : at 14.5 m/s (solid line), 8.5-11 m/s (dotted line), and less than 8 m/s (dashed line). Only for the highest gas velocity considered (14.5 m/s), is the residual gradient positive. For all other gas velocities the residual gradient decreases continuously with the solids flux. A residual gradient of -350 Pa/m was computed for a glass flux of 130 kg/m^{2}s, and gas velocities of 7 to 8 m/s. Between 8.5 to 11 m/s the residual gradient is -200 Pa/m for a glass flux of 200 kg/m^{2}s. In corroboration of these experimental results, Miller and Gidaspow (1992) have also noted that the residual pressure gradient becomes increasingly negative as the solids flux increases. Moreover, the magnitude of this residual gradient in their study, increased with the height in the vertical riser, to a maximum at about 4.5 m upstream of the test section. This is roughly the same length of line preceding the test section in this thesis research.

The residual gradient is negative over 95% of the time for the glass beads data shown in Fig. 4.4.2. Forty per cent of the experiments had a residual pressure gradient contribution of about -25%. Van Swaiij et al. (1970) observed residual gradients of -22% for the same range of conditions. They

Fig. 4.4.2 : Residual Pressure Gradient for Glass Vertical Line Orientation

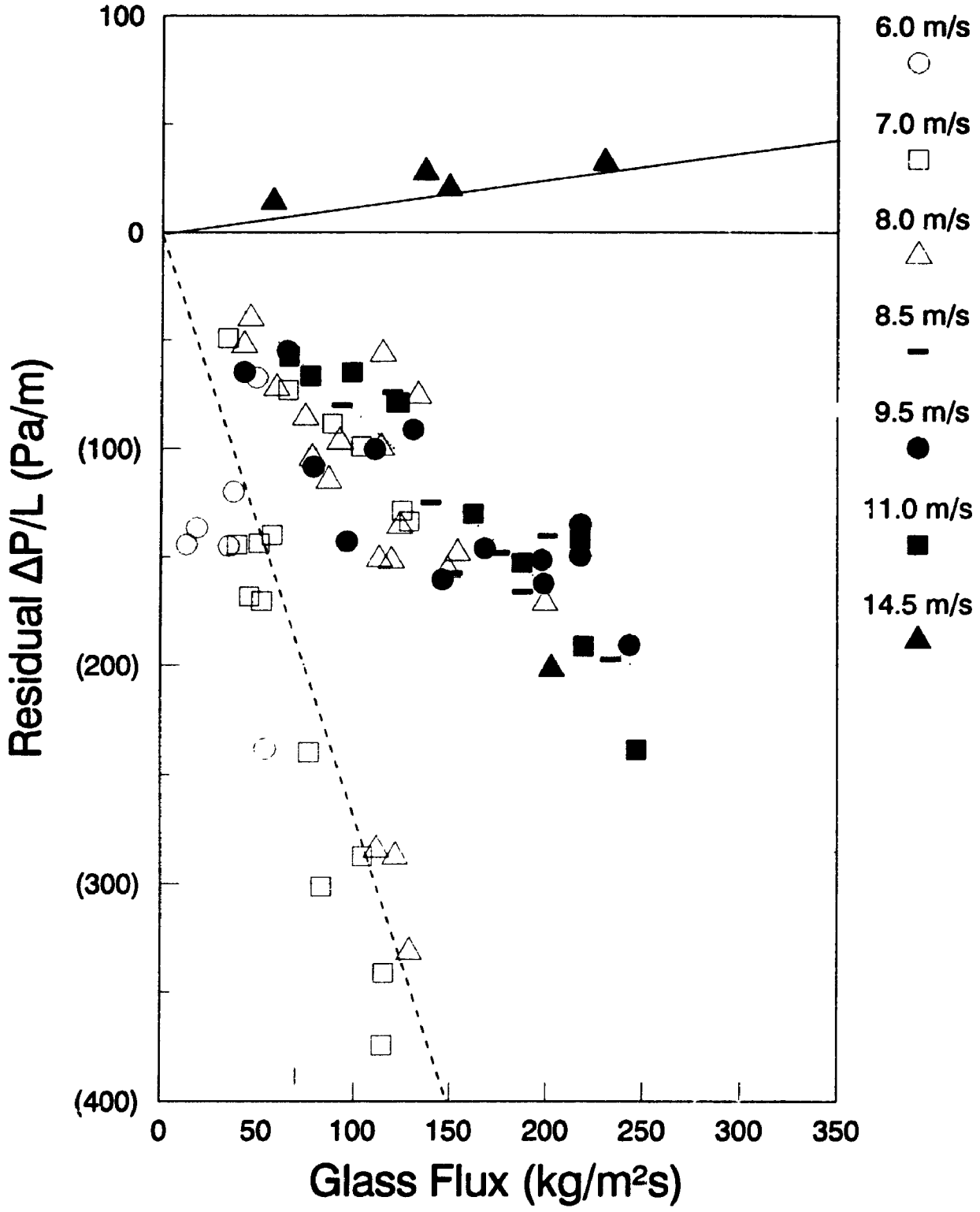

believed it was due to the localised solids down flow in the vicinity of the pipe wall, and this speculation has been confirmed by the Miller and Gidaspow (1992) vertical riser study.

4.5 EVALUATION OF PRESSURE DROP CORRELATIONS

For non-slugging dense phase flows there are very few experimental data available for pressure drop estimation. The correlations are based upon limited pools of data and there are many uncertainties in using any correlation for packed moving beds or fluidized-bed regimes. Arastoopour et al. (1979) used a relative velocity model and the assumption that particles form together in clumps of the same density as the particles. They showed that by adjusting the clump size the calculated pressure drop could be made to agree with the observed results of Yerushalmi et al. (1976) for fast fluidization. It is not as yet possible to predict a clump size a priori however, and their model does not account for solids backflow.

4.5.1 COMPARISON OF PRESSURE DROP WITH CORRELATIONS

The experimental pressure gradient data taken in this thesis was compared with the correlations of Capes and Nakamura (1973), Yang (1975), and Jones (Rohatgi, 1988) based on the solids friction factor predictions for each of these correlations. The results are shown in Fig. 4.5.1 for sand particles and Fig. 4.5.2 for glass beads, both for the vertical orientation. None of

Fig. 4.5.1 : Pressure Gradient Correlations

Sand Particles in Vertical Riser Transport

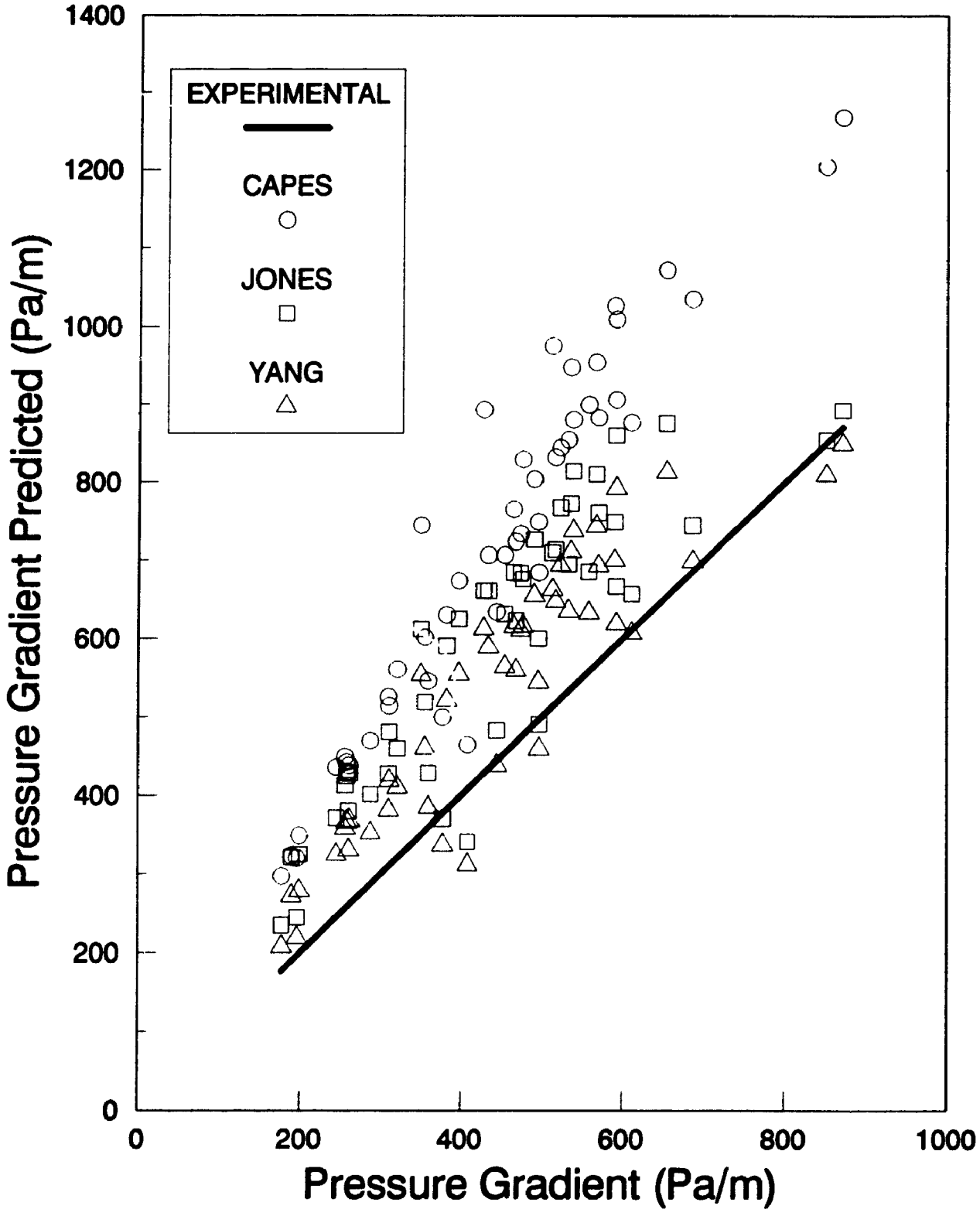

Fig. 4.5.2 : Pressure Gradient Correlations

Glass Particles in Vertical Riser Transport

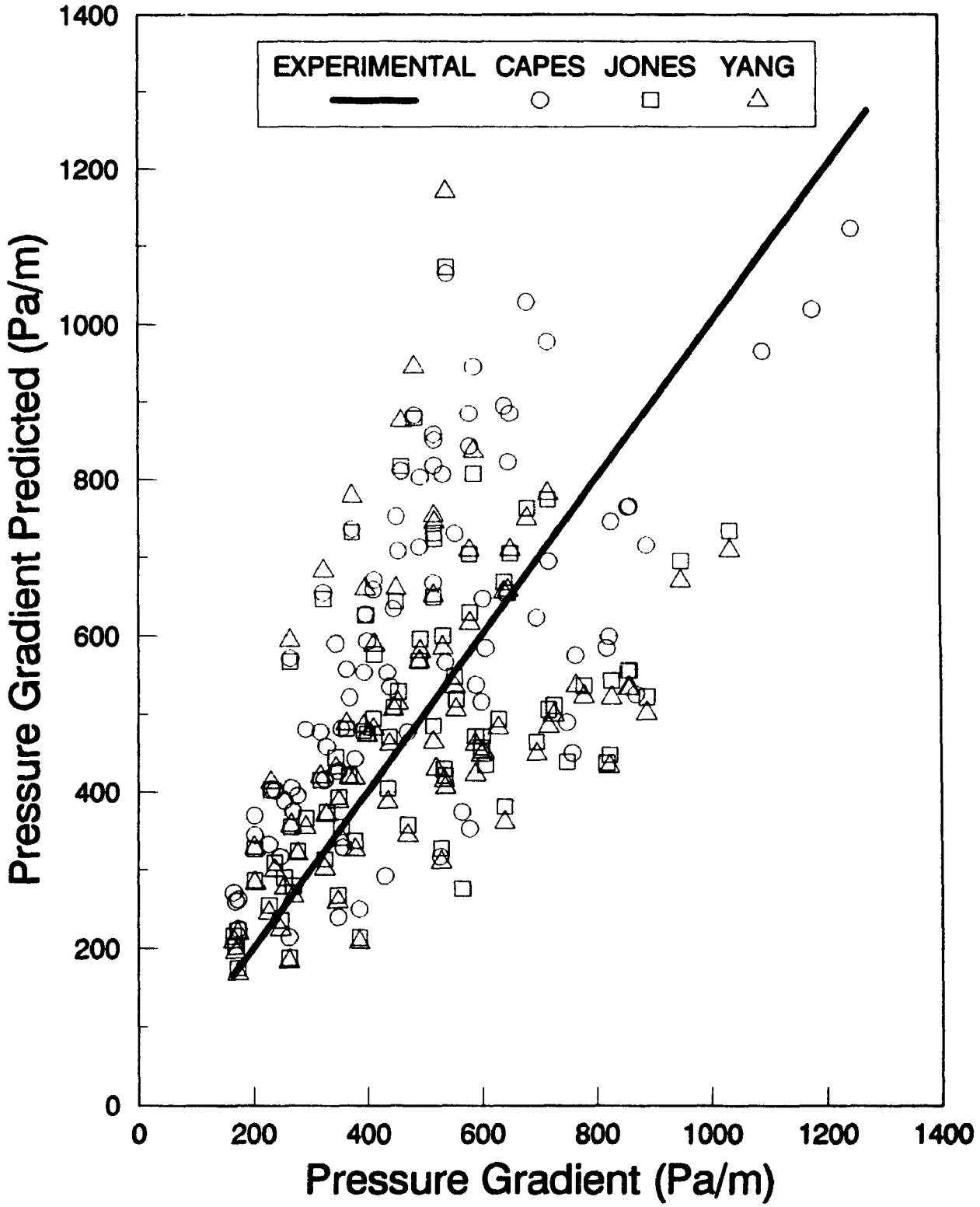

these correlations were developed for inclined riser transport. The correlation predictions were obtained from the FORTRAN program PDROP (Appendix D).

Fig. 4.5.1 shows that the sand pressure gradient data is over estimated by the Capes and Jones correlations. The Yang correlation seems the most adequate for this data. In Fig. 4.5.2 glass pressure gradient data is reasonably well represented at higher gas velocities away from the choking point. None of the correlations are able to predict the pressure gradient near choking for either particle type. This is not surprising because these correlations were originally developed for dilute phase pneumatic transport where the particles are dispersed homogeneously through the pipe.

4.5.2 OTHER MODEL FORMS

The Li and Kwauk (1988) model was reasonably successful in correlating the pressure gradient data, but failed for inclined lines. The Michaelides (1987) model was unsuccessful for all except the most dilute flows. Polynomial and purely empirical smoothing correlations were satisfactory for pressure gradient and solids holdup data, but too many parameters were required. Many of these parameters were statistically insignificant at the 95% confidence level. A more insightful approach was clearly required for better representation of the data.

The Klinzing thermodynamic approach (Klinzing et al., 1989), used for modelling oblique pneumatic transport lines operated in the dilute phase, was tested with partial success. It is the only one currently available in the literature for inclined transport lines. The model was capable of predicting those data obtained at high gas velocities where entrainment of particles is complete (as expected), but failed for conditions where there was significant amounts of solids refluxing at the pipe walls. The change of sign associated with solids friction factor, with the onset of solids refluxing could not be handled by any of the specific forms given by Zaltash (1987). The standard deviation associated with the various Zaltash model forms ranged from 40 Pa/m for dilute phase flows (load less than 10 and gas velocity above 8 m/s) to 200 Pa/m for flows with refluxing. This represents an average deviation of 10% for dilute phase transport, and 50% for non-slugging dense phase transport. As a result this form of model was eliminated from further consideration, and an alternative form was sought.

4.6 EFFECT OF PARTICLE VELOCITY ON FRICTION FACTOR

There is presently no reliable method to compute solids-wall frictional pressure drop directly. Since there are experimental errors inherent with the measurement of pressure gradient, solids holdup, and gas velocity, the relative error associated with solids frictional pressure drop computed by difference will be the sum of the previous three. Moreover, the friction

factor can also be influenced by the particle sphericity which is about 0.84 for sand and 1.0 for glass beads. Since the solids holdup pressure gradient equivalent is comparable in magnitude to the total gradient in this study for all line inclinations, small measurement errors in solids holdup can result in gross uncertainties with the solids-wall frictional component. When there is any solids deposition of particles, the pressure gradient due to solids holdup will also be over estimated, leading to erroneous estimates for the friction factor.

Usually the pressure gradient contribution due to the frictional component of the solids phase, $\Delta P_{f_s}/L$, is expressed analogously to that employed for the gas phase using equation (43), originally defined by equation (31b) in § 2.9.

$$\frac{\Delta P_{f_s}}{L} = \frac{2 f_s \rho_p (1 - \epsilon) U_p^2}{D} \qquad (43)$$

Here, D denotes the diameter of the pipe and f_s designates the frictional coefficient of the particulate phase.

The solids friction factor obtained from equation (43) was compared with correlations from the literature. These included : Capes and Nakamura (1973), Konno and Saito (1969), and Yang (1988). The FORTRAN program CORANA (Appendix D) was used to compute f_s. None of the correlations (shown in § 1.7) account for line inclination effects. The Capes and

Nakamura correlation was high in comparison with the other two, and with the experimental data.

4.6.1 FRICTION FACTOR FOR SAND PARTICLES

Fig. 4.6.1 shows the effect of particle velocity on the friction factor (computed using equation 43) for a range of gas velocities in vertical transport. The scatter of data associated with the friction factor is due to the multiple sources of error associated with the estimation of the solids friction factor. For particle velocities below 4 m/s the friction factor is negative. This is because the line is at the choking point and there is extensive solids reversal at the pipe boundaries. This leads to the negative friction factors (discussed in §4.4) which is corroborated by the results of Leung and Wiles (1976), who noted that for non-slugging systems, solids are carried upwards with considerable internal recirculation. This results in a negative solids friction factor due to solid down flow at the wall. Above 4 m/s, the friction factor increases consistently to above zero values because the gas velocity is sufficient to entrain most of the particles at the pipe wall in an upwards flow.

Fig. 4.6.2 shows the effect of particle velocity on friction factor (using equation 43) for sand at a line inclination of 4°. The friction factor is negative for a narrow range of particle velocities between 2 to 3 m/s. It

Fig. 4.6.1: Friction Factor vs. Sand Velocity

Vertical Line Orientation

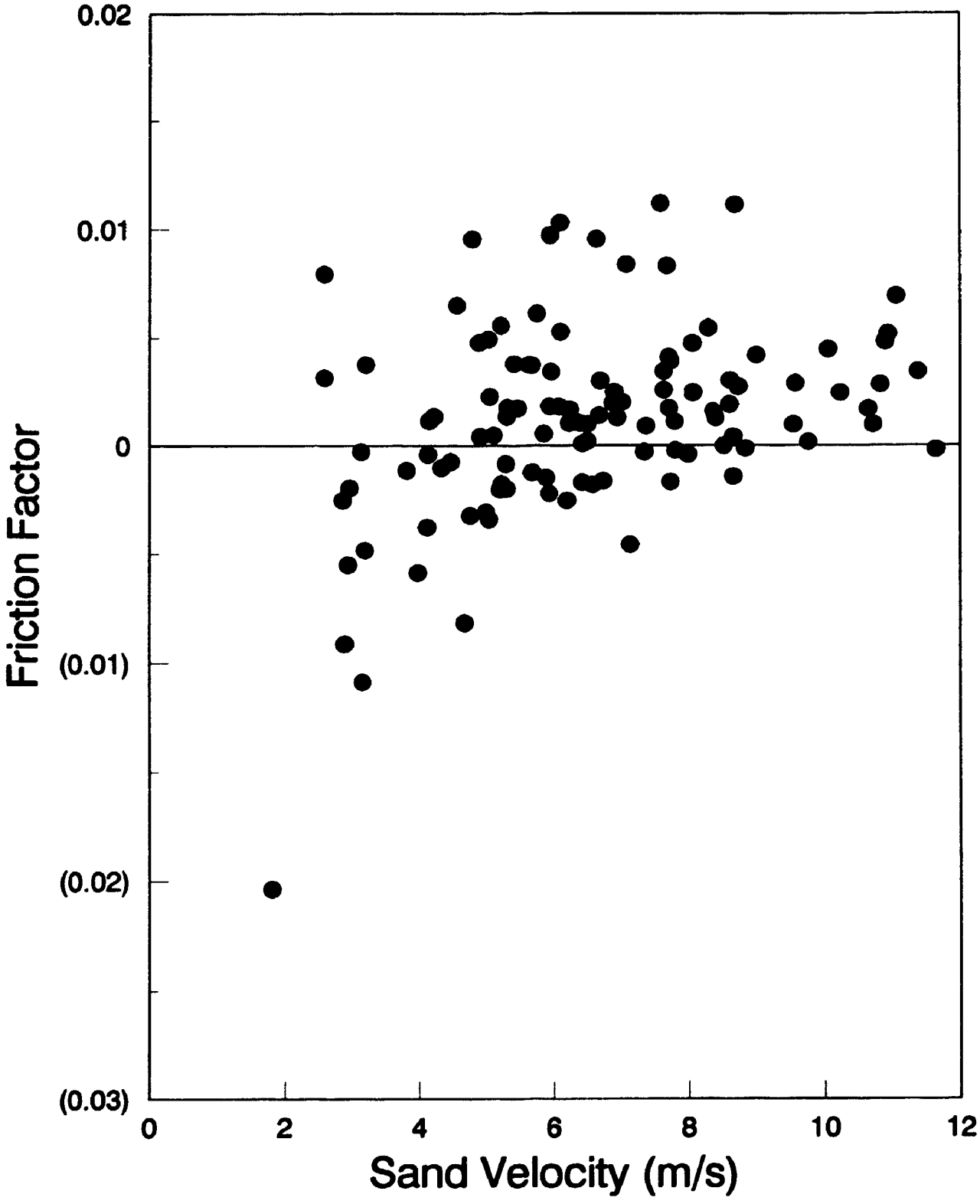

Fig. 4.6.2: Friction Factor vs. Sand Velocity

4° Inclined Line Orientation

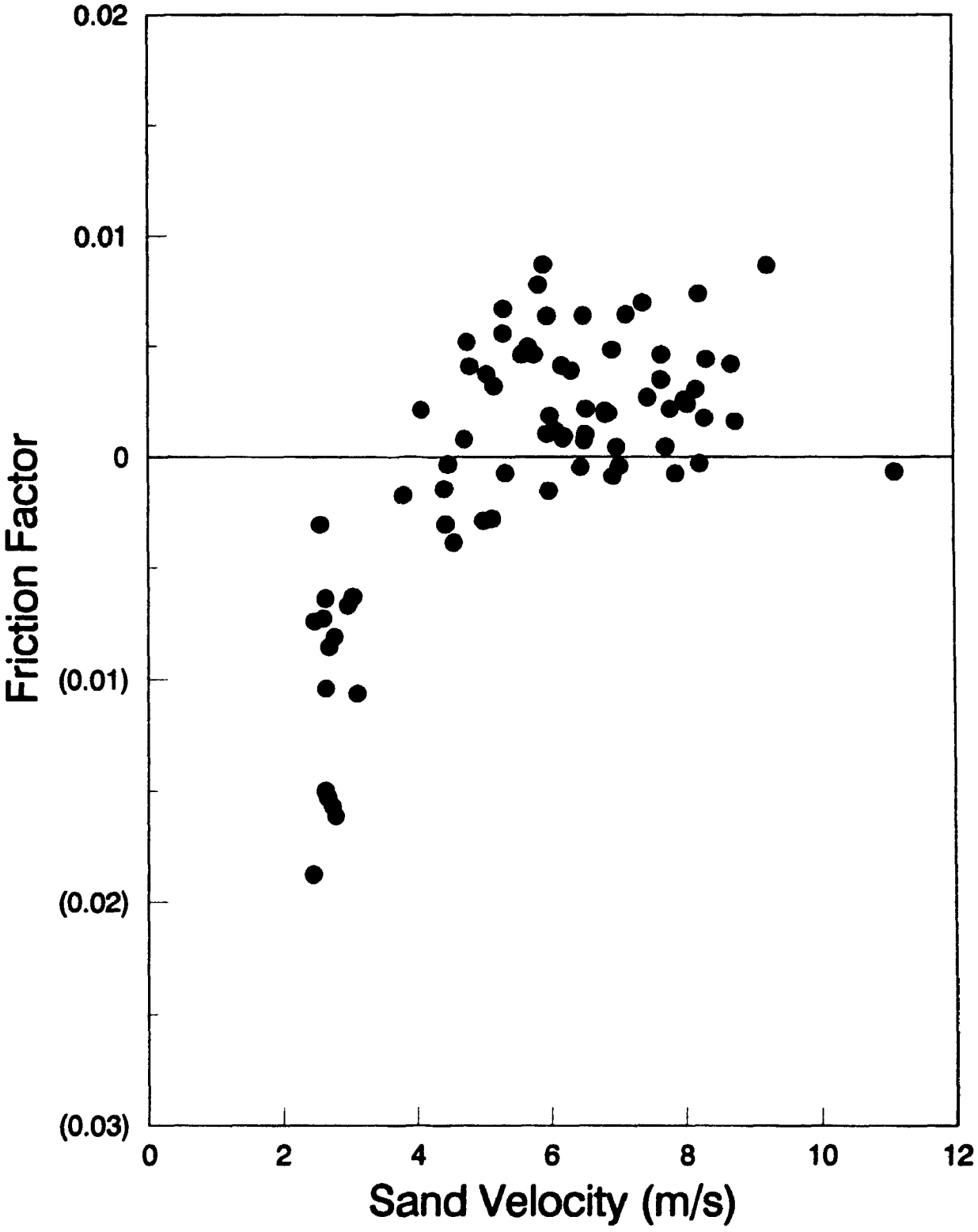

increases rapidly with particle velocity to a maximum of 0.008 before levelling off, as the particle velocity increases from 3 to 9 m/s.

The friction factor at a line inclination of 11° (using equation 43) is shown in Fig. 4.6.3. It is negative for particle velocities below 2 m/s, but increases sharply from -0.05 to about 0.01, as the particle velocity increases from 1 m/s to 4 m/s. The steep decrease of friction factor for particle velocities less than 3 m/s is expected, based upon visual observations which indicated massive streamers of refluxing particles in the vicinity of the choking point for the line inclined at 11°.

At 18° (Fig. 4.6.4) the friction factor is negative for the range of particle velocities between 1.0 and 1.5 m/s. The solids refluxing is so severe in this flow regime that the friction factor decreases to about -0.4. After increasing to 0.01 at a particle velocity of 3 m/s (Fig. 4.6.4), f_s remains constant at this value for the range of particle velocities above 3 m/s.

The negative friction factors observed for sand particles in Figs. 4.6.1 to 4.6.4 (using equation 43) were for gas velocities less than 6 m/s, where the line is approaching choking conditions. At these gas velocities the solids holdup collected between pinch valves could have been over estimated due to localised pockets of deposited solids. This may have led to the under

Fig. 4.6.3: Friction Factor vs. Sand Velocity

11° Inclined Line Orientation

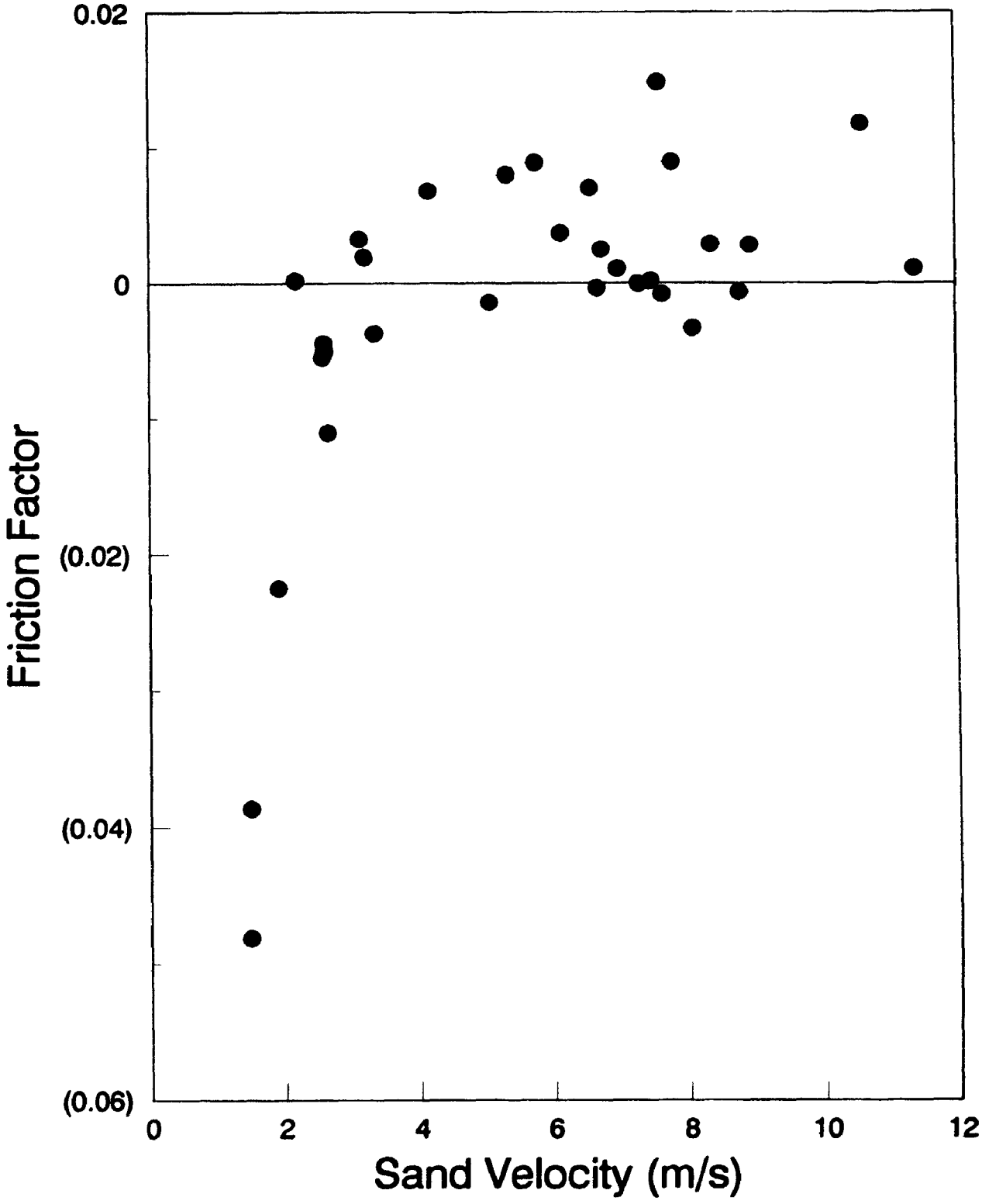

Fig. 4.6.4: Friction Factor vs. Sand Velocity

18° Inclined Line Orientation

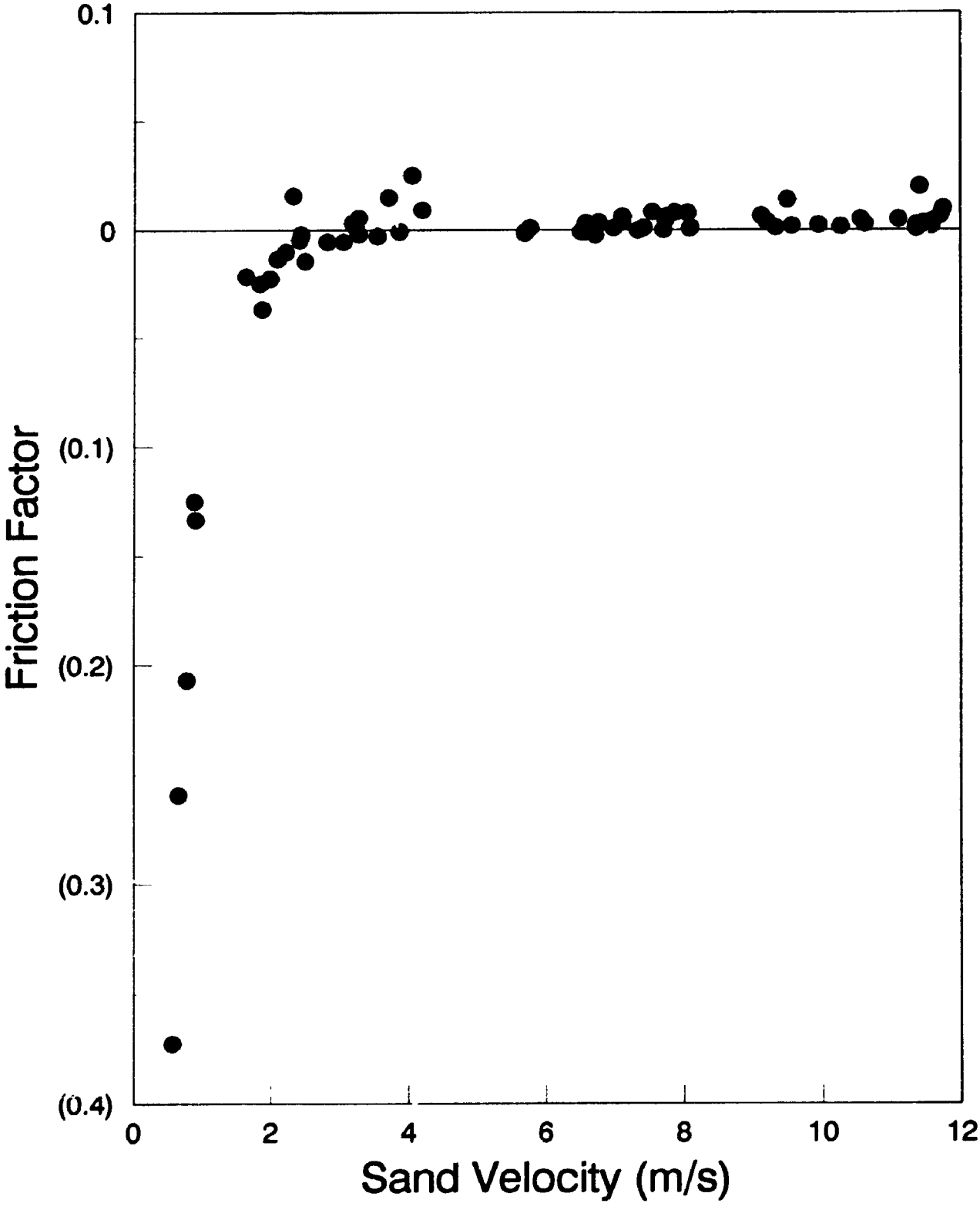

prediction of the residual pressure gradient, and the negative wall friction, f_s. Clearly, estimation of the friction factor under these conditions using the traditional 3-component pressure drop method (equation 42) is inappropriate.

The physical significance of the negative solids frictional component is that solids at the pipe boundary where refluxing occurs are flowing opposite (downwards) to the net bulk flow of solids through the core of the pipe. There are presently no reliable correlations to predict the solids friction factor in the transition regime, and none of the correlations available (Michaelides and Roy, 1987) can predict a negative friction factor where there is solids flow reversal.

4.6.2 FRICTION FACTOR FOR GLASS PARTICLES

The effect of particle velocity on the friction factor (using equation 43) for glass is shown for the vertical orientation in Fig. 4.6.5. The value of f_s is negative for particle velocities below 4 m/s, but increases to about 0.005 as the particle velocity increases beyond 2 m/s. Negative friction factors were also observed for line inclinations of 7° (Fig. 4.6.6) and 17° (Fig. 4.6.7) for similar conditions. None of the friction factor correlations were reliable for prediction of the friction factor of glass beads.

Fig. 4.6.5: Friction Factor vs. Glass Velocity
Vertical Line Orientation

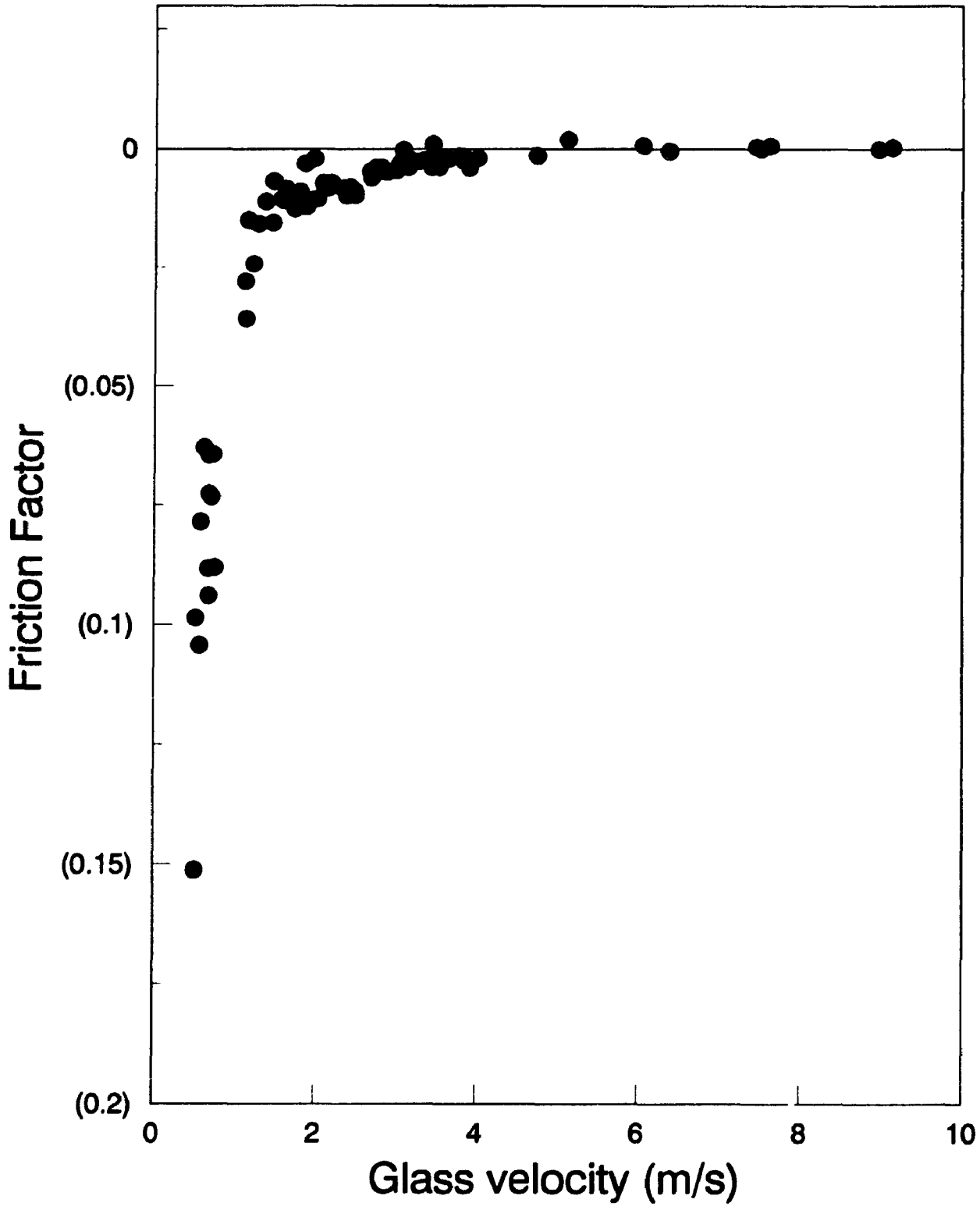

Fig. 4.6.6: Friction Factor vs. Glass Velocity
7° Inclined Line Orientation

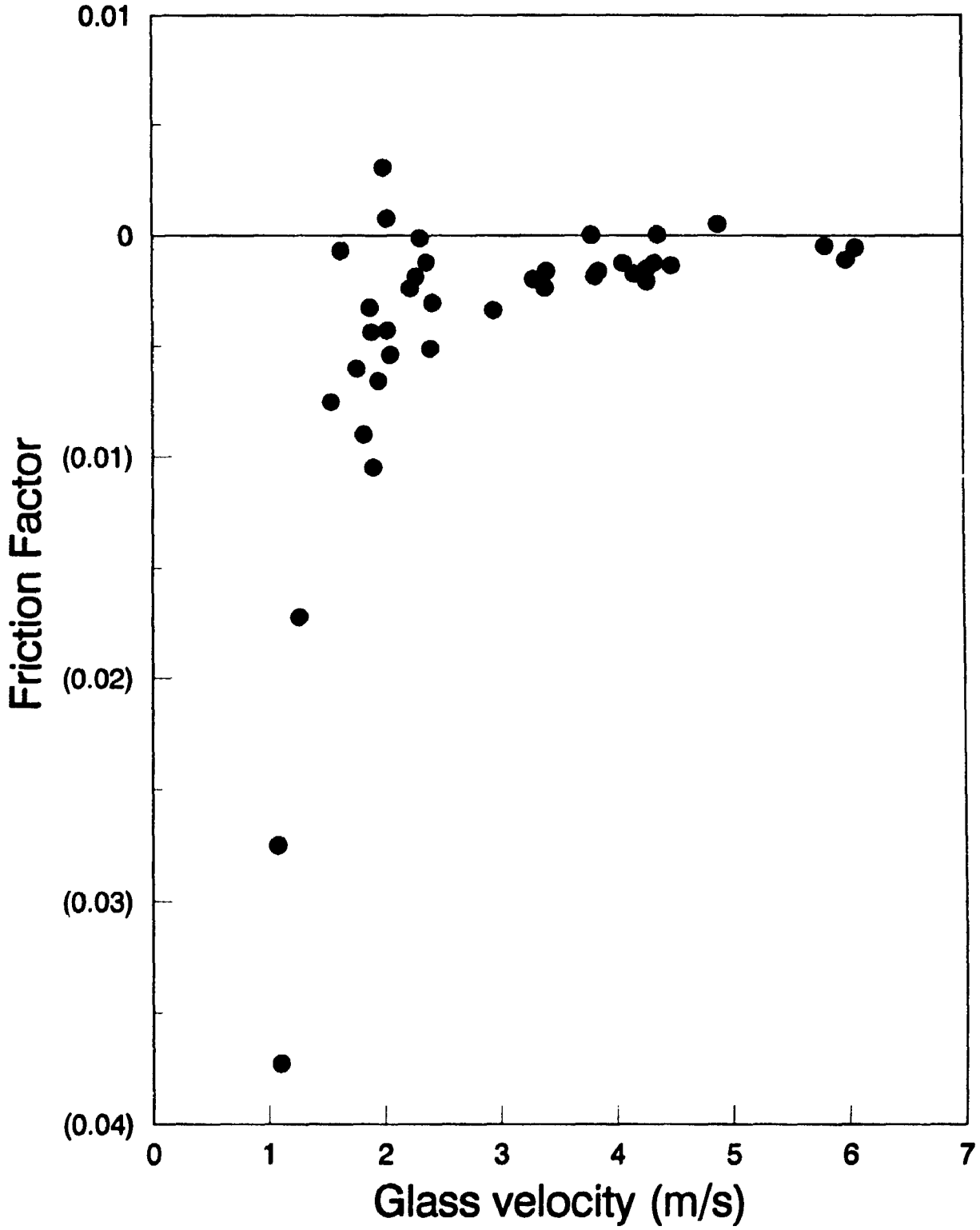

Fig. 4.6.7: Friction Factor vs. Glass Velocity
17° Inclined Line Orientation

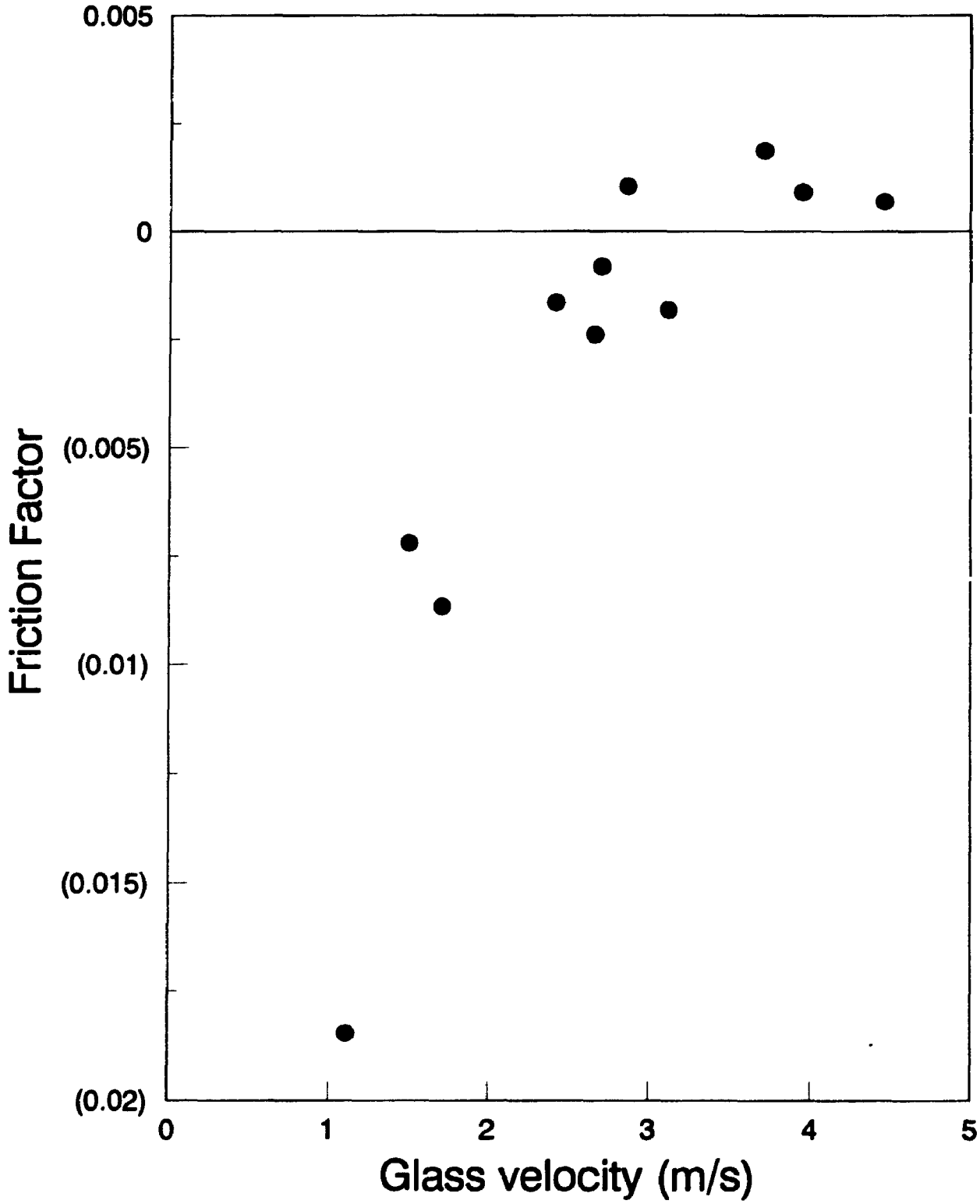

From visual observations made in the laboratory, the glass particles travelled a short distance upwards after being reentrained from the static state in the vicinity of the pipe walls. After this short upward flight, which was usually terminated by streams of particles hitting the pipe wall, the momentum of the clusters would fall to zero. This phenomenon was more apparent as the gas velocity was reduced at constant solids flux for the vertical and inclined lines. In comparison with the smaller diameter sand particles, where the majority of solids refluxing occurred for the inclined lines, evidence of solids refluxing was apparent for all line orientations (including the vertical), and gas velocities tested, for the glass beads.

4.7 CORRELATION ANALYSIS

To evaluate which variables had the most significant impact on the observed pressure gradient, a correlation analysis using the software package NCSS (Hintze, 1990) was performed. The effects of variables on the pressure gradient ($\Delta P/L$) including : the solids holdup (α), line inclination angle from the vertical (θ), solids flux (W_s), solids to gas mass loading (m^*), and gas velocity (U_g) were examined for sand particles (Appendix G1) and glass beads (Appendix G3).

4.7.1 CORRELATION ANALYSIS FOR SAND

For sand particles (Appendix G1) the pressure gradient is correlated 0.84

with α and 0.69 with the solids loading ratio, m^*. The decrease of the pressure gradient with gas velocity (-0.37) is expected since the experiments were conducted in the non-slugging dense phase flow regime, to the left of the Zenz minimum (Figs. 3.4.1 to 3.4.4).

A variable selection program was used to determine which combination of variables was most significant on the observed pressure gradient. This is shown in the Variable Selection Report in Appendix G1. For sand particles the hierarchy of variable importance is : solids holdup, inclination angle, solids flux, and gas velocity.

Appendix G2 shows the effects of the variables on the calculated solids-wall friction factor (f_s) for sand particles. The friction factor decreases with solids holdup (correlation of -0.39), and shows no dependence with any other variable. The decrease of f_s with the solids holdup is the expected trend due to solids refluxing at the pipe wall.

4.7.2 CORRELATION ANALYSIS FOR GLASS

The correlation of pressure gradient ($\Delta P/L$) with the independent variables for glass beads is shown in Appendix G3. $\Delta P/L$ is correlated 0.96 with the solids holdup (α), 0.64 with the load (m^*), -0.15 with θ, 0.43 with solids flux (W_s), and -0.27 with gas velocity (U_g). The effect of line inclination on the

observed pressure gradient is minimal for the glass beads.

The relative importance of the variables, including the possible interaction effects, is summarised in the variable selection report in Appendix G3. In priority of importance the variables are : α, θ, W_s, U_g, and m^*. However, the only parameter of any statistical significance is α.

The friction factor for the glass beads (Appendix G4) is correlated slightly with all parameters including : -0.2 with α, 0.1 with θ, and about 0.28 with each of solids flux, gas velocity, and solids loading.

4.7.3 CORRELATION OF DILUTE PHASE DATA FROM ZALTASH (1987)

Dilute phase pressure gradient data (Zaltash, 1987) was also correlated with NCSS. The results, shown in Appendix G5, indicate that the pressure drop in the dilute phase for the lower hemisphere of the tube ($\Delta P_{S,L}$), is correlated with gas velocity, tube diameter, and solids flux (W_{SL}); no significant correlation with line inclination was observed. This is the expected result, because in the dilute phase there is no significant amount of solids refluxing, except at extreme line inclinations. The particles should all be entrained, and it is not expected that there would be any significant impact of line inclination on the observed pressure gradient.

4.8 PRESSURE GRADIENT MODEL

A semi-empirical model to predict the pressure gradient data for both glass beads and sand particles has been developed in this research for oblique risers operated in the non-slugging dense phase. The form of the model is equivalent to equation 42 (§ 4.4) used for vertical pneumatic transport. It assumes that the pressure gradient can be broken down into three components, including : frictional pressure losses of the gas with the pipe wall; pressure losses from the solids holdup; and pressure losses due to the gas-solids friction. The model form also accounts for line inclination and the possibility of negative solids-wall friction factors arising from solids refluxing at the wall. No other model presently available can account for negative solids-wall friction which occurs near the choking gas velocity, even though this phenomenon is well documented in the literature.

The basic form of the model is given in equation (44):

$$\left(\frac{\Delta P}{L}\right)_{total} = \left(\frac{\Delta P}{L}\right)_{gas\ friction} + \left(\frac{\Delta P}{L}\right)_{holdup} + \left(\frac{\Delta P}{L}\right)_{solids\ friction} \qquad (44)$$

(i) *(ii)* *(iii)*

4.8.1 GAS-WALL FRICTION COMPONENT

The first component (i) of equation (44) is computed from equation (45): From empirical correlation (Fig. 2.9.2), the gas-wall friction factor, f_g, is

$$\left(\frac{\Delta P}{L}\right)_{gas\ friction} = \frac{2 f_g \epsilon \rho_g U_g^2}{D} \qquad (45)$$

given by equation (46). It was obtained from this research by performing several experiments with gas flowing at different velocities through the empty tube. The results were correlated with the software package NCSS.

$$f_g = 0.0114\ U_g^{-0.25} \qquad (46)$$

where U_g is in units of m/s. Substituting (46) into (45) an expression for pressure gradient due to gas-wall friction is then given by equation (47).

$$\left(\frac{\Delta P}{L}\right)_{gas} = 0.94\ U_g^{1.75} \qquad (47)$$

4.8.2 SOLIDS HOLDUP COMPONENT

The pressure gradient due to solids holdup in the transport line (component [ii] in equation 44) is given by equation (48):

$$\left(\frac{\Delta P}{L}\right)_{holdup} = \alpha\ \rho_p\ g\ \cos(\theta) \qquad (48)$$

An empirical correlation for predicting the line voidage (obtained through reiterative methods in NCSS) is given by equation (49):

Equation (49) accounts for the dependence of the solids holdup with solids

$$\left(\frac{1-\epsilon}{\epsilon}\right) = 3.5x10^{-5}\left(\frac{D}{d_p}\right)\left(\frac{U_t}{U_g - U_t}\right) m^* \cos(1-\theta) \qquad (49)$$

loading, m^*, inclination angle, θ, and the gas velocity, U_g. The particle diameter (d_p) and tube diameter (D) have also been introduced into the correlation as a dimensionless ratio. After algebraic reorganization of the

$$\alpha = \frac{3.5x10^{-5}\left(\frac{D}{d_p}\right)\left(\frac{U_t}{U_g - U_t}\right) m^* \cos(1-\theta)}{\left(3.5x10^{-5}\left(\frac{D}{d_p}\right)\left(\frac{U_t}{U_g - U_t}\right) m^* \cos(1-\theta) + 1\right)} \qquad (50)$$

terms in equation (49) the solids holdup, $\alpha(1-\epsilon)$, is given by equation (50).

Substituting equation (50) into (48), an expression for the pressure gradient

$$\left(\frac{\Delta P}{L}\right)_{holdup} = \frac{3.5x10^{-5}\,\rho_p\, g \cos(\theta)\left(\frac{D}{d_p}\right)\left(\frac{U_t}{U_g - U_t}\right) m^* \cos(1-\theta)}{\left(3.5x10^{-5}\left(\frac{D}{d_p}\right)\left(\frac{U_t}{U_g - U_t}\right) m^* \cos(1-\theta) + 1\right)} \qquad (51)$$

due to the solids holdup is given by equation (51).

4.8.3 SOLIDS-WALL FRICTIONAL COMPONENT

The pressure gradient due to solids-wall friction is normally given by equation (52).

$$\left(\frac{\Delta P}{L}\right)_{solid-wall} = \frac{2\,\rho_p\,\alpha U_p^2 f_s}{D} \qquad (52)$$

The well-known Yang (1988) correlation (equation 13; § 1.7) was somewhat successful for the prediction of sand friction factor (f_s) data at gas velocities in the dilute phase regime where f_s was positive, but failed when tested in the presence of negative friction factor data. The only correlation that was suitable for both positive and negative values of f_s is given by equation (53).

$$f_s = 115\left(\frac{d_p}{D}\right)^2 \log\left(\frac{U_p}{U_g - U_t}\right) \qquad (53)$$

It accounts for the tube wall diameter (D) and particle size (d_p). The particle velocity, U_p, is averaged over the pipe cross-section as defined by equation (26).

Substituting equations (50) and (53) into equation (52) for pressure gradient due to solids-wall friction, equation (54) is obtained.

$$\left(\frac{\Delta P}{L}\right)_{solid} = 230\rho_p\left(\frac{U_p^2}{D}\right)\left(\frac{d_p}{D}\right)^2 \log\left(\frac{U_p}{U_g - U_t}\right) \frac{\left(3.5x10^{-5}\left(\frac{D}{d_p}\right)\left(\frac{U_t}{U_g - U_t}\right) m^{*}\cos(1-\theta)\right)}{\left(3.5x10^{-5}\left(\frac{D}{d_p}\right)\left(\frac{U_t}{U_g - U_t}\right) m^{*}\cos(1-\theta) + 1\right)} \qquad (54)$$

4.8.4 CALCULATION OF TOTAL PRESSURE GRADIENT

Equations (47), (51), and (54) are pressure gradient components due to gas-wall friction, solids holdup, and solid-wall friction respectively. When substituting these equations into equation (44) for the total pressure gradient from the three independent sources, an overall pressure gradient expression is given by equation (55).

$$\left(\frac{\Delta P}{L}\right)_{tot} = 0.94U_g^{1.75} + \left(\rho_s g\cos(\theta) + 230\rho_s\left(\frac{U_p^2}{D}\right)\left(\frac{d_p}{D}\right)^3\log\left(\frac{U_p}{U_g - U_t}\right)\right)\left(\frac{3.5\times10^{-4}\left(\frac{D}{d_p}\right)\left(\frac{U_t}{U_g - U_t}\right)^m\cos(1-\theta)}{\left(3.5\times10^{-4}\left(\frac{D}{d_p}\right)\left(\frac{U_t}{U_g - U_t}\right)^m\cos(1-\theta)+1\right)}\right) \quad (55)$$

4.8.5 FIT OF THE MODEL TO THE SAND PRESSURE GRADIENT DATA

Equation (55) was compared with the experimental data for the sand particles, and this is shown in Fig. 4.8.1 for all line inclinations. The solid oblique line is the "equal value line", representing experimental data collected at all line inclinations. Model predictions are given by a combination of open and closed symbols, representing the different gas velocity ranges which were studied.

The cluster of points observed in the lower half of Fig. 4.8.1 corresponds to gas velocities in the fully entrained flow regime, where there is good agreement with the data. At gas velocities less than 5 m/s (open triangles

Fig. 4.8.1 : Pressure Gradient Model [1]

Sand Particles at All Line Orientations

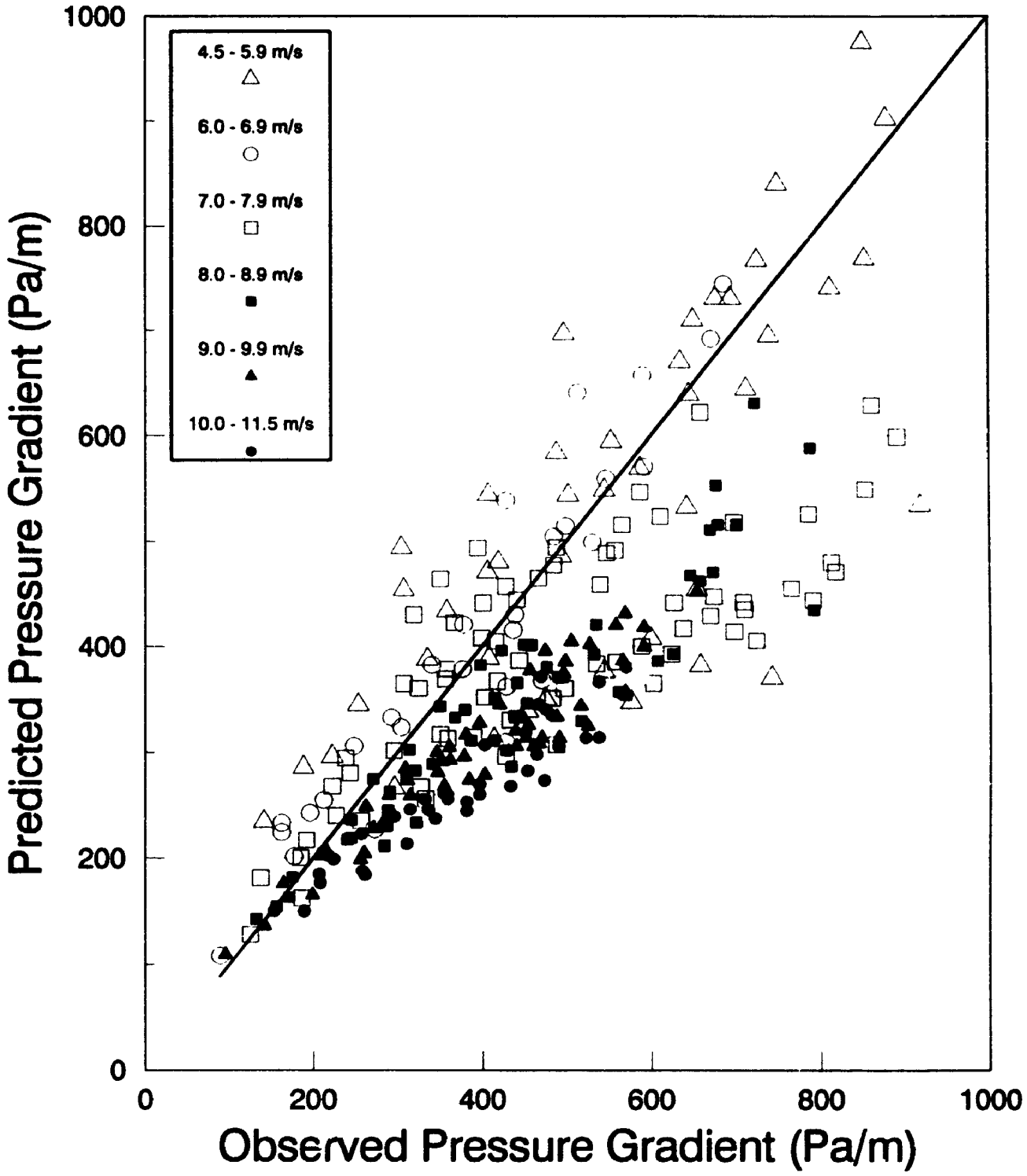

1. Symbols are model predictions

at pressure gradients above 800 Pa/m), the riser chokes at all inclinations (Table 4.1.2). The model, which is unable to accurately predict the extensive solids reversal that accompanies choking, fails only under these conditions. Reasonable agreement is observed for all gas velocities away from the choking point.

4.8.6 ESTIMATION OF SAND HOLDUP

The correlation analysis of § 4.7 demonstrated that the most critical parameter affecting the observed pressure gradient was the contribution from solids holdup (Appendices G1, G3). Based on this result the model prediction of solids holdup (equation 51) was compared with the experimental data, to evaluate how effectively this contribution had been captured in the estimation of the total pressure gradient.

A comparison of the predicted solids holdup (equation 51) with the actual observed holdup from equation (25a), § 2.9, is shown in Fig. 4.8.2 for the sand particles at all line inclinations. Model predictions are indicated by a variety of symbols representing different gas velocities. For a solids volumetric fraction of less than 0.02 the agreement with the model is excellent. In this region most of the particles were entrained with the gas, and solids deposition at the pipe wall was minimal. For those experiments where $\alpha > 0.03$ the riser choked at all line inclinations (Table 4.1.2). Where

Fig. 4.8.2 : Solids Holdup Model [1]

Sand Particles at All Line Orientations

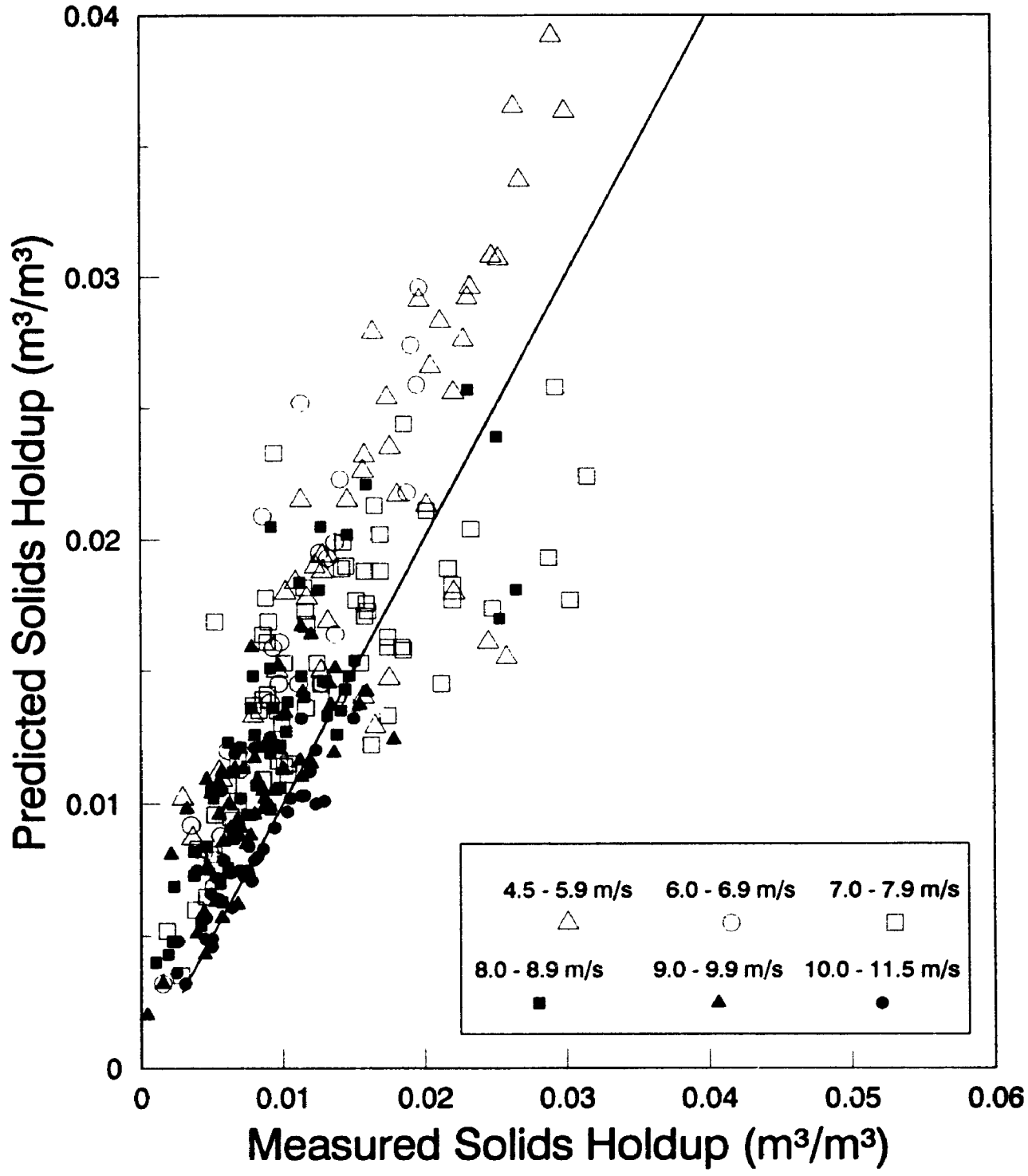

1. Symbols represent model predictions.

the solids holdups exceed 0.03 in Fig. 4.8.2, a significant fraction of the particles were deposited at the wall, particularly for line inclinations greater than or equal to 11°. The model form fails for the choking riser conditions only.

4.8.7 MODEL FIT OF GLASS PRESSURE GRADIENT DATA

Fig. 4.8.3 compares the pressure gradient model (equation 55) for all line inclinations with the glass beads pressure gradient data. Reliable predictions are obtained for gas velocities of up to about 10 m/s. More data for the glass beads in the fully entrained flow regime would improve the model fit for gas velocities above 10 m/s. Most of the friction factor data in this research was obtained for extensive solids refluxing conditions (Figs. 4.6.5 to 4.6.7), where f_s is negative.

4.8.8 ESTIMATION OF GLASS HOLDUP

The prediction of the glass beads holdup is shown in Fig. 4.8.4. Considering the multiple flow regimes which are possible at the three line inclinations considered, the model agreement is reasonable.

4.8.9 CONCLUDING REMARKS ON MODEL APPLICABILITY

A semi-empirical model has been developed for the prediction of the pressure gradient (equation 55) and solids holdup (equation 50) in oblique

Fig. 4.8.3 : Pressure Gradient Model [1]

Glass Beads at All Line Orientations

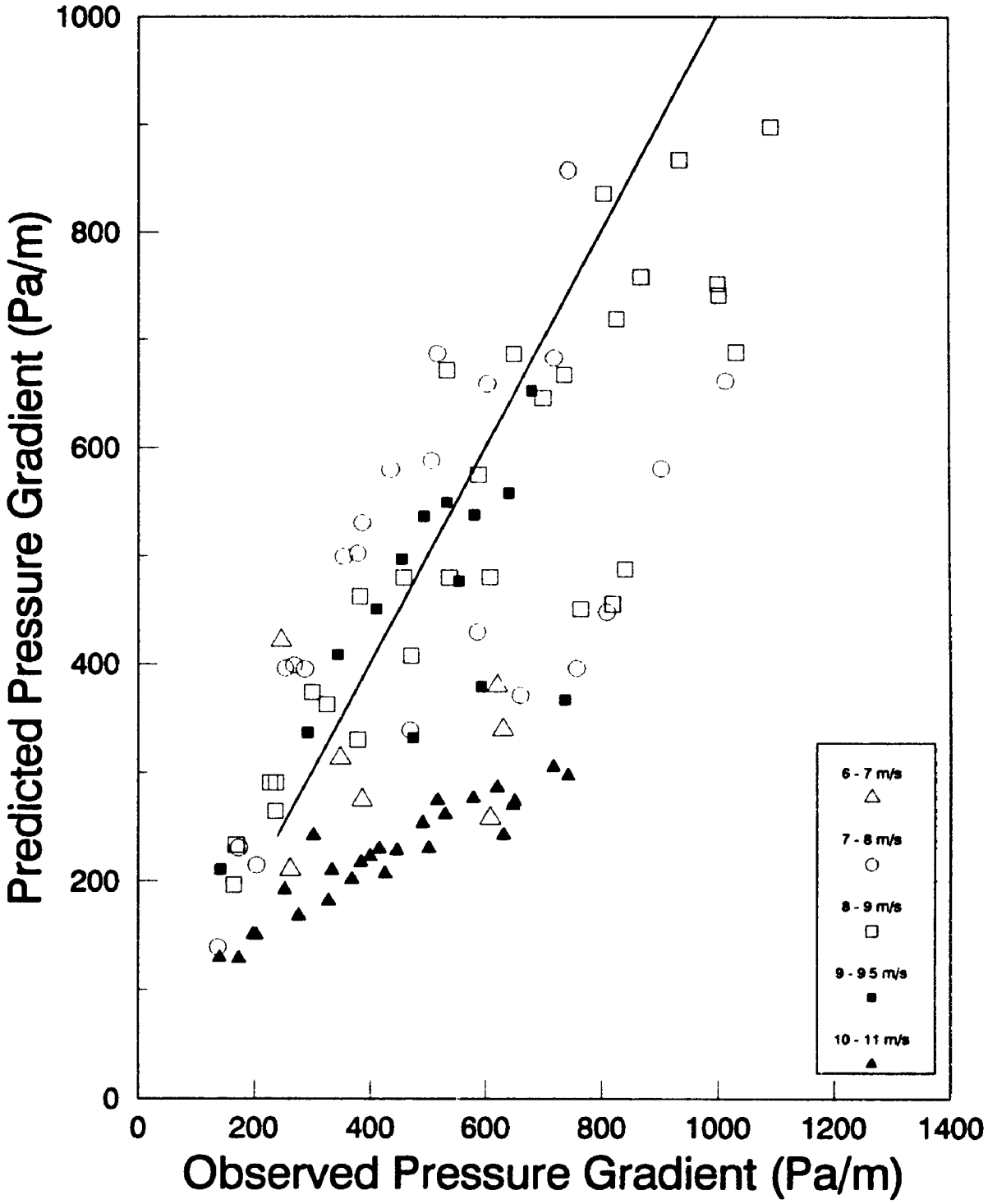

1. Symbols represent predicted values.

Fig. 4.8.4 : Solids Holdup Model [1]

Glass Beads at All Line Orientations

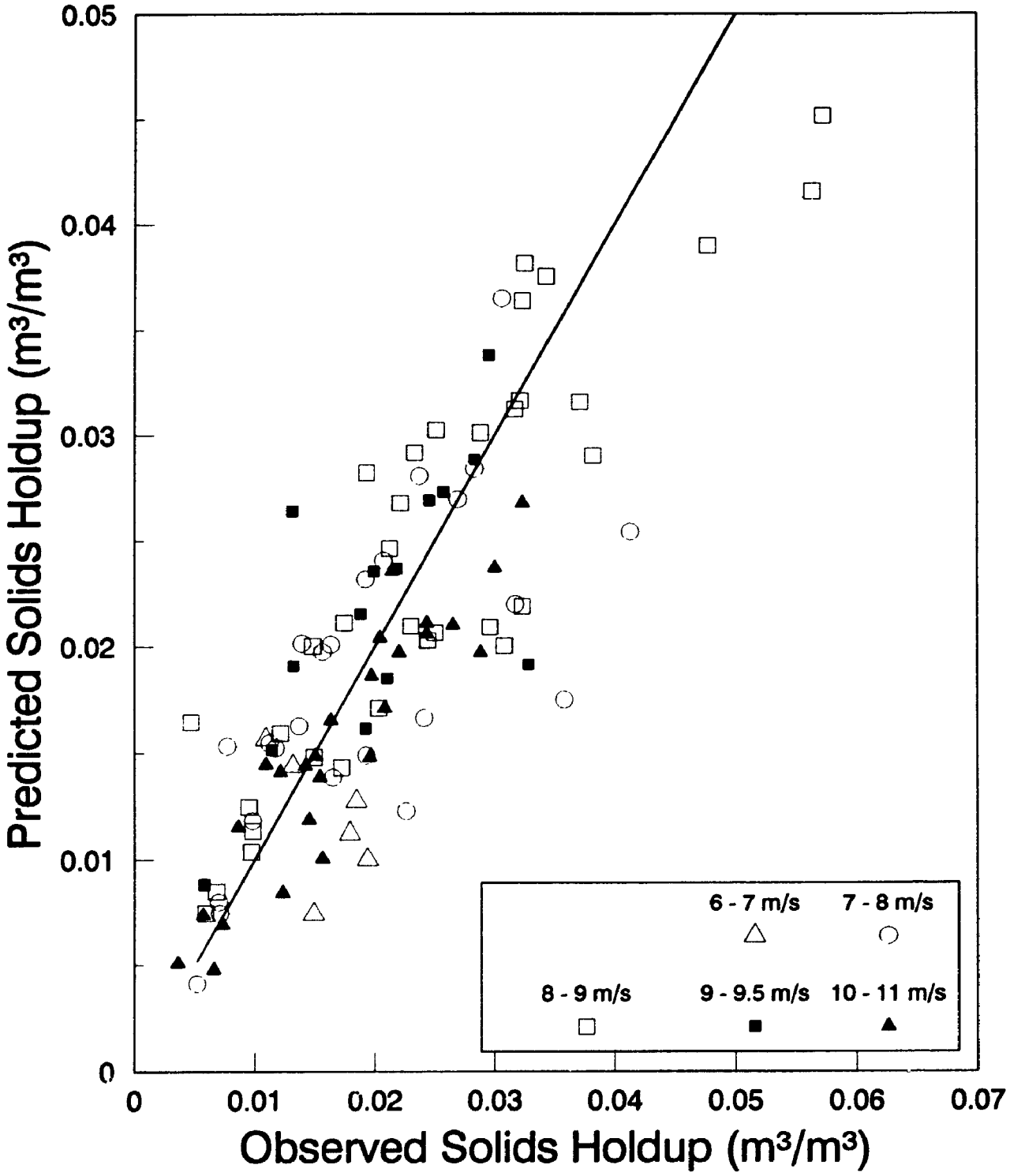

1. Symbols represent predicted values.

risers operated in the non-slugging (fast fluidization) flow regime. The model assumes that the total pressure gradient is the sum of three components including : gas-wall friction pressure drop, solids holdup pressure loss, and solids-wall frictional pressure loss. It is an adaptation of the method used to treat dilute phase pressure gradient data in vertical pneumatic transport lines.

The model accounts for negative friction factors (resulting from solids refluxing at low gas velocities), and variations of particle diameter, tube diameter, and line inclination. The functional form of the solids holdup model includes terms which account for its dependence on the transport loading ratio, gas velocity, and riser inclination. Prediction of the gas-wall frictional contribution was obtained in the usual manner.

The overall fit of the pressure gradient model prediction to the experimental data is quite good considering the wide range of hydrodynamic conditions which have been analysed, and the applicability to different particle types and line inclinations.

4.9 INTRODUCTION TO TIME SERIES CHARACTERISATION OF DATA

Although many flow-regime maps for vertical 2-phase gas-solid riser-type flows have been empirically developed (Yerushalmi and Cankurt, 1979) the

observations are not always reproducible from one rig to another (Gajdos and Bierl, 1978). This is because the observations are often subjective in nature, being made from visual observations in the laboratory (Shingles and Dry, 1986). Another important reason could be that the flows are not fully developed (Tutu, 1984).

In this thesis a more objective approach to characterise the hydrodynamics of riser flows -both vertical and oblique- has been presented. It investigates the use of statistical and time series methods for flow characterisation of riser transport (non-slugging dense phase transport). It employs various methods of time series analyses using the pressure signals collected from the transducer (used to collect pressure gradient), mounted along the fully developed section of the riser, which measured 4.769 m in length.

The use of pressure fluctuations to characterise time series data in fluidization studies is not new. The statistical study of pressure fluctuations in a bubbling fluidized bed has been well documented in the literature (Leu and Lan, 1990). Use of pressure fluctuations for characterising flow transitions in gas-liquid two phase flows has also been studied (Matsui, 1984; Tutu, 1984). Wang et al. (1990) have used statistical methods for characterisation of the turbulence in 2-phase gas-liquid pipe flows. Tsuji and Morikawa (1982) and Dhodapkar and Klinzing (1993)

examined the statistical analysis of pressure fluctuations in horizontal pneumatic transport. Arena et al. (1988, 1992) have studied pressure gradient fluctuation data for vertical gas-solids riser transport. In this thesis pressure gradient fluctuation data are used to better characterise oblique riser flow.

4.9.1 METHODS OF DATA ANALYSIS

A pressure transducer was used to collect 2050 differential pressure gradient signals from the riser test section, which was 4.769 m in length (Fig. 2.1). Schnitzlein and Weinstein (1988) have found that the differential pressure and its fluctuations are determined by the properties of the dense annular region at the wall, which is composed of partly stagnant down-flowing solid, and solid rolling along it upward in the form of waves. The method employed here was adapted from Matsumoto and Harakawa (1987) who employed a differential pressure transducer for measurement of pressure fluctuations in vertical pneumatic transport, and for use in determination of power spectral functions.

The set of 2050 pressure gradient signals collected for each run was stored on a microcomputer floppy drive as an ASCII file. Storage in this format allowed easy analysis of the data, with auxiliary import capabilities to commercial software packages. Analysis of the time series was done

predominantly with the use of time series analysis software packages for the IBM PC including NCSS, IDENTP and UNIFITP. IDENTP and UNIFITP were developed by Jutan (1990) at the University of Western Ontario. NCSS is a commercial software package by Hintze (1990).

All time series were examined for trends and serial correlations by the pattern of autocorrelations and partial autocorrelations obtained from the IDENTP program. Spectral analyses of the data (obtained from the NCSS package) revealed information pertaining to the dominant frequencies associated with the process. Spectral analysis of the pressure gradient time series data is discussed in § 4.10.

A stochastic model based upon Box-Jenkins methodology (Box and Jenkins, 1970) was employed to collapse time series pressure gradient data. This included the search for an appropriate autoregressive integrated moving average model (ARIMA) to simulate the data. The serial pattern of partial autocorrelations was used to obtain estimates of the parameters. This analysis is presented in § 4.11.

4.9.2 TIME SERIES GENERATED AT VARIOUS LINE INCLINATIONS

Fig. 4.9.1 shows the first 225 data points (225 time lags) generated for the pressure gradient in the 18° line orientation for a typical run at a gas

Fig. 4.9.1: Pressure Gradient Time Series [1]

Sand Particles at 18°, 8.5 m/s, and 195 kg/m²s

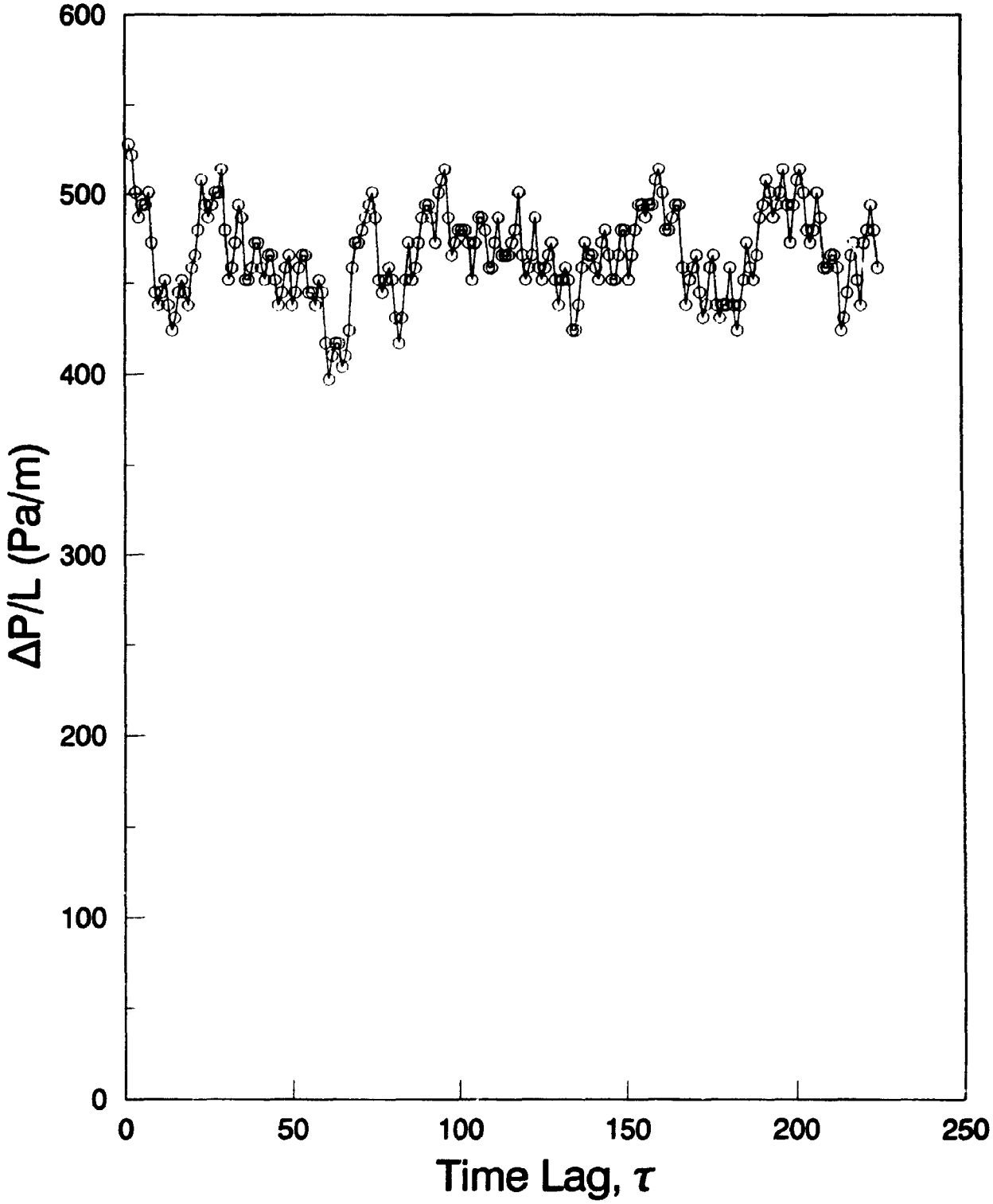

1. A time lag represents 0.081 elapsed seconds.

velocity of 8.5 m/s and a solids flux of 195 kg/m^{2}s. A 'time lag', used as the abscissa for many of the time series figures to be presented, is defined as an integer multiple of 0.081s, which was the sampling interval used in this research. Hence, a time lag of 10 would correspond to an elapsed time of 8.1 s.

Fig. 4.9.2 shows a probability density function (PDF) of the time series shown for the 18° inclined line in Fig. 4.9.1. The distribution is Gaussian, as defined by the characteristics in § 3.2, having a skewness of 0.065 and kurtosis of 0.449.

A typical pressure gradient series for glass beads is given in Fig. 4.9.3 for the 17° inclined line orientation. It was obtained at experimental conditions of 150 kg/m^{2}s and a gas velocity of 12 m/s. It is characterised by the Gaussian PDF shown in Fig. 4.9.4. The values of the skewness and kurtosis are 0.063 and 0.335 respectively.

There is no fundamental difference in the manner in which data was collected for sand as compared with the glass beads. The two types of particles should therefore be amenable to the same types of data analysis, and the results should be comparable on the same basis. Sections 4.10 and 4.11 will compare the time series for the two types of particles, and discuss

Fig. 4.9.2 : PDF of Pressure Gradient [1]

Sand Particles at 18°, 8.5 m/s, and 195 kg/m²s

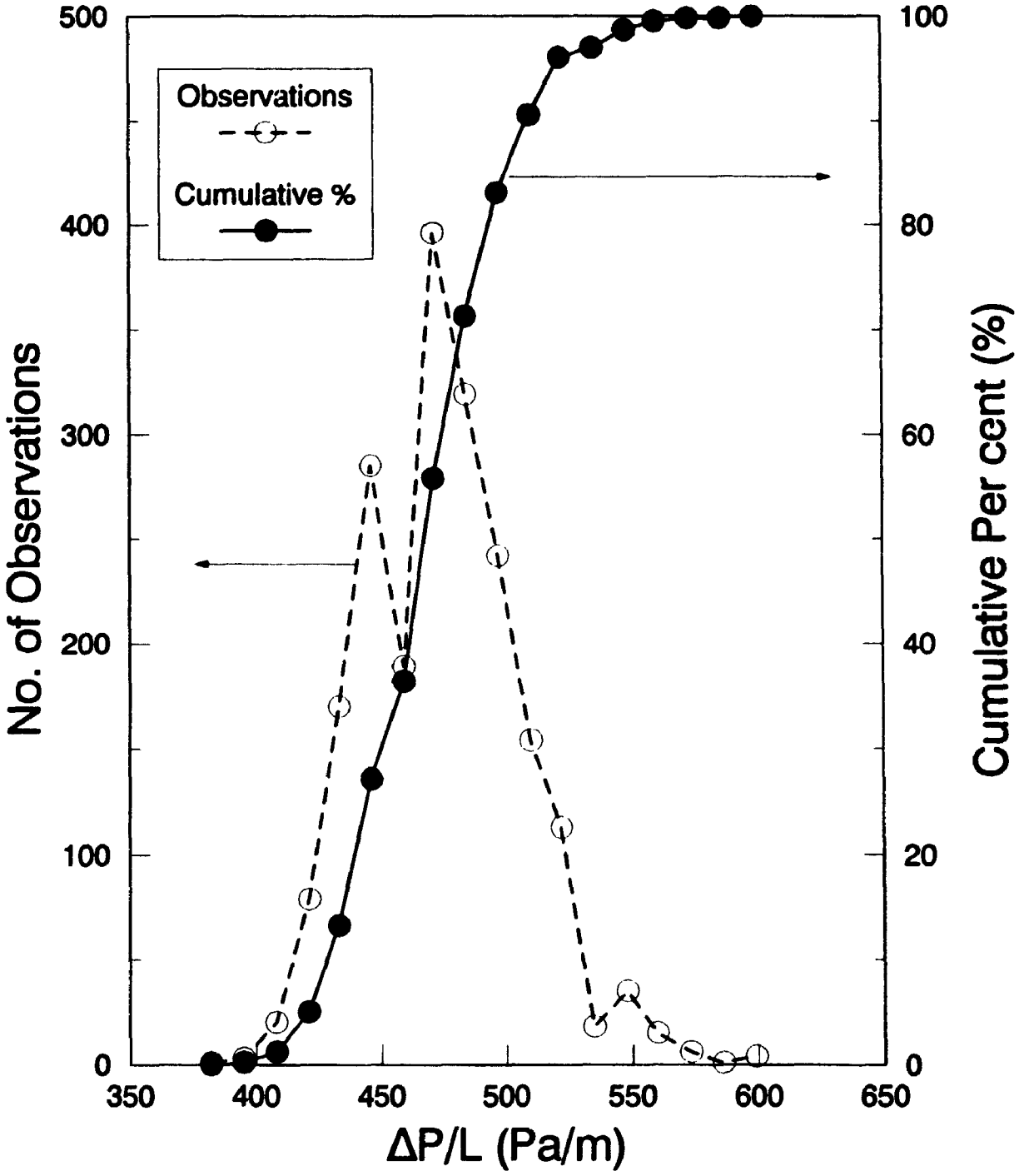

1. μ = 475 Pa/m σ = 31 Pa/m
Skewness = 0.065
Kurtosis = 0.449

Fig. 4.9.3: Pressure Gradient Time Series [1]

Glass Particles at 17°, 12 m/s, and 150 kg/m²s

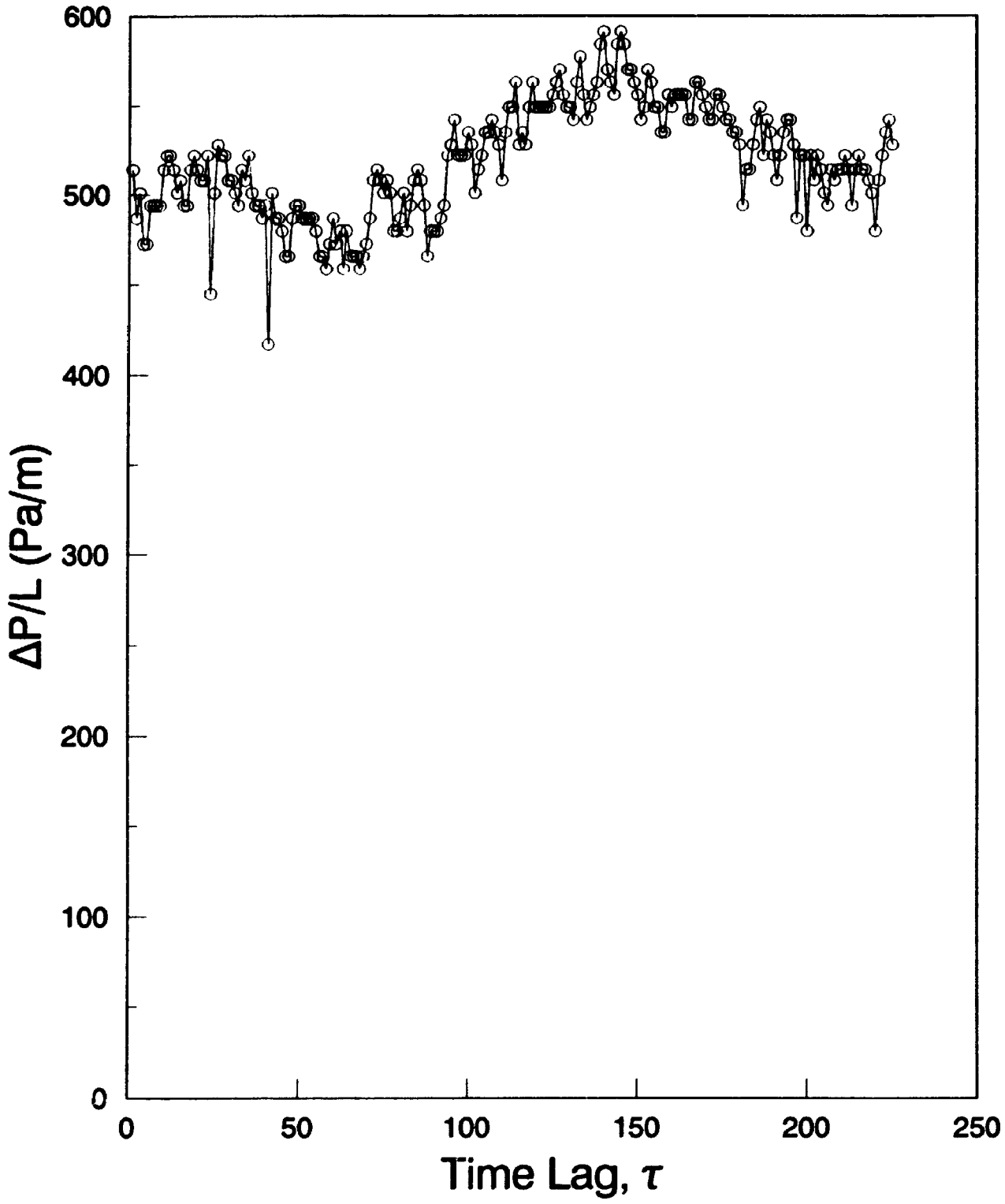

1. A time lag represents 0.081 s

Fig. 4.9.4 : PDF of Pressure Gradient [1]

Glass Particles at 17°, 12 m/s, and 150 kg/m²s

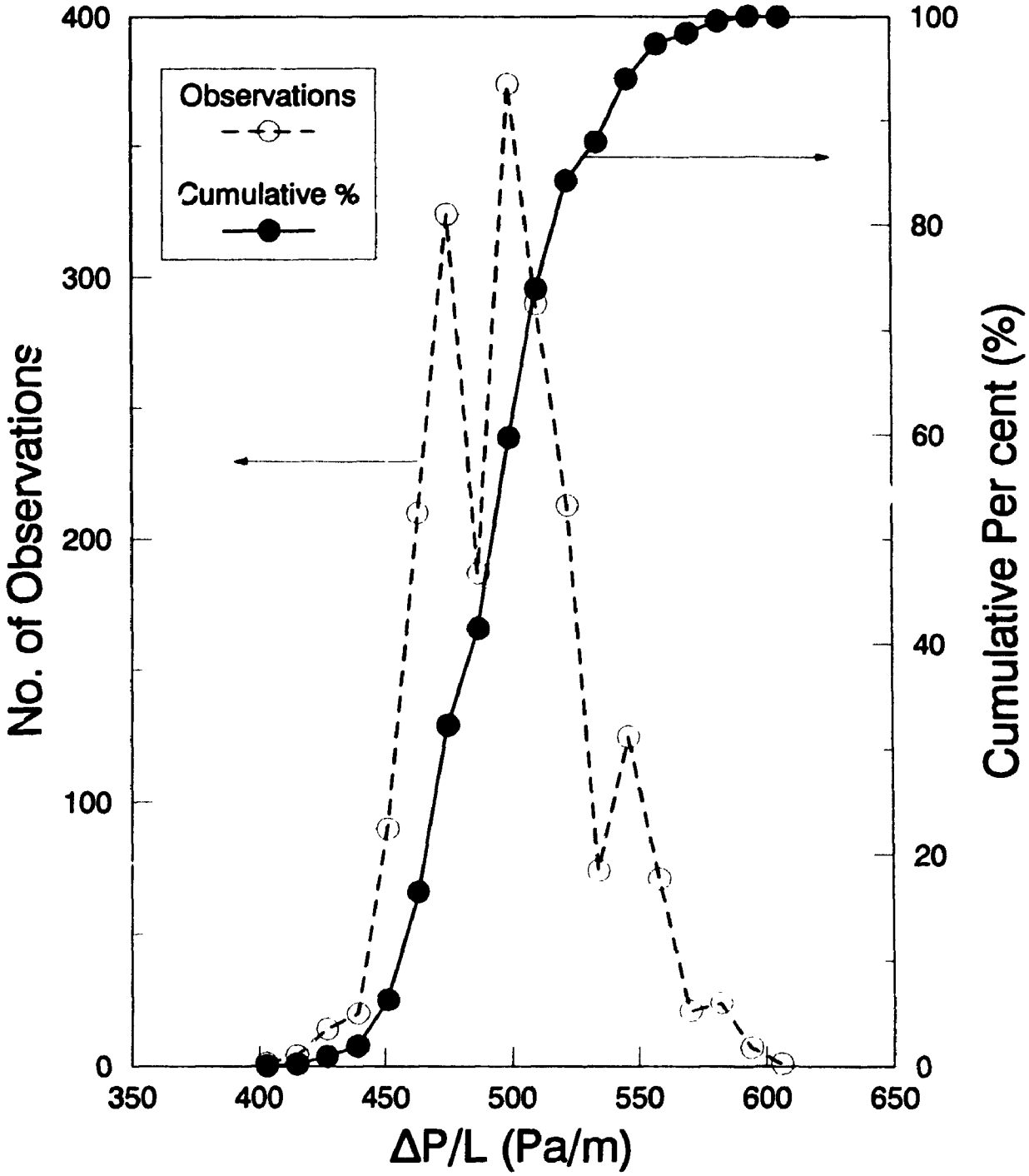

1. μ = 500 Pa/m σ = 31.4 Pa/m
Skewness = 0.063
Kurtosis = 0.335

the impact of line inclination, and other manipulated variables.

4.10 SPECTRAL ANALYSIS

The power spectral density function (PSD) is a frequency-domain description of the time series, and is appropriate for detection of the frequency component embedded in a random process (Bendat and Piersol, 1971). The power spectral density was calculated using the fast Fourier Transform of the autocorrelation function. The autocorrelation function is defined by equation (56) :

$$Rp(\tau) = \lim_{\tau_m \to \infty} \frac{1}{\tau_m} \int_{-\tau_m/2}^{\tau_m/2} P(t) \times P(t+\tau)\, dt \qquad (56)$$

The power spectral density function is given by equation (57):

$$\Gamma(f) = \frac{2}{\tau_m} \int_{-\tau_m/2}^{\tau_m/2} R\,p(\tau) \cos(2\pi f\tau)\, d(\tau) \qquad (57)$$

The Fast Fourier Transform method (Press et al., 1986) is used here in all computations for the power spectrum estimation.

4.10.1 SAMPLING FREQUENCY

A sampling frequency of 12.3 Hz was used in this research. Preliminary experiments demonstrated that the spectrum distributed over 90% of its

power in the range of frequencies between two and eight hertz, which was the rationale for the selection of the 12.3 Hz cut-off frequency. This observation agrees with the results of Louge et al. (1990) who found no significant fluctuations above 20 Hz. Drahos and Cermak (1988) found that the limitation of the band-width used in this work agrees with the frequency content of typical pressure fluctuations.

4.10.2 POWER SPECTRA FOR SAND PARTICLES

Spectral coherence refers to the amplitude of the peak in the power spectrum at the dominant frequency, and has units of Pa^2 (Dhodapkar and Klinzing, 1993). A typical power spectrum obtained for the vertical line transport of sand particles is shown in Fig. 4.10.1. The dominant frequency occurs at approximately 4.9 Hz, and has an amplitude, Γ, (or spectral coherence) of 28×10^6 Pa^2. The experiment was conducted at a gas velocity of 6.7 m/s and a solids flux of 185 kg/m^2s.

The spectrum in Fig. 4.10.1 has negligible power distributed before 4 Hz or after 8 Hz. Dhodapkar and Klinzing (1993) have noted that the particles absorb all of the high frequency fluctuations (above 10 Hz), for the case of gas-only flow in horizontal pneumatic dilute transport with 450 μm glass beads.

Fig. 4.10.1: Power Spectrum for Vertical Line

Pressure Gradient Series for Sand at 6.7 m/s and 185 kg/m²s

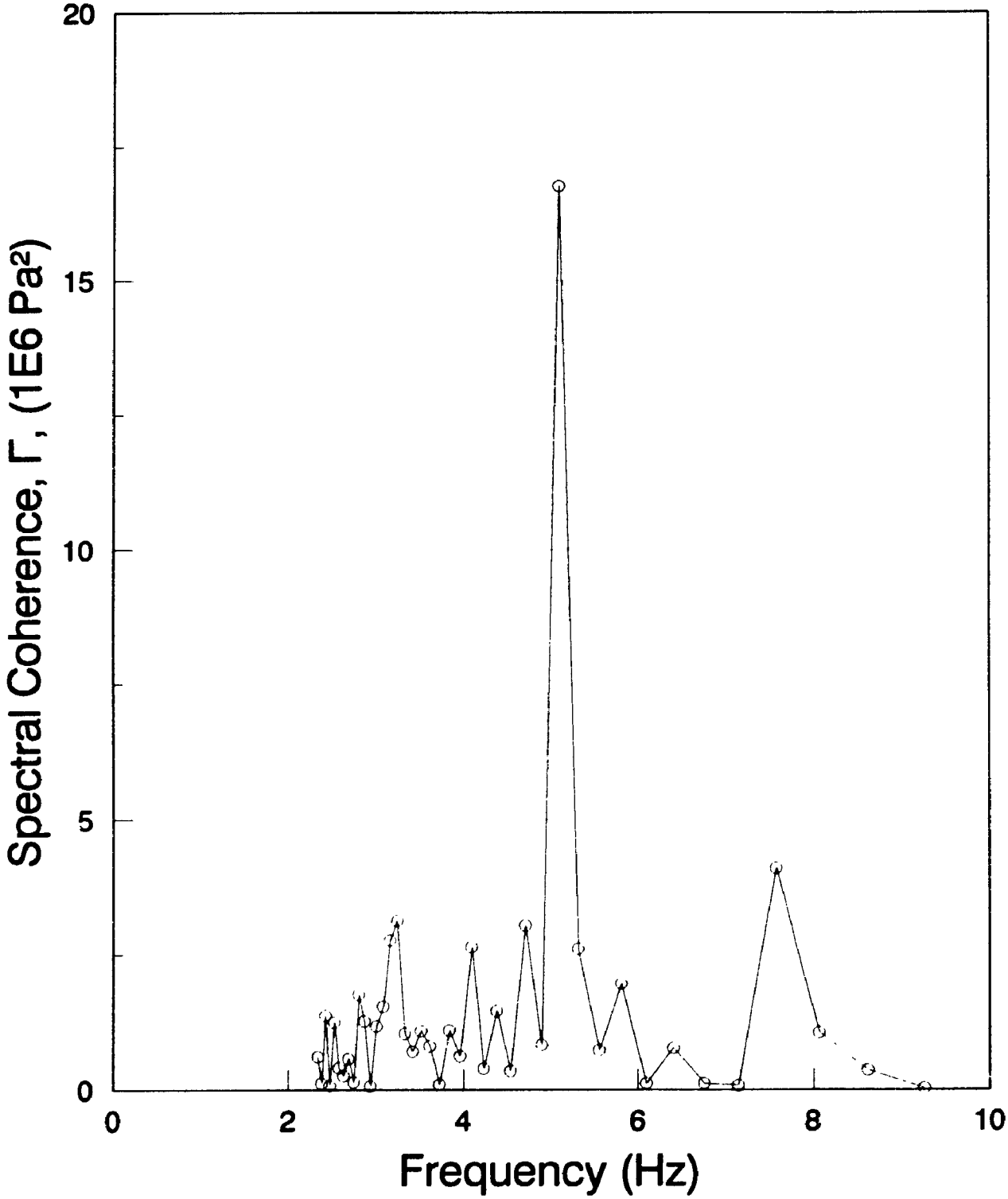

At a gas velocity of 5.6 m/s and a solids flux of 170 kg/m^{2}s (Fig. 4.10.2), most of the power in the spectrum was distributed in a band of frequencies between 4.5 and 6.5 Hz. Louge et al. (1990) observed that the shape of the power spectrum and the dominant frequency in vertical riser transport are insensitive to the superficial gas velocity. They concluded that near the wall the voidage fluctuations are not primarily governed by the gas turbulence, but by local instabilities of the granular motion in the dense annular region.

Based on the observation that the dominant frequency from spectral analysis is about 5 Hz (Figs. 4.10.1, 4.10.2), several runs were examined for the impacts of various controlled variables on the power spectrum in this frequency range for vertical lines. Fig. 4.10.3 shows the results of this study at a gas velocity of 5.6 m/s (where there is refluxing) for a range of solid fluxes in a narrow band of frequencies between 2 and 8 Hz. (There was no significant distribution of power on either side of these frequencies). As the sand flux increases from 135 to 195 kg/m^{2}s (Fig. 4.10.3), the spectral coherence at 5 Hz increases from about 9 x 10^6 Pa^2 to 17x 10^6 Pa^2.

Further evidence of a dependence of the spectral coherence on the sand flux for vertical lines is examined in Fig. 4.10.4 for the choking gas velocity of 4.5 m/s. The coherence increases from virtually undetectable at 100 kg/m^{2}s,

Fig. 4.10.2: Power Spectrum for Vertical Line

Pressure Gradient for Sand at 5.6 m/s and 170 kg/m²s [1,2]

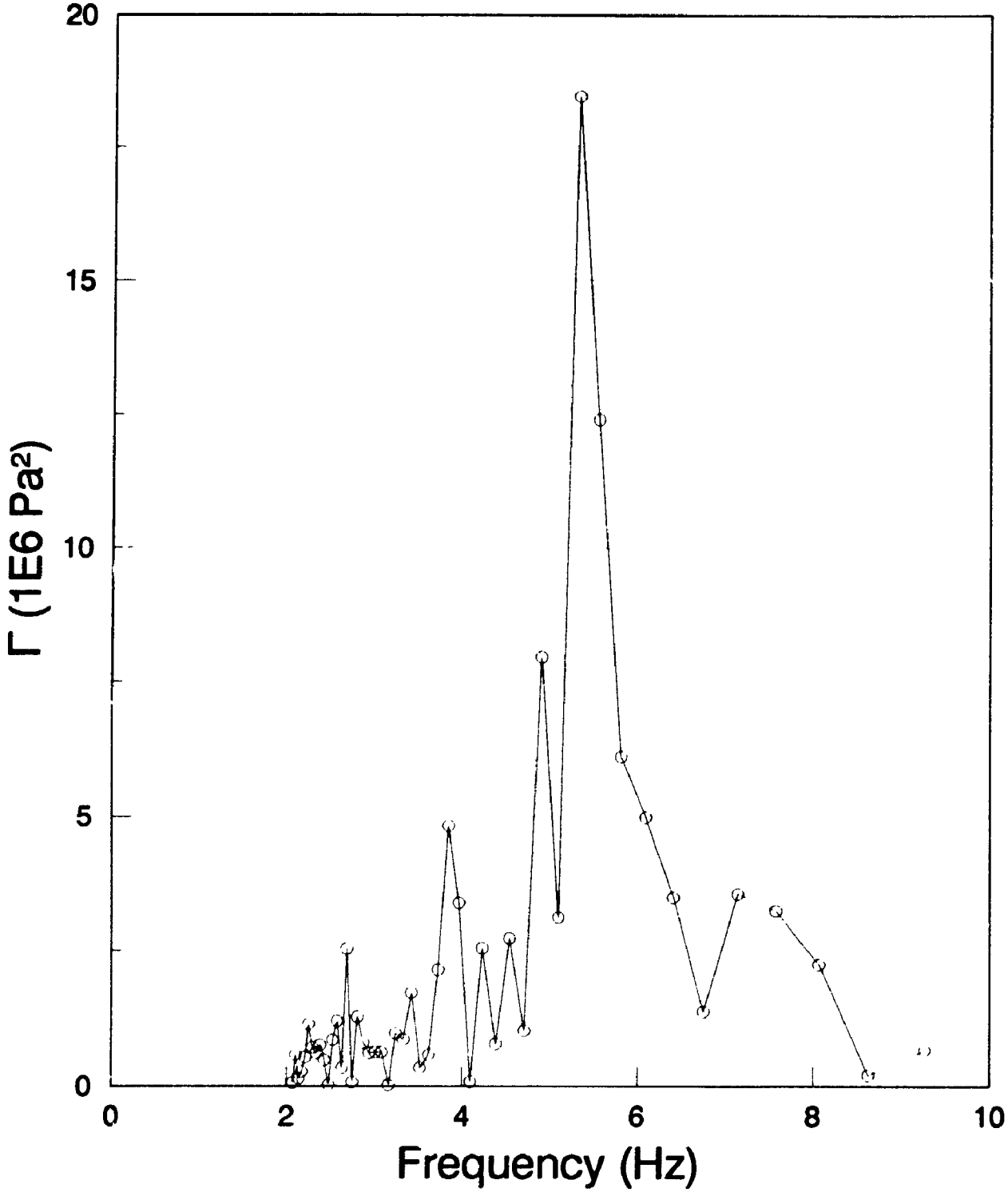

1. Solids Flux = 170 kg/m²s
2. Gas Velocity = 5.6 m/s

Fig. 4.10.3: Effect of Solids Flux on Spectra

Comparison of Pressure Gradient Spectra with Sand at 5.6 m/s

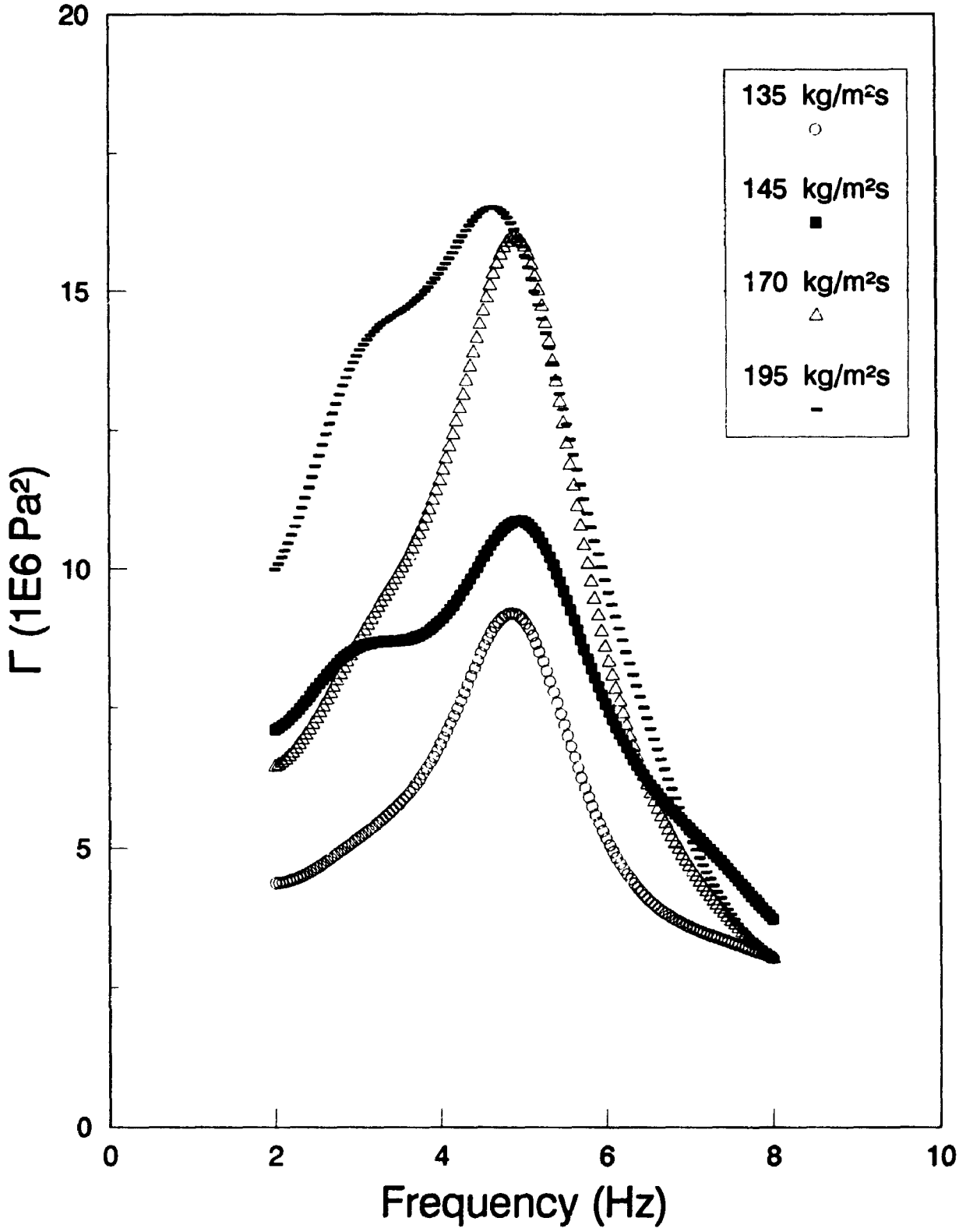

Fig. 4.10.4: Effect of Solids Flux on Spectra

Comparison of Pressure Gradient Spectra with Sand at 4.5 m/s

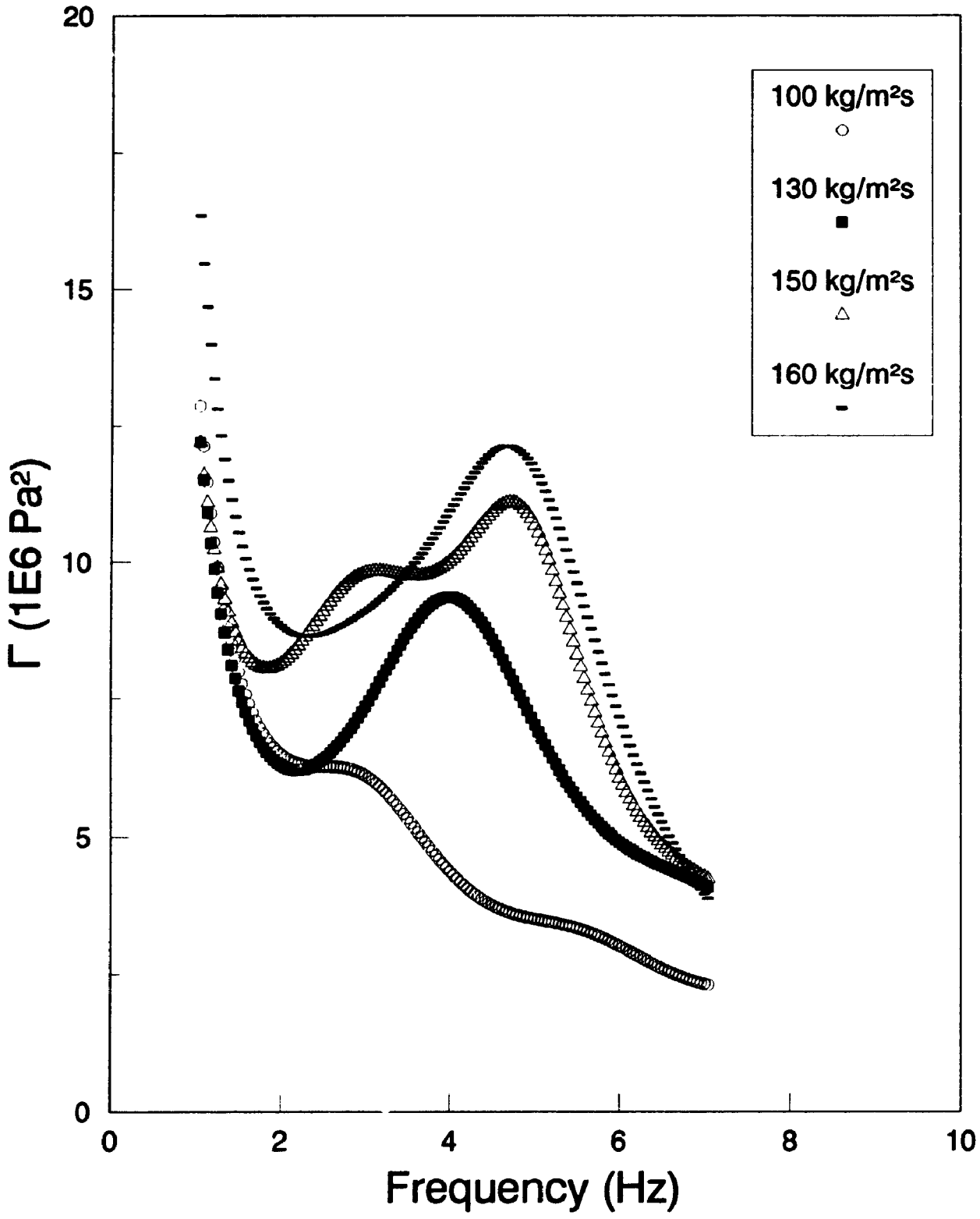

to 12 x 10^6 Pa^2 at 160 kg/m^2s. Based upon numerous investigations there was no significant peak in the power spectrum when the solids flux was less than 100 kg/m^2s. It seems, therefore, that there is some change of flow which is responsible for the manifestation of the peak in the power spectrum at a frequency of about 5 Hz, for a solids flux above 100 kg/m^2s.

Fig. 4.10.5 shows the power spectrum for the transport of sand in a riser inclined at 18°. The power spectrum was generated from the time series data presented in Fig. 4.9.1. A single spike in the power spectrum is observed at a (dominant) frequency of 5.1 Hz. The spectral coherence of the peak is 26 x 10^6 Pa^2, where over 95% of the power is distributed. Similar results for dominant frequency were observed at the intermediate line inclinations, indicating that the dominant frequency is not affected by line orientation. There was no significant correlation (< 0.2) of the dominant frequency with any of the independent variables.

As the gas velocity was increased beyond 10 m/s, a second peak in the power spectrum was detected at a frequency of about 8 Hz. Due to the relatively few number of experiments conducted in the high gas velocity regime, however, this observation could not be further investigated. Drahos and Cermak (1988) found that the dominant frequency from power spectral analysis decreased from 18 Hz (for gas-only flow) to about 5 Hz in

Fig. 4.10.5: Power Spectrum for 18° Line

Pressure Gradient for Sand at 8.5 m/s and 195 kg/m²s [1,2]

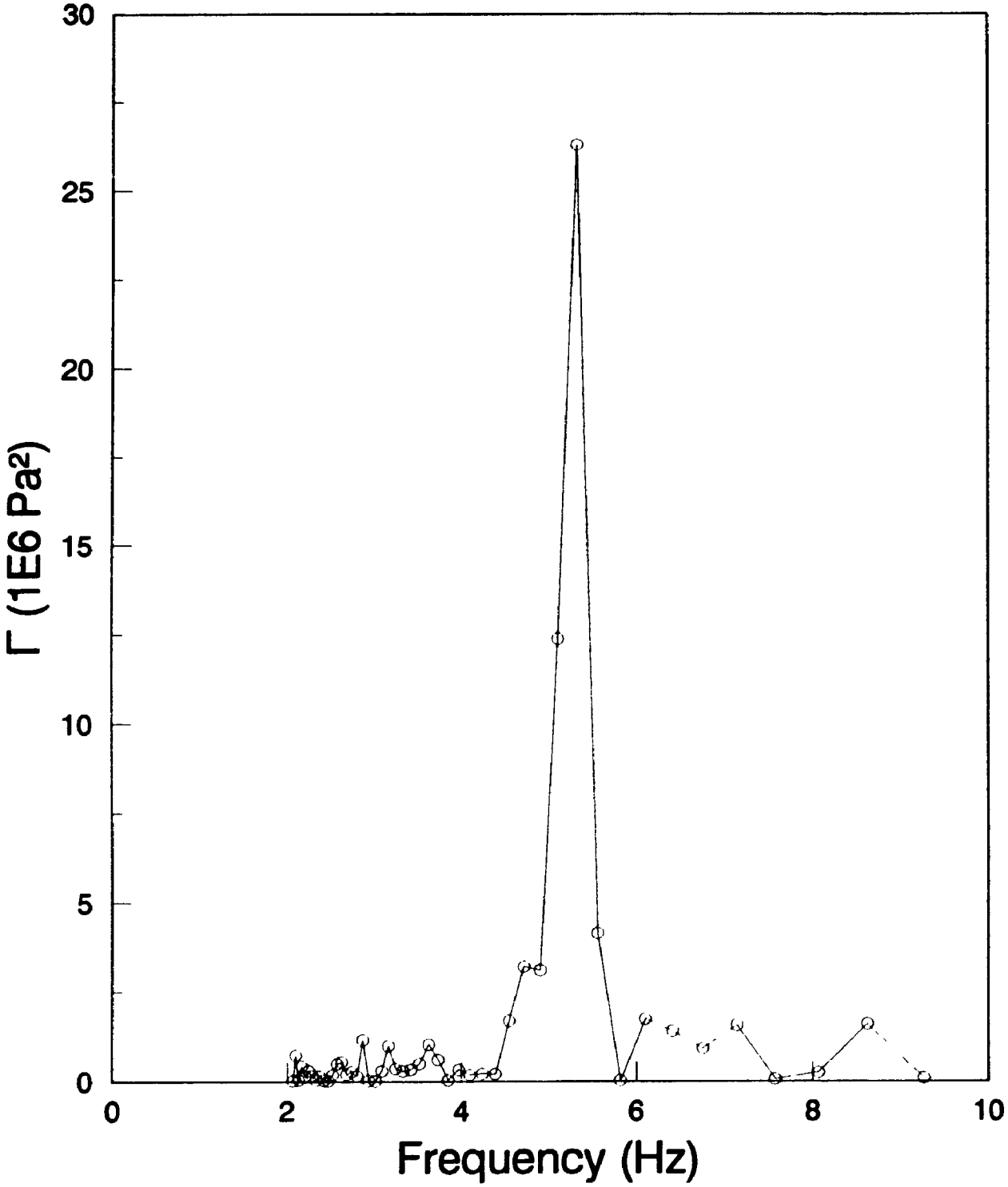

1. Solids Flux = 195 kg/m²s
2. Gas Velocity = 8.5 m/s

the fast fluidization regime. Soo (1987) has found that the wave length, wave velocity, and frequency all increase with increasing air velocity.

4.10.3 DOMINANT FREQUENCY OF POWER SPECTRA

In light of the results observed in Figs. 4.10.1 to 4.10.5 for the power spectra of sand pressure gradient series, a PDF was generated based upon the dominant frequency from spectral analysis. The number of observations is plotted on the left ordinate (representing the number of experiments), and the cumulative percentage of observations is shown on the right ordinate of Fig. 4.10.6. Since line inclination did not affect the position of the dominant frequency (0.18 correlation with θ), data for all line inclinations was included in this analysis. In some instances, where a dominant frequency could not be detected in the power spectrum (for those runs carried out at low solids flux conditions and at high gas velocities), the data was excluded.

The average dominant frequency, f_D , obtained from spectral analysis of the pressure gradient time series data is 4.90 Hz, with a standard deviation of 1.30 Hz. The distribution is approximately Gaussian (dotted line) and the PDF is concentrated in the frequency range of 4 Hz to 6 Hz for approximately 60% of the data. About 20% of the data was at frequencies of between 2 and 4 Hz, while about 20% was also associated with frequencies between 6 and 8 Hz. A complete tabulation of the dominant frequencies for

Fig. 4.10.6: PDF of Pressure Gradient Spectra

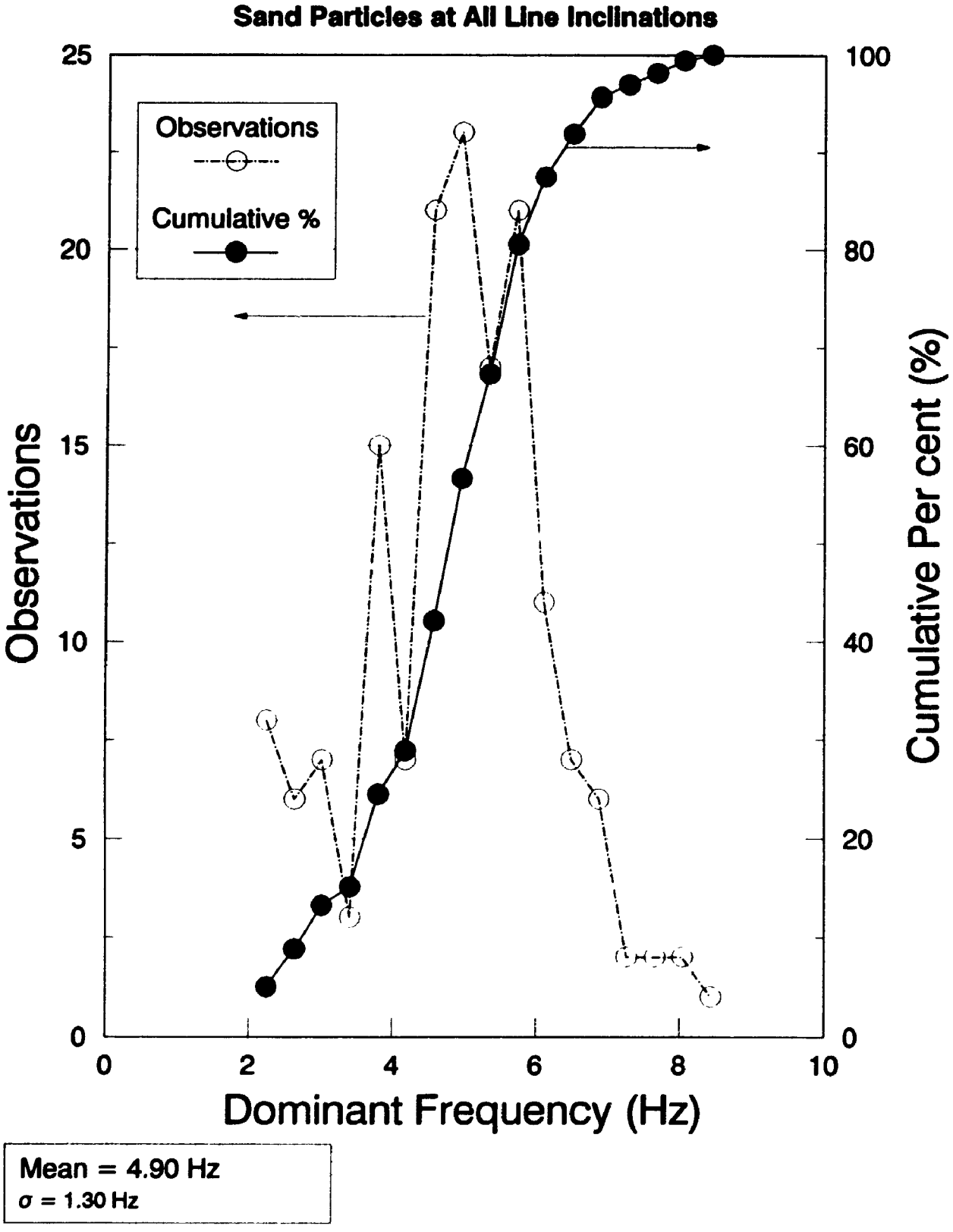

each experimental run is given in Appendix H2.

Arena et al. (1992) have noted that the dominant frequency obtained from spectral analysis of the pressure gradient time series data (analogous to the methods employed here) is a "plug frequency", where a plug represents a packet or cluster of particles travelling through the riser. For the experimental conditions covered by this research, Arena et al. (1992) observed a plug frequency of about 5 Hz. Based on their observations the dominant frequency obtained from pressure gradient data may represent the frequency of solid plugs moving through the riser.

Matsumoto and Harakawa (1987) have found a 5 Hz peak in the power spectral density profile at the point of transition from dilute phase flow to fast fluidization. Soo et al. (1991) observed that the dominant frequency from power spectral analysis for mass flow fluctuation was about 5.5 Hz. The results of these authors corroborate the observations made in this research. It would appear from these results that there is a fundamental property of dense phase transport (characterised by the dominant frequency in the power spectrum) which is not affected by line inclination, as demonstrated in Figs. 4.10.1 and 4.10.5.

4.10.4 STATIC PRESSURE POWER SPECTRA

Dhodapkar and Klinzing (1993) have found that the power spectrum from a static pressure transducer in horizontal pneumatic transport can be used to characterise gas-solids flows under homogeneous or stratified flow conditions. Under such flow conditions the power spectra from two static pressure transducers were the same within experimental variation. Satija et al. (1985) also used power spectra generated from static pressure time series to characterise the transition of flow regimes in vertical pneumatic transport. There are several limitations associated with this technique, however, including that the static pressure is influenced by both upstream and downstream conditions.

Based upon the results of Dhodapkar and Klinzing (1993) for horizontal dilute transport, power spectra were generated for the static pressure signals collected in this research by a transducer situated 1.769 m upstream of the test section. Fig. 4.10.7 shows the PDF (for the dominant frequency from power spectra) for the signals collected by the static pressure transducer. The PDF has a mean of 5.10 Hz and a standard deviation of 0.11 Hz, which are in close agreement with those obtained from the spectral analysis of pressure gradient time series in Fig. 4.10.6. In comparison, Dhodapkar and Klinzing observed that two static pressure transducers separated by some distance had the same basic shape, but there was a

Fig. 4.10.7: PDF of Static Pressure Spectra

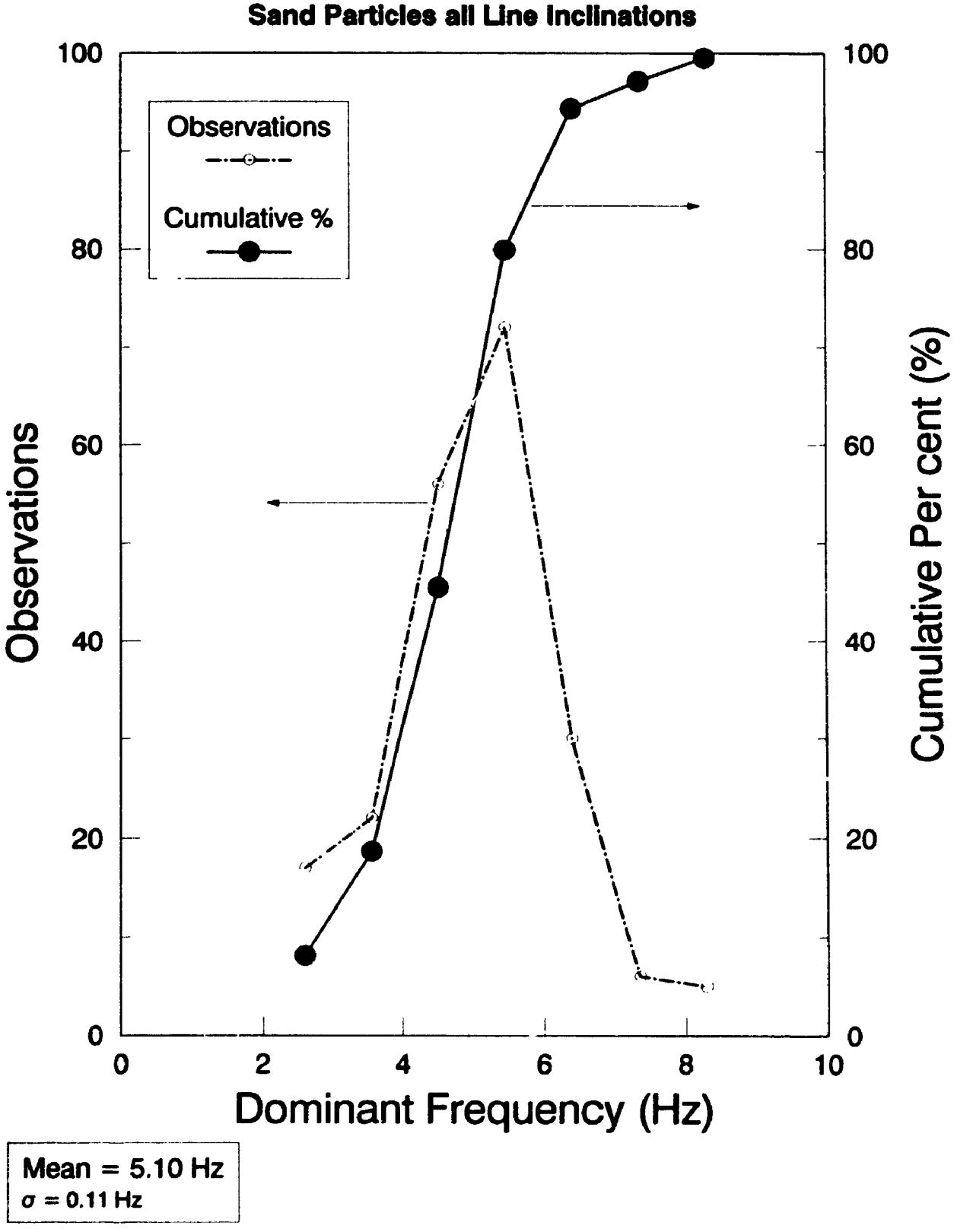

small shift of the dominant frequency in the spectra.

4.10.5 POWER SPECTRA FOR GLASS PARTICLES

A striking difference between the power spectra of the 197 μm sand particles and 441 μm glass beads, is the difference of dominant frequency in the power spectra. A listing of the dominant frequency for all runs for glass beads is tabulated in Appendix H4. There is no single dominant frequency for vertical riser transport of glass. It ranges from 2.0 to 6.4 Hz, and is not significantly correlated with any of the controlled variables. This could be because the sand particles flow in a regular "dune" flow, whereas the glass beads flow resemble a more chaotic and irregular flow pattern (Dhodapkar and Klinzing, 1993).

Fig. 4.10.8 shows a typical power spectrum obtained for the glass beads at 17° orientation, for a gas velocity of 8.5 m/s, and at a solids flux of 180 kg/m^{2}s. A single dominant frequency at about 3 Hz is observed in the spectrum. There was some fluctuation of the dominant frequency in the power spectra at different conditions, similar to the observations made for the vertical line. However, the dominant frequency was always less than 8 Hz for all line orientations.

Fig. 4.10.9 shows the PDF of the dominant frequency for glass beads at all

Fig. 4.10.8: Power Spectrum for Glass at 17°

Pressure Gradient at 8.5 m/s and 180 kg/m²s [1, 2]

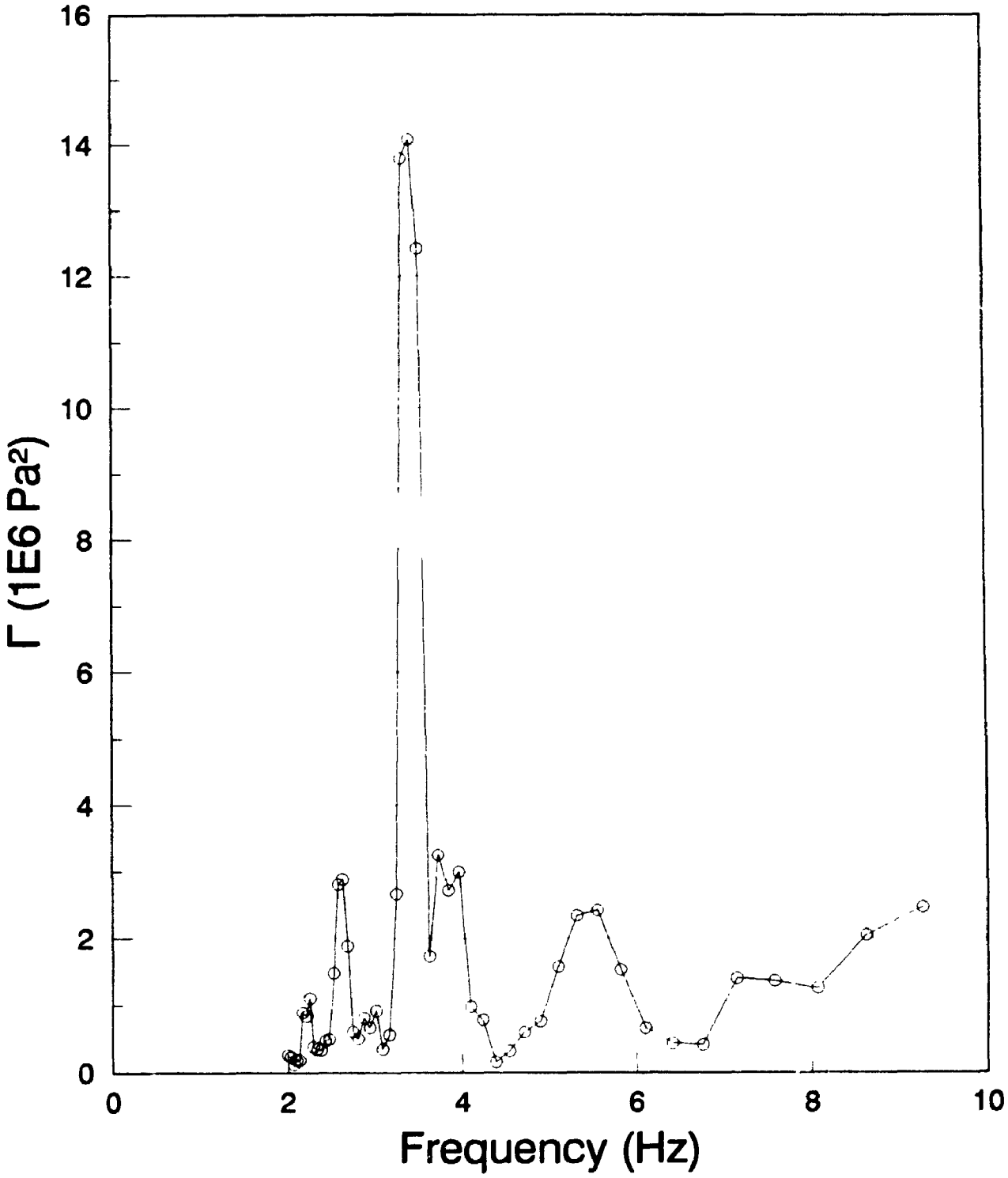

1. Solids Flux = 180 kg/m²s
2. Gas Velocity = 8.5 m/s

Fig. 4.10.9: PDF of Pressure Gradient Spectra
Glass Beads all Line Inclinations

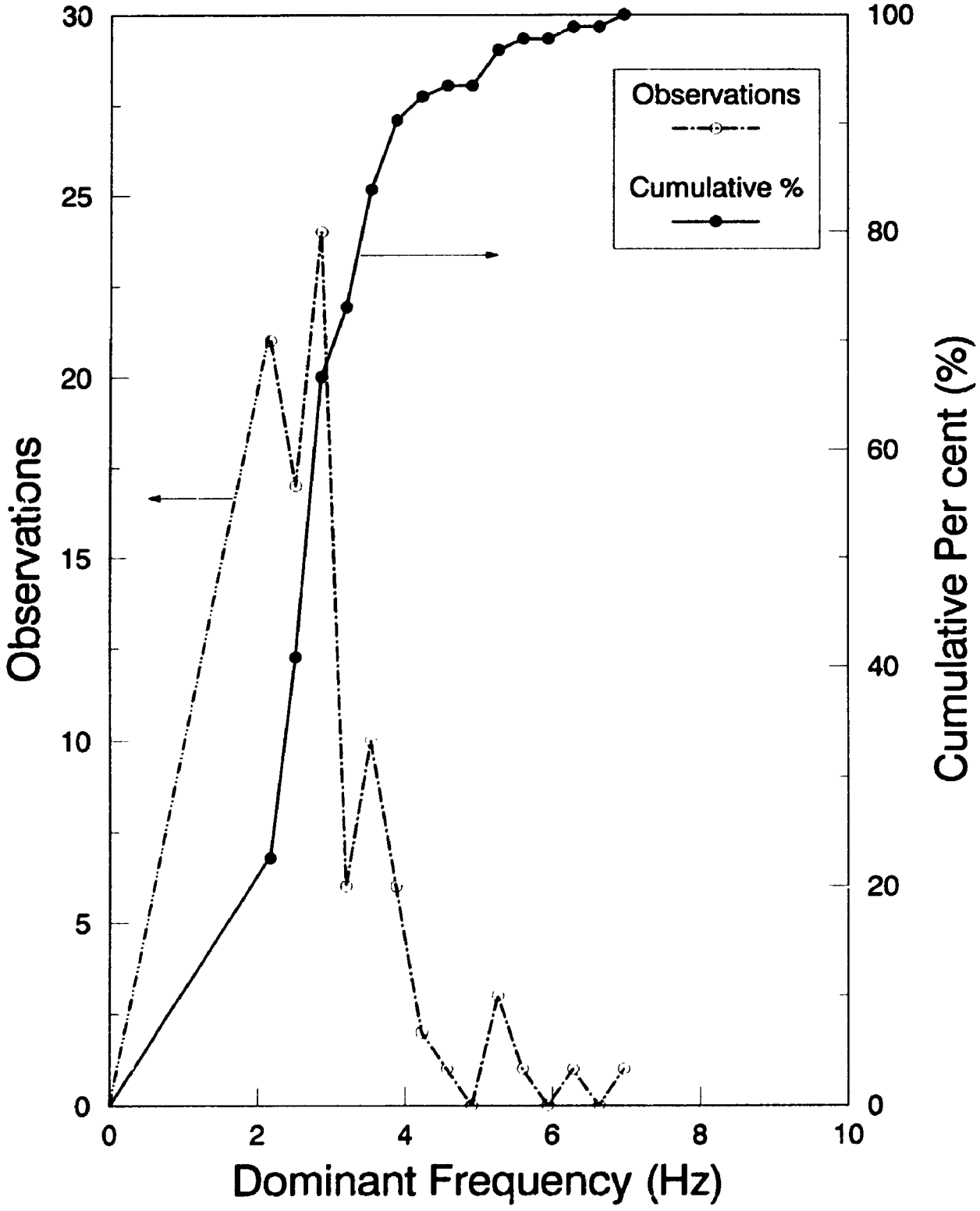

line inclinations. For 70% of all experiments, the dominant frequency is between 2.17 Hz and 2.86 Hz. At 17 degrees the dominant frequency is greater than 3 Hz (Appendix H4). Zhu and Soo (1992) observed a dominant frequency (for mass flow fluctuations) of about 3 Hz for the type of glass beads particles used in this research. Dhodapkar and Klinzing (1993) observed a dominant frequency of about 2.5 Hz for 450 μm glass beads (similar to those used here) for horizontal transport.

The spectral coherence at the dominant frequency for glass beads was strongly influenced by line inclination. Fig. 4.10.10 shows the effects of solids flux and line inclination on Γ (f) using a surface plot format, generated by the scientific software AXUM (Trimetrix, 1993). The grid is an exact replica of the computed spectral data at the dominant frequency for the glass beads. It is apparent that there is a strong interaction effect between the solids flux and line inclination. The spectral coherence appears to increase in synchronization with both of these variables, from a lower limit of less than 5×10^6 Pa^2 (for the vertical line and up to 250 kg/m^2s solids flux), to about 28×10^6 Pa^2 at a line inclination of 17°, and a solids flux of 300 kg/m^2s. The simultaneous increase of Γ(f) with both of these variables may suggest that the phenomenon observed is a "moving slug" or wave frequency, analogous to the observations of Schnitzlein and Weinstein (1988) and Arena et al. (1992). Such a slug is known from experiment to

Fig. 4.10.10: Effect of Inclination, θ, on Spectral Coherence, Γ
Glass Beads Pressure Gradient Spectra

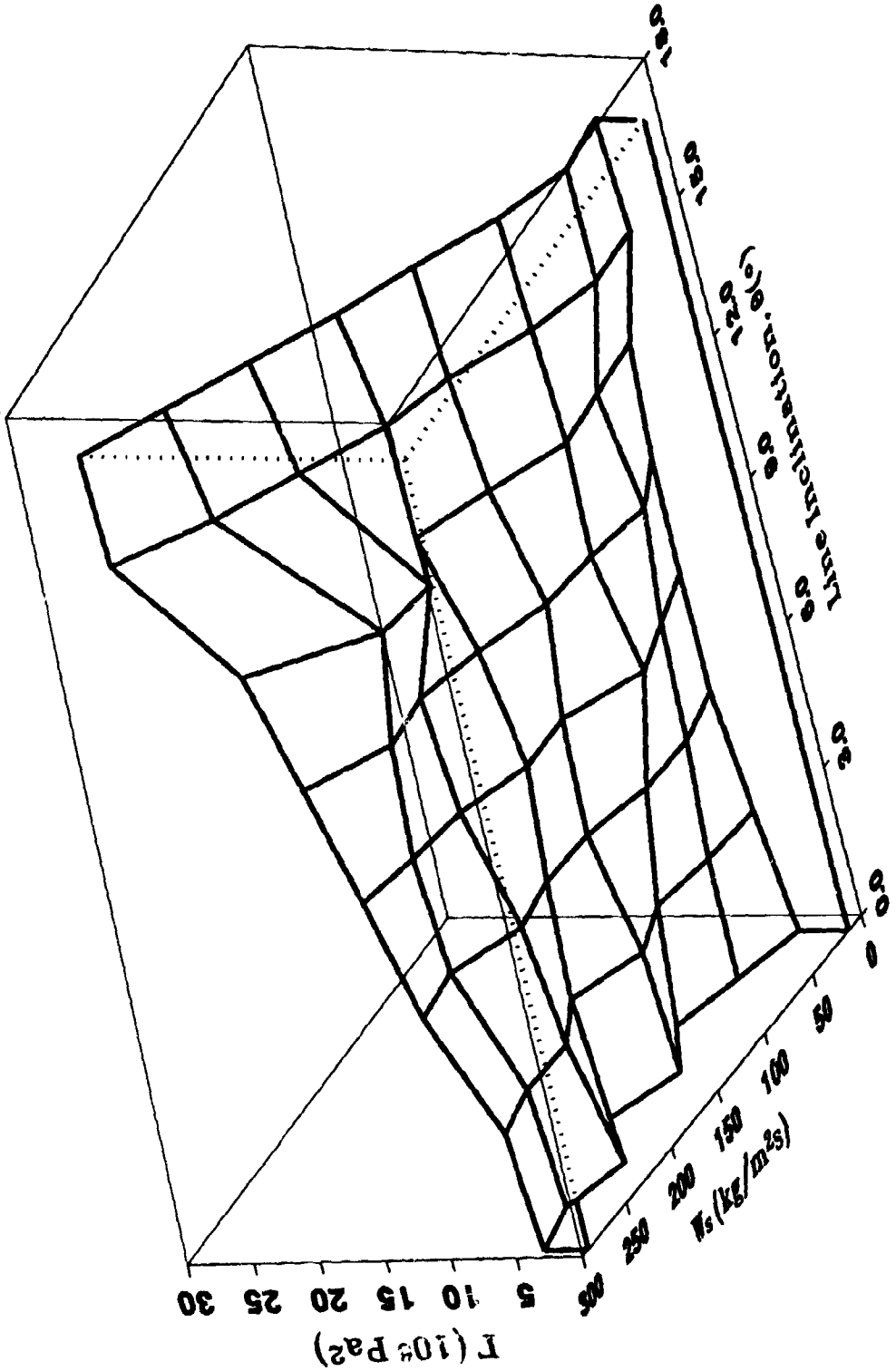

increase with both the solids flux and line inclination.

4.11 ARIMA MODEL FOR TIME SERIES DATA

In § 4.10 a non-parametric approach, using the dominant frequency in the power spectrum, was used for oblique riser flow characterisation. Another method that could be employed for representing the time series of pressure gradient data, is a linear stationary autoregressive integrated moving average (ARIMA) model (Box and Jenkins, 1970). Subsequent analysis of the ARIMA model would presumably correlate either the optimal order of the model, or the numerical values of model coefficients, with the flow patterns such as gas velocity, solids flux, or line inclination.

A detailed Box-Jenkins time series analysis has shown that an ARIMA (n,0,0) model is appropriate for over 80% of the data analysed, where n is an integer that varies between one and five. For simplicity the ARIMA(n,0,0) model will be referred to as an AR(n) model. The precise number of parameters is determined from a statistical analysis (based upon 95% confidence bands) of the partial autocorrelation function. The AR(n) model is given by equation (58):

$$P_t = a_1 P_{t-1} + a_2 P_{t-2} + \ldots + a_k P_{t-k} + w_t \qquad (58)$$

Here k is the order of the model; P_t ,..., P_{t-k} are pressure gradient values

(centred around the mean) at times t,..., t-k; a_1,..., a_k are model coefficients determined from the Yule-Walker equations using the autocorrelation function (Jutan, 1990); and w_t is a white noise process with zero mean.

4.11.1 NUMBER OF ARIMA PARAMETERS FOR SAND

The autocorrelation function of the pressure gradient time series decreases exponentially with time. However, it is the partial autocorrelation function, $\Phi(\tau)$, which is useful for estimation of the number of parameters required in the ARIMA model (Box and Jenkins, 1970).

Fig. 4.11.1 shows the partial autocorrelation function, $\Phi(\tau)$, generated for sand particles in the vertical orientation. Solid bars represent the magnitude of the parameters a_i used to estimate the parameters of the AR(n) model. Each time lag represents a single sampling interval of 0.081 s, as noted in § 4.9.2. The dotted horizontal line at 0.2 (normalized units) designates the 99% confidence band (or three standard deviation band from χ^2 distribution) for the parameters. (A 95% confidence band, representing two standard deviations, would be at 0.115 on the ordinate). Numerical values are printed on each bar because of the importance of the magnitude of the numbers, in determining whether they will be accepted or rejected based on the χ^2 test. An inspection of Fig. 4.11.1 shows that the order of the AR(n) model is 1; parameters after the first (AR1) are not significant at

Fig. 4.11.1: Partial Autocorrelation Function [1]

Vertical Transport of Sand at 100 kg/m²s and 4.5 m/s

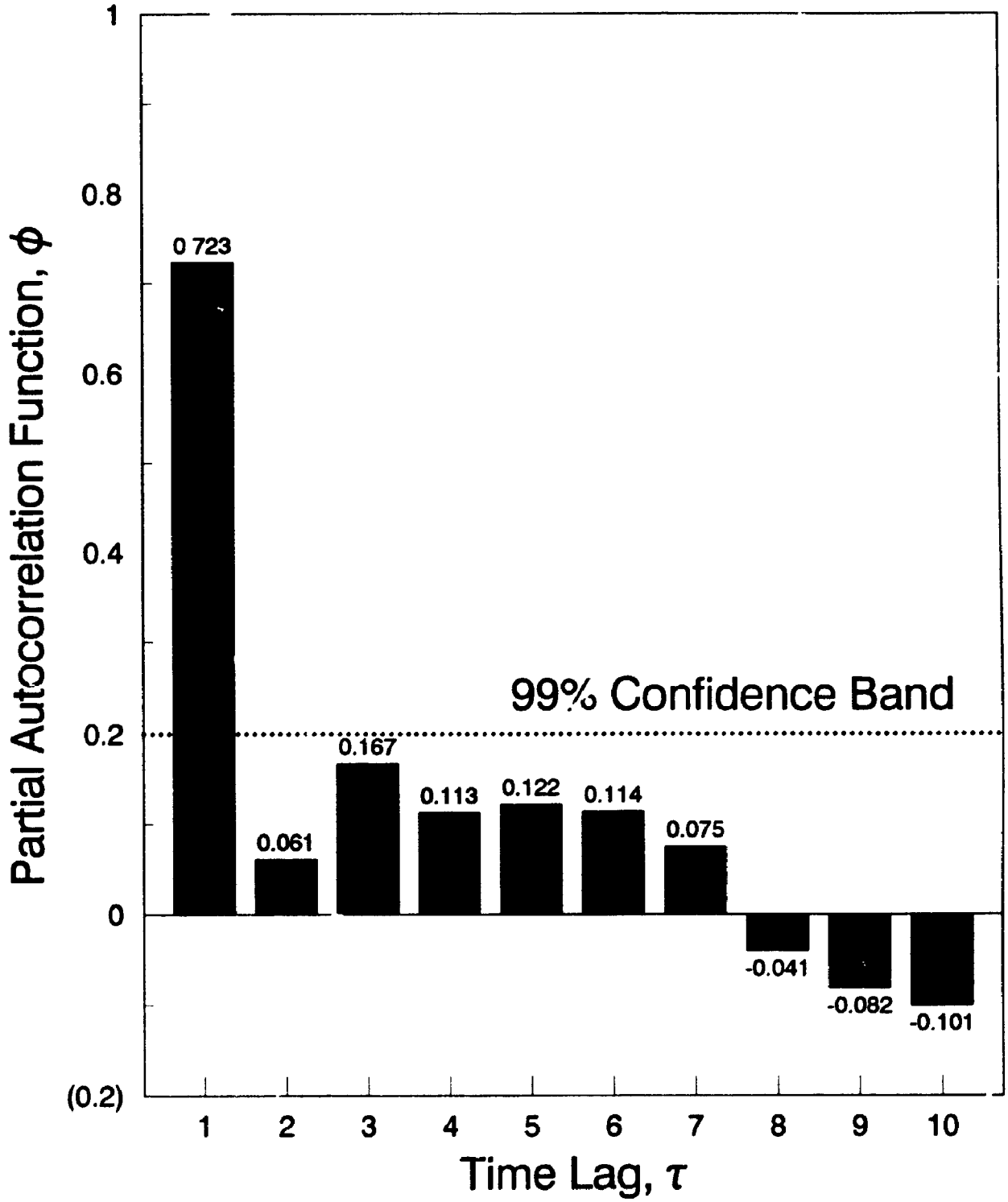

1. Each time lag, τ, is 0.081 s

the 99% level of confidence.

For a line inclination of 11° (Fig. 4.11.2) the second parameter (AR2 at time lag 2) is negative. However it is not significant at the 99% level of confidence, so the order of the ARIMA model is still 1. When the line inclination is increased to 18° (Fig. 4.11.3), the number of significant parameters increases to 2; the first, AR1, is positive, and the second, AR2, is negative.

A summary of the parameter estimates for all experimental conditions for sand particles is tabulated in Appendix H2. The run number from which these data were computed is shown in the left-most column. This run number can be used to obtain the experimental conditions from Appendix H1.

The ARIMA model adequacy for the time series (Appendix H2) is given by the R^2 (%), which is the correlation squared, expressed as a percentage. Not all of the experimental data were amenable to the ARIMA type of analysis. For the sand particles, 82% of the data were fit to an AR(n) type model, with n ranging from 2 to 3. Of these data, 76% of the models required at least two parameters, whereas three parameters were needed for 42% of the cases considered. A 2-parameter AR(n) model (a_1 positive; a_2 negative) could

Fig. 4.11.2: Partial Autocorrelation Function [1]

11° Transport of Sand at 100 kg/m²s and 4.5 m/s

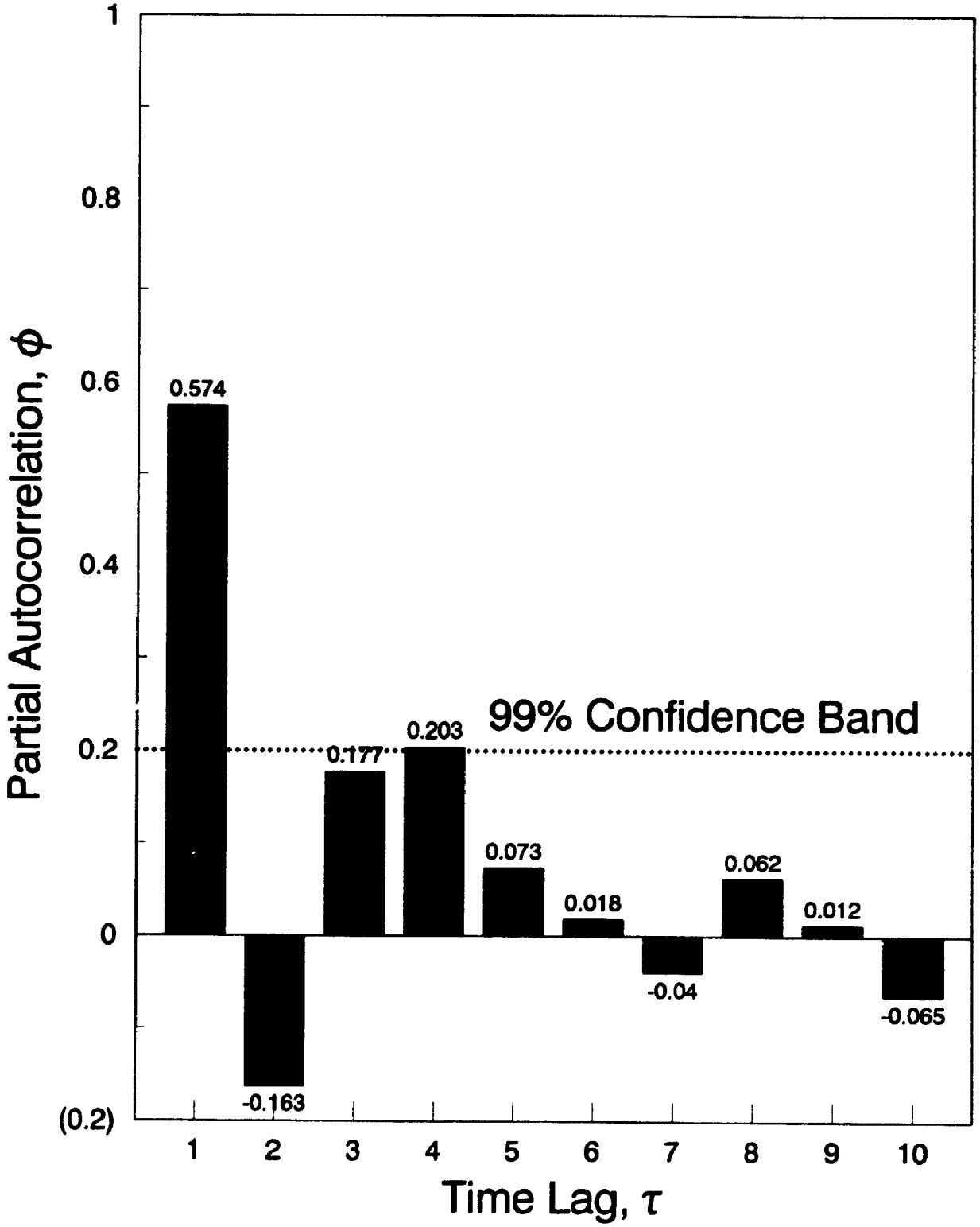

1. Each time lag is 0.081 s

Fig. 4.11.3: Partial Autocorrelation Function [1]

18° Transport of Sand at 100 kg/m²s and 4.5 m/s

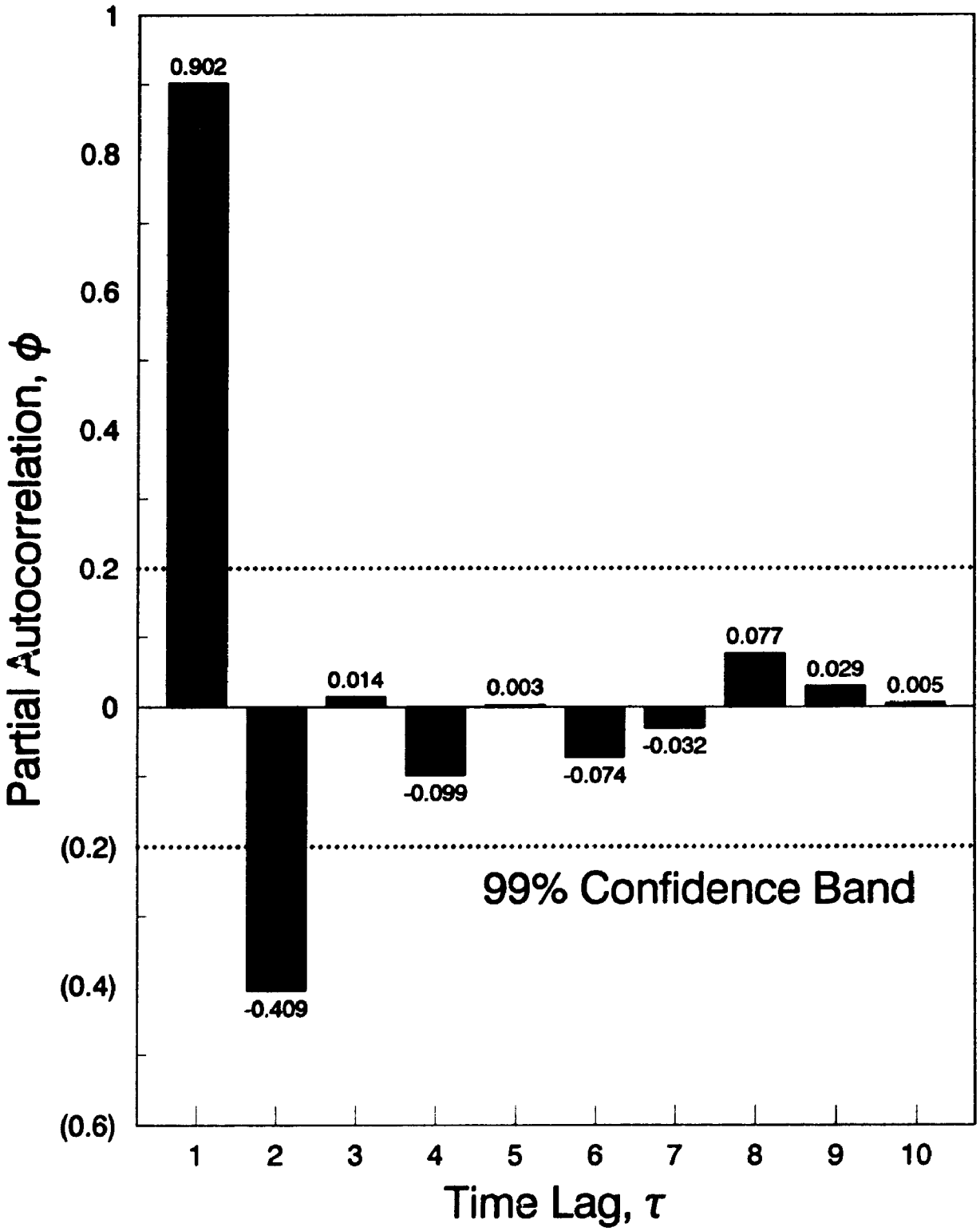

1. Each time lag is 0.081 s

suffice for the entire range of experimental conditions covered by this study.

The value of AR1 is positive over the entire range of conditions studied for sand particles, which agrees with Drahos and Cermak (1988). They observed that a single AR parameter (AR1) was often adequate for on-line flow characterisation of vertical risers in pneumatic transport flows, and that AR1 was positive for fast fluidization, but negative for dilute phase flow. The validity of AR1 changing sign as the flow regime shifted from dilute to dense flow conditions, as indicated by Drahos and Cermak (1988), could not be checked in this research since all of the experiments conducted here were in the non-slugging dense phase (Figs. 3.4.1 to 3.4.7).

No strong effect of any of the controlled variables on the model order was observed. The magnitude of the coefficients was not strongly dependent on changes of experimental conditions, including line inclination. The AR(n) model may have applications for time series forecasting, but there is no evidence to suggest that the model could be used to predict the transition to choking.

4.11.2 FORM OF ARIMA FOR GLASS BEADS

The time series obtained from experiments with glass beads were also modelled using an ARIMA (n,0,0) form. Fig. 4.11.4 shows the partial

Fig. 4.11.4: Partial Autocorrelation Function [1]

Vertical Transport of Glass Beads at 120 kg/m²s and 8.5 m/s

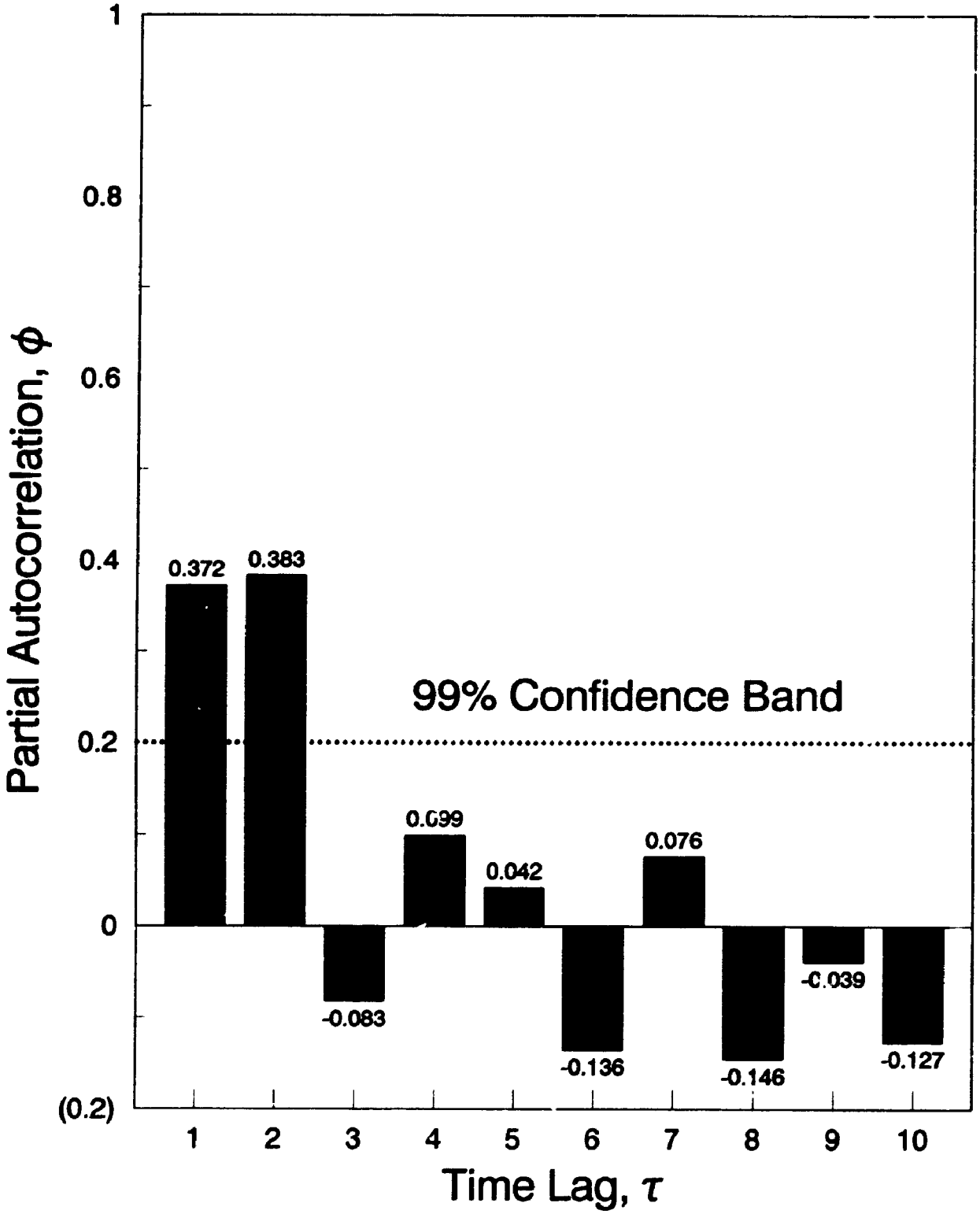

1. Each time lag is 0.081 s

autocorrelation profile for glass beads (vertical orientation), for the time series characterised in Figs. 4.9.5 and 4.9.6. Two parameters are statistically significant, and both are about 0.38 in magnitude. At 7° (Fig. 4.11.5) two parameters are also required, and both are also positive. At 17° (Fig. 4.11.6) three parameters, all positive, are statistically significant. This partial autocorrelation function was obtained from the time series data characterised in Figs. 4.9.7 and 4.9.8.

A common characteristic of the pressure gradient time series data for glass beads is the exponential decay of the partial autocorrelation function (Figs. 4.11.4 to 4.11.6). AR1 is negative for about 20% of all experiments, while AR2 is usually negative for solids fluxes less than 100 kg/m^{2}s. A detailed listing of all the values of the model coefficients for experiments with glass beads is given in Appendix H4. The experimental conditions for these runs (from which the ARIMA parameters are derived) are given in Appendix H3. Of the total number of experiments analysed, 90% could be adequately fit with an AR(n) model. Of these, 88% required at least 2 parameters, 62% needed three parameters, and 32% used four parameters. The average number of parameters estimated was 2.93 for glass beads compared with 1.94 for sand.

Fig. 4.11.5: Partial Autocorrelation Function [1]

7° Transport of Glass Beads at 120 kg/m²s and 8.5 m/s

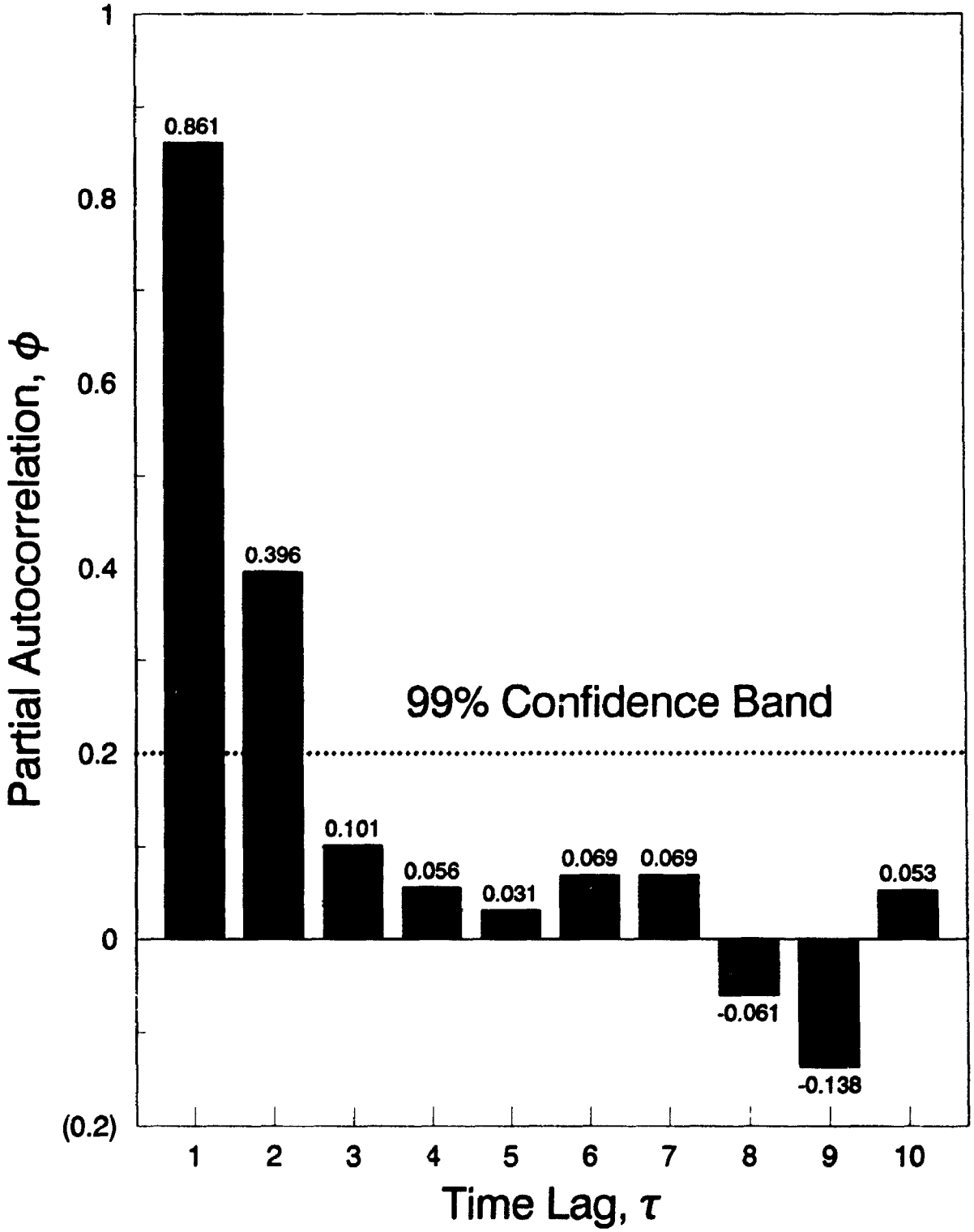

1. Each time lag is 0.081 s

Fig. 4.11.6: Partial Autocorrelation Function [1]

17° Transport of Glass Beads at 120 kg/m²s and 8.5 m/s

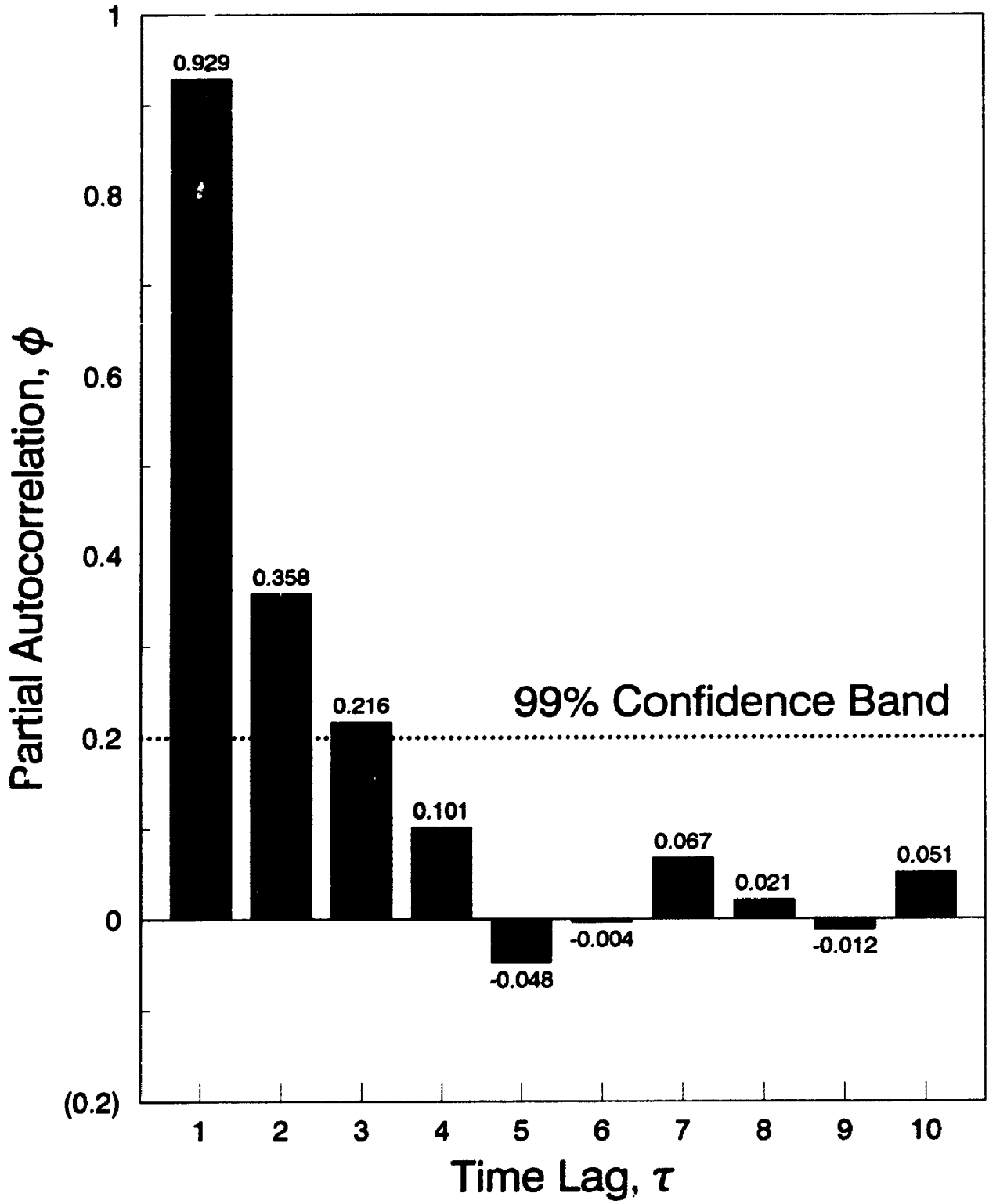

1. Each time lag is 0.081 s

4.11.3 MODEL ADEQUACY

Model adequacy of the AR(n) model was assessed in two ways by an R^2 (expressed as a percentage) shown for each of the fitted data points in Appendix H. An average R^2 of 55% was observed for sand, and 75% for glass beads.

5. CONCLUSIONS

For the non-slugging dense phase, and for the range of particle sizes covered by Geldart Group B powders and some Geldart Group A powders, it is concluded that :

1a. The average riser pressure gradient in the fully-developed test section is influenced primarily by the solids holdup and the line inclination. The effect of θ on the fully developed pressure gradient is prominent primarily in the low gas velocity region, within 2 m/s of the choking velocity.

1b. Where the line inclination is above 7°, and the gas velocity is within 2 m/s of the choking velocity, α cannot be used to estimate the pressure gradient due to solids holdup, because of solids deposition with refluxing at the pipe wall.

2a. The gross lifting efficiency is higher for the non-slugging dense phase in comparison with the dilute phase.

2b. Line inclination for a commercial-scale oblique riser should be maintained below 7° from the vertical to minimize excessive frictional losses and erosion from an annulus displaced to the underside of the pipe.

3a. The standard deviation of the pressure gradient fluctuations is proportional to the solids holdup at all line inclinations. There is potential for it to be used as a leading indicator for the on-line estimation of the choking velocity.

3b. There is a characteristic (dominant) frequency in the power spectra generated from the pressure gradient time series data, which is 5.1 Hz for sand and about 3 Hz for glass. The dominant frequency is observed for solids fluxes above 100 kg/m^2s, and its value is invariant with θ. The spectral coherence at the dominant frequency increases with the solids flux.

3c. The pressure gradient time series can be adequately modelled using a linear stationary ARIMA model of form AR(n), with n varying between 2 and 4. The model is valid at all line inclinations.

4a. The choking solids flux decreases with line inclinations above 7°, but $\alpha \approx 3\%$ at the choking point for all line inclinations.

4b. The choking velocity increases linearly with particle velocity for all line inclinations.

4c. Solids friction factors are negative whenever there is solids refluxing or deposition at the pipe wall. This phenomenon is

exacerbated at higher line inclinations. The friction factor can not be estimated from the methods used for dilute phase transport because of solids refluxing and deposition at pipe boundaries.

4d. The empirical correlations available in the literature for dilute vertical pneumatic transport flows (particle velocity and solids friction factor), cannot be applied to the non-slugging dense phase at any line orientation, including the vertical. Assumptions upon which they are based are invalid due to refluxing of solids.

5. A semi-empirical model that takes into account negative friction factors which result from solids refluxing, has been developed for oblique riser transport. It correlates the pressure gradient with solids loading, particle velocity, and line inclination, using a basic mathematical form developed for vertical pneumatic transport.

6. RECOMMENDATIONS

It is recommended that future oblique and vertical riser studies endeavour to investigate:

- the effect of tube diameter (up to 0.5 m) on the solids refluxing, annulus formation, and maximum solids throughput;

- methods of computing solids friction factor directly at tube diameters of up to 0.5m;

- the radial dependence of particle velocity and slip velocity in oblique riser transport operated in the refluxing flow regime for a tube diameter of up to 0.5 m.

7. REFERENCES

Adewumi, M. and Arastoopour, H., "Pseudo-two-dimensional Steady-state Two-phase Flow Model for Gas-Solids Vertical Pneumatic Conveying Systems", Int. J. Eng. Fluid Mech. 3(1) : 53-70 (1990).

Amos, G., Rhodes, M., and Mineo, H., "Gas Mixing in Gas-Solids Risers", Chem. Eng. Sci. 48(5): 943-949 (1993).

Al Taweel, A., Militzer, J., Kan, J., and Hamdullahpur, F., "Motion of Hydrodynamic Aggregates", Powder Tech., 59 : 173-181 (1989).

Ally, M., "Electrostatic Effects in Dilute and Dense Phase Gas-Solid Pneumatic Transport", Ph.D. Dissertation, University of Pittsburgh, Pittsburgh, Penn. (1981).

Annunziato, M., "A Measuring System for Two-Phase Flow Pattern Recognition Using Statistical Analysis", from "Multiphase Flow and Heat Transfer Second Int. Symp.", Vol. 2, pp. 1356-1366, Xue-Jue Chen, T.N. Veziroglu, C.L. Tien Eds., Hemisphere Pub. Co. N.Y. (1991).

Arastoopour, H., and Gidaspow, D., "Vertical Pneumatic Conveying

Using Four Hydrodynamic Models", Ind. Eng. Chem. Fundam., 18 (2):123-130 (1979).

Arastoopour, H., "Pneumatic Transport of Solids", in Encyclopedia of Fluid Mechanics Solids and Gas-Solids Flows,Vol. 4, Chapter 11, pp. 349-362, N. Cheremisinoff Ed., Gulf Pub. Co., Houston (1986).

Arena, U., Commarota, A., Massimilla, L., and Pirozzi, D., "The Hydrodynamic Behaviour of Two CFBs of Different Sizes" in Circulating Fluidized Bed Tech. II: pp. 223-230, P. Basu and J. Large Eds., Pergamon Press, Toronto (1988).

Arena, U., Marzochella, A., Massimilla, L., and Malandrino, A., "Hydrodynamics of CFBs with Risers of Different Shape and Size", Powder Tech. 70 : 237-247 (June 1992).

Azzi, M. Turlier, P., Large, J., Bernard, J. and Guignon, P., "Use of a Momentum Probe and Gamma Densitometry to Study Local Properties of Fast Fluidized Beds", in Circulating Fluidized Bed Tech. III : pp. 189-194, P. Basu, M. Horio and M. Hasatani Eds., Pergamon Press, Toronto (1991).

Bader, R., Findlay, J. and Knowlton, T., "Gas/Solids Flow Patterns in a

30.5 cm Diameter CFB" in Circulating Fluidized Bed Tech. II, pp. 123-138, P. Basu and J. Large Eds., Pergamon Press, Toronto (1988).

Bartholomew, R. and Casagrande, R., "Measuring Solids Concentration in Fluidized Systems by Gamma-Ray Absorption", Ind. Eng. Chem., 49(3) : 428-431 (Mar. 1957).

Base, T., "Turbulence I", ES 617A Course Notes, The University of Western Ontario, London, Ontario (1987).

Beeckmans, J., "Solids Volume Fraction at the Injection Point in a Pneumatic Transport Line", Powder Tech. J. 67 : 67-69 (1991).

Bendat, J.S. and Piersol, A.G., "Random Analysis and Measurement Procedures", Wiley, New York (1971).

Berker, A. and Tulig, T., "Hydrodynamics of Gas-Solids Flow in a Catalytic Cracker Riser", Chem. Eng. Sci. 41(4) : 821-827 (1986).

Bi, H. and Zhu, J., "Static Instability Analysis of CFBs and Concept of High-Density Risers", AIChE J. 39(8): 1272-1280 (1993).

Bi, H., Grace, J.R., and Zhu, J., "On Types of Choking in Vertical Pneumatic Systems", Int. J. Multiphase Flow 19: 1077-1092 (1993).

Boothroyd, R.G., "Pressure Drop in Duct Flow of Gaseous Suspensions of Fine Particles", Trans. Inst. Chem. Eng., 44 : T306-T313 (1966).

Box, E.P. and Jenkins, G.M., Time Series Analysis : Forecasting and Control, Chapter 3, pp. 46-84, Holden Day, San Francisco (1970).

Brereton, C. and Stromberg., L., "Some Aspects of the Fluid Dynamic Behaviour of Fast Fluidized Beds", in Circulating Fluidized Bed Tech., pp. 133-144, P. Basu Ed., Pergamon Press, Toronto (1985).

Brereton, C. and Grace, J., "Microstructural Aspects of the Behaviour of CFBs", Chem. Eng. Sci. 48(14): 2565-2572 (1993).

Capes, C. and Nakamura, K., "An Experimental Study with Particles in the Intermediate and Turbulent Flow Regimes", Can. J. Chem. Eng. 51 : 31-38 (Feb. 1973).

Cooley, J.W. and Turkey, W., Mathematics and Computation, 19: 297-301 (1965).

Dhodapkar, S., Zaltash, A., Myler, C., and Klinzing, G., "Acceleration Zone Studies in Pneumatic Conveying Systems at Various Inclinations", AIChE Symp. Ser. 270, Vol. 85 : 1-10 (1987).

Dhodapkar, S. and Klinzing, G., "Pressure Fluctuations in Pneumatic Conveying Systems", Powder Tech. 74: 179-195 (1993).

Drahos, J., and Cermak, J., "Characterization of Flow Regime Transition in a Circulating Fluidized Bed", Powder Tech. 56, 41-46 (1988).

Dry, R. and Christensen, I., "Periodic Density Inversion Effects in a High Velocity Fluidized Bed", Chem. Eng. Sci. 43(3) : 731-733 (1988).

Dry, R. and White, C., "Gas Residence Time Characteristics in a High Velocity CFB of FCC", Powder Tech. 58 : 17-23 (1989).

Gajdos, L. and Bierl, T., "Studies in Support of Recirculating Bed Reactors for the Processing of Coal", Topical Report Contract No. EX-76-C-01-2449, Carnegie-Mellon U., Pittsburgh, Penn. (Sept. 1978).

Galtier, P., Pontier, R., and Patureaux, T., "Near Full-Scale Flow Model for the R2R Catalytic Cracking Process", in Fluidization VI, pp. 17-

24, J.R. Grace, L.W. Shemilt, M.A. Bergougnou Eds., Engineering Foundation, New York (1989).

Geldart, D., "Types of Gas Fluidization", Powder Tech. 7: 285-292 (1973).

Geldart, D. and Rhodes, M., "From Minimum Fluidization to Pneumatic Transport", in Circulating Fluidized Bed Tech., pp. 21-32, P. Basu Ed., Pergamon Press, Toronto (1986).

Ginestet, A., Guignon, P., Large, J., Sen Gupta, S.K., and Beeckmans, J., "Hydrodynamics of a Flowing Gas-Solids Suspension at High Angles of Inclination", Can. J. Chem. Eng. 71: 177-182 (April 1993).

Gianetto, A., Pagliolico, S., Roven, G., and Ruggen, B., "Theoretical and Practical Aspects of CFBs for Complex Chemical Systems", Chem. Eng. Sci. 45(8) : 2219-2225 (1990).

Grace., J., "High Velocity Fluidized Bed Reactors", Chem. Eng. Sci. 45(8) : 1953-1966 (1990).

Hariu, O.H., and Molstad, M.C., "Pressure Drop in Vertical Transport of Solids by Gases", Ind. Eng. Chem., 41: 1148- 1160 (1949).

Hellinckx, L., "Slip Velocity in Carrier Lines", from Interaction Between Fluids and Particles, London, Instn. Chem. Engrs., pp. 67-74 (1962).

Hinkle, B.L., Ph.D. Thesis, Georgia Inst. Tech., Georgia (1953).

Hintze, J.L., "Number Cruncher Statistical System", Pacific Ease Co., Santa Monica, CA. (1990).

Hirama, T., Takeuchi, H., and Chiba, T., "Regime Classification of Macroscopic Gas-Solid Flow in a CFB Riser", Powder Tech. 70 : 215-222 (June 1992).

Horio, M., Ishii, H., and Nishimuro, M., "On the Nature of Turbulent and Fast Fluidized Beds", Powder Tech. 70 : 229-236 (June 1992).

Jenkins, G.M. and Watts, D.G., "Spectral Analysis and its Applications", Holden-Day, San Francisco (1968).

Jiang,. P., Jean, R., and Fan, L., "Baffle Effects on Performance of Catalytic CFB Reactor", AIChE J. 37(9) : 1392-1400 (Sept. 1991).

Jutan, A., "Process Identification and Control", ES660B Course Notes, The

University of Western Ontario, London, Ontario (1990).

Karri, S. and Knowlton, T., "A Practical Definition of the Fast Fluidization Regime" in Circulating Fluidized Bed Tech. III, pp. 67-72, P. Basu, M. Horio and M. Hasatani Eds., Pergamon Press, Toronto (1991).

Klinzing, G., Rohatgi, N., Myler, C., Dhodapkar, S., Zaltash, A., and Mathur, M., "Pneumatic Transport of Solids in an Inclined Geometry", Can. J. Chem. Eng. 67 : 237-244 (Apr. 1989).

Knowlton, T.M., and Bachovchin, D.M., Fluidization Tech., 253-258, D. Keairns (Ed.), Washington: Hemisphere Pub. Corp., Washington (1976).

Kokal, S. and Stanislav, J., "An Experimental Study of Two-Phase Flow in Slightly Inclined Pipes", Chem. Eng. Sci. 44(3) : 665-679 (1989).

Konno, H., and Saito, S., "Pneumatic Conveying of Solids Through Straight Pipes", J. Chem. Eng. Japan, 2 : 211-217 (1969).

Konrad, K., "Dense Phase Pneumatic Conveying Through Long Pipelines", Powder Tech. 48 : 193-203 (1986).

Kunni, D. and Levenspiel, O., "Fluidization Engineering", pp. 72-73, Robert E. Kreiger Publishing Co. Inc., Malabar, Florida (1969).

Kwauk, M., Ningde, W., Youchu, L., Bingyu, C., and Zhiyuan, S., "Fast Fluidization at ICM" in Circulating Fluidized Bed Tech., pp. 33-62, P. Basu Ed., Pergamon Press, Toronto (1986).

Lee, S., "Particle Drag in a Dilute Turbulent Two-Phase Suspension Flow", Int. J. Multiphase Flow 17(3) : 421-424 (1991).

Leu, L. and Lan, C., "Measurement of Pressure Fluctuations in Two-Dimensional Gas-Solid Fluidized Beds at Elevated Temperatures", J. Chem. Eng. Japan 23(5), 555-562 (1990).

Leung, L., Wiles, R., and Nicklin, D., "Correlation for Predicting Choking Flowrates", Ind. Eng. Chem. Process Des. Dev. 10(2) : 183-189 (1971).

Leung, L. and Wiles, R., "Design Procedure for Vertical Pneumatic Conveying Systems", Ind. Eng. Chem. Process Des. Dev. 15(4) : 552-557 (1976).

Leung, L., Jones, P., and Knowlton, T., "Analysis of Moving-Bed Flow of

Solids down Standpipes and Slide Valves", Powder Tech. 19 : 7-15 (1978).

Leung, L.S., "The Ups and Downs of Gas-Solids Flow: A Review", in Fluidization, pp. 25-68, J.R. Grace and J.M. Matsen (Eds.), NY: Plenum Press (1980).

Li, H. and Kwauk, M., "Analysis of Flow Dynamics", Chem. Eng. Sci. 44(2) : 249-259 (1988).

Li, H., Xia, Y., Tung, Y , and Kwauk, M., "Micro-visualization of Two-Phase Flow Structure in a Fast Fluidized Bed", in Circulating Fluidized Bed Tech. III, pp. 183-188, P. Basu, M. Horio and M. Hasatani Eds., Pergamon Press (1991).

Louge, M., Lischer, D., and Chang, H., "Measurements of Voidage Near the Wall of a Circulating Fluidized Bed Riser", Powder Tech. 62: 269-276 (1990).

Martin, M., Turlier, P., and Bernard, J., "Gas and Solid Behaviour in Cracking CFBs", Powder Tech. 70 : 249-258 (June 1992).

Matsen, J., "Mechanism of Choking and Entrainment", Powder Tech. 32 :

21-33 (1982).

Matsen, J., "Some Characteristics of Large Solids Circulation Systems", in Fluidization Tech. Vol. 2, pp. 135-141, D.L. Keairns Ed., Hemisphere Pub. Co., New York (1976).

Matsui, G., "Identification of Flow Regimes Using Differential Pressure Transducers", Int. J. Multiphase Flow 10(6) : 711- 720 (1984).

Matsumoto, S. and Harakawa, H., "Statistical Analysis of the Transition of the Flow Pattern in Vertical Pneumatic Conveying", Int. J. Multiphase Flow 13(1) : 123-129 (1987).

Matsumoto, S., Harakawa, H., Suzuki, M., and Ohtani, S., "Solid Particle Velocity in Vertical Gaseous Suspension Flows", Int. J. Multiphase Flow 12(3): 445-448 (1986).

Matsui, G., "Identification of Flow Regimes in Vertical Gas- Liquid Two-Phase Flow Using Differential Pressure Fluctuations", Int. J. Multiphase Flow 10(6): 711-720 (1984).

Michaelides, E., and Roy, I., "Evaluation of Several Correlations Used

for the Prediction of Pressure Drop in Particulate Flows", Int. J. Multiphase Flow 13(3) : 433-442 (1987).

Michaelides, E., "Motion of Particles in Gases", J. Fluids Eng. 109 : 172-178 (June 1987).

Miller, A. and Gidaspow, D., "Dense, Vertical Gas-Solid Flow in a Pipe", AIChE J. 38(11): 1801-1815 (Nov. 1992).

Mok, S., Molodtsof, Y., Large, J., and Bergougnou, M.A., "Characterization of Dilute and Dense Phase Vertical Upflow", Can. J. Chem. Eng. 67 : 10-16 (Feb. 1989).

Muzyka, D., "The Use of Probabilistic Multiphase Flow Equations in the Study of the Hydrodynamics and Heat Transfer of Gas- Solids Suspensions", Ph.D. Dissertation, The University of Western Ontario, London, Ont. (Oct. 1985).

Myler, C., "Use of a Thermodynamic Analogy for Pneumatic Transport in Horizontal Pipes", Ph.D. Dissertation, University of Pittsburgh, Pittsburgh, Pensylvannia (1987).

Nakamura, K. and Capes, C., "A Theoretical Study of Uniform and Annular Particle Flow Models", Can. J. Chem. Eng. 51 : 39-46 (Feb. 1973).

Ocone, R., Sundaresan, S., and Jackson, R., "Gas-Particle Flow in a Duct of Arbitrary Inclination with Particle-Particle Interactions", AIChE J. 39(8): 1261-1271 (Aug. 1993).

Patience, G., Chaouki, J., Berruti, F., and Wong, R., "Scaling Considerations for CFB Risers", Powder Tech. 73 : 31-37 (1992).

Pita, J. and Sundaresan, S., "Gas-Solid Flow in Vertical Tubes", AIChE J. 37(7) : 1009-1018 (Jul. 1991).

Pita, J. and Sundaresan, S., "Developing Flow of a Gas-Particle Mixture in a Vertical Riser", AIChE J. 39(4): 541-552 (April 1993).

Press., W., Flannery, B., Teukolsky, S., and Vetterling, W., "Numerical Recipes" Chapter 12, pp. 381-452, Cambridge University Press, Cambridge (1986).

Punwani. D., Modi, M., and Tarman, P., "Generalized Correlation for Estimating Choking Velocity in Vertical Solids Transport", Proc. Int.

Powder and Bulk Solids Handling and Processing Conf., pp. 16-20, Powder Advisory Centre, Chicago (1976).

Reeks, M. and Hall, D., "Deposition and Resuspension of Gas-Borne Particles in Recirculating Turbulent Flows", J. Fluids Eng. 110 : 165-171 (June 1988).

Rhodes, M., "Modelling of Flow Structure in Upward-Flowing Suspension", Powder Tech. 60 : 27-38 (1990).

Rhodes, M., Hirama, T., Cerutti, G., and Geldart, G., "Non- uniformities of Solids Flow in the Risers of CFBs", in Fluidization VI, pp. 73-79, L.W. Shemilt and M.A. Bergougnou Eds., Engineering Foundation, NY (1989).

Rhodes, M., Mineo, H., and Hirama, T., "Particle Motion at the Wall of the 305 mm Diameter Riser of a Cold CFB", in Circulating Fluidized Bed Tech. III, pp. 171-176, P. Basu, M. Horio and M. Hasatani Eds., Pergamon Press (1991).

Rhodes, M., Wang, X., Cheng, H., Hiroma, T., and Gibbs, B., "Similar Profiles in CFB Risers", Chem. Eng. Sci. 47(7) : 1634-1643 (1992a).

Rhodes, M., Zhou, S., and Benkreira, H., "Flow of Dilute Gas- Particle Suspensions", AIChE J. 38(12) : 1913-1915 (Dec. 1992b).

Rhodes, M., Mineo, H., and Hirama, T., "Particle Motion at the Wall of a CFB", Powder Tech. 70 : 207-214 (June 1992c).

Rohatgi, N., "Pneumatic Transport in a Variable Inclined Test Loop", Ph.D. Dissertation, University of Pittsburgh, Pittsburgh, Pennsylvania (1988).

Rose, H. and Duckworth, R., "Transport of Solid Particles in Liquids and Gases I", The Engineer 392-396 (14 Mar. 1969a).

Rose, H. and Duckworth, R., "Transport of Solid Particles in Liquids and Gases II", The Engineer: 430-433 (21 Mar. 1969b).

Rose, H. and Duckworth, R., "Transport of Solid Particles in Liquids and Gases III", The Engineer: 478-483 (28 Mar. 1969c).

Saiz-Jabardo, J. and Boure, J., "Experiments on Void Fraction Waves", Int. J. Multiphase Flow 15(4) : 483-493 (1989).

Sandy, C.W., Daubert, T.E., and Jones, J.E., "Vertical Dense Phase Gas-Solids Transport", Chem. Eng. Prog. Symp. Ser., 66 (105): 133-142 (1970).

Satija, S., Young, J.B., and Fan, L.S., "Pressure Fluctuations and Choking Criterion for Vertical Pneumatic Conveying of Fine Particles", Powder Tech. 43: 257-271 (1985).

Saxton, A. and Worley, A., "Modern Catalytic Cracking Design", Oil Gas J. 68(20) : 82-89 (1970).

Schnitzlein, M. and Weinstein, H., "Flow Characterization in High-Velocity Fluidized Beds Using Pressure Fluctuations", Chem. Eng. Sci. 43(10): 2605-2614 (1988).

Schuurmans, H., "Measurements in a Commercial Catalytic Cracking Unit", Ind. Eng. Chem. Process Des. Dev. 19 : 267-271 (1980).

Senior, R. and Brereton, C., "Modelling of CFB Solids Flow and Distribution", Chem. Eng. Sci. 47(2) : 281-296 (1992).

Shingles, T. and Dry, R., "Circulating Fluidized Beds", in Encyclopedia of

Fluid Mechanics Vol. 4 : Solids and Gas- Solids Flows, Chapter 33, pp. 1063-1076, N. Cheremisinoff Ed., Gulf Pub. Co., Houston (1986).

Shingles, T. and McDonald, A., "Commercial Experience with Synthol CFB Reactors" in Circulating Fluidized Bed Tech. II, pp. 43-50, P. Basu and J. Large Eds., Pergamon Press, Toronto (1988).

Sinclair, J. and Jackson, R., "Gas-Particle Flow in a Vertical Pipe with Particle-Particle Interactions", AIChE J. 35(9) : 1473-1486 (Sept. 1989).

Smith, T., "Limiting Volume Fractions in Vertical Pneumatic Transport", Chem. Eng. Sci. 33 : 745-749 (1978).

Soo, S., "Pipe Flow of a Dense Suspension", J. Pipelines 6 : 193- 203 (1987).

Soo, S., Zhu, C., and Lucht, T., "Statistical Properties of Dense Suspensions in Pipeflow" from "Multiphase Flow and Heat Transfer Second Int. Symp.", Vol. 2, pp. 1047-1055, Xue-Jue Chen, T.N. Veziroglu, C.L. Tien Eds., Hemisphere Pub. Co. N.Y. (1991).

Staub, F.W., "Steady-State and Transient Gas-Solids Flow Characteristics in Vertical Transport Lines", Powder Tech., 26: 147-159 (1980).

Streeter, V. and Wylie, E., "Fluid Mechanics", p 236, McGraw-Hill Book Co. 7th Ed., New York (1979).

Takeuchi, H. and Hirama, T., "Flow Visualization in the Riser of a CFB", in Circulating Fluidized Bed Tech. III, pp. 177-182, P. Basu, M. Horio and M. Hasatani Eds., Pergamon Press, Toronto (1991).

Tsuji, Y. and Morikawa, Y., "Flow Pattern and Pressure Fluctuation in Air-Solid Two-Phase Flow in a Pipe at Low Air Velocities", Int. J. Multiphase Flow 8(4): 329-341 (1982).

Tsuo, Y. and Gidaspow, D., "Computation of Flow Patterns in CFBs", AIChE J. 36(6) : 885-896 (June 1990).

TRIMETRIX, Inc., *"Axum Technical Graphics and Data Analysis"*, The Scientific Endeavours Corp. Pub., Seattle, WA (1993).

Tutu, N.K., "Pressure Drop Fluctuations and Bubble-Slug Transition in a Vertical Two Phase Air-Water Flow", Int. J. Multiphase Flow 10(2): 211-216 (1984).

van Swaiij, W., Buurman, C., and van Breugel, J., "Shear Stresses on

the Wall of a Dense Gas-Solids Riser", Chem. Eng. Sci. 25 : 1818-1820 (1970).

Wang, S.K., Lee, S.J., Jones, O.C., and Lahey, R., "Statistical Analysis of Turbulent Two-Phase Pipe Flow", J. Fluids Eng. 112: 89-95 (Mar. 1990).

Wang, T., Lin, Z.J., Zhu, C.M., Liu, D.C., and Saxena, S.C., "Particle Velocity Measurements in a CFB", AIChE J. 39(8): 1406-1410 (Aug. 1993).

Wedding, J.B., Robertson, J.M., Peterka, J.A., and Akins, R.E., "Spectral and Probability-Density Nature of Square-Prism Separation-Reattachment Wall Pressures", J. Fluids Eng. 100: 485-492 (1978).

Westphalen, D. (M.I.T.), "Experimental Verification of Scaling Relationships for CFBs", Prepared for Electric Power Research Institute, J.W. Stallings Project Manager, EPRI Report GS-7228, Project 979-21 (April 1991).

White, C. and Dry, R., "Transmission Characteristics of Gas in a CFB", Powder Tech. 57 : 89-94 (1989).

Wirth, E., "Critical Transport Velocity with Vertical Pneumatic

Conveying", in World Congress Particle Tech. III : Mechanics of Particulate Solids Pneumatic and Hydraulic Conveying Mixing, I. Leschonski Ed., pp. 339-349, NMA Nurnberger Messe Pub., Fed Rep. Germany (1986).

Wirth, K. and Seiter, M., "Solids Concentration and Solids Velocity in the Wall Region of CFBs", in 11th Int. Conf. on Fluidized Bed Combustion Vol. 1, pp. 311-316, E. Anthony Ed., ASME Pub. (April 1991).

Wolny, A. and Kabata, M., "Mixing of Solid Particles in Vertical Pneumatic Transport", Chem. Eng. Sci. 40(11) : 2113-2118 (1985).

Wong, R., Pugsley, T., and Berruti, F., "Modelling the Axial Voidage Profile and Flow Structure in Risers of CFBs", Chem. Eng. Sci. 47 (9-11): 2301-2306 (1992).

Yang, W., "Estimating the Solid Particle Velocity in Vertical Pneumatic Conveying Lines", Ind. Eng. Chem. Fund. 12 (12) : 349-352 (1973).

Yang, W.C., "A Mathematical Definition of Choking Phenomenon and a Mathematical Model for Predicting Choking Velocity and Choking Voidage", A.I.Ch.E. J., 21 : 1013-1015 (1975).

Yang, W.G., "United Theory on Dilute Phase Pneumatic Transport", Paper presented at International Powder Tech. and Bulk Solids Handling Conf. Exhibition 1 : 89-95, Chicago, May 11- 13 (1976).

Yang, W., "Criteria for Choking in Vertical Pneumatic Conveying Lines", Powder Tech. 35 : 143-150 (1983).

Yang, W., "A Model for the Dynamics of a CFB Loop" in Circulating Fluidized Bed Tech. II, pp. 181-192, P. Basu and J. Large Eds., Pergamon Press, Toronto (1988).

Yang, Y.L., Jin, Y., Yu, Z., and Wang, Z., "Investigation on Slip Velocity Distributions in the Riser of Dilute Circulating Bed", Powder Tech., 73 : 67-73 (1992).

Yang, Y.L., Jin, Y., Yu, Z., Zhu, J., and Bi, H., "Local Slip Velocity Behaviors in the Circulating Fluidized", AIChE Symp. Ser. 296(89): 81-90 (1993).

Yerushalmi, J., Turner, D., and Squires, A., "The Fast Fluidized Bed", Ind. Eng. Chem. Process Des. Dev. 15(1) : 47-53 (1976).

Yerushalmi, J. and Cankurt, N., "High Velocity Fluidized Beds", Chemtech (9): 564-572 (1978).

Yerushalmi, J. and Cankurt, N., "Further Studies of the Regimes of Fluidization", Powder Tech. 24 : 187-205 (1979).

Yousfi, Y. and Gau, G., "Vertical Pneumatic Conveying I", Chem. Eng. Sci. 29 : 1939-1946 (1974a).

Yousfi, Y. and Gau, G., "Vertical Pneumatic Conveying II", Chem. Eng. Sci. 29 : 1947-1953 (1974b).

Zaltash, A., "Application of Thermodynamic Approach to Pneumatic Transport at Pipe Orientations Above the Horizontal", Ph.D. Dissertation, University of Pittsburgh, Pittsburgh, Pennsylvania (1987).

Zaltash, A., Myler, C., Dhodapkar, S., and Klinzing, G., "Application of Thermodynamic Approach to Pneumatic Transport at Various Pipe Orientations", Powder Tech. 59 : 199-207 (1989).

Zenz, F., "Nine Variables in Catalyst Flow", Petroleum Refiner 36(7) : 175-183 (Jul. 1957).

Zenz, F. and Othmer, D., Fluidization and Fluid-Particle Systems, Chapter 10, pp. 332-350, Reinhold Pub. Corp., New York (1960).

Zhang, W. and Tung, Y., "Radial Voidage Profiles in Fast Fluidized Beds of Different Diameters", Chem. Eng. Sci. 46(12) : 3045-3052 (1991).

Zhu, C. and Soo, S.L., "Statistical Properties of Unsteady Gas- Solid Suspensions with Strong Particle-Particle Interactions in Horizontal Pipe Flows", Powder Tech. 73 : 51-60 (1992).

APPENDIX A - PRESSURE TRANSDUCER CALIBRATION CURVES

Fig. A1 : Schaevitz P-3091 Transducer (Upstream Test Section Pressure Determination)

Fig. A2 : Setra C-239 Transducer (Test Section Pressure Drop Determination)

Fig. A3 : Taylor #1 3402-T Transducer (Pneumatic Transport Flowrate Determination)

Fig. A4 : Taylor #2 3402-T Transducer (Upstream Pressure Pneumatic Transport Line)

Fig. A1: Schaevitz P-3091 Transducer Calibration

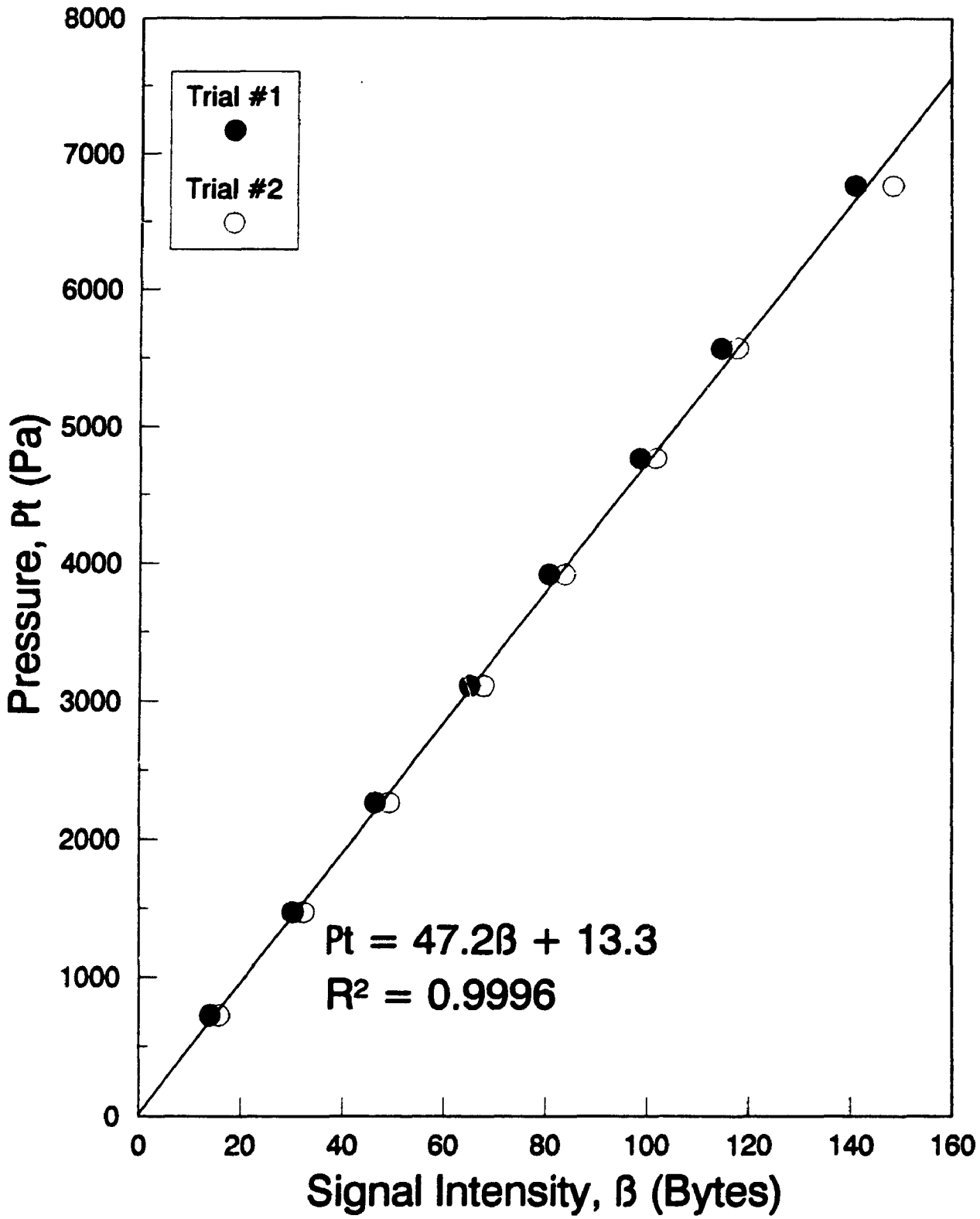

Fig. A2: Setra (C-239) Transducer Calibration

Test Section Pressure Drop Determination

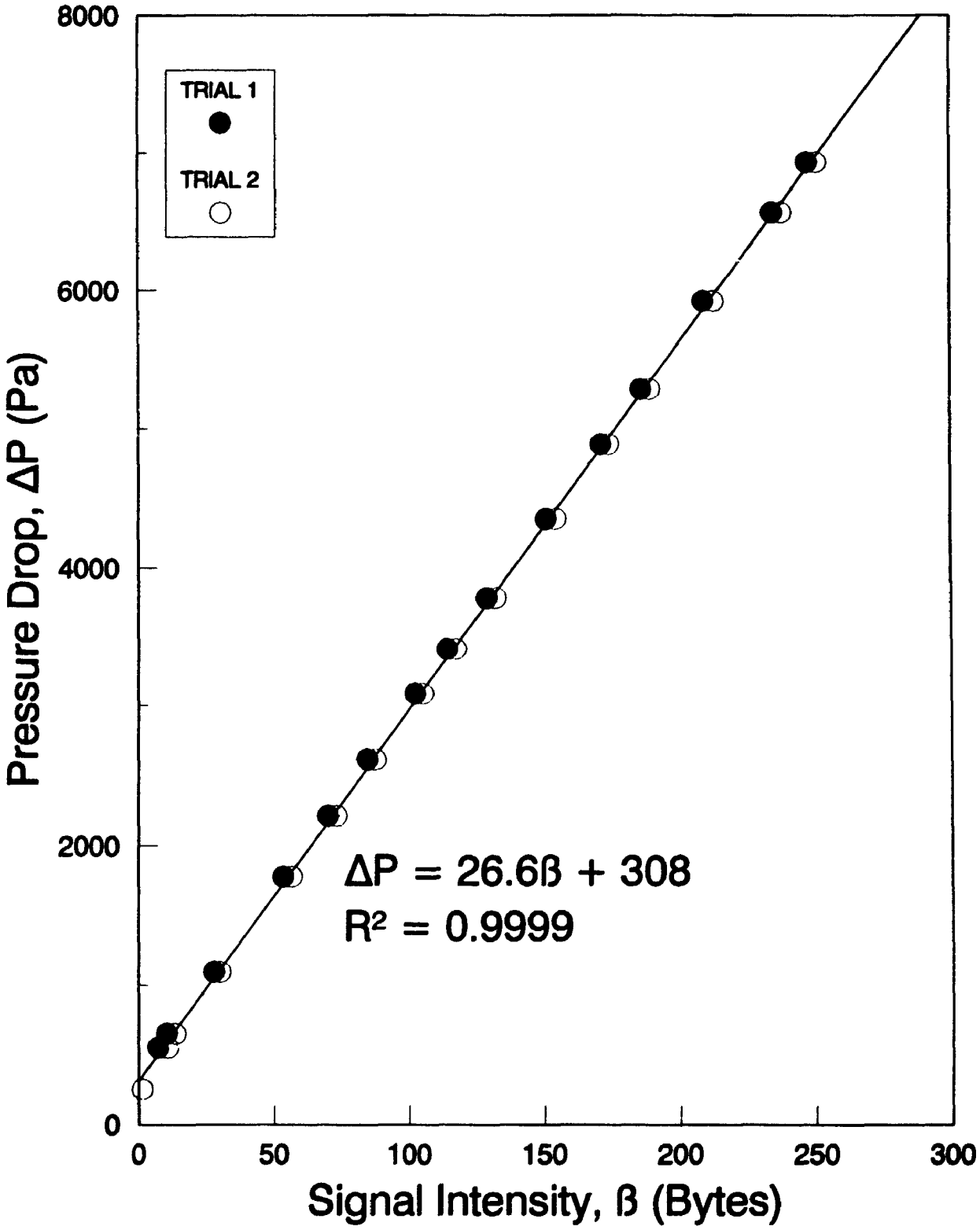

Fig. A3 : Taylor #3402T Transducer Calibration

Pneumatic Transport Flowrate Determination

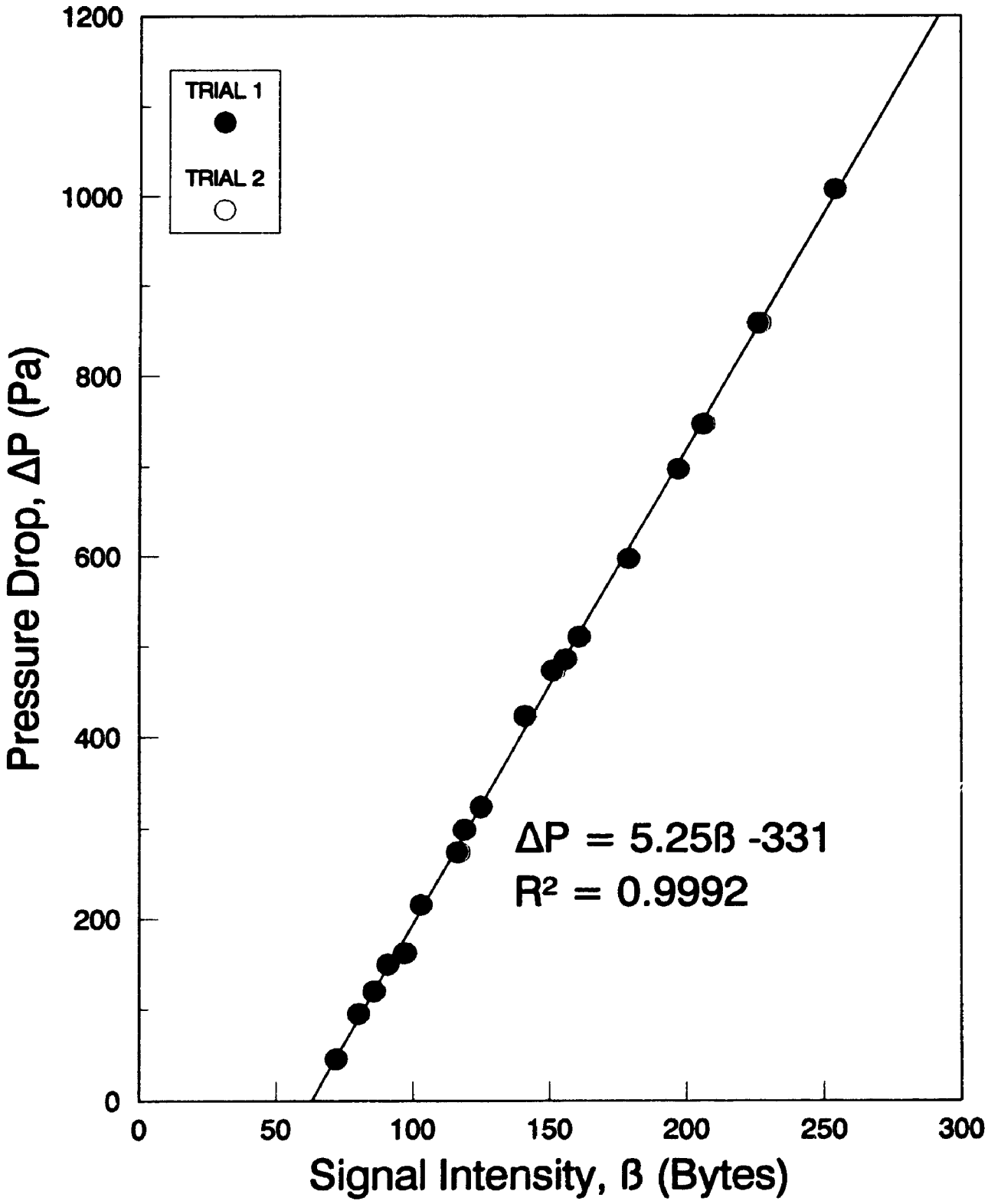

Fig. A4: Taylor #3402T Transducer Calibration

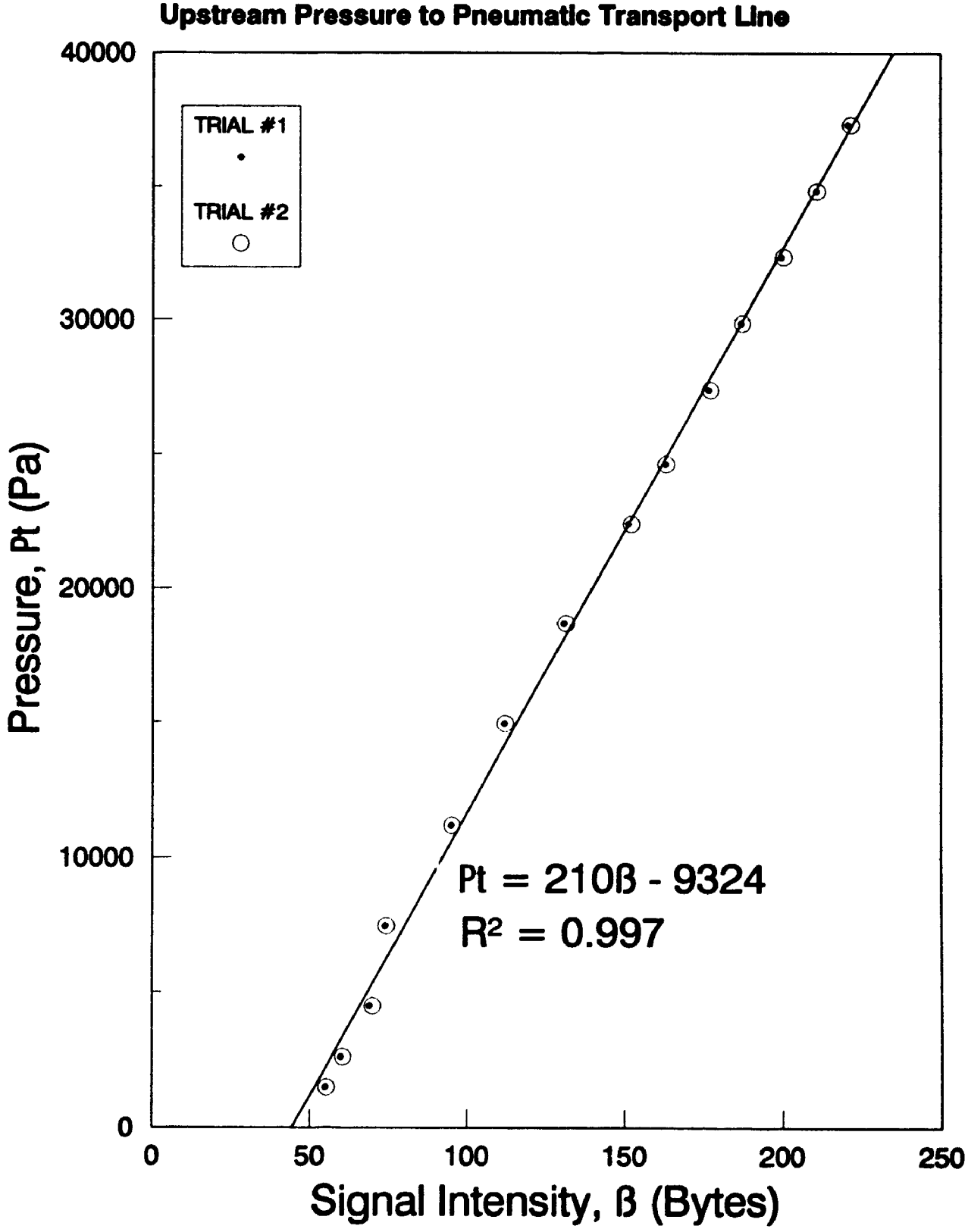

APPENDIX B - DATA ACQUISITION PROGRAM IN APPLESOFT BASIC

```
1  REM  THIS PROGRAM IS WRITTEN FOR THE
2  REM  PURPOSE OF DATA ACQUISITION
3  REM  DATA IS READ FROM FILE ORIFDATA
4  REM  THE PROGRAM COLLECTS DATA FROM
5  REM  4 TRANSDUCERS. MASS FLOWS ARE
6  REM  CALCULATED, AVERAGE AND STANDARD
7  REM  DEVIATIONS ARE COMPUTED AND STORE
8  REM  THE PROGRAM IS INTERACTIVE AND
9  REM  USER FRIENDLY.
10 D$ =  CHR$ (4):PR$ = "OFF"
15 DR$(1) = ",D1":DR$(2) = ",D2"
20  PRINT D$;"OPENORIFDATA,D1"
30  PRINT D$;"READORIFDATA"
35  REM  INPUT DATA
40  INPUT N,LE,LU,PUP,TP
42  INPUT NZ,LE,DR,VS,FUP,FDROP,FLP,FPP,FR
50  PRINT D$;"CLOSE"
51  REM  INITIALIZE OUTPUT VARS.
55 DA$ = "?":RN$ = "?":AP$ = "?":F1$ = "?":F2$ = "?":F3$ = "?":OF$ = "?"
57 BL$ = "                                        "
58  REM  DEFINE CALIBRATION RANGES
60  GOSUB 6010
61  DEF  FN Q(F) = 5.2528561 * (F - 63.206933)
62 OQ$ = "TAYLOR TRANSDUCER"
63 OP$ = "PLIN DROP"
64  DEF  FN S(V) = 205.7 * (V - 42)
65  TEXT : HOME : VTAB 10: HTAB 8: FLASH : PRINT " TURN PRINTER ON!": NORMAL

66  VTAB 12: HTAB 8: INVERSE : PRINT " CHECK SOLIDS CORRELATIONS!": NORMAL

67  REM  CREATE DISPLAY TABLE ON SCREEN
70 LL$ = "                                  "
80 L$ = "-----------------------------------"
90 S$ = "|": DIM Z%(2500): DIM Y%(2500): DIM W(3),Q(3)
95  GOTO 280
100  TEXT : HOME :J = 1:CK = 0
170  VTAB 23: INVERSE : PRINT " M(ENU)/A(VE)/P(RINT)/F(AST)/E(XIT)": NORMAL

180  VTAB 4: INVERSE : PRINT LL$: NORMAL
190  PRINT "| AV (Pa) | STDV (Pa)|VEL. (m/s)|"
200  PRINT L$
210  VTAB (7): FOR I = 1 TO 11
220  PRINT S$; TAB( 6); TAB( 11);S$;: HTAB (14): PRINT "    ";: HTAB (22): PRIN
     S$;: HTAB (25): PRINT "    ";: HTAB (33): PRINT S$
230  NEXT I
240  INVERSE : PRINT LL$: NORMAL : PRINT
245  REM  DETERMINE CHANNEL
252  IF K >  = 11 THEN K = 0
253  IF K = 4 THEN PL = 49329
254  IF NT = 2 THEN  IF K = 5 THEN  VTAB (K + 7): INVERSE : PRINT S$; TAB(
     6);AV; TAB( 11);S$;: HTAB (14): PRINT STD;"    ";: HTAB (22): PRINT S$
     ;: HTAB (25): PRINT VS;"    ";: HTAB (33): PRINT S$: NORMAL : GOTO 262

255  VTAB (K + 7)
256  INVERSE : PRINT S$; TAB( 6); INT (AV); TAB( 11);S$;: HTAB (14): PRINT
      INT (STD);"    ";: HTAB (22): PRINT S$;: HTAB (25): PRINT VS;"    ";: HTAB
     (33): PRINT S$: NORMAL
262  VTAB 20: INVERSE
```

```
264  PRINT "  EPS(%)    LD (KG/KG) SL (G/S)    "
265  NORMAL
266  VTAB (21): PRINT S$; TAB( 6);EPS; TAB( 11);S$;: HTAB (14): PRINT LD;"
       ";: HTAB (22): PRINT S$;: HTAB (25): PRINT SL;"    ";: HTAB (33): PRINT
     S$
268  INVERSE : PRINT LL$: NORMAL : PRINT
270  REM  INPUT AN OPTION FOR ASCII
280 K% =  PEEK ( - 16384)
290  IF K% < 128 THEN 970
300  IF K% = 193 THEN 970
310  IF K% = 205 THEN  TEXT : HOME : GOSUB 6010: GOTO 280
320  IF K% = 208 THEN 490
330  IF K% = 198 THEN 700
340  IF K% = 197 THEN 1300
360 SB = 0:VA = 0: VTAB (6 + PB)
365  REM  DATA ACQUISITION INITIATED
366  REM  COLLECT DATA
370  FOR I = 1 TO N
380 Z%(I) =  PEEK (PL)
381  IF  PEEK (PL) >  = 254 THEN  VTAB 2: PRINT BL$: FLASH : VTAB 2: HTAB
     7: PRINT "WARNING: EXCEEDING A/D": NORMAL
382  IF NT = 1 THEN Z%(I) =  FN Q(Z%(I)): GOTO 390
383  REM  DETERMINE PRESSURE FROM SIGNAL
384  IF PL = 49330 THEN Z%(I) =  FN P(Z%(I))
386  IF PL = 49328 THEN Z%(I) =  FN H(Z%(I))
388  IF PL = 49329 THEN Z%(I) =  FN Q(Z%(I))
389  REM  SUM SIGNALS
390 SB = SB + Z%(I)
400  NEXT I
404  IF NT = 2 THEN  IF K = 5 THEN  VTAB (K + 7): PRINT S$; TAB( 6);AV; TAB(
     11);S$;: HTAB (14): PRINT STD;"    ";: HTAB (22): PRINT S$;: HTAB (25)
     : PRINT VS;"    ";: HTAB (33): PRINT S$: NORMAL : GOTO 410
405  VTAB (K + 7): PRINT S$; TAB( 6); INT (AV); TAB( 11);S$;: HTAB (14): PRINT
      INT (STD);"    ";: HTAB (22): PRINT S$;: HTAB (25): PRINT VS;"    ";: HTAB
     (33): PRINT S$
410 AV = SB / N
415  REM  CALCULATE STANDARD DEVIATION
420  FOR I = 1 TO N
430 VA = VA + (Z%(I) - AV) * (Z%(I) - AV): NEXT
440 STD =  SQR (VA / (N - 1)): IF STD < 0 THEN STD = 0
443  IF NT = 2 THEN  IF PL = 49330 THEN NAV =  INT (AV)
444  REM  CALCULATE UPSTREAM P
445  IF PL = 49328 THEN AV = AV - LU * NAV / LE
450  REM  CALCULATE VOIDAGE
453  IF RR = 1 THEN  IF PL = 49330 THEN EPS = AV / (2560 * 9.81 * LE):EPS =
      INT (EPS * 10000) * 0.01
456  IF NT = 2 THEN  IF K = 4 THEN 470
457  IF NT = 1 THEN  GOSUB 1630: GOTO 465
463  VTAB 2: PRINT BL$: INVERSE : VTAB 2: HTAB 7: PRINT TR$: NORMAL
465  VTAB 1: PRINT BL$: VTAB 1: HTAB 7: INVERSE : PRINT HE$: NORMAL
470  IF NT = 2 THEN  IF K = 4 THEN  VTAB 2: PRINT BL$: INVERSE : VTAB 2: HTAB
     7: PRINT OQ$: NORMAL : GOSUB 1630: GOSUB 1760: GOSUB 1760:AV =  INT (
     MF * 100000) * 0.01:STD =  INT ((W(1) / MF) * 10000) * 0.01
471 K = K + 1
472  IF RR = 1 THEN  IF PL = 49330 THEN  GOSUB 4000
473  IF NT = 1 THEN  VTAB 2: PRINT BL$: INVERSE : VTAB 2: HTAB 7: PRINT TR
     $: NORMAL : GOTO 475
474  GOSUB 5100
475  IF CK = 1 THEN 100
485  IF PR$ = "OFF" THEN 252
486  REM      RUN PRINT          MENU
490 T1$(1) = "Application:":A$(1) = M$(CH):P(1) = 1
495 T1$(2) = "Printer ------------> ":A$(2) = PR$:P(2) = 1
500 T1$(3) = "Run Number ---------> ":A$(3) = RN$:P(3) = 1
520 T1$(4) = "Gas Velocity--------> ":A(4) = VS
539 T1$(5) = "Date ---------------> ":A$(5) = DA$:P(5) = 1
```

```
540 T1$(6) = "FBEDUP (CM H2O)-----> ":A(6) = FUP
541 T1$(7) = "FBED DROP (IN. H2O)-> ":A(7) = FDROP
542 T1$(8) = "FLINE UP (IN H2O)---> ":A(8) = FLP
543 T1$(9) = "FLINE DROP (IN. H2O-> ":A(9) = FPP
548  REM   INPUT AN OPTION FOR ASCII
549 NL = 9: GOSUB 1020:R% = 1
550 M$(CH) = A$(1):PR$ = A$(2):RN$ = A$(3):VS = A(4):DA$ = A$(5):FUP = A(6
    ):FDROP = A(7):FLP = A(8):FPP = A(9)
551  IF K% = 193 THEN 970
552  IF K% = 197 THEN 1300
553  IF K% = 205 THEN 310
554  IF K% = 208 THEN 490
556  IF K% = 198 THEN 700
559  TEXT : HOME
560  PRINT D$;"PR#1"
570  PRINT  TAB( 5);"TODAY'S DATE";DA$; SPC( 5);" RUN NUMBER";RN$
575  PRINT  TAB( 5);"CURRENT AVERAGE DROP=";  SPC( 2); INT (NAV);"  +/-"; SPC(
    2); INT (STD);"  Pa"
576  PRINT  TAB( 5);"CURRENT AVERAGE UPSTREAM PRESS.="; SPC( 2); INT (AV);
    "  +/-"; SPC( 2); INT (STD);"  Pa"
577  PRINT  TAB( 5);"CURRENT TEST SECTION (M)="; SPC( 2);LE
578  PRINT  TAB( 5);"CURRENT UPSTREAM TEST POINT (M)="; SPC( 2);LU
579  PRINT  TAB( 5);"GAS VELOCITY (M/S)="; SPC( 2);VS
580  PRINT  TAB( 5);"SL= ";SL; SPC( 3);"VS=  ";VS; SPC( 3);"LD= ";LD
582  PRINT  TAB( 5);"ANGLE FROM VERTICAL="; SPC( 2);PHI
584  PRINT  TAB( 5);"SAUTER MEAN DIA. (MICRONS)="; SPC( 2);SD
586  PRINT  TAB( 5);"SOLIDS INVENTORY (KG)="; SPC( 2);SI
587  PRINT  TAB( 5);"LOAD (KG/KG)="; SPC( 2);LD
588  PRINT  TAB( 5);"SOLIDS VOID (%)="; SPC( 2);EPS
592  IF RR = 2 THEN  PRINT "THE STATIC PRESSURE IS:"; INT (AV); SPC( 1);"+
    /-"; SPC( 1); INT (STD); SPC( 2);"PA"
593  IF RR = 1 THEN  IF PL = 49328 THEN  PRINT "THE UPSTREAM PRESSURE IS:
    "; INT (AV);"                PA"
594  IF RR = 1 THEN  IF PL = 49330 THEN  PRINT "THE AVERAGE PRESSURE GRADI
    ENT IS:"; SPC( 2); INT (AV / LE); SPC( 1);"+/-"; SPC( 1); INT (STD /
    LE); SPC( 2);"PA/M"
595  IF PL = 49329 THEN  PRINT "THE AVERAGE PRESSURE DROP IS:"; SPC( 2); INT
    (AV); SPC( 1);"+/-"; SPC( 1); INT (STD); SPC( 2);"PA."
596  PRINT "SAMPLE SIZE="; SPC( 2);NZ
598  FOR PP = 1 TO 3: PRINT : NEXT
600  PRINT D$;"PR#0"
605  IF P#$ = "OFF" THEN K% = 193
610  GOTO 100
620  REM      RUN FAST SAMPLING MENU
700 T1$(1) = "File SETRA----------> ":A$(1) = F1$:P(1) = 1
730 T1$(2) = "File SCHAEVITZ------> ":A$(2) = F2$:P(2) = 1
731 T1$(3) = "File TAYLOR---------> ":A$(3) = F3$:P(3) = 1
732 T1$(4) = "Fast sample points--> ":A(4) = NZ
735 T1$(5) = "Test section (m)----> ":A(5) = LE
736 T1$(6) = "Upstream Pt. (m)----> ":A(6) = LU
737 T1$(7) = "Drive Number--------> ":A(7) = DR
738 T1$(8) = "Freq. Range (Hz)----> ":A(8) = FR
739  REM  DECIDE PATH FOR SAMPLING
740 NL = 8: GOSUB 1020:F1$ = A$(1):F2$ = A$(2):F3$ = A$(3):NZ = A(4):LE =
    A(5):LU = A(6):DR = A(7):FR = A(8)
741 R% = 2
742  IF K% = 193 THEN 970
744  IF K% = 197 THEN 1300
746  IF K% = 205 THEN 310
748  IF K% = 208 THEN 490
749  IF K% = 198 THEN 700
750  IF NT = 1 THEN 785
760  IF F1$ = "?" THEN 700
780  IF F2$ = "?" THEN 700
785  IF NT = 1 THEN  IF F3$ = "?" THEN 700
786  REM  CALCULATE SAMPLING RATE
```

```
790  IF DA$ = "?" OR RN$ = "?" THEN 490
791  IF FR >  = 100 THEN TL = 1: GOTO 800
793 TL =  INT ((1 / (FR * 2)) * 1000 / 1.15): REM   ADD 5 FOR NATURAL COMP
    ILATION TIME
795 EST =  INT (((TL + 5) * 0.002 * NZ / 60) * 10) * 0.1
800  TEXT : HOME : VTAB 6: HTAB 11: FLASH : PRINT "SAMPLING !": NORMAL
805  VTAB 8: PRINT BL$: VTAB 8: HTAB 5: INVERSE : PRINT M$(CH): NORMAL
807  VTAB 10: PRINT BL$: VTAB 10: HTAB 5: INVERSE : PRINT "FREQ. RANGE (HZ
    ) = "; - 1 * FR;" TO ";FR;" HZ": NORMAL
808  VTAB 12: PRINT BL$: VTAB 12: HTAB 5: INVERSE : PRINT "SAMPLING LAG (M
    S) = ";TL + 5: NORMAL
809  VTAB 14: PRINT BL$: VTAB 14: HTAB 5: INVERSE : PRINT "EST. SAMPLING T
    IME (MIN.) = ";EST: NORMAL
810 FG = 1: GOSUB 5100
820  REM  FULLY DEVELOPED DACQ
830  FOR I = 1 TO NZ
840  FOR J = 1 TO TL: NEXT
850 Z%(I) =  PEEK (PL)
852  IF NT = 1 THEN 855
853  FOR J = 1 TO TL: NEXT
854  GOSUB 5100:Y%(I) =  PEEK (PL): GOSUB 5100
855  NEXT I
856  TEXT : HOME : VTAB 10: HTAB 11: FLASH : PRINT "COMPUTING STATISTICS!"
    : NORMAL
857  VTAB 12: PRINT BL$: VTAB 12: HTAB 11: INVERSE : PRINT M$(CH): NORMAL

858  REM  SAVE TO DATA FILE
860  GOSUB 1400
861  TEXT : HOME : VTAB 12: HTAB 16: FLASH : PRINT " SAVING ! ": NORMAL
862  IF NT = 2 THEN 875
863  VTAB 14: PRINT BL$: VTAB 14: HTAB 16: INVERSE : PRINT M$(CH): NORMAL

864  VTAB 16: HTAB 16: INVERSE : PRINT "FILE: ";F3$: NORMAL
865  PRINT D$;"OPEN";F3$;DR$(DR)
866  PRINT D$;"DELETE";F3$
867  PRINT D$;"OPEN";F3$
868  PRINT D$;"WRITE";F3$
869  GOSUB 5100
870  FOR I = 1 TO NZ
871  PRINT  INT (Z%(I)): NEXT
872  GOTO 948
875  VTAB 14: HTAB 16: INVERSE : PRINT "FILE: ";F1$: NORMAL
876  VTAB 10: PRINT BL$: VTAB 10: HTAB 11: INVERSE : PRINT M$(CH): NORMAL

880  PRINT D$;"OPEN";F1$;DR$(DR)
890  PRINT D$;"DELETE";F1$
900  PRINT D$;"OPEN";F1$
910  PRINT D$;"WRITE";F1$
915 FG = 1: GOSUB 5100
917  REM  WRITE GRADIENT DATA
920  FOR I = 1 TO NZ
930  PRINT  INT (Z%(I) / LE): NEXT
948  PRINT D$;"CLOSE"
949  IF NT = 1 THEN  IF CH = 1 THEN  GOSUB 1630: GOSUB 6010: GOTO 280
950  IF NT = 1 THEN  IF CH <  > 1 THEN  GOSUB 6010: GOTO 280
951 FG =  - 1: GOSUB 5100
952  VTAB 14: HTAB 16: INVERSE : PRINT "FILE: ";F2$: NORMAL
953  PRINT D$;"OPEN";F2$;DR$(DR)
955  PRINT D$;"DELETE";F2$
957  PRINT D$;"OPEN";F2$
959  PRINT D$;"WRITE";F2$
961  FOR I = 1 TO NZ
963  PRINT  INT (Y%(I)): NEXT
965  REM  REM AVERAGING MENU
969  PRINT D$;"CLOSE"
```

```
972 T1$(2) = "No. of points-------> ":A(2) = N
980 T1$(3) = "Upstream Pt. (m)----> ":A(3) = LU
1005 T1$(4) = "Test section (m)----> ":A(4) = LE
1007 T1$(5) = "Temperature(C)------> ":A(5) = TP
1008 T1$(6) = "Up Press. (Pa)------> ":A(6) = UP
1009 T1$(7) = "Test Drop (Pa)------> ":A(7) = NAV
1010 T1$(8) = "Load (Kg/Kg)--------> ":A(8) = LD
1011 T1$(9) = "Void Solids (%)-----> ":A(9) = EPS
1012 NL = 9: GOSUB 1020:OF$ = A$(1):N = A(2):LU = A(3):LE = A(4):TP = A(5)
     :UP = A(6):NAV = A(7):LD = A(8):EPS = A(9)
1013 R% = 3
1014  IF K% = 198 THEN 700
1015  IF K% = 208 THEN 490
1016  IF K% = 193 THEN 970
1017  IF K% = 19  THEN 1300
1018  IF K% = 195 THEN 100
1019  IF K% = 205 THEN 310
1020 J = 1:CL$ = "                ": TEXT : HOME
1025  REM  PROGRAM FOR MENU ACCESS
1030  POKE  - 16368,0: VTAB 6: FOR I = 1 TO NL
1040  PRINT T1$(I);
1050  IF P(I) = 1 THEN  PRINT A$(I);"       ": GOTO 1070
1060  PRINT A(I);"       "
1070  PRINT
1080  NEXT I
1090  VTAB (4 + 2 * J): PRINT T1$(J);: FLASH
1100  IF P(J) = 1 THEN  PRINT A$(J): GOTO 1120
1110  PRINT A(J)
1120  NORMAL
1130  VTAB 23: INVERSE : PRINT "C(TD)/E(XIT)/A(V)/F(AST)/M(ENU)/P(RINT)": NORM
1140  WAIT  - 16384,128
1150 K% =  PEEK ( - 16384)
1160  IF K% = 139 THEN J = J - 1: POKE  - 16368,0: IF J < 1 THEN J = 1: GOTO
     1030
1170  IF K% = 195 THEN 1290
1172  IF K% = 197 THEN 1290
1174  IF K% = 193 THEN 1290
1176  IF K% = 205 THEN 1290
1177  IF K% = 208 THEN 1290
1178  IF K% = 198 THEN 1290
1180  IF K% = 138 THEN J = J + 1: POKE  - 16368,0: IF J > NL THEN J = NL: GOTO
     1030
1190  IF K% = 141 THEN J = J + 1: POKE  - 16368,0: IF J > NL THEN J = 1: GOT
     1030
1200  IF K% < 171 THEN 1030
1210  IF K% > 185 THEN 1030
1220  ONERR  GOTO 1280
1230  VTAB (4 + 2 * J): HTAB (22): PRINT CL$: VTAB (4 + 2 * J): HTAB (22)
1240  IF P(J) = 1 THEN  INPUT " ";A$(J): GOTO 1260
1250  INPUT " ";A(J)
1260  IF J < NL THEN J = J + 1
1270  POKE 216,0: GOTO 1030
1280  PRINT  CHR$ (7): POKE 216,0: GOTO 1030
1290  FOR I = 1 TO NL:P(I) = 0: NEXT I: RETURN
 300  POKE  - 16368,0
1305  REM  WRITE TO OUPUT FILE
1310  PRINT D$;"OPENORIFDATA,D1"
1315  PRINT D$;"DELETE ORIFDATA"
1317  PRINT D$;"OPEN ORIFDATA"
1320  PRINT D$;"WRITE ORIFDATA"
1330  PRINT N: PRINT LE: PRINT LU: PRINT PUP: PRINT TP
1335  PRINT NZ: PRINT LE: PRINT DR: PRINT VS: PRINT FUP: PRINT FDROP: PRINT
     FLP: PRINT FPP: PRINT FR
1360  PRINT D$;"CLOSE"
1362  IF OF$ = "?" THEN 970
```

```
1366  PRINT SL: PRINT VS: PRINT W: PRINT OD: PRINT Q: PRINT DEN
1368  PRINT D$;"CLOSE";OF$
1370  TEXT : HOME : VTAB 12: HTAB 11: FLASH : PRINT "LOADING !": NORMAL
1375  VTAB 14: HTAB 11: INVERSE : PRINT "FILE: PR.MF5": NORMAL
1376  VTAB 16: HTAB 11: INVERSE : PRINT "# POINTS SAMPLED=  ";NZ: NORMAL
1380  PRINT D$;"RUNPR.MF5,D1"
1400  REM  SUBROUTINE FAST SAMPLING
1450  REM  STATISTICS ARE COMPUTED
1500 SF = 0:VA = 0:AV = 0:STD = 0:SP = 0:YVA = 0:YAV = 0:YSTD = 0
1510  FOR I = 1 TO NZ
1520 SF = SF + Z%(I):SP = SP + Y%(I)
1530  NEXT I
1540 AV = SF / NZ:YAV = SP / NZ
1571  IF NT = 1 THEN AV =  FN Q(AV): FOR I = 1 TO NZ:Z%(I) =  FN Q(Z%(I)):
      NEXT : GOTO 1576
1573  REM  CONVERT AVERAGE TO PRESSURE
1575 FG = 1: GOSUB 5100:AV =  FN P(AV): FOR I = 1 TO NZ:Z%(I) =  FN P(Z%(I
     )): NEXT : GOSUB 5100:YAV =  FN H(YAV) - LU * AV / LE: FOR I = 1 TO N
     Z:Y%(I) =  FN H(Y%(I)) - LU * Z%(I) / LE: NEXT
1576  FOR I = 1 TO NZ
1577 VA = VA + (Z%(I) - AV) * (Z%(I) - AV):YVA = YVA + (Y%(I) - YAV) * (Y%
     (I) - YAV)
1578  NEXT I
1580 STD =  SQR (VA / (NZ - 1)):YSTD =  SQR (YVA / (NZ - 1))
1600  PRINT D$;"PR#1"
1602  PRINT : PRINT : PRINT
1605  PRINT  TAB( 5);M$(CH)
1606  PRINT : PRINT : PRINT
1610  PRINT DA$
1612  PRINT : PRINT : PRINT
1615  PRINT "GAS VELOCITY="; SPC( 2);VS; SPC( 2);"M/S"
1617  PRINT  TAB( 5);"SOLID FLOW RATE ="; SPC( 1);SL; SPC( 1);"G/S"
1618  IF NT = 1 THEN  PRINT  TAB( 5);"THE AVERAGE UPSTREAM PRESSURE VALUE
     FROM TAYLOR TRANSDUCER IS:"; SPC( 2);UP; SPC( 1);"Pa"
1619  IF NT = 1 THEN  PRINT  TAB( 5);"THE AVERAGE VALUE FROM TAYLOR TRANSD
     UCER IS:"; SPC( 2); INT (AV); SPC( 1);"+/-"; SPC( 1); INT (STD); SPC(
     1);"Pa"
1620  PRINT  TAB( 5);"THE AVERAGE VALUE FROM SETRA TRANSDUCER IS:"; SPC( 2
     ); INT (AV); SPC( 1);"+/-"; SPC( 1); INT (STD); SPC( 1);"Pa"
1625  PRINT  TAB( 5);"THE AVERAGE VALUE FROM SCHAEVITZ TRANSDUCER IS:"; SPC(
     2); INT (YAV); SPC( 1);"+/- "; SPC( 1); INT (YSTD); SPC( 1);"Pa"
1627  PRINT  TAB( 5);"TEST SECTION="; SPC( 2);LE; SPC( 1);"M"
1628  PRINT D$;"PR#0"
1629  RETURN
1630  REM      PROGRAM ORIFICE FLOWRATE
1635  VTAB 2: PRINT BL$: INVERSE : VTAB 2: HTAB 7: PRINT OQ$: NORMAL
1637  VTAB 1: PRINT BL$: VTAB 1: HTAB 7: INVERSE : PRINT OP$: NORMAL
1638 DP = 0.0381:OD = 0.02286
1639  IF CH = 2 OR CH = 3 OR CH = 4 THEN DP = 0.01905
1641  IF CH = 2 OR CH = 3 OR CH = 4 THEN OD = 0.0127
1643  IF CH = 5 THEN OD = 0.03048
1650 CK = 0
1670  REM   OPEN ORIFICE DATA FILE
1680  REM   INPUT ORIFICE FILE NAME
1690  REM   INPUT ORIFICE FILE DATA
1700 UAV = 0:SUB = 1
1705  FOR M = 1 TO N
1710 UAV = UAV +  PEEK (49331)
1715  NEXT M
1717 UR = UAV / N
1718 UP =  INT ( FN S(UR))
1720 PUP = UP + 101325
1750 PDN = PUP - AV
1760  REM  ORIFICE PROGRAM
1780  REM  THIS PROGRAM COMPUTES THE MASS FLOWRATE OF AIR THROUGH A
```

```
1800  REM  SHARP EDGED ORIFICE METER WITH CORNER TAPS.
1820  REM  INITIALIZATION AND FILE OPENING
2055 GMW = 28.8
2080 GVIS = 0.0000178
2100 GK = 1.4
2110  IF SUB = 2 THEN DP = 0.01905:OD = 0.01397:UP = FLP * 248.84:PC = FPP
     * 248.84
2115  IF SUB = 3 THEN DP = 0.01905:OD = 0.01397:UP = FUP * 98.064:PC = FDR
     OP * 248.84
2116  IF SUB <  > 1 THEN PUP = UP + 101325:PDN = PUP - PC
2120  REM
2140  REM  CALCULATIONS
2160 DEN = GMW * PUP / (8314.32 * (TP + 273.15))
2180 PI = 3.1415927
2200 PR = PDN / PUP
2220 BETA = OD / DP
2240 Y = 1 - (1 - PR) * (0.41 + 0.35 * BETA ^ 4) / GK
2260 KO = 0.6004 + 0.35 * BETA ^ 4
2280  IF BETA < 0.5 THEN KO = KO - 0.052 * (0.5 - BETA) ^ 1.5
2300 AO = (PI * OD ^ 2) / 4
2320 B = (0.002 + 0.026 * BETA ^ 4) * KO
2340 TM = AO *  SQR (2 * (PUP - PDN) * DEN)
2360 RY = 30000
2380  REM
2400  FOR I = 1 TO 1000
2420 L = 1000 /  SQR (RY)
2440 KK = KO * (1 + B * L)
2460 W(SUB) = KK * Y * TM
2480 RN = 4 * W(SUB) / (GVIS * PI * DP)
2500 RSID = 1 - RN / RY
2520  IF  ABS (RSID) < 0.001 THEN 2610
2540 RY = RN
2560  NEXT I
2580  PRINT "DID NOT CONVERGE"
2600  STOP
2610 MF = W(1) + W(2) - W(3)
2620 Q(SUB) = W(SUB) / DEN
2640 VO = Q(SUB) / AO
2650 VS = MF / DEN / 0.0007917
2655 VS =  INT (VS * 100) * 0.01
2660 RO = DEN * VO * OD / GVIS
2680  REM  PRINT OUT RESULTS
2720  TEXT : HOME
2740  PRINT D$;"PR#1"
2750  INVERSE : PRINT  TAB( 5);"ORIFICE METER CALCS": NORMAL
2780  PRINT
2830  PRINT
2831  PRINT  TAB( 5);"SAMPLING FREQ. (HZ)"; SPC( 2);FR
2832  PRINT  TAB( 5);"ORIFICE FILE"; SPC( 2);OF$
2833  PRINT  TAB( 5);"DATE"; SPC( 2);DA$
2835  PRINT  TAB( 5);"RUN NUMBER"; SPC( 2);RN$
2837  PRINT  TAB( 5);"LOOP ="; SPC( 2);SUB
2840  PRINT  TAB( 5);"THE MASS FLOWRATE OF AIR (KG/S)="; SPC( 2);W(SUB)
2860  PRINT  TAB( 5);"PRESSURE DROP (PA) ="; SPC( 2); INT (AV * 10) * 0.1
2880  PRINT  TAB( 5);"ORIFICE DIAMETER (M) ="; SPC( 2);OD
2900  PRINT  TAB( 5);"ORIFICE VELOCITY (M/S) ="; SPC( 2);VO
2920  PRINT  TAB( 5);"ORIFICE REYNOLDS# ="; SPC( 2);RO
2940  PRINT
2960  PRINT "VOLUMETRIC FLOWRATE (CU.M/S)="; SPC( 2);Q(SUB)
2965  FOR Q = 1 TO 3: PRINT : NEXT
2970  IF SUB <  > 3 THEN 3990
2975  PRINT  TAB( 5);"THE TOTAL MASS FLOWRATE OF AIR (KG/S)="; SPC( 2);MF
2976  PRINT "EFFECTIVE VOLUMETRIC FLOWRATE (CU.M/S)="; SPC( 2);MF / DEN
2980  PRINT  TAB( 5);"SUPERFICIAL GAS  VELOCITY (M/S)="; SPC( 2);VS
2990  PRINT  TAB( 5);"THE DENSITY OF AIR (KG/CU. M)="; SPC( 2); INT (DEN *
     100) * 0.01
```

```
      DPDLG = RHOP*ALPHA / 100 * 9.81 * COS(ANGLE)
      DPLFL = 2 * FG * RHOF * UF**2 / D
      DPDLS = GRADP - DPDLG  - DPLFL
      FS = DPDLS * D / 2 / RHOP/ ALPHA / UP**2 *100
      WRITE(6,1000) NRUN,GS*1000,G*1000,GRADP,DPDLG,DPLFL,DPDLS,ALPHA
      WRITE(8,1000) NRUN,GS*1000,G*1000,GRADP,DPDLG,DPLFL,DPDLS,ALPHA
C
C     END OF OUTER LOOP ... CONTINUE TO NEXT RUN SERIES
C
 1000 FORMAT(I2,7F10.2)
 1011 FORMAT('RUN SERIES ',A3,'   THETA = ',F7.1,/)
 1040 FORMAT(A3)
*********************************************************************
      CALL DPNEUV( ID, D, XL, WS, ROP, DP, UG, ROG, XMUG, DELTP,
     1 DPFS,DPFG,DPHS,EPSCS)
      IF (NRUN .EQ. 1) WRITE(9,1011) L, THETA
      IF (NRUN .EQ. 1) WRITE(9,1150)
 1150 FORMAT(T7,'SOLIDS',T19,'GAS',T27,'DPRESS',
     1T37,'DPGRAV',T48,'DPFLUID',T58,'DP SOL',T68,'HOLDUP%')
      WRITE(6,1200) NRUN,GS*1000,G*1000,DELTP,DPHS,DPFG,DPFS,EPSCS
     1 *100
      WRITE(9,1201) NRUN,GS*1000,G*1000,DELTP,DPHS,DPFG,DPFS,EPSCS
     1 *100
 1200 FORMAT(I2,7F10.2/)
 1201 FORMAT(I2,7F10.2)
      NRUN = NRUN + 1
      GOTO 10
  100 CLOSE(UNIT=7)
      CLOSE(UNIT=8)
*     START NEW RUN SERIES
      CLOSE(UNIT=9)
      GOTO 70
 2000  END
      SUBROUTINE DPNEUV( ID, D, XL, WS, ROP, DP, UG, ROG, XMUG, DELTP,
     1 DPFS,DPFG,DPHS,EPSCS)
*********************************************************************
c  computes the total pressure drop through a straight section
c    of vertical pneumatic transport line
*********************************************************************
c INPUT
c      id       identification of solids friction factor correlation
c      d        pipe id
c      xl       length of straight section considered
c      ws        solids flux density (in kg/s/m2)
c      rop      particle density
c      dp       particle diameter
c      ug       superficial gas velocity
c      rog      gas density
c      xmug     gas viscosity
*********************************************************************
c OUTPUT
c      deltp    pressure drop across the straight section
```

```
10100 M$(1) = "TEST-UP & TEST-DOWN"
10200 M$(2) = "ACCEL-UP & ACCEL-DOWN"
10210 M$(3) = "DIPLEG-UP & DIPLEG-DOWN"
10250 NT = 2:FG = 1
10300 RR = 2:MEN = 3:H$ = "SUB": GOTO 6100
11200 M$(1) = "PNEUMATIC LINE"
11300 M$(2) = "FBEDIN"
11400 M$(3) = "FBEDOUT"
11500 M$(4) = "SPARGER"
11600 M$(5) = "EXHAUST"
11650 NT = 1:FG = 1
11700 RR = 3:MEN = 5:H$ = "SUB": GOTO 6100
12000  IF RR > 1 THEN 13000
12100  IF CH = 1 THEN P1$ = "TEST PRESSURE DROP":P2$ = "TEST UPSTREAM PRES
     SURE"
12200  IF CH = 2 THEN P1$ = "ACCEL PRESSURE DROP":P2$ = "ACCEL UPSTREAM PR
     ESSURE"
12300  IF CH = 3 THEN P1$ = "DIPLEG PRESSURE DROP":P2$ = "DIPLEG UPSTREAM
     PRESSURE"
12400  RETURN
13000  IF RR = 3 THEN 14000
13100  IF CH = 1 THEN P1$ = "TEST DOWNSTEAM PRESSURE":P2$ = "TEST UPSTREAM
      PRESSURE"
13200  IF CH = 2 THEN P1$ = "ACCEL DOWNSTREAM PRESSURE":P2$ = "ACCEL UPSTR
     EAM PRESSURE"
13300  IF CH = 3 THEN P1$ = "DIPLEG DOWNSTREAM PRESSURE":P2$ = "DIPLEG UPS
     TREAM PRESSURE"
13400  RETURN
14000  IF CH = 1 THEN P1$ = "PNEUMATIC LINE DELTA P"
14100  IF CH = 2 THEN P1$ = "FBEDIN DELTA P"
14200  IF CH = 3 THEN P1$ = "FBEDOUT DELTA P"
14300  IF CH = 4 THEN P1$ = "SPARGER DELTA P"
14400  IF CH = 5 THEN P1$ = "EXHAUST DELTA P"
14450 P2$ = ""
14500  RETURN
```

APPENDIX C - SCHEMATIC OF PINCH VALVE WITH DIMENSIONS

Appendix C: Schematic of Pinch Valve with Dimensions

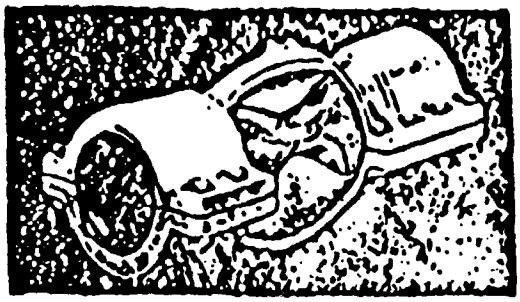

SERIES SGE

The SGE valve is the simplest and consequently the lowest cost remotely operated pinch valve available to industry.

OPERATION: Operation of the SGE valve is by application of hydraulic or pneumatic pressure through the pipe connection in the housing to the annular volume surrounding the elastomeric tube. As pressure is applied the central portion of the tube collapses from opposite sides effecting centered, straight line closure. Only straight line closure can provide gas-tight closure on slurries, gases and liquids. Upon reduction of applied pressure to atmosphere (or to vacuum if line pressure is a vacuum), the elasticity of the liner opens the valve to full-round configuration. If a vacuum condition exists in the flow line, a vacuum source, such as a vacuum generator, may be applied to the operating line to fully open the valve.
The SGE valve is generally specified for on-off service, but approximate flow control (throttling) can be effected by using a PRV (pressure reducing valve) to vary the operating pneumatic or hydraulic pressure.
To insure maximum cycle life, a PRV should be installed and set no higher than is necessary to close the valve tight.

CONSTRUCTION: The SGE pinch valve is constructed with a split housing for easy change of elastomeric bodies, meaning less down-time for maintenance. Standard housing is cast aluminum, but cast iron is available upon request. Body construction is tailored to operating conditions, and bodies are available in a wide range of elastomers including: pure gum rubber, (natural rubber), Neoprene, Buna N, Butyl, Hypalon®, Silicone, Viton®, EPDM (Nordel®) and food grade elastomers. Other elastomers available upon application.

MAINTENANCE: No maintenance or cleaning is necessary for the life of the valve, since there are no moving parts, no packing glands, and no seals. Length of service of the elastomeric body is dependent upon the material handled, line and operating pressures, frequency of cycling, and other factors.

APPLICATIONS: The SGE pinch valve is being successfully employed in air and vacuum vaying systems, handling dry powders as well as a wide range of slurries and for controlling pump discharge and hopper unloading. It can be employed in almost any aspect of pollution abatement due to its ability to close bubble tight over solid particles.

OPTIONAL ACCESSORIES: PRV (Pressure Reducing Valve), 3-Way Solenoid Valve, Air Pressure Gauge (Specify if installation and adjustment is desired).

NOTE: Air supply should be approximately 40 psig higher than line pressure in order to insure full closure of valve.

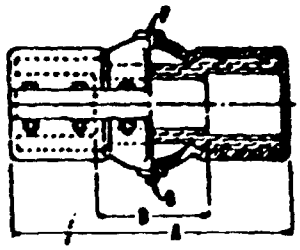

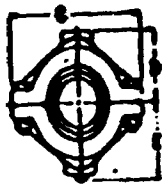

®E. I. duPont Co. trademarks

SERIES SGE DIMENSIONS

VALVE SIZE	1/4	1/2	3/4	1	1 1/4	1 1/2	2	2 1/2	3	4
A. LENGTH	4 1/4	5 3/8	6 1/8	7 3/16	8 1/2	10 1/8	11 3/16	14 1/4	16 1/8	20 1/8
B. BETWEEN PIPE	1 5/8	2	2 1/2	3	3 1/2	4 1/4	5 1/2	7	8 3/8	10 1/2
C. WIDTH	2 7/8	3 1/4	3 1/2	4 1/8	4 1/2	4 3/4	5 3/8	6 5/8	7 1/2	9 3/4
D.	1 1/16	1 1/4	1 7/16	1 11/16	2	2 3/16	2 5/8	3 3/16	3 5/8	4 5/8
E.	1 3/8	1 9/16	1 3/4	2	2 5/16	2 1/2	2 15/16	3 1/2	4	5 1/2
F. NPT (SUPPLY)	1/8	1/8	1/8	1/8	1/8	1/8	1/8	1/4	1/4	1/4
G. NPT (DRAIN)	1/8	1/8	1/8	1/8	1/8	1/8	1/8	1/4	1/4	1/4
WEIGHT (ALUM.)	1 lb	1 lb	1	1 lb	2 lb	2 lb	10	21	25	38
WEIGHT (C.I.)	3	4	4 lb	10	10	17	22	44	57	84

APPENDIX D : FORTRAN PROGRAMS FOR DATA ANALYSIS

Program PDROP : Pressure Gradient Using Literature Correlations

Program CORANA : Particle Velocity Using Literature Correlations

Program CORREL : Klinzing Thermodynamic Approach

Program LIFTD2 : Lifting Efficiency Calculations, Experimental

Program TRDAT : Calculation of Particle Velocity, Friction factor

```
      PROGRAM PDROP
C
C     THIS PROGRAM ANALYSES THE RESULTS OF THE PNEUMATIC
TRANSPORT
C     EXPERIMENTS.
C
C     COMPUTES FLUID AND PARTICLE VELOCITY, SOLIDS FRICTION FACTOR,
C     COMPONENTS OF THE TOTAL PRESSURE DROP.  INPUTS FROM FILE
'*.DAT'
C     AND OUTPUTS TO FILES '*.OUT' AND '*.RAW'
C
C     IFLE, OFLE, OFLE2 : INPUT AND OUTPUT FILE NAMES
C     UP : PARTICLE VELOCITY
C     UF : ACTUAL FLUID VELOCITY
C     USUPER : SUPERFICIAL FLUID VELOCITY
C     ALPHA : VOLUME FRACTION OF THE SOLIDS * 100
C     EPS : VOID FRACTION
C     D : PIPE DIAMETER
C     AREA : PIPE CROSS-SECTIONAL AREA
C     RHOF : GAS DENSITY
C     VISC : GAS VISCOSITY
C     ATM : STANDARD ATMOSPHERE IN PASCALS
C     THETA : ANGLE OF INCLINATION IN DEGREES
C     ANGLE : ANGLE OF INCLINATION IN RADIANS
C     L : CHARACTER INDICATING RUN SERIES
C     NRUN : RUN NUMBER WITHIN SERIES
C     G : MASS FLOWRATE OF THE GAS
C     GS : SOLIDS MASS FLOWRATE
C     M : RATIO GS / G
C     T : TEMPERATURE (DEGREES CELSIUS)
C     PUP : GAUGE PRESSURE AT BOTTOM OF TEST SECTION
C     GRADP : TOTAL PRESSURE GRADIENT IN TEST SECTION
C     DELP : ONE HALF PRESSURE DROP ACROSS TEST SECTION
C     RE : REYNOLDS NUMBER FOR PIPE FLOW
C     FG : FRICTION FACTOR FOR GAS
C     DPDLG : PRESSURE GRADIENT DUE TO GRAVITY
C     DPDFL : PRESSURE GRADIENT DUE TO GAS FRICTION
C     DPDLS : PRESSURE GRADIENT DUE TO SOLIDS FRICTION
C     FS : FRICTION FACTOR FOR SOLIDS
C
C
      INTEGER NRUN
      CHARACTER  ID,OFLE*7 , IFLE*7, L*3, OFLE2*7
C
*     INITIALIZE VARIABLES
      D = 0.03175
      AREA = D**2*ACOS(-1.0) / 4
      RHOP = 2600.0
      ATM = 1.013E05
      VISC = 1.81E-05
       DP=197E-06
       ROP=RHOP
```

```
      UT=1.484
      XL=1
      XMUG = VISC
C
C     START OF LOOP FOR DIFFERENT RUN SERIES
C
   70 WRITE(6,*) 'ENTER RUN SERIES LETTER (Q TO EXIT):'
      READ(5,1040) L
      IF (L.EQ.'Q') GOTO 2000
      IFLE(4:7) = '.ALL'
      IFLE(1:3) = L
      OFLE(4:7) = '.EXP'
      OFLE(1:3) = L
      OFLE2(1:3) = L
      OPEN(UNIT=6,FILE='TERMINAL')
      OPEN(UNIT=7,FILE=IFLE)
      READ(7,*) THETA, INDX
      ANGLE = THETA * ACOS(-1.0) / 180.0
      OPEN(UNIT=8,FILE=OFLE)
      WRITE(6,*) 'ENTER IDENTIFIER FOR FRICTION FACTOR : (C)APES,
     1(J)ONES, (Y)ANG'
      READ(6,1041) ID
 1041 FORMAT(A1)
      IF (ID .EQ. 'C') OFLE2(4:7) = '.CAP'
      IF (ID .EQ. 'J') OFLE2(4:7) = '.JON'
      IF (ID .EQ. 'Y') OFLE2(4:7) = '.YNG'
      OPEN(UNIT=9,FILE=OFLE2)
      WRITE(6,1011) L, THETA
      WRITE(8,1011) L, THETA
      NRUN = 1
C
C     START OF FIRST LOOP FOR DIFFERENT RUNS WITHIN A SERIES
C
   10 READ(7,*,END=100) GS, G, ALPHA, T, PUP, GRADP
      IF (NRUN .EQ. 1) WRITE(6,1150)
      IF (NRUN .EQ. 1 ) WRITE(8,1150)
      IF (INDX.EQ.1) PUP = PUP / 98.1
      GS = GS / 1000
      WS = GS/AREA
      G = G / 1000
      M = GS / G
      EPS = 1.0 - ALPHA/100
      PUP = PUP * 98.1
      DELP = 4.55 * GRADP / 2
      RHOF = (29/22.414)*(PUP - DELP + ATM) / ATM* 273 /(273 + T)
      ROG = RHOF
      UP = GS / RHOP / AREA / (1.0 -EPS)
      UF = G / RHOF / EPS / AREA
      UG = UF
      USUPER = G / RHOF / AREA
      RE = D * UF * RHOF / VISC
      FG = 0.0791 / RE**0.25
```

```
      DPDLG = RHOP*ALPHA / 100 * 9.81 * COS(ANGLE)
      DPLFL = 2 * FG * RHOF * UF**2 / D
      DPDLS = GRADP - DPDLG  - DPLFL
      FS = DPDLS * D / 2 / RHOP/ ALPHA / UP**2 *100
      WRITE(6,1000) NRUN,GS*1000,G*1000,GRADP,DPDLG,DPLFL,DPDLS,ALPHA
      WRITE(8,1000) NRUN,GS*1000,G*1000,GRADP,DPDLG,DPLFL,DPDLS,ALPHA
C
C     END OF OUTER LOOP ... CONTINUE TO NEXT RUN SERIES
C
 1000 FORMAT(I2,7F10.2)
 1011 FORMAT('RUN SERIES ',A3,'   THETA = ',F7.1,/)
 1040 FORMAT(A3)
*****************************************************************
      CALL DPNEUV( ID, D, XL, WS, ROP, DP, UG, ROG, XMUG, DELTP,
     1 DPFS,DPFG,DPHS,EPSCS)
      IF (NRUN .EQ. 1) WRITE(9,1011) L, THETA
      IF (NRUN .EQ. 1) WRITE(9,1150)
 1150 FORMAT(T7,'SOLIDS',T19,'GAS',T27,'DPRESS',
     1T37,'DPGRAV',T48,'DPFLUID',T58,'DP SOL',T68,'HOLDUP%')
      WRITE(6,1200) NRUN,GS*1000,G*1000,DELTP,DPHS,DPFG,DPFS,EPSCS
     1 *100
      WRITE(9,1201) NRUN,GS*1000,G*1000,DELTP,DPHS,DPFG,DPFS,EPSCS
     1 *100
 1200 FORMAT(I2,7F10.2/)
 1201 FORMAT(I2,7F10.2)
      NRUN = NRUN + 1
      GOTO 10
  100 CLOSE(UNIT=7)
      CLOSE(UNIT=8)
*     START NEW RUN SERIES
      CLOSE(UNIT=9)
      GOTO 70
 2000  END
      SUBROUTINE DPNEUV( ID, D, XL, WS, ROP, DP, UG, ROG, XMUG, DELTP,
     1 DPFS,DPFG,DPHS,EPSCS)
*****************************************************************
c  computes the total pressure drop through a straight section
c    of vertical pneumatic transport line
*****************************************************************
c INPUT
c      id       identification of solids friction factor correlation
c      d        pipe id
c      xl       length of straight section considered
c      ws        solids flux density (in kg/s/m2)
c      rop      particle density
c      dp       particle diameter
c      ug       superficial gas velocity
c      rog      gas density
c      xmug     gas viscosity
*****************************************************************
c OUTPUT
c      deltp    pressure drop across the straight section
```

```
157   ************************************************************************
158   c     si units
159   ************************************************************************
160
161         CHARACTER ID
162         EXTERNAL DPIPE, UTERM
163
164   c     gas friction pressure drop
165   c      assume pipe wall roughness affected by particle diameter
166         ROUGH = 2. * DP
167         CALL DPIPE( D, XL, ROUGH, UG, ROG, XMUG, RE, F, DPFG)
168
169   c     terminal velocity
170         CALL UTERM( ROG, XMUG, ROP, DP, UTER)
171
172   c     estimate particle velocity.  then solids holdup
173         UP = UG - UTER
174         EPSCS = WS / UP / ROP
175
176   c     hydrostatic pressure drop due to solids
177         DPHS = ROP * EPSCS * 9.81 * XL
178
179   c     solids friction pressure drop
180         CALL DPNFS( ID, D, XL, UG, ROG, ROP, WS, UTER, FS, DPFS, DP)
181
182         DELTP = DPFS + DPFG + DPHS
183         RETURN
184         END
185
186         SUBROUTINE DPNFS( ID, D, XL, UG, ROG, ROP, WS, UTER, FS, DPFS, DP)
187   ************************************************************************
188   c  computes the pressure drop due to the solids friction in
189   c   vertical pneumatic transport lines
190   ************************************************************************
191   c  uses the simple relationship: fs = k / (up**n)
192   c   (for more sophisticated model see Yang: subroutine ???????)
193   ************************************************************************
194   c INPUT
195   c      id       identification of solids friction factor correlation
196   c      d        pipe id
197   c      xl       length of straight section considered
198   c      ug        superficial gas velocity
199   c      rog      gas density
200   c      rop      particle density
201   c      ws       solids flux density (in kg/s/m2)
202   c      uter     particle terminal velocity
203   ************************************************************************
204   c OUTPUT
205   c      fs       solids friction factor (warning fs = fp/4)
206   c      dpfs     pressure drop from solids friction
207   ************************************************************************
208   c      all correlations taken from Yang w.c., AIChE J, 24, 1978, 548-552
```

```
209   c     except Capes, taken from capes, nakamura, CJChE, 51, 1973, 31-38
210   ************************************************************************
211   c     for spherical particles
212   ************************************************************************
213   c     si units
214   ************************************************************************
215
216         CHARACTER ID
217
218   c     approximation for particle velocity
219         UP = UG - UTER
220
221         XINT = 2. * WS * UP * XL / D
222
223         IF ( ID .EQ. 'C') THEN
224   c       capes and nakamura
225           FP = 0.206 * UP**(-1.22)
226           FS = FP / 4.
227           DPFS = FS * XINT
228           RETURN
229
230         ELSE IF ( ID .EQ. 'J' ) THEN
231   c       jones (based on ug)
232           FS = 0.
233           A0 = 6./ DP * .3048
234           THETA = WS / ROG / UG
235           IF ( A0 .GT. 6300. ) THEN
236             X = (6300./A0)**.333333333
237           ELSE
238             X = 1.
239           ENDIF
240           FPS = 1.89 E-6 * A0 * THETA**X
241           DPFS = FPS * ROG * UG * UG * XL / 2. / D
242           RETURN
243
244         ELSE IF ( ID .EQ. 'Y' ) THEN
245   c       yang (1978) (note: yang assumes a sophisticated formula for
246   c         up, which we do not use here)
247           RERAT = UTER / (UG - UP)
248           EPSCS = WS / ROP / UP
249           EPS = 1 - EPSCS
250           R = UG / UTER
251           IF ( R .GT. 1.5 ) THEN
252             FP = 0.0126 * EPSCS / EPS/EPS/EPS * (EPSCS * RERAT)**(-.979)
253           ELSE
254             FP = 0.0410 * EPSCS / EPS/EPS/EPS * (EPSCS * RERAT)**(-1.021)
255           ENDIF
256           FS = FP / 4.
257           DPFS = FS * XINT
258           RETURN
259
260         ELSE
```

```
      WRITE (*, 11)
 11    FORMAT(' WRONG ID ')
      DPFS = 1.E 22
      RETURN

     ENDIF

     END

     SUBROUTINE DPIPE( D, XL, EPS, V, ROF, XMUF, RE, F, DP)
*************************************************************************
c    computes the pressure drop through a pipe for turbulent flow of
c      a single phase incompressible fluid
*************************************************************************
c    uses equation for friction factor from serghides t.k., chem. eng.
c     91, no 5, march 5, 1984, 63-64
c    simpler, less general equation from haaland s.f., trans. asme, jfe,
c     105, 1983, 89-90
*************************************************************************
c     SI units
*************************************************************************
c INPUT
c     d       pipe id
c     xl      length of straight section for which we want dp
c     eps      pipe wall roughness (see program dpipem for values)
c     v       fluid velocity
c     rof     fluid density
c     xmuf     fluid dynamic viscosity
*************************************************************************
c OUTPUT
c     re      reynolds number
c     f       friction factor WARNING such as dp = 2 f rog l v*v /  d
c     dp       pressure drop
*************************************************************************

     RE = ROF * V * D / XMUF

     IF ( RE .LT. 2000.) THEN
      WRITE(*,11) RE
 11    FORMAT(' non turbulent: reynolds number =', E16.7)
      F = 16. / RE
     ELSE
      R = EPS / D / 3.7
      IF (((RE.GT.4.E4).AND.(RE.LT.1.E8)).AND.(R.LT.1.4E-2)) THEN
       F = -3.6 * ALOG10( 6.9/RE + R**1.11 )
       F = 1./F/F
      ELSE
       A = - 2.0 * ALOG10( R + 12./ RE )
       B = - 2.0 * ALOG10( R + 2.51 * A / RE )
       C = - 2.0 * ALOG10( R + 2.51 * B / RE )
       DD = C - 2.*B + A
       F = A - (B-A)*(B-A) / DD
```

```
313           F = 1./F/F
314           F = F / 4.
315         ENDIF
316       ENDIF
317
318       DP = 2. * ROF * F * XL * V * V / D
319
320       RETURN
321       END
322
323
324       SUBROUTINE UTERM ( ROF, XMUF, ROP, DP, UTER)
325     C*********************************************************************
326     C     computes the terminal velocity of a free-falling single particle
327     C*********************************************************************
328     C computes aa and n such that CD = aa * (REp)**(-n)
329     C  with CD as drag coefficient and REp as particle Reynolds number
330     C uses interpolation formulae developed by cedric briens from
331     C published experimental data (see terminal velocity file)
332     C
333     C then computes uterm with Zenz's dimensionless numbers
334     C
335     C WARNING: strictly valid only for spherical particles
336     C*********************************************************************
337     C INPUT:  rof: fluid density
338     C         xmuf: fluid viscosity (dynamic)
339     C         rop: particle density
340     C         dp : particle diameter
341     C*********************************************************************
342     C OUTPUT:  uter: terminal velocity
343     C*********************************************************************
344
345         G = 9.81
346
347         OMEGA = ( 4.* XMUF * G * (ROP-ROF) / 3.  /ROF/ROF) ** (1./3.)
348         DELTA = ( 3.* XMUF * XMUF / 4. / ROF / G / (ROP-ROF) ) ** (1./3.)
349         X = DP / DELTA
350
351
352         IF ( X .LT. 2.1 ) THEN
353            AA = 24
354            XN = 1
355
356         ELSE IF ( X .LT. 3.) THEN
357            AA = 26.5
358            XN = .892
359
360         ELSE IF ( X .LT. 7 4) THEN
361            AA = 26.5
362            XN = .810
363
364         ELSE IF ( X .LT. 22. ) THEN
```

```
365           AA = 15.7
366           XN = .583
367
368         ELSE IF ( X .LT. 76. ) THEN
369           AA = 6.48
370           XN = .391
371
372         ELSE IF ( X .GT. 76. ) THEN
373           AA = .44
374           XN = 0.
375
376         ENDIF
377
378         Y = ( 1./ AA * X ** (1.+XN) ) ** ( 1./(2.-XN) )
379         UTER = Y * OMEGA
380         RETURN
381         END
382
```

```
      PROGRAM CORANA
C
C     THIS PROGRAM COMPARES THE RESULTS OF THE PNEUMATIC
TRANSPORT
C     EXPERIMENTS WITH CORRELATIONS IN THE LITERATURE
C
C
C     USES FILES OF TYPE '*.REG' AND OUTPUTS FILES OF TYPE '*.ANA'.
C     PRODUCES ONE FILE PER RUN SERIES, BUT ALSO AN OVERALL
SUMMARY
C     IN FILE 'ALL.ANA'.
C
C     IFLE, OFLE : INPUT AND OUTPUT FILE NAMES
C     UP : PARTICLE VELOCITY
C     UF : ACTUAL FLUID VELOCITY
C     USUPER : SUPERFICIAL FLUID VELOCITY
C     ALPHA : VOLUME FRACTION OF THE SOLIDS
C     EPS : VOID FRACTION
C     D : PIPE DIAMETER
C     THETA : ANGLE OF INCLINATION IN DEGREES
C     ANGLE : ANGLE OF INCLINATION IN RADIANS
C     L : CHARACTER INDICATING RUN SERIES
C     I : RUN NUMBER WITHIN SERIES
C     G : MASS FLOWRATE OF THE GAS
C     GS : SOLIDS MASS FLOWRATE
C     M : RATIO GS / G
C     T : TEMPERATURE (DEGREES CELSIUS)
C     GRADP : TOTAL PRESSURE GRADIENT IN TEST SECTION
C     FG : FRICTION FACTOR FOR GAS
C     DPDLG : PRESSURE GRADIENT DUE TO GRAVITY
C     DPDFL : PRESSURE GRADIENT DUE TO GAS FRICTION
C     DPDLS : PRESSURE GRADIENT DUE TO SOLIDS FRICTION
C     FS : FRICTION FACTOR FOR SOLIDS
C     UPKON : PARTICLE VELOCITY PREDICTION BY METHOD OF KONNO &
SAITO
C     UPMAT : PARTICLE VELOCITY PREDICTION BY METHOD OF MATSEN
C     UPMYL : PARTICLE VELOCITY PREDICTION BY METHOD OF MYLER
C     UPZAL : PARTICLE VELOCITY PREDICTION BY METHOD OF ZALTASH
C     UPHINK : METHOD OF HINKLE-IGT
C     FSKON : SOLIDS FRICTION FACTOR PREDICTION ACCORDING TO
KONNO & SAITO
C     FSYANG : PREDICTION OF YANG FOR FS
C     FSNAK : PREDICTION OF NAKAMURA & CAPES
C
      CHARACTER OFLE*6 , IFLE*6, L*3
      REAL M, FSKON(50), FSYANG(50), FSNAK(50), FSA(50)
      INTEGER COUNT(10), TCOUNT(10), UPA(50)
C
      OPEN(UNIT=6,FILE='TERMINAL')
      OPEN(UNIT=5,FILE='TERMINAL')
      WRITE(6,*) 'ENTER ERROR LEVEL'
```

```
      READ(5,*) ERR
      D = 0.03175
      AREA = D**2*ACOS(-1.0) / 4
      RHOP = 2600.0
      ATM = 1.013E05
      VISC = 1.82E-05
      UTERM = 3.2
      TSUM2 = 0
      TSUM3 = 0
      TSUM4 = 0
      TSUM6 = 0
      TSUM7 = 0
      TSUM8 = 0
      TSUM9 = 0
      TSUM10 = 0
      TSU2 = 0
      TSU8 = 0
      TS2 = 0
      DO 33 I = 1,10
   33 TCOUNT(I) = 0
C
C     START OF LOOP FOR DIFFERENT RUN SERIES
C
   70 WRITE(6,*) 'ENTER RUN SERIES LETTER (Z TO EXIT):'
      READ(5,1040) L
      IF (L.EQ.'Z') GOTO 90
      IFLE(3:6) = '.REG'
      IFLE(1:2) = L
      OFLE(3:6) = '.ANA'
      OFLE(1:2) = L
      OPEN(UNIT=7,FILE=IFLE)
      READ(7,1010) THETA
      ANGLE = THETA * ACOS(-1.0) / 180.0
      OPEN(UNIT=8,FILE=OFLE)
      WRITE(8,1111) L
 1111 FORMAT(///'RUN SERIES ',A2,//)
      I = 1
      SUM2 = 0
      SUM3 = 0
      SUM4 = 0
      SUM5 = 0
      SUM6 = 0
      SUM7 = 0
      SUM8 = 0
      SUM9 = 0
      SUM10 = 0
      SU8 = 0
      SU2 = 0
      S2 = 0
      DO 34 K = 1, 10
   34 COUNT(K) = 0
      WRITE(8,300)
```

```
104          300 FORMAT(' I',T10,'UP',T20,'UP-UPKON',T32,'UP-UPMAT',T44,'UP-UPMYL'
105            1,T56,'UP-UPZAL',T68,'UP-UPHINK',//)
106          C
107          C     START OF FIRST LOOP FOR DIFFERENT RUNS WITHIN A SERIES
108          C
109            10 READ(7,*,END=2000) GS,G,GRADP,DPDLG,DPLFL,DPDLS
110              READ(7,*)  EPS, UP, UF, USUPER,RHOF,M,FS
111              UPA(I) = 0
112              IF (UF.GT.UP) THEN
113              FSA(I) = FS
114              FS = FS / 1000
115              GS = GS / 1000
116              G = G / 1000
117              M = GS / G
118              RE = D * UF * RHOF / VISC
119              FG = 0.0791 / RE**0.25
120              UPKON=(UF-UTERM)
121              UPMAT = UF - 10.8 * UTERM * (1.0 - EPS)**0.293
122              UPMYL = (UF - UTERM**0.71) * D**0.019
123              SQGD = SQRT(9.81 * D)
124              UPZAL = SQGD * (USUPER/SQGD - (UTERM/SQGD)**0.87)*(1.0 - 0.5 *
125             1COS(ANGLE))**0.0765*(D/191.0E-06)**0.031*(RHOP/RHOF)**(-0.0321)
126              UPHINK = UF*(1.0 - 0.68*(191.0E-06)**0.92*SQRT(RHOP)/RHOF**0.2
127             1/D**0.54)
128              FSKON(I) = 28.5*SQRT(9.81*D)/UP
129              WRITE(8,1000) I, UP, (UP -UPKON), (UP -UPMAT),
130             1                (UP - UPMYL), (UP -UPZAL), (UP -UPHINK)
131              IF (FS .GT. 0) THEN
132                SUM8 = SUM8 + ABS(FS * 1000 - FSKON(I))
133                SU8 = SU8 + 1000*FS
134                UPA(I) = 1
135                FSYANG(I) = 3.15 *(1.0 - EPS) / EPS**3 * ( (1.0 - EPS)
136             1  * UTERM / (UF - UP))**(-0.979)
137                FSNAK(I) = 48.0 / UP**1.22
138                COUNT(9) = COUNT(9) + 1
139                SUM9 = SUM9 + ABS(FS*1000 - FSYANG(I))
140                SUM10 = SUM10 + ABS(FS*1000 - FSNAK(I))
141                COUNT(8) = COUNT(8) + 1
142                ENDIF
143              IF (ABS(UPKON-UP)/UP.LT.ERR) THEN
144                SUM2 = SUM2 + ABS(UPKON - UP)
145                SU2 = SU2 + UP
146                S2 = UPKON - UP
147                COUNT(2) = COUNT(2) + 1
148                ENDIF
149              IF (ABS(UPMAT - UP)/UP.LT.ERR) THEN
150                COUNT(3) = COUNT(3) + 1
151                SUM3 = SUM3 + ABS(UPMAT - UP)
152                ENDIF
153              IF (ABS(UPMYL - UP)/UP.LT.ERR) THEN
154                SUM4 = SUM4 + ABS(UPMYL - UP)
155                COUNT(4) = COUNT(4) + 1
```

```
156             ENDIF
157           IF (ABS(UPZAL-UP)/UP.LT.ERR) THEN
158             COUNT(6) = COUNT(6) + 1
159             SUM6 = SUM6 + ABS(UPZAL - UP)
160             ENDIF
161           IF (ABS(UPHINK - UP)/UP.LT.ERR) THEN
162             SUM7 = SUM7 + ABS(UPHINK - UP)
163             COUNT(7) = COUNT(7) + 1
164             ENDIF
165           ELSE
166             WRITE(8,1001) I
167       1001 FORMAT(I2,'  UP > UF')
168           ENDIF
169           I = I + 1
170       C
171           GOTO 10
172       2000 CONTINUE
173           N = I - 2
174           WRITE(8,1060)
175       1060 FORMAT(/T10,'FS',T22,'FSKON',T34,'FSYANG',T46,'FSNAK',/)
176           DO 150 I = 1, N
177        150 IF (UPA(I).EQ.1)
178          1WRITE(8,1000) I, FSA(I), FSKON(I), FSYANG(I), FSNAK(I)
179       C
180       C     END OF INNER LOOP ... BEGIN SUMMARY FOR RUN SERIES
181       C
182           COUNT(1) = I - 1
183           TCOUNT(10) = TCOUNT(10) + COUNT(1)
184           AAD2 = 1000
185           AAD3 = 1000
186           AAD4 = 1000
187           AAD6 = 1000
188           AAD7 = 1000
189           AVFS = SU8 / COUNT(8)
190           AADFSK = SUM8 / COUNT(8)
191           AADFSY = SUM9 / COUNT(9)
192           AADFSN = SUM10 / COUNT(9)
193           AVUP = SU2 / COUNT(2)
194           IF (COUNT(2).GT.0) THEN
195             AAD2 = SUM2 / COUNT(2)
196             AV2 = S2 / COUNT(2)
197             ENDIF
198           IF (COUNT(3).GT.0) AAD3 = SUM3 / COUNT(3)
199           IF (COUNT(4).GT.0) AAD4 = SUM4 / COUNT(4)
200           AADFS = SUM8 / COUNT(8)
201           IF (COUNT(6).GT.0) AAD6 = SUM6 / COUNT(6)
202           IF (COUNT(7).GT.0) AAD7 = SUM7 / COUNT(7)
203           DO 37 I = 1, 10
204        37 TCOUNT(I) = TCOUNT(I) + COUNT(I)
205           TSUM2 = TSUM2 + SUM2
206           TSUM3 = TSUM3 + SUM3
207           TSUM4 = TSUM4 + SUM4
```

```
208           TSUM6 = TSUM6 + SUM6
209           TSUM7 = TSUM7 + SUM7
210           TSUM8 = TSUM8 + SUM8
211           TSUM9 = TSUM9 + SUM9
212           TSUM10 = TSUM10 + SUM10
213           TSU2 = TSU2 + SU2
214           TSU8 = TSU8 + SU8
215           TS2 = TS2 + AV2
216           WRITE(8,320) COUNT(1), ERR
217           WRITE(8,223) AAD2, COUNT(2), AV2, AVUP
218           WRITE(8,224) AAD3, COUNT(3)
219           WRITE(8,225) AAD4, COUNT(4)
220           WRITE(8,226) AAD6, COUNT(6)
221           WRITE(8,227) AAD7, COUNT(7)
222           WRITE(8,228) AADFSK, COUNT(8), AVFS, AADFSY, COUNT(9), AADFSN
223
224           CLOSE(UNIT=7)
225           CLOSE(UNIT=8)
226         C
227         C    END OF CALCULATIONS FOR SERIES . . PROCEED TO NEXT SERIES
228         C
229           GOTO 70
230         C
231         C    END OF ALL SERIES . . OVERALL SUMMARY
232         C
233          90 AAD2 = TSUM2 / TCOUNT(2)
234           AAD3 = TSUM3 / TCOUNT(3)
235           AAD4 = TSUM4 / TCOUNT(4)
236           AAD6 = TSUM6 / TCOUNT(6)
237           AAD7 = TSUM7 / TCOUNT(7)
238           AVUP = TSU2 / TCOUNT(2)
239           AADFSK = TSUM8 / TCOUNT(8)
240           AADFSY = TSUM9 / TCOUNT(9)
241           AADFSN = TSUM10 / TCOUNT(9)
242           AVFS = TSU8 / TCOUNT(2)
243           AV2 = TS2 / TCOUNT(2)
244           OPEN(UNIT=8,FILE='ALL.ANA')
245           WRITE(8,*) 'OVERALL DATA'
246           WRITE(8,320) TCOUNT(10), ERR
247           WRITE(8,223) AAD2, TCOUNT(2), AV2, AVUP
248           WRITE(8,224) AAD3, TCOUNT(3)
249           WRITE(8,225) AAD4, TCOUNT(4)
250           WRITE(8,226) AAD6, TCOUNT(6)
251           WRITE(8,227) AAD7, TCOUNT(7)
252           WRITE(8,228) AADFSK, TCOUNT(8), AVFS, AADFSY, TCOUNT(9)
253          1,AADFSN
254         223 FORMAT('CORRELATION OF KONNO AND SAITO'/'AAD = ',F12.4,
255          1'  COUNT = ',I4,'  AVERAGE DEVIATION = ',F12.4,/
256          2'AVERAGE UP = ',F8.2)
257         224 FORMAT('CORRELATION OF MATSEN'/'AAD = ',F12.4,
258          1'  COUNT = ',I4)
259         225 FORMAT('CORRELATION OF MYLER'/'AAD = ',F12.4,
```

```
260           1'  COUNT = ',I4)
261          226 FORMAT('CORRELATION OF ZALTASH'/'AAD = ',F12.4,
262           1'  COUNT = ',I4)
263          227 FORMAT('CORRELATION OF HINKLE-IGT'/'AAD = ',F12.4,
264           1'  COUNT = ',I4)
265          228 FORMAT('CORRELATION OF KONNO AND SAITO FOR FS : AADFS = ',
266           1F12.4,'  COUNT = ',I4,/  AVG FS = ',F8.3,/
267           2'CORRELATION OF YANG FOR FS : AADFS = ',F12.4,'  COUNT = ',
268           3I4,/'CORRELATION OF NAKAMURA & CAPES FOR FS : AADFS = ',F12.4,/)
269          320 FORMAT(//'TOTAL NUMBER OF DATA POINTS :',I3,'  ERROR LEVEL :',
270           1F8.2,//)
271          1000 FORMAT(I2,6F12.3)
272          1010 FORMAT(F10.2)
273          1030 FORMAT(I2,7F11.4)
274          1040 FORMAT(A2)
275          3000 FORMAT(7F10.3)
276              END
```

```
 1            PROGRAM CORREL
 2        C
 3        C    THIS PROGRAM ANALYSES THE RESULTS OF THE PNEUMATIC
 4        TRANSPORT
 5        C    EXPERIMENTS.
 6        C
 7        C    COMPUTES FLUID AND PARTICLE VELOCITY, SOLIDS FRICTION
 8        FACTOR,
 9        C    COMPONENTS OF THE TOTAL PRESSURE DROP.  INPUTS FROM FILE
10        '*.DAT'
11        C    AND OUTPUTS TO FILES '*.OUT' AND '*.RAW'
12        C
13        C    IFLE, OFLE, OFLE2 : INPUT AND OUTPUT FILE NAMES
14        C    UP : PARTICLE VELOCITY  (M/S)
15        C    UF : ACTUAL FLUID VELOCITY (M/S)
16        C    UT : CALCULATED MEAN TERMINAL SETTLING VELOCITY (M/S)
17        C    USUPER : SUPERFICIAL FLUID VELOCITY (M/S)
18        C    ALPHA : VOLUME FRACTION OF THE SOLIDS * 100
19        C    EPS : VOID FRACTION
20        C    D : PIPE DIAMETER (M)
21        C    AREA : PIPE CROSS-SECTIONAL AREA (M*M)
22        C    RHOF : GAS DENSITY (KG/(M*M*M))
23        C    VISC : GAS VISCOSITY (KG/M*M*M)
24        C    ATM : STANDARD ATMOSPHERE IN PASCALS  (PA)
25        C    THETA : ANGLE OF INCLINATION IN DEGREES
26        C    ANGLE : ANGLE OF INCLINATION IN RADIANS
27        C    L : CHARACTER INDICATING RUN SERIES
28        C    NRUN : RUN NUMBER WITHIN SERIES
29        C    G : MASS FLOWRATE OF THE GAS (G/S)
30        C    GS : SOLIDS MASS FLOWRATE (G/S)
```

```
C     M : RATIO GS / G
C     T : TEMPERATURE (DEGREES CELSIUS)
C     PUP : GAUGE PRESSURE AT BOTTOM OF TEST SECTION (PA OR CM
WG)
C     GRADP : TOTAL PRESSURE GRADIENT IN TEST SECTION (PA/M)
C     DELP : ONE HALF PRESSURE DROP ACROSS TEST SECTION (PA)
C     RE : REYNOLDS NUMBER FOR PIPE FLOW
C     FG : FRICTION FACTOR FOR GAS
C     DPDLG : PRESSURE GRADIENT DUE TO GRAVITY (PA/M)
C     DPDFL : PRESSURE GRADIENT DUE TO GAS FRICTION  (PA/M)
C     DPDLS : PRESSURE GRADIENT DUE TO SOLIDS FRICTION (PA/M)
C     FS : FRICTION FACTOR FOR SOLIDS
C     INDX : FLAG; = 1 IF PUP IN PA, = 0 IF PUP IN CM WG
C     JGSTAR : DIMENSIONLESS GAS FLUX
C     JPSTAR : DIMENSIONLESS SOLIDS FLUX
C     RSTAR : DIMENSIONLESS GAS CONSTANT
C     JCONST : PARAMETER USED IN COMPUTING DIMENSIONLESS
FLUXES
C     SEGPAR : SEGREGATION PARAMETER
C     K1, K2, K3, K4 : PARAMETERS USED IN CALCULATING UP (KLINZING)
C     DP : MEAN PARTICLE SIZE (M)
C
      EXTERNAL FCT, FUT
      CHARACTER  OFLE*9 , IFLE*9, L*5
      DIMENSION UP(250), UF(250), USUPER(250), EPS(250), FS(250)
      REAL M(250), JGSTAR(250), JPSTAR(250), JGCON, JPCON, RSTAR(250),
     1SEGPAR(250), K1, K2, K3, K4, UTCALC(250), F(250), UTTHEO(250),
     2REP(250), CD(250)
      COMMON K1, K2, K3, K4, UG, ANGLE
C
      OPEN(UNIT=6,FILE='TERMINAL')
      OPEN(UNIT=5,FILE='TERMINAL')
      D = 0.03175
      AREA = D**2*ACOS(-1.0) / 4
      RHOP = 2600.0
      DP = 441.0E-06
      ATM = 1.013E05
      VISC = 1.82E-05
      K1 = 18 * VISC / RHOP / DP**2
      K2 = 0.057 * SQRT(9.81 / D)
      JPCON = 1.0/AREA/SQRT(9.81*D)
      JGCON = 1.0 / AREA / SQRT(9.81 * D * RHOP)

C
C     START OF LOOP FOR DIFFERENT RUN SERIES
C
   70 WRITE(6,*) 'ENTER RUN SERIES LETTER (Z TO EXIT):'
      READ(5,1040) L
      IF (L.EQ.'Q') GOTO 2000
      IFLE(1:2) = 'A:'
      OFLE(1:2) = 'A:'
      IFLE(6:9) = '.ALL'
```

```
      IFLE(3:5) = L
      OFLE(6:9) = '.REV'
      OFLE(3:5) = L
      OPEN(UNIT=7,FILE=IFLE)
      READ(7,*) THETA, INDX
      ANGLE = THETA * ACOS(-1.0) / 180.0
      OPEN(UNIT=8,FILE=OFLE)
      WRITE(8,1011) L, THETA
      WRITE(8,1012)
      NRUN = 1
C
C     START OF FIRST LOOP FOR DIFFERENT RUNS WITHIN A SERIES
C
   10 READ(7,*,END=100) GS, G, ALPHA, T, PUP, GRADP
      IF (INDX.EQ.1) PUP = PUP / 98.1
      GS = GS / 1000
      G = G / 1000
      M(NRUN) = GS / G
      EPS(NRUN) = 1.0 - ALPHA/100
      PUP = PUP * 98.1
      DELP = 4.55 * GRADP / 2
      RHOF = (29/22.414)*(PUP - DELP + ATM) / ATM* 273 /(273 + T)
      UP(NRUN) = GS / RHOP / AREA / (1.0 -EPS(NRUN))
      UF(NRUN) = G / RHOF / EPS(NRUN) / AREA
      JGSTAR(NRUN) = G  / RHOF * JGCON * SQRT(RHOF)
      JPSTAR(NRUN) = GS / RHOP * JPCON
      RSTAR(NRUN) = JPSTAR(NRUN) / JGSTAR(NRUN) / ALPHA * 100
      SEGPAR(NRUN) = 0
      IF (UF(NRUN).GT.UP(NRUN))  SEGPAR(NRUN) = (UF(NRUN) - UP(NRUN))
     1 * SIN(ANGLE) / UF(NRUN) * 100
      USUPER(NRUN) = G / RHOF / AREA
      RE = D * UF(NRUN) * RHOF / VISC
      FG = 0.0791 / RE**0.25
      DPDLG = RHOP*ALPHA / 100 * 9.81 * COS(ANGLE)
      DPLFL = 2 * FG * RHOF * UF(NRUN)**2 / D
      DPDLS = GRADP - DPDLG  - DPLFL
      FS(NRUN) = DPDLS * D / 2 / RHOP/ ALPHA / UP(NRUN)**2 *100
      K3 = 3 * SQRT(RHOF * VISC) / RHOP / DP**1.5
      K4 = 0.3 * RHOF / RHOP / DP
      UG = UF(NRUN)
      IER = 3
      IAR = 3
      AL = 0.2
      DO 550  I = 1, 5
      IF (IER.GT.0)
     1CALL RTMI(UTCALC(NRUN),F(NRUN),FCT,AL,AL+2,0.01,50,IER)
  550 AL = AL + 1
      AL = 0.2
      DO 557  I = 1, 5
      IF (IAR.GT.0)
     1CALL RTMI(UTTHEO(NRUN),F(NRUN),FUT,AL,AL+2,0.01,50,IAR)
  557 AL = AL + 1
```

```
135           IF (IER.EQ.1) UTCALC(NRUN) = -1.0
136           IF (IER.EQ.2) UTCALC(NRUN) = -2.0
137           IF (IAR.EQ.1) UTTHEO(NRUN) = -1.0
138           IF (IAR.EQ.2) UTTHEO(NRUN) = -2.0
139           WRITE(8,1000) NRUN,GS*1000,G*1000,GRADP,DPDLG,DPLFL,DPDLS
140           WRITE(9,1300) NRUN,GS*1000,G*1000,UF(NRUN),UP(NRUN),GRADP,
141          1DPDLG,DPLFL,DPDLS, RHOF, FS(NRUN), ALPHA
142           REP(NRUN) = UTTHEO(NRUN)*RHOF*DP / VISC
143           AA = DP * (9.81*RHOF*RHOP/VISC**2)**0.3333
144           IF (AA.LT.3.3) THEN
145             CD(NRUN) = 24 / REP(NRUN)
146           ELSE
147             CD(NRUN) = 24/REP(NRUN) + 4/SQRT(REP(NRUN)) + 0.4
148             ENDIF
149           NRUN = NRUN + 1
150           GOTO 10
151       C
152       C     END OF FIRST INNER LOOP
153       C     SECOND INNER LOOP BEGINS :
154       C
155         100 WRITE(8,1020)
156           DO 20  I = 1, NRUN - 1
157          20 WRITE(8,1030) I, EPS(I), UP(I), UF(I), USUPER(I),(UF(I)-UP(I))
158            1, M(I), FS(I)* 1000
159       C
160       C     END OF SECOND INNER LOOP
161       C     THIRD OUTPUT LOOP BEGINS
162       C
163           WRITE(8,1060)
164           DO 30  I = 1, NRUN - 1
165          30 WRITE(8,1030) I, JGSTAR(I), JPSTAR(I), RSTAR(I), SEGPAR(I)
166            1,UTCALC(I), UTTHEO(I), REP(I)
167           GOTO 70
168       C
169       C     END OF OUTER LOOP ... CONTINUE TO NEXT RUN SERIES
170       C
171          2000 CLOSE(UNIT=7)
172           CLOSE(UNIT=8)
173           CLOSE(UNIT=9)
174          1000 FORMAT(I2,6F12.3)
175          1011 FORMAT('RUN SERIES ',A3,'   THETA = ',F7.1,/)
176          1012 FORMAT(T8,'SOL FLUX',T20,'GAS FLUX',T30,'PRESS GRAD.',
177            1T44,'DP GRAV',T56,'DP FLUID',T69,'DP SOL'//)
178          1020 FORMAT(///' RUN',T9,'EPS',T20,'UP',T31,'UF',T40,'U_SUPER',T52,
179            1'UF - UP',T63,'  M',T73,'FS*1000'//)
180          1030 FORMAT(I2,7F11.4)
181          1040 FORMAT(A3)
182          1050 FORMAT(A6)
183          1060 FORMAT(///,T8,'JGSTAR',T19,'JPSTAR',T30,'RSTAR',T40,'SEGPAR',
184            1T52,'UTCALC',T63,'UTERM',T73,'REP',/)
185          1300 FORMAT(I3,5E12.4,/1X,6E12.4)
186          1400 FORMAT(5E12.4)
```

```
      STOP
      END
C
      SUBROUTINE RTMI(X,F,FCT,XLI,XRI,EPS,IEND,IER)
C     PREPARE ITERATION
      IER=0
      XL=XLI
      XR=XRI
      X=XL
      TOL=X
      F=FCT(TOL)
      IF (F) 10,160,10
   10 FL=F
      X=XR
      TOL=X
      F=FCT(TOL)
      IF (F) 20,160,20
   20 FR=F
      IF (SIGN(1.,FL)+SIGN(1.,FR)) 250,30,250
C     BASIC ASSUMPTION FL*FR LESS THAN 0 IS SATISFIED.
C     GENERATE TOLERANCE FOR FUNCTION VALUES.
   30 I=0
      TOLF=100.*EPS
C     START ITERATION LOOP
   40 I=I+1
C     START BISECTION LOOP
      DO 130 K=1,IEND
      X=.5*(XL+XR)
      TOL=X
      F=FCT(TOL)
      IF (F) 50,160,50
   50 IF (SIGN(1.,F)+SIGN(1.,FR)) 70,60,70
C     INTERCHANGE XL AND XR IN ORDER TO GET THE SAME SIGN IN F
AND FR
   60 TOL=XL
      XL=XR
      XR=TOL
      TOL=FL
      FL=FR
      FR=TOL
   70 TOL=F-FL
      A=F*TOL
      A=A+A
      IF (A-FR*(FR-FL)) 80,90,90
   80 IF (I-IEND) 170,170,90
   90 XR=X
      FR=F
C     TEST ON SATISFACTORY ACCURACY IN BISECTION LOOP
      TOL=EPS
      A=ABS(XR)
      IF (A-1.) 110,110,100
  100 TOL=TOL*A
```

```
239         110 IF (ABS(XR-XL)-TOL) 120,120,130
240         120 IF (ABS(FR-FL)-TOLF) 140,1'^  30
241         130 CONTINUE
242       C     END OF BISECTION LOOP
243       C     NO CONVERGENCE AFTER IEND ITERATION STEPS FOLLOWED BY
244       IEND
245       C     SUCCESSIVE STEPS OF BISECTION OR STEADILY INCREASING
246       FUNCTION
247       C     VALUES AT RIGHT BOUNDS. ERROR RETURN.
248             IER=1
249         140 IF (ABS(FR)-ABS(FL)) 160,160,150
250         150 X=XL
251             F=FL
252         160 RETURN
253       C     COMPUTATION OF ITERATED X-VALUE BY INVERSE PARABOLIC
254       INTERPOLATION
255         170 A=FR-F
256             DX=(X-XL)*FL*(1.+F*(A-TOL)/(A*(FR-FL)))/TOL
257             XM=X
258             FM=F
259             X=XL-DX
260             TOL=X
261             F=FCT(TOL)
262             IF (F) 180,160,180
263       C     TEST ON SATISFACTORY ACCURACY IN ITERATION LOOP
264         180 TOL=EPS
265             A=ABS(X)
266             IF (A-1.) 200,200,190
267         190 TOL=TOL*A
268         200 IF (ABS(DX)-TOL; 210,210,220
269         210 IF (ABS(F)-TOLF) 160,160,220
270       C     PREPARATION OF NEXT BISECTION LOOP
271         220 IF (SIGN(1.,F)+SIGN(1.,FL)) 240,230,240
272         230 XR=X
273             FR=F
274             GO TO 40
275         240 XL=X
276             FL=F
277             XR=XM
278             FR=FM
279             GO TO 40
280       C     END OF ITERATION LOOP
281       C     ERROR RETURN IN CASE OF WRONG INPUT DATA
282         250 IER=2
283             RETURN
284             END
285       C
286             FUNCTION FCT(X)
287             REAL K1, K2, K3, K4
288             COMMON K1, K2, K3, K4, UG, ANGLE
289             FCT = K4*X**2+ K3*X**1.5 +(K1+K2)*X - 9.81*COS(ANGLE)-K2*UG
290             RETURN
```

```
      END
C
      FUNCTION FUT(X)
      REAL K1, K2, K3, K4
      COMMON K1, K2, K3, K4, UG, ANGLE
      FUT = K4*X**2+ K3*X**1.5 +K1*X - 9.81*COS(ANGLE)
      RETURN
      END
C
       PROGRAM LIFTD2
*     THIS PROGRAM CALCULATES THEORETICAL LIFTING ENERGY
EFFICIENCIES
*     FOR SOLID PARTICLES IN A PIPE.
*
*     M - SOLIDS/GAS MASS FLOW RATIO
*     ANGLE - PIPE INCLINATION IN RADIANS
*     THETA - PIPE INCLINATION IN DEGREES
*     DP - PARTICLE SIZE (M)
*     DPM - PARTICLE SIZE (MICRONS)
*     EPS - VOIDAGE
*     ALPHA - SOLIDS HOLDUP (%)
*     T - TEMPERATURE (DEGREES C)
*     P - ABS. PRESSURE (ATM)
*     UT - TERMINAL SETTLING VELOCITY (M/S)
*     UG - ACTUAL GAS VELOCITY (M/S)
*     UGS - SUPERFICIAL GAS VELOCITY (M/S)
*     IER - ERROR CODE RETURNED IN ROOT-SOLVING SUBROUTINE RTMI
*     D - PIPE DIAMETER (M)
*     RE - PARTICLE REYNOLDS NUMBER
*     CD - DRAG COEFFICIENT
*     RED - REYNOLDS NUMBER FOR PIPE
*     F - PIPE FRICTION FACTOR
*     DPDLF - PIPE FRICTION PRESSURE GRADIENT (PA/M)
*     DPDLG - SOLIDS HOLDUP GRADIENT (PA/M)
*     DPDLSF - SOLIDS FRICTION GRADIENT (PA/M)
*     DPTOT - TOTAL PRESSURE GRADIENT (PA/M)
*     EFFNET - NET SOLIDS LIFTING EFFICIENCY (%) (GAS FRICTION
*           ENERGY DEDUCTED)
*     EFFGRO - GROSS SOLIDS LIFTING EFFICIENCY (%)
*     EFF - SINGLE PARTICLE LIFTING EFFICIENCY (%)
*
      REAL M
      CHARACTER  OFLE*7,IFLE*7,L*3
      REAL LD(250)
      OPEN(UNIT=1,FILE='TERMINAL')
   70 WRITE(1,*) 'ENTER RUN SERIES LETTER (Z TO EXIT):'
      READ(1,1040) L
      IF (L.EQ.'Z') GOTO 30
      IFLE(4:7) = '.DAT'
      IFLE(1:3) = L
      OPEN(UNIT=5,FILE=IFLE)
```

```
43            OFLE(4:7) = '.THE'
44            OFLE(1:3) = L
45            OPEN(UNIT=6,FILE=OFLE)
46            READ(5,*) THETA, INDX
47            ANGLE = THETA * ACOS(-1.0) / 180.0
48            WRITE(6,1011) L, THETA
49            WRITE(6,1012)
50            NRUN = 1
51          99 READ(5,*,END=70) GS, G, HUP, T, PUP, GRADP
52            IF (INDX.EQ.1) PUP = PUP / 98.1
53            IF (THETA.EQ.0) UT=1.34
54            IF (THETA.EQ.4) UT=1.63
55            IF (THETA.EQ.11) UT=2.26
56            IF (THETA.EQ.18) UT=2.83
57            DPM=197
58            RHOP=2600
59            D=0.03175
60            GS = GS / 1000
61            G = G / 1000
62            LD(NRUN) = GS / G
63            PUP = PUP * 98.1
64            DELP = 4.55 * GRADP / 2
65            M=LD(NRUN)
66            P=(101325+PUP)/101325
67            VISC = 1.81E-05
68            DP = DPM/1.0E06
69            RHOG = 29/22.414*273.0/(273.0 + T)*P
70            AREA=3.1415927/4*((1.25/12)*0.3048)**2
71            UG = G / RHOG / (1-HUP*0.01) / AREA
72            UP=UG-UT
73        *
74        *     TERMINAL VELOCITY CALCULATED USING RTMI & FCT
75        *
76            EFF = (1.0 - UT/UG) * COS(ANGLE)*100.0
77            ALPHA = HUP/100
78         1011 FORMAT('RUN SERIES ',A3,'   THETA = ',F7.1,/)
79         1012 FORMAT(T1,'THETA',T8,'SOL FLUX',T20,'GAS FLUX',T34,'LOAD.',
80           1T47,'EFFNET',T59,'EFFGRO',T71,'EFF %',//)
81         1040 FORMAT(A3)
82        *
83        *     COMPUTE PRESSURE GRADIENTS
84        *
85            RED = RHOG * D * UG / VISC
86            F = 0.0791 / RED**0.25
87            DPDLF = 2 * F * RHOG * UG**2 / D
88            DPDLG = ALPHA/100 * RHOP * 9.81 * COS(ANGLE)
89            FS = 0.0285 * SQRT(9.81 * D) / UP
90            DPDLSF = 2 * FS * RHOP*ALPHA/100 * UP**2 / D
91            DPTOT = GRADP
92        *
93        *     CALCULATION OF EFFICIENCIES BASED ON PRESSURE GRADIENTS
94        *
```

```
      EFFNET = 9.81*M *  RHOG * COS(ANGLE) / (DPTOT - DPDLF)*100
      EFFGRO = 9.81 * RHOG * M * COS(ANGLE) / DPTOT * 100
      WRITE(6,1000) THETA,GS*1000,G*1000,M,EFFNET,EFFGRO,EFF
 1000 FORMAT(F5.2,6F12.3)
      GOTO 99
  30  STOP
      END

      PROGRAM TRDAT
C
C     THIS PROGRAM ANALYSES THE RESULTS OF THE PNEUMATIC
TRANSPORT
C     EXPERIMENTS AND PRODUCES FILES FOR PROGRAM DATANA.
C     .
C
C     INPUT FILE OF FORM '*.DAT', OUTPUT FILE OF FORM '*.REG'
C
C     IFLE, OFLE : INPUT AND OUTPUT FILE NAMES
C     UP : PARTICLE VELOCITY
C     UF : ACTUAL FLUID VELOCITY
C     USUPER : SUPERFICIAL FLUID VELOCITY
C     ALPHA : VOLUME FRACTION OF THE SOLIDS
C     EPS : VOID FRACTION
C     D : PIPE DIAMETER
C     AREA : PIPE CROSS-SECTIONAL AREA
C     RHOF : GAS DENSITY
C     VISC : GAS VISCOSITY
C     ATM : STANDARD ATMOSPHERE IN PASCALS
C     THETA : ANGLE OF INCLINATION IN DEGREES
C     ANGLE : ANGLE OF INCLINATION IN RADIANS
C     L : CHARACTER INDICATING RUN SERIES
C     I : RUN NUMBER WITHIN SERIES
C     G : MASS FLOWRATE OF THE GAS
C     GS : SOLIDS MASS FLOWRATE
C     M : RATIO GS / G
C     T : TEMPERATURE (DEGREES CELSIUS)
C     PUP : GAUGE PRESSURE AT BOTTOM OF TEST SECTION
C     GRADP : TOTAL PRESSURE GRADIENT IN TEST SECTION
C     RE : REYNOLDS NUMBER FOR PIPE FLOW
C     FG : FRICTION FACTOR FOR GAS
C     DPDLG : PRESSURE GRADIENT DUE TO GRAVITY
C     DPDFL : PRESSURE GRADIENT DUE TO GAS FRICTION
C     DPDLS : PRESSURE GRADIENT DUE TO SOLIDS FRICTION
C     FS : FRICTION FACTOR FOR SOLIDS
C     INDX : PUP IN CM IF INDX = 0, IN PASCALS IF INDX = 1
C
      CHARACTER OFLE*7 , IFLE*7, L*3
      DIMENSION UP(50), UF(50), USUPER(50), EPS(50), FS(50)
      REAL M(50)
C
      D = 0.03175
```

```
44          AREA = D**2*ACOS(-1.0) / 4
45          RHOP = 2600.0
46          ATM = 1.013E05
47          VISC = 1.82E-05
48      C
49      C     START OF LOOP FOR DIFFERENT RUN SERIES
50      C
51        70 WRITE(6,*) 'ENTER RUN SERIES LETTER (Z TO EXIT):'
52          READ(5,1040) L
53          IF (L.EQ.'Z') GOTO 2000
54          IFLE(4:7) = '.DAT'
55          IFLE(1:3) = L
56          OFLE(4:7) = '.REG'
57          OFLE(1:3) = L
58          OPEN(UNIT=7,FILE=IFLE)
59          OPEN(UNIT=8,FILE=OFLE)
60          READ(7,*) THETA, INDX
61          WRITE(8,1000) THETA
62          ANGLE = THETA * ACOS(-1.0) / 180.0
63          I = 1
64      C
65      C     START OF FIRST LOOP FOR DIFFERENT RUNS WITHIN A SERIES
66      C
67        10 READ(7,*,END=70) GS, G, ALPHA, T, PUP, GRADP
68          IF (INDX.EQ.1) PUP = PUP / 98.1
69          GS = GS / 1000
70          G = G / 1000
71          M(I) = GS / G
72          EPS(I) = 1.0 - ALPHA/100
73          PUP = PUP * 98.1
74          RHOF = (29/22.414)*(PUP + ATM) / ATM* 273 /(273 + T)
75          UP(I) = GS / RHOP / AREA / (1.0 -EPS(I))
76          UF(I) = G / RHOF / EPS(I) / AREA
77          USUPER(I) = G / RHOF / AREA
78          RE = D * UF(I) * RHOF / VISC
79          FG = 0.0791 / RE**0.25
80          DPDLG = RHOP*ALPHA / 100 * 9.81 * COS(ANGLE)
81          DPLFL = 2 * FG * RHOF * UF(I)**2 / D
82          DPDLS = GRADP - DPDLG  - DPLFL
83          FS(I) = DPDLS * D / 2 / RHOP/ ALPHA / UP(I)**2 *100
84          WRITE(8,1000) GS*1000,G*1000,GRADP,DPDLG,DPLFL,DPDLS
85          WRITE(8,1030) EPS(I), UP(I), UF(I), USUPER(I),RHOF
86         1, M(I), FS(I)* 1000
87          I = I + 1
88      C
89          GOTO 10
90      C
91      C     END OF INNER LOOP ... CONTINUE TO NEXT RUN SERIES
92      C
93       2000 CLOSE(UNIT=7)
94          CLOSE(UNIT=8)
9        1000 FORMAT(6F10.3)
```

```
 1030 FORMAT(7F10.4)
 1040 FORMAT(A3)
      STOP
      END
```

APPENDIX E : DERIVATION OF LIFTING EFFICIENCY

APPENDIX E : LIFTING EFFICIENCY DERIVATION

The basic definition of lifting efficiency can be defined by the expression given by equation (E1).

$$\eta = \frac{\textit{Gain of Potential Energy of Solids } (\Delta U_s)}{\textit{Consumption of Energy by Gas } (\Delta U_g)} \times 100\% \qquad \textbf{(E1)}$$

The gain of potential energy of solids (ΔU_s) is given by equation (E2).

$$\Delta U_s = W_{sf}\, g \cos\theta \qquad \textbf{(E2)}$$

and the solids flux, W_{sf}, is given by equation (E3a).

$$W_{sf} = m^* \rho_g U_g A \qquad \textbf{(E3a)}$$

where m^* is the solids loading (kg solid / kg gas).

Also, the energy consumption of the gas is given by equation (E4a).

$$\Delta U_g = A U_g \left(-\frac{\partial P}{\partial z} \right) \qquad \textbf{(E4a)}$$

Noting that,

$$A \alpha U_p \rho_p = W_{sf} = m^* W_g = m^* A \rho_g U_g \qquad \textbf{(E4b)}$$

The 'gross' lifting efficiency is obtained from substituting equations (E2) , (E4a) and (E4b) into (E1) to obtain equation (E5a).

$$\eta = \frac{m^* \rho_g U_g A g \cos\theta}{A U_g \left(-\frac{\partial P}{\partial z}\right)} \qquad \text{(E5a)}$$

Simplifying equation (E5b) is obtained.

$$\eta_{gross} = \frac{m^* \rho_g g \cos\theta}{\left(-\frac{\partial p}{\partial z}\right)} \qquad \text{(E5b)}$$

If the gross lifting efficiency η_{gross} is corrected for the gas-wall frictional pressure gradient in equation (E5b), an expression for the net lifting efficiency, η_{net}, is given by equation (E5c).

$$\eta_{net} = \frac{m^* \rho_g g \cos\theta}{\left(-\frac{\partial P}{\partial z}\right)_{tot.} - \left(-\frac{\partial P}{\partial z}\right)_{wall}} \qquad \text{(E5c)}$$

Assuming that the solids holdup is the primary component of the pressure drop, then the total pressure gradient term is given by equation (E6).

$$\left(-\frac{\partial P}{\partial z}\right) = \alpha \rho_p g \cos\theta \qquad \text{(E6)}$$

An expression for α is given by equation (E7).

$$\alpha = \frac{m^* \rho_g U_g}{U_p \rho_p} \qquad \text{(E7)}$$

Substituting (E7) into (E6) for α, equation (E8a) is obtained for the total pressure gradient term.

$$\left(-\frac{\partial P}{\partial z}\right) = \left(\frac{m^* \rho_g U_g}{U_p \rho_p}\right) \rho_p \, g\cos\theta \qquad \text{(E8a)}$$

Simplifying we get equation (E8b).

$$\left(-\frac{\partial P}{\partial z}\right) = \frac{m^* \rho_g \, U_g \, g\cos\theta}{U_p} \qquad \text{(E8b)}$$

Substituting equation (E8b) into (E5b) an expression for the gross lifting efficiency is given by equation (E9).

$$\eta_{gross} = \frac{(m^* \rho_g g\cos\theta) \, U_p}{m^* \rho_g U_g \, g\cos\theta} = \frac{U_p}{U_g} \qquad \text{(E9)}$$

Since the theoretical particle velocity (for a single particle in dilute-phase flow) is given by the difference of the terminal settling velocity from the gas velocity (equation E10),

$$U_p = U_g - U_t \qquad \text{(E10)}$$

then equation (E9) can equivalently be written as equation (E11).

$$\eta_{gross\%} = \left(\frac{U_g - U_t}{U_g}\right) \times 100\% = \left(1 - \frac{U_t}{U_g}\right) \times 100\% \qquad \text{(E11)}$$

Then the (particle) lifting efficiency expressed as a per cent is given by equation (E12).

$$\eta_p\,(\%) = 100\left(1 - \frac{U_t}{U_g}\right)\cos\theta \qquad \text{(E12)}$$

The particle lifting efficiency from equation (E12) is compared with the actual (experimental) lifting efficiencies (gross and net) from equations (E5b) and (E5c) respectively using observed values of total and gas-wall pressure gradient terms.

Alternatively, the particle lifting efficiency can be rederived as follows. For a single particle streaming through the center of the pipe (and assuming no gas-wall frictional effects) the pressure drop can be written by equation (E13).

$$\Delta P = \frac{m_p\, g\cos\theta}{A} \qquad \text{(E13)}$$

The power of the gas required to move the particle is given by equation

$$Power = \frac{\Delta P\, M_g}{\rho_g} \qquad \text{(E14)}$$

(E14), noting that the mass of the gas is M_g.

The work done by the gas is given by equation (E15) where t_p is the flight time of the particle.

$$Work = \left(\frac{\Delta P}{L}\right)\left(\frac{M_g}{\rho_g}\right) t_p = \left(\frac{\Delta P}{U_p}\right)\left(\frac{M_g}{\rho_g}\right) = \frac{\Delta P U_g \rho_g A}{U_p \rho_g} = \frac{\Delta P U_g A}{U_p} \qquad \text{(E15)}$$

Substituting equation (E13) for pressure drop into equation (E15), equation (E16) is obtained for work done by the gas:

$$\frac{Work_{[gas]}}{L} = \frac{m_p\, g \cos(\theta)\, U_g\, A}{A\, U_p} = \frac{m_p\, g \cos(\theta)\, U_g}{U_p} \qquad \text{(E16)}$$

The gain of potential energy of the particle, ΔU_s , is $m_p g\cos(\theta)$, and the work done by the gas, ΔU_g , in getting it there is $m_p g\cos(\theta)/U_p$. Hence the efficiency is given by equation (E17).

$$\eta_p = \frac{m_p\,(g\cos\theta)}{\left(\frac{m_p\,(g\cos\theta)\,U_g}{U_p}\right)} = \frac{U_p}{U_g} = \frac{U_g - U_t}{U_g} \qquad \text{(E17)}$$

which is equivalent to equation (E12).

APPENDIX F: LIFTING EFFICIENCY CORRELATIONS

APPENDIX F1: CORRELATION OF NET LIFTING EFFICIENCY (THIS THESIS) WITH EXPERIMENTAL PARAMETERS FOR SAND DATA

APPENDIX F2: CORRELATION OF NET LIFTING EFFICIENCY (THIS THESIS) WITH EXPERIMENTAL PARAMETERS FOR GLASS DATA

APPENDIX F3: CORRELATION OF NET LIFTING EFFICIENCY WITH EXPERIMENTAL PARAMETERS FOR ALL THESIS DATA

APPENDIX F4 : CORRELATION OF DILUTE PHASE GROSS LIFTING EFFICIENCY (ZALTASH, 1987) WITH EXPERIMENTAL PARAMETERS

APPENDIX F5 : CORRELATION OF DILUTE PHASE ENERGY DISSIPATED (ZALTASH, 1987) WITH EXPERIMENTAL PARAMETERS

APPENDIX F1: CORRELATION OF NET LIFTING EFFICIENCY (THIS THESIS) WITH EXPERIMENTAL PARAMETERS FOR SAND DATA

----------Correlation Matrix----------

Date/Time 09-22-1993 09:22:18
Data Base Name C:\ncss\efsand
Description Copy of data in spreadsheet file: C:\123r3\efsand.wk1

Pearson Correlations

	α	Θ	W_s	U_g	m^*	U_p	U_{slip}	η_p
α	1.00000	0.09925	0.24643	-0.37209	0.52975	-0.59583	0.51588	-0.47339
Θ	0.09925	1.00000	-0.19769	0.03864	-0.24850	0.00926	-0.09275	0.09568
W_s	0.24643	-0.19769	1.00000	0.31677	0.77958	0.07350	0.12208	0.33014
U_g	-0.37209	0.03864	0.31677	1.00000	-0.29139	0.49539	0.17166	0.94402
m^*	0.52975	-0.24850	0.77958	-0.29139	1.00000	-0.25503	0.07307	-0.29262
U_p	-0.59583	0.00926	0.07350	0.49539	-0.25503	1.00000	-0.70831	0.56511
U_{slip}	0.51588	-0.09275	0.12208	0.17166	0.07307	-0.70831	1.00000	0.02164
η_p	-0.47339	0.09568	0.33014	0.94402	-0.29262	0.56511	0.02164	1.00000
η_{net}	-0.34519	-0.75017	0.26997	0.03175	0.25196	0.18533	-0.20912	0.05962
E_{diss}	0.23936	0.75075	-0.18629	0.18707	-0.31691	-0.04592	0.20662	0.17593

Pearson Correlations

	η_{net}	E_{diss}
α	-0.34519	0.23936
Θ	-0.75017	0.75075
W_s	0.26997	-0.18629
U_g	0.03175	0.18707
m^*	0.25196	-0.31691
U_p	0.18533	-0.04592
U_{slip}	-0.20912	0.20662
η_p	0.05962	0.17593
η_{net}	1.00000	-0.97032
$E_{diss.}$	-0.97032	1.00000

APPENDIX F2: CORRELATION OF NET LIFTING EFFICIENCY (THIS THESIS) WITH EXPERIMENTAL PARAMETERS FOR GLASS DATA

----------Correlation Matrix----------
Date/Time 09-22-1993 09:24:05
Data Base Name C:\ncss\effglass
Description Copy of data in spreadsheet file: C:\123r3\effglass.wk1

Pearson Correlations

	α	Θ	W_s	U_g	m^*	U_p	U_{slip}	η_p
α	1.00000	-0.26072	0.30281	-0.39896	0.55348	-0.50780	0.24715	-0.39352
Θ	-0.26072	1.00000	-0.06487	0.07938	-0.12492	0.25650	-0.25411	0.14231
W_s	0.30281	-0.06487	1.00000	0.48858	0.89360	0.19901	0.25475	0.54132
U_g	-0.39896	0.07938	0.48858	1.00000	0.09696	0.66583	0.18066	0.96241
m^*	0.55348	-0.12492	0.89360	0.09696	1.00000	-0.05404	0.17385	0.19681
U_p	-0.50780	0.25650	0.19901	0.66583	-0.05404	1.00000	-0.61354	0.64968
U_{slip}	0.24715	-0.25411	0.25475	0.18066	0.17385	-0.61354	1.00000	0.16207
η_p	-0.39352	0.14231	0.54132	0.96241	0.19681	0.64968	0.16207	1.00000
η_{net}	-0.36057	0.06378	0.34188	0.28436	0.26828	0.36850	-0.18472	0.37840
E_{diss}	0.27491	-0.03170	-0.19980	-0.02471	-0.23134	-0.19520	0.23059	-0.11971

Pearson Correlations

	η_{net}	$E_{diss.}$
α	-0.36057	0.27491
Θ	0.06378	-0.03170
W_s	0.34188	-0.19980
U_g	0.28436	-0.02471
m^*	0.26828	-0.23134
U_p	0.36850	-0.19520
U_{slip}	-0.18472	0.23059
η_p	0.37840	-0.11971
η_{net}	1.00000	-0.96082
$E_{diss.}$	-0.96082	1.00000

APPENDIX F3: CORRELATION OF NET LIFTING EFFICIENCY WITH EXPERIMENTAL PARAMETERS FOR ALL THESIS DATA

----------Correlation Matrix----------
Date/Time 09-22-1993 09:20:19
Data Base Name C:\ncss\efftot
Description Copy of data in spreadsheet file: C:\123r3\efftot.wk1

Pearson Correlations

	d_p	α	Θ	W_s	U_g	m^*	U_p	U_{slip}
d_p	1.00000	0.41522	-0.19301	-0.19001	0.28831	-0.41295	-0.39935	0.64285
α	0.41522	1.00000	-0.10583	0.15925	-0.20544	0.24422	-0.60292	0.53155
Θ	-0.19301	-0.10583	1.00000	-0.11754	-0.01097	-0.12006	0.12946	-0.23884
W_s	-0.19001	0.15925	-0.11754	1.00000	0.29534	0.79426	0.16946	0.00224
U_g	0.28831	-0.20544	-0.01097	0.29534	1.00000	-0.28497	0.35273	0.31588
m^*	-0.41295	0.24422	-0.12006	0.79426	-0.28497	1.00000	-0.01433	-0.20059
U_p	-0.39935	-0.60292	0.12946	0.16946	0.35273	-0.01433	1.00000	-0.74304
U_{slip}	0.64285	0.53155	-0.23884	0.00224	0.31588	-0.20059	-0.74304	1.00000
η_p	-0.31141	-0.56156	0.20372	0.39539	0.28651	0.27765	0.61948	-0.48601
η_{net}	-0.60247	-0.49374	-0.32662	0.34386	-0.09244	0.43565	0.40537	-0.50813
E_{diss}	0.37043	0.36514	0.41181	-0.24508	0.20729	-0.39656	-0.21979	0.38216

Pearson Correlations

	η_p	η_{net}	E_{diss}
d_p	-0.81141	-0.60247	0.37043
α	-0.56156	-0.49374	0.36514
Θ	0.20372	-0.32662	0.41181
W_s	0.39539	0.34386	-0.24508
U_g	0.28651	-0.09244	0.20729
m^*	0.27765	0.43565	-0.39656
U_p	0.61948	0.40537	-0.21979
U_{slip}	-0.48601	-0.50813	0.38216
η_p	1.00000	0.57374	-0.27854
η_{net}	0.57374	1.00000	-0.93604
E_{diss}	-0.27854	-0.93604	1.00000

APPENDIX F4 : CORRELATION OF DILUTE PHASE GROSS LIFTING EFFICIENCY (ZALTASH, 1987) WITH EXPERIMENTAL PARAMETERS

Date/Time 01-10-1993 14:50:49
Data Base Name C:\ncss\zaldata
Description Copy of data in spreadsheet file: C:\zaltash\zaleff.wk1

Pearson Correlations $\eta_{gross,L}$

	Θ	d_p (μm)	d_{tube} (m)	ρ_p	U_g	U_{PL}	W_{SL}	$\eta_{gross,L}$
Θ	1.00000	-0.00631	0.50909	0.00415	0.14105	0.15239	0.12559	-0.30808
d_p (μm)	-0.00631	1.00000	-0.01279	-0.11287	0.02591	-0.26792	-0.01164	-0.13109
d_{tube} (m)	0.50909	-0.01279	1.00000	-0.00686	0.46057	0.42904	0.71878	-0.04434
ρ_p	0.00415	-0.11287	-0.00686	1.00000	0.03477	-0.03038	-0.09181	-0.08869
U_g	0.14105	0.02591	0.46057	0.03477	1.00000	0.88310	0.33906	-0.36925
U_{PL}	0.15239	-0.26792	0.42904	-0.03038	0.88310	1.00000	0.29984	-0.31546
W_{SL}	0.12559	-0.01164	0.71878	-0.09181	0.33906	0.29984	1.00000	0.15468
$\eta_{gross,L}$	-0.30808	-0.13109	-0.04434	-0.08869	-0.36925	-0.31546	0.15468	1.00000

Dependent Variables: $\eta_{gross,L}$

No.	R-Squared	Variables
1	0.13634332509	U_g
2	0.22485077320	U_g ,W_{SL}
3	0.31932588591	Θ,U_g ,W_{SL}
4	0.33863135215	Θ,U_g ,W_{SL} ,d_p (μm)
5	0.34212582451	Θ,U_g ,W_{SL} ,d_p (μm),ρ_p
6	0.34437566426	Θ,U_g ,W_{SL} ,d_p (μm),ρ_p ,d_{tube} (m)
7	0.34454939759	Θ,U_g ,U_{PL} ,W_{SL} ,d_p (μm),ρ_p ,d_{tube} (m)

Pearson Correlations $\eta_{gross,U}$

	Θ	d_p (μm)	d_{tube} (m)	ρ_p	U_g	$U_{P,U}$	$W_{S,U}$	$\eta_{gross,U}$
Θ	1.00000	-0.00631	0.50909	0.00415	0.14105	0.10291	0.76502	0.65291
d_p (μm)	-0.00631	1.00000	-0.01279	-0.11287	0.02591	-0.26468	0.05593	-0.16099
d_{tube} (m)	0.50909	-0.01279	1.00000	-0.00686	0.46057	0.40769	0.54358	0.27489
ρ_p	0.00415	-0.11287	-0.00686	1.00000	0.03477	0.00136	-0.07527	-0.14484
U_g	0.14105	0.02591	0.46057	0.03477	1.00000	0.88266	0.24941	-0.15612
$U_{P,U}$	0.10291	-0.26468	0.40769	0.00136	0.88266	1.00000	0.13367	-0.16507
$W_{S,U}$	0.76502	0.05593	0.54358	-0.07527	0.24941	0.13367	1.00000	0.70302
$\eta_{gross,U}$	0.65291	-0.16099	0.27489	-0.14484	-0.15612	-0.16507	0.70302	1.00000

Variable Selection Report One $\eta_{gross,U}$

Dependent Variables: $\eta_{gross,U}$

No.	R-Squared	Variables
1	0.49423865728	$W_{S,U}$
2	0.61139114585	U_g ,$W_{S,U}$
3	0.64996812020	U_g ,$W_{S,U}$,d_p (µm)
4	0.66885537762	Θ,U_g ,$W_{S,U}$,d_p (µm)
5	0.68594189842	Θ,$U_{P,U}$,$W_{S,U}$,d_p (µm),ρ_p
6	0.68764621049	Θ,U_g ,$U_{P,U}$,$W_{S,U}$,d_p (µm),ρ_p
7	0.68844923086	Θ,U_g ,$U_{P,U}$,$W_{S,U}$,d_p (µm),ρ_p ,d_{tube} (m)

APPENDIX F5 : CORRELATION OF DILUTE PHASE ENERGY DISSIPATED (ZALTASH, 1987) WITH EXPERIMENTAL PARAMETERS

Date/Time 01-10-1993 19:15:40
Data Base Name C:\ncss\zaldata
Description Copy of data in spreadsheet file: C:\zaltash\zaleff.wk1

Pearson Correlations $E_{Diss\%}$

	Θ	d_p (µm)	d_{tube} (m)	ρ_p	U_g	U_{PL}	W_{SL}	$U_{SLIP,L}$
Θ	1.00000	-0.00631	0.50909	0.00415	0.14105	0.15239	0.12559	-0.03782
d_p (µm)	-0.00631	1.00000	-0.01279	-0.11287	0.02591	-0.26792	-0.01164	0.61681
d_{tube} (m)	0.50909	-0.01279	1.00000	-0.00686	0.46057	0.42904	0.71878	0.02101
ρ_p	0.00415	-0.11287	-0.00686	1.00000	0.03477	-0.03038	-0.09181	0.13391
U_g	0.14105	0.02591	0.46057	0.03477	1.00000	0.88310	0.33906	0.14773
U_{PL}	0.15239	-0.26792	0.42904	-0.03038	0.88310	1.00000	0.29984	-0.33358
W_{SL}	0.12559	-0.01164	0.71878	-0.09181	0.33906	0.29984	1.00000	0.05468
$U_{SLIP,L}$	-0.03782	0.61681	0.02101	0.13391	0.14773	-0.33358	0.05468	1.00000
$E_{Diss\%}$	0.05245	-0.34990	0.29600	-0.07403	0.35533	0.49387	-0.05921	-0.33172

Variable Selection Report One

Dependent Variables: $E_{Diss\%}$

No.	R-Squared	Variables
1	0.24390782639	U_{PL}
2	0.29112351984	U_{PL} ,W_{SL}
3	0.38389100800	U_{PL} ,W_{SL} ,d_{tube} (m)
4	0.43946045871	U_{PL} ,W_{SL} ,d_p (µm),d_{tube} (m)
5	0.45803819717	U_{PL} ,W_{SL} ,d_p (µm),ρ_p ,d_{tube} (m)
6	0.46923935701	Θ,U_{PL} ,W_{SL} ,d_p (µm),ρ_p ,d_{tube} (m)
7	0.47206486159	Θ,U_g ,U_{PL} ,W_{SL} ,d_p (µm),ρ_p ,d_{tube} (m)

Date/Time 01-10-1993 19:16:45

Data Base Name C:\ncss\zaldata
Description Copy of data in spreadsheet file: C:\zaltash\zaleff.wk1

Pearson Correlations E_{DISSu}

	Θ	d_p (μm)	d_{tube} (m)	ρ_p	U_g	$U_{P,U}$	$W_{S,U}$	$U_{SLIP,U}$
Θ	1.00000	-0.00631	0.50909	0.00415	0.14105	0.10291	0.76502	0.07403
d_p (μm)	-0.00631	1.00000	-0.01279	-0.11287	0.02591	-0.26468	0.05593	0.60400
d_{tube} (m)	0.50909	-0.01279	1.00000	-0.00686	0.46057	0.40769	0.54358	0.09255
ρ_p	0.00415	-0.11287	-0.00686	1.00000	0.03477	0.00136	-0.07527	0.06823
U_g	0.14105	0.02591	0.46057	0.03477	1.00000	0.88266	0.24941	0.20618
$U_{P,U}$	0.10291	-0.26468	0.40769	0.00136	0.88266	1.00000	0.13367	-0.27792
$W_{S,U}$	0.76502	0.05593	0.54358	-0.07527	0.24941	0.13367	1.00000	0.23147
$U_{SLIP,U}$	0.07403	0.60400	0.09255	0.06823	0.20618	-0.27792	0.23147	1.00000
EDISS.,	-0.03939	-0.00243	-0.02030	0.01266	0.00794	0.00741	-0.05175	0.00081

Dependent Variables: EDISS.,U

No.	R-Squared	Variables
1	0.02344638820	U_g
2	0.03467928948	Θ,U_g
3	0.04491952156	Θ,U_g ,U_{PL}
4	0.05382838899	Θ,U_g ,U_{PL} ,d_{tube} (m)
5	0.05702786003	Θ,U_g ,U_{PL} ,W_{SL} ,d_{tube} (m)
6	0.05878098957	Θ,U_g ,U_{PL} ,W_{SL} ,d_p (μm),d_{tube} (m)
7	0.05901659952	Θ,U_g ,U_{PL} ,W_{SL} ,d_p (μm),ρ_p ,d_{tube} (m)

APPENDIX G: CORRELATIONS OF PRESSURE GRADIENT AND FRICTION FACTOR FOR SAND AND GLASS

APPENDIX G1 : CORRELATION OF PRESSURE GRADIENT FOR SAND

APPENDIX G2 : CORRELATION OF FRICTION FACTOR FOR SAND

APPENDIX G3 : CORRELATION OF PRESSURE GRADIENT FOR GLASS BEADS

APPENDIX G4 : CORRELATION OF FRICTION FACTOR FOR GLASS BEADS

APPENDIX G5 : CORRELATION OF DILUTE PHASE PRESSURE GRADIENT (ZALTASH, 1987) WITH EXPERIMENTAL PARAMETERS

APPENDIX G1 : CORRELATION OF PRESSURE GRADIENT FOR SAND

Date/Time 06-14-1992 11:16:35
Data Base Name C:\ncss\sandrev
Description Backup of sandm created 05-29-1992

Correlations

	α	Θ	W_s	U_ξ	m^*	$\Delta P/L$
α	1.0000	0.1002	0.2432	-0.3716	0.5296	0.8384
Θ	0.1002	1.0000	-0.2014	0.0316	-0.2481	0.2709
W_s	0.2432	-0.2014	1.0000	0.3251	0.7759	0.4342
U_ξ	-0.3716	0.0316	0.3251	1.0000	-0.2891	-0.3716
m^*	0.5296	-0.2481	0.7759	-0.2891	1.0000	0.6922
$\Delta P/L$	0.8384	0.2709	0.4342	-0.3716	0.6922	1.0000

----------Multiple Regression----------
Date/Time 06-14-1992 11:16:35
Data Base Name C:\ncss\sandrev
Description Backup of sandm created 05-29-1992

Multiple Regression Report

Dependent Variable: $\Delta P/L$

Independent Variable	Parameter Estimate	Stndized Estimate	Standard Error	t-value (b=0)	Prob. Level	Seq. R-Sqr	Simple R-Sqr
Intercept	114.2049	0.0000	34.4488	3.32	0.0009		
α	13442.32	0.5475	590.7644	22.75	0.0000	0.7029	0.7029
Θ	8.825147	0.3312	.5341252	16.52	0.0000	0.7381	0.0734
W_s	.7507603	0.2193	.2469623	3.04	0.0024	0.8219	0.1885
U_ξ	-14.24133	-0.1735	3.836938	-3.71	0.0002	0.8870	0.1381
m^*	.806364	0.2641	2.216955	3.52	0.0004	0.8912	0.4791

Analysis of Variance Report

Dependent Variable: $\Delta P/L$

Source	df	Sums of Squares (Sequential)	Mean Square	F-Ratio	Prob. Level
Constant	1	6.23455E+07	6.23455E+07		
Model	5	9957975	1991595	520.92	0.000
Error	318	1215778	3823.201		
Total	323	1.117375E+07	34593.66		

Root Mean Square Error 61.83204
Mean of Dependent Variable 438.6621
Coefficient of Variation .140956

R Squared 0.8912
Adjusted R Squared 0.8895

Variable Selection Report

Dependent Variables: ΔP/L

No.	R-Squared	Variables
1	0.70286	α
2	0.78844	α, m^*
3	0.88630	α, Θ, m^*
4	0.88803	α, Θ, U_g, m^*
5	0.89119	$\alpha, \Theta, W_s, U_g, m^*$

APPENDIX G2 : CORRELATION OF FRICTION FACTOR FOR SAND

Date/Time 06-14-1992 11:13:47
Data Base Name C:\ncss\sandrev
Description Backup of sandm created 05-29-1992

Correlations

	α	Θ	W_s	U_g	m^*	f_s
α	1.0000	0.1002	0.2432	-0.3716	0.5296	-0.3892
Θ	0.1002	1.0000	-0.2014	0.0316	-0.2481	0.0123
W_s	0.2432	-0.2014	1.0000	0.3251	0.7759	0.0398
U_g	-0.3716	0.0316	0.3251	1.0000	-0.2891	-0.0842
m^*	0.5296	-0.2481	0.7759	-0.2891	1.0000	0.0758
f_s	-0.3892	0.0123	0.0398	-0.0842	0.0758	1.0000

----------MultipleRegression----------

Date/Time 06-14-1992 11:13:47
Data Base Name C:\ncss\sandrev
Description Backup of sandm created 05-29-1992

Multiple Regression Report

Dependent Variable: f_s

Independent Variable	Parameter Estimate	Stndized Estimate	Standard Error	t-value (b=0)	Prob. Level	Seq. R-Sqr	Simple R-Sqr
Intercept	.3452E-02	0.0000	.4172E-02	0.83	0.4079		
α	-.9022834	-0.7453	.7154E-01	-12.61	0.0000	0.1515	0.1515
Θ	.2757E-03	0.2099	.6468E-04	4.26	0.0000	0.1542	0.0002
W_s	-.301E-04	-0.1783	.2991E-04	-1.01	0.3142	0.1782	0.0016
U_g	-.525E-03	-0.1296	.4646E-03	-1.13	0.2588	0.3201	0.0071
m^*	.9088E-03	0.6235	.2685E-03	3.39	0.0007	0.3438	0.0057

Analysis of Variance Report

Dependent Variable: f_s

Source	df	Sums of Squares (Sequential)	Mean Square	F-Ratio	Prob. Level
Constant	1	2.577391E-04	2.577391E-04		
Model	5	9.339858E-03	1.867972E-03	33.32	0.000
Error	318	1.782753E-02	5.606142E-05		
Total	323	2.716739E-02	8.410956E-05		

Root Mean Square Error 7.487418E-03
Mean of Dependent Variable 8.919031E-04
Coefficient of Variation 8.394878

R Squared 0.3438
Adjusted R Squared 0.3335

Variable Selection Report

Dependent Variables: f_s

No.	R-Squared	Variables
1	0.15151	α
2	0.26203	α, m^*
3	0.30572	α, U_g, m^*
4	0.34170	α, Θ, U_g, m^*
5	0.34379	$\alpha, \Theta, W_s, U_g, m^*$

APPENDIX G3 : CORRELATION OF PRESSURE GRADIENT FOR GLASS BEADS

Date/Time 06-14-1992 11:17:13
Data Base Name C:\ncss\glrev
Description Backup of glassm created 05-29-1992

Correlations

	α	Θ	W_s	U_g	m^*	$\Delta P/L$
α	1.0000	-0.2226	0.2970	-0.4058	0.5459	0.9593
Θ	-0.2226	1.0000	-0.0502	0.0938	-0.0996	-0.1475
W_s	0.2970	-0.0502	1.0000	0.4932	0.8938	0.4269
U_g	-0.4058	0.0938	0.4932	1.0000	0.1008	-0.2650
m^*	0.5459	-0.0996	0.8938	0.1008	1.0000	0.6400
$\Delta P/L$	0.9593	-0.1475	0.4269	-0.2650	0.6400	1.0000

----------MultipleRegression----------

Date/Time 06-14-1992 11:17:14
Data Base Name C:\ncss\glrev
Description Backup of glassm created 05-29-1992

Multiple Regression Report

Dependent Variable: ΔP/L

Independent Variable	Parameter Estimate	Stndized Estimate	Standard Error	t-value (b=0)	Prob. Level	Seq. R-Sqr	Simple R-Sqr
Intercept	-162.6985	0.0000	48.64713	-3.34	0.0011		
α	18705.17	0.9513	544.2591	34.37	0.0000	0.9202	0.9202
Θ	341177	0.0655	.9963402	3.35	0.0010	0.9248	0.0218
W_s	-.8581723	-0.2069	.4109884	-2.09	0.0387	0.9466	0.1822
U_g	20.311	0.1874	5.001662	4.06	0.0001	0.9486	0.0702
m^*	7.660201	0.2932	2.312939	3.31	0.0012	0.9526	0.4096

Analysis of Variance Report

Dependent Variable: ΔP/L

Source	df	Sum of Squares (Sequential)	Mean Square	F-Ratio	Prob. Level
Constant	1	3.591578E+07	3.591578E+07		
Model	5	8793168	1758634	526.41	0.000
Error	131	437643.3	3340.789		
Total	136	9230812	67873.62		

Root Mean Square Error 57.79955
Mean of Dependent Variable 512.0146
Coefficient of Variation .1128865

R Squared 0.9526
Adjusted R Squared 0.9508

Variable Selection Report

Dependent Variables: ΔP/L

No.	R-Squared	Variables
1	0.92025	α
2	0.94234	α, W_s
3	0.94659	α, Θ, W_s
4	0.95101	α, Θ, U_g, m^*
5	0.95259	α, Θ, W_s, U_g, m^*

APPENDIX G4 : CORRELATION OF FRICTION FACTOR (f_s) FOR GLASS BEADS

Date/Time 06-14-1992 11:17:41
Data Base Name C:\ncss\glrev
Description Backup of glassm created 05-29-1992

Correlations

	α	Θ	$\Delta P/L$	U_g	m^*	f_s
α	1.0000	-0.2226	0.2970	-0.4058	0.5459	-0.2010
Θ	-0.2226	1.0000	-0.0502	0.0938	-0.0996	0.1178
$\Delta P/L$	0.2970	-0.0502	1.0000	0.4932	0.8938	0.2914
U_g	-0.4058	0.0938	0.4932	1.0000	0.1008	0.2804
m^*	0.5459	-0.0996	0.8938	0.1008	1.0000	0.2719
f_s	-0.2010	0.1178	0.2914	0.2804	0.2719	1.0000

----------Multiple Regression----------
Date/Time 06-14-1992 11:17:41
Data Base Name C:\ncss\glrev
Description Backup of glassm created 05-29-1992

Multiple Regression Report
Dependent Variable: f_s

Independent Variable	Parameter Estimate	Stndized Estimate	Standard Error	t-value (b=0)	Prob. Level	Seq. R-Sqr	Simple R-Sqr
Intercept	-.8590251	0.0000	.192212	-4.47	0.0000		
α	-9.788825	-0.4711	2.150448	-4.55	0.0000	0.0404	0.0404
Θ	.3118E-02	0.0578	.3937E-02	0.79	0.4297	0.0460	0.0139
$\Delta P/L$	-.664E-02	-1.5155	.1624E-02	-4.09	0.0001	0.1804	0.0849
U_g	.7413E-01	0.6473	.1976E-01	3.75	0.0003	0.1836	0.0786
m^*	.5037E-01	1.8242	.9139E-02	5.51	0.0000	0.3373	0.073

Analysis of Variance Report

Dependent Variable: f_s

Source	df	Sums of Squares (Sequential)	Mean Square	F-Ratio	Prob. Level
Constant	1	.5990145	.5990145		
Model	5	3.477296	.6954592	13.33	0.000
Error	131	6.832299	5.215496E-02		
Total	136	10.3096	7.580584E-02		

Root Mean Square Error .2283746
Mean of Dependent Variable -6.612389E-02
Coefficient of Variation -3.453738

R Squared 0.3373
Adjusted R Squared 0.31

Variable Selection Report

Dependent Variables: f_s

No.	R-Squared	Variables
1	0.08494	W_s
2	0.24786	α, m^*
3	0.26244	α, W_s, m^*
4	0.33411	α, W_s, U_g, m^*

APPENDIX G5 : CORRELATION OF DILUTE PHASE PRESSURE GRADIENT (ZALTASH, 1987) WITH EXPERIMENTAL PARAMETERS

----------Correlation Matrix----------

Date/Time 01-10-1993 15:50:47
Data Base Name C:\ncss\zaldata
Description Copy of data in spreadsheet file: C:\zaltash\zaleff.wk1

Pearson Correlations

	Θ	d_p (μm)	d_{tube} (m)	ρ_p	U_g	U_{PL}	W_{SL}	$U_{SLIP,L}$
Θ	1.00000	-0.00631	0.50909	0.00415	0.14105	0.15239	0.12559	-0.03782
d_p (μm)	-0.00631	1.00000	-0.01279	-0.11287	0.02591	-0.26792	-0.01164	0.61681
d_{tube} (m)	0.50909	-0.01279	1.00000	-0.00686	0.46057	0.42904	0.71878	0.02101
ρ_p	0.00415	-0.11287	-0.00686	1.00000	0.03477	-0.03038	-0.09181	0.13391
U_g	0.14105	0.02591	0.46057	0.03477	1.00000	0.88310	0.33906	0.14773
U_{PL}	0.15239	-0.26792	0.42904	-0.03038	0.88310	1.00000	0.29984	-0.33358
W_{SL}	0.12559	-0.01164	0.71878	-0.09181	0.33906	0.29984	1.00000	0.05468
$U_{SLIP,}$	-0.03782	0.61681	0.02101	0.13391	0.14773	-0.33358	0.05468	1.00000
$\Delta P_{S,L}$	-0.09041	0.24455	-0.20946	0.08584	0.36646	0.16743	0.12922	0.39835

Variable Selection Report One

Dependent Variables: $\Delta P_{S,L}$

No.	R-Squared	Variables
1	0.13429349915	U_g
2	0.32707180074	U_g ,d_{tube} (m)
3	0.49324312398	U_g ,W_{SL} ,d_{tube} (m)
4	0.57158185000	U_g ,U_{PL} ,W_{SL} ,d_{tube} (m)
5	0.58625086213	Θ,U_g ,U_{PL} ,W_{SL} ,d_{tube} (m)
6	0.59470711269	Θ,U_g ,U_{PL} ,W_{SL} ,d_p (μm),d_{tube} (m)
7	0.60509326906	Θ,U_g ,U_{PL} ,W_{SL} ,d_p (μm),ρ_p ,d_{tube} (m)

Pearson Correlations

	Θ	d_p (μm)	d_{tube} (m)	ρ_p	U_g	$U_{P,U}$	$W_{S,U}$	$U_{SLIP,U}$
Θ	1.00000	-0.00631	0.50909	0.00415	0.14105	0.10291	0.76502	0.07403
d_p (μm)	-0.00631	1.00000	-0.01279	-0.11287	0.02591	-0.26468	0.05593	0.60400
d_{tube} (m)	0.50909	-0.01279	1.00000	-0.00686	0.46057	0.40769	0.54358	0.09255
ρ_p	0.00415	-0.11287	-0.00686	1.00000	0.03477	0.00136	-0.07527	0.06823
U_g	0.14105	0.02591	0.46057	0.03477	1.00000	0.88266	0.24941	0.20618
$U_{P,U}$	0.10291	-0.26468	0.40769	0.00136	0.88266	1.00000	0.13367	-0.27792
$W_{S,U}$	0.76502	0.05593	0.54358	-0.07527	0.24941	0.13367	1.00000	0.23147
$U_{SLIP,U}$	0.07403	0.60400	0.09255	0.06823	0.20618	-0.27792	0.23147	1.00000
$\Delta P_{S,L}$	-0.07578	0.28775	-0.18087	0.13925	0.40307	0.22192	0.12648	0.36178

Variable Selection Report One

Dependent Variables: $\Delta P_{S,L}$

No.	R-Squared	Variables
1	0.16246553726	U_g
2	0.33296269922	U_g ,d_{tube} (m)
3	0.41341728449	U_g ,$U_{P,U}$,d_{tube} (m)
4	0.46585016753	U_g ,$W_{S,U}$,d_p (μm),d_{tube} (m)
5	0.49338955249	U_g ,$W_{S,U}$,d_p (μm),ρ_p ,d_{tube} (m)
6	0.51079224928	Θ,U_g ,$W_{S,U}$,d_p (μm),ρ_p ,d_{tube} (m)
7	0.51345079357	Θ,U_g ,$U_{P,U}$,$W_{S,U}$,d_p (μm),ρ_p ,d_{tube} (m)

APPENDIX H : RAW EXPERIMENTAL DATA AND TIME SERIES DERIVED DATA

APPENDIX H1 : SAND PRESSURE GRADIENT RAW DATA

APPENDIX H2 : SAND PRESSURE GRADIENT TIME SERIES DATA

APPENDIX H3 : GLASS PRESSURE GRADIENT RAW DATA

APPENDIX H4 : GLASS PRESSURE GRADIENT TIME SERIES DATA

APPENDIX H1 : PRESSURE GRADIENT RAW DATA FOR SAND

RUN #	Θ (°)	W_s kg/m²s	U_g (m/s)	α (%)	UPSTREAM PRESSURE (Pa)	ΔP/L (Pa/m)
1	0	150.0	4.73	2.19	4747	634
2	0	158.8	4.66	2.10	5009	676
3	0	144.4	6.27	1.24	3898	418
4	0	143.8	5.75	1.46	3860	439
5	0	120.1	6.23	1.11	3396	350
6	0	160.0	8.67	0.67	4358	336
7	0	114.1	6.25	0.92	3053	295
8	0	150.0	8.53	0.58	3877	290
9	0	100.0	6.10	0.72	2706	243
10	0	97.5	8.38	0.39	2924	194
11	0	94.5	6.09	0.67	2593	222
12	0	197.3	6.94	1.57	4496	450
13	0	184.0	6.90	1.23	4120	398
14	0	50.4	4.39	0.61	1956	188
15	0	160.0	6.89	1.05	3853	380
16	0	62.5	4.41	0.84	2335	253
17	0	140.0	6.92	1.04	4208	429
18	0	76.3	4.55	1.02	2866	335
19	0	212.9	6.43	1.51	4482	488
20	0	92.5	4.52	1.16	3278	406
21	0	193.6	6.35	1.62	4247	467
22	0	99.6	4.60	1.31	3846	494
23	0	162.9	6.27	1.32	3871	399
24	0	114.3	4.63	1.21	3985	502
25	0	153.8	8.72	0.83	4625	344
26	0	127.5	4.66	1.88	4220	553

RUN #	Θ (°)	W_s kg/m²s	U_g (m/s)	α (%)	UPSTREAM PRESSURE (Pa)	ΔP/L (Pa/m)
27	0	168.8	8.65	0.85	4416	359
28	0	176.3	6.93	1.40	4331	442
29	0	196.3	5.81	2.01	4649	547
30	0	168.8	5.71	1.34	4198	485
31	0	191.3	6.37	1.24	4098	428
32	0	62.5	5.51	0.55	2048	162
33	0	113.8	8.47	0.45	3244	224
34	0	92.9	5.61	0.75	2646	248
35	0	155.0	6.84	0.92	3841	378
36	0	105.0	5.68	0.88	2901	292
37	0	167.5	8.62	0.62	4208	332
38	0	202.6	6.40	1.23	4416	485
39	0	192.9	6.92	1.37	4298	423
40	0	135.0	5.65	1.05	3506	378
41	4	169.6	4.89	2.69	5272	725
42	4	153.6	7.69	0.93	4427	346
43	4	175.0	7.78	1.06	4938	397
44	4	76.6	4.40	1.09	2004	202
45	4	198.0	4.85	3.19	6379	879
46	4	87.5	12.35	0.77	4986	178
47	4	236.3	7.95	1.41	5928	506
48	4	104.4	10.28	0.89	4408	190
49	4	65.8	5.51	0.37	2792	212
50	4	234.0	10.68	1.96	6900	465
51	4	90.4	5.63	0.65	3321	304
52	4	97.5	8.02	0.47	3687	210
53	4	121.1	5.66	0.99	4183	437
54	4	146.8	8.81	0.77	5362	290

RUN #	Θ (°)	W_s kg/m²s	U_g (m/s)	α (%)	UPSTREAM PRESSURE (Pa)	ΔP/L (Pa/m)
55	4	92.4	4.61	1.36	2728	304
56	4	26.1	7.10	0.19	1899	89
57	4	157.5	5.82	1.40	4968	531
58	4	179.0	4.80	2.85	6128	749
59	4	213.9	5.69	2.03	6042	671
60	4	154.0	10.48	1.12	5446	279
61	4	86.1	4.65	1.25	3273	307
62	4	41.5	8.58		2532	93
63	4	103.1	4.62	1.55	4031	407
64	4	222.6	9.07	1.22	5881	452
65	4	111.1	4.62	1.68	4365	488
66	4	78.1	10.01	2.14	3698	522
67	4	144.5	4.73	2.26	5470	649
68	4	172.4	8.27	0.92	5209	379
69	4	193.4	10.71	1.57	6135	368
70	4	139.1	7.55	0.85	4182	309
71	4	156.4	4.83	2.46	5779	694
72	11	140.9	7.17	0.85	6855	453
73	11	153.0	6.71	1.16	7508	552
74	11	86.8	6.94	0.49	4769	288
75	11	153.0	6.71	1.16	7508	552
76	11	162.5	8.04	0.77	7437	455
77	11	99.9	6.39	0.73	5149	3[illegible]0
78	11	114.0	7.76	0.62	5642	315
79	11	99.9	6.39	0.73	5149	390
80	11	50.9	7.38	0.20	2370	156
81	11	80.1	6.29	0.55	4387	327
82	11	159.4	9.12	0.72	8092	439

RUN #	Θ (°)	W_s kg/m²s	U_g (m/s)	α (%)	UPSTREAM PRESSURE (Pa)	ΔP/L (Pa/m)
83	11	106.9	6.42	1.73	5535	433
84	11	147.9	8.84	0.64	6801	351
85	11	122.9	6.54	1.02	6479	498
86	11	103.3	8.60	0.27	5145	247
87	11	122.9	6.54	1.02	6479	498
88	11	86.8	6.94	0.49	4769	288
89	11	122.9	6.54	1.02	6479	498
90	11	107.6	6.98	0.54	5365	341
91	11	175.6	6.71	2.83	8634	673
92	11	135.0	7.16	0.74	6674	438
93	11	138.1	6.67	2.26	7442	559
94	11	158.3	7.29	0.99	7655	490
95	11	95.9	5.79	0.97	4329	429
96	11	97.5	6.27	0.61	5083	389
97	11	108.8	5.96	1.46	6256	536
98	11	111.3	6.45	0.88	5713	136
99	11	108.8	5.96	1.46	6256	536
100	11	133.0	6.57	1.09	6795	502
101	11	96.6	5.91	1.86	5578	484
102	11	120.6	6.54	0.86	6378	481
103	11	96.6	5.91	1.86	5578	484
104	11	145.0	7.89	0.91	7109	441
105	11	128.8	5.99	1 69	7179	627
106	11	98.0	7.72	0.51	5123	282
107	11	136.3	6.11	1.71	7868	674
108	11	147.9	8.84	0.64	6801	351
109	11	49.4	4.61	1.01	3862	414
110	11	73.9	8.53	0.26	4253	186

RUN #	Θ (°)	W_s kg/m²s	U_g (m/s)	α (%)	UPSTREAM PRESSURE (Pa)	ΔP/L (Pa/m)
111	11	49.4	4.61	1.01	3862	414
112	11	119.6	7.04	0.69	5962	387
113	11	57.4	4.66	1.57	4453	476
114	11	140.9	7.17	0.85	6855	453
115	11	57.4	4.66	1.57	4453	476
116	11	111.3	6.45	0.88	5713	136
117	11	72.8	4.81	2.61	5726	600
118	11	120.6	6.54	0.86	6378	481
119	11	72.8	4.81	2.61	5726	600
120	11	164.5	8.96	0.67	7475	426
121	11	66.4	4.80	1.87	5172	545
122	11	107.6	6.98	0.54	5365	341
123	11	66.4	4.80	1.87	5172	545
124	11	97.5	6.27	0.61	5083	389
125	11	97.6	4.82	2.15	6461	642
126	11	137.5	7.89	0.66	6378	362
127	11	97.6	4.82	2.15	6461	642
128	11	135.0	7.16	0.74	6674	438
129	11	122.8	8.71	0.43	5959	294
130	11	133.0	6.57	1.09	6795	502
131	11	83.4	4.85	2.36	6378	654
132	18	71.3	5.68	0.74	4748	428
133	18	117.5	7.01	0.66	6254	518
134	18	131.3	7.06	0.82	7000	562
135	18	85.8	7.59	0.49	4673	271
136	18	185.0	7.17	1.19	7742	646
137	18	137.5	7.86	0.61	7145	492
138	18	208.8	7.20	1.35	8269	679

RUN #	Θ (°)	W_S kg/m²s	U_g (m/s)	α (%)	UPSTREAM PRESSURE (Pa)	ΔP/L (Pa/m)
139	18	76.3	7.52	0.25	4540	284
140	18	213.8	7.28	0.98	8413	701
141	18	41.1	7.30	0.10	2875	132
142	18	147.5	7.15	0.85	7296	608
143	18	193.1	8.95	0.70	1815	476
144	18	68.9	6.23	0.69	4470	333
145	18	131.5	8.79	0.48	6704	354
146	18	85.6	6.37	1.10	5249	428
147	18	70.5	8.55	0.28	4631	208
148	18	90.9	6.42	1.03	5810	488
149	18	200.8	9.05	0.85	8145	467
150	18	112.8	6.47	1.47	6833	603
151	18	138.8	8.84	0.72	7261	397
152	18	135.0	6.58	1.86	7898	698
153	18	147.5	10.52	0.56	7466	296
154	18	138.8	6.54	0.55	6943	670
155	18	151.3	10.65	0.49	8075	334
156	18	125.0	6.53	1.65	7103	624
157	18	87.4	10.17	0.31	5312	198
158	18	131.3	6.57	1.96	8072	724
159	18	150.0	7.90	0.89	7643	489
160	18	208.8	6.71	2.68	9110	788
161	18	211.3	7.28	1.56	9001	670
162	18	181.3	6.66	2.15	8907	786
163	18	183.8	7.19	1.34	7989	658
164	18	226.3	6.72	2.46	9301	722
165	18	151.3	7.17	0.97	7614	626
166	18	156.4	6.88	2.70	8703	792

RUN #	Θ (°)	W_s kg/m²s	$^{T}J_g$ (m/s)	α (%)	UPSTREAM PRESSURE (Pa)	ΔP/L (Pa/m)
167	18	73.0	6.81	0.39	4398	322
168	18	185.6	6.14	3.13	9330	861
169	18	51.4	7.39	0.24	3325	171
170	18	136.3	6.11	3.07	8680	813
171	18	113.1	7.66	0.34	5823	403
172	18	158.3	6.11	3.36	9214	853
173	18	165.5	8.85	0.61	7398	403
174	18	125.0	6.11	3.23	8428	791
175	18	43.4	8.26	0.16	2431	142
176	18	123.5	6.00	2.35	8074	765
177	18	222.5	9.10	1.21	8762	470
178	18	116.6	5.93	2.35	7033	709
179	18	66.6	10.10	0.20	4524	158
180	18	115.0	5.94	2.64	7620	710
181	18	212.5	8.05	1.28	8051	570
182	18	90.0	5.78	1.18	5628	471
183	18	183.8	7.19	1.34	7989	658
184	18	102.5	5.88	1.86	6633	589
185	18	85.8	7.59	0.49	4673	271
186	18	132.5	6.09	2.31	8336	818
187	18	202.5	7.98	0.83	7875	559
188	18	51.3	4.61	1.67	4458	577
189	18	164.5	8.93	0.74	7617	431
190	18	58.6	4.67	2.75	5248	658
191	18	107.5	7.74	0.67	5880	358
192	18	60.9	4.82	3.30	6184	742
193	18	95.8	6.88	0.52	5251	435
194	18	88.8	4.91	5.72	8314	995

RUN #	Θ (°)	W_s kg/m²s	U_g (m/s)	α (%)	UPSTREAM PRESSURE (Pa)	ΔP/L (Pa/m)
195	18	113.1	8.65		5774	295
196	18	103.1	4.86	5.41	9041	1096
197	18	230.0	7.26	1.70	8458	677
198	18	107.4	10.21	0.39	4868	239
199	18	132.5	7.83	0.49	6736	461
200	18	72.9	4.86	5.42	7676	974
201	18	95.4	4.93	4.57	7937	918

APPENDIX H2 : SAND PRESSURE GRADIENT TIME SERIES DATA

RUN#	f_D (Hz)	AR (n)	AR[1]	AR[2]	AR[3]	R^2 (%)
1	5.55	1	0.90			80.9
2	5.32	3	1.06	-0.34	0.16	74.6
3	5.32	2	0.67	-0.22		34.1
4	5.55	3	0.90	-0.35	0.20	57.0
5	5.10	3	0.78	-0.41	0.27	42.4
6	4.71	1	0.71			50.0
7	4.10	1	0.60			37.0
8	6.41	3	1.15	-0.53	0.20	72.4
9	3.62	1	0.45			20.8
10	3.42	2	0.79	-0.11		51.7
11	5.55	1	0.64			42.0
12	5.10	3	0.96	-0.46	0.19	55.9
13	5.32	3	0.92	-0.34	0.20	60.6
14	4.90	1	0.72			50.3
15	5.55	3	-0.90	-0.32	0.21	60.8
16	6.10	3	0.90	-0.16	0.12	71.8
17	5.32	3	0.96	-0.53	0.32	57.5
18	3.85	1	0.66			45.6
19	5.81	3	0.92	-0.41	0.18	54.2
20	6.41	1	0.72			53.1
21	6.10	3	0.90	-0.37	0.18	53.6
22	6.76	1	0.77			68.3
23	4.71	3	0.81	-0.21	0.14	53.3
24	5.81	2	0.71	0.17		73.0
25	4.89	3	0.86	-0.31	0.20	55.7
26	5.34	1	0.84			73.3
27	5.32	3	0.92	-0.48	0.35	59.1

RUN#	f_D (Hz)	AR (n)	AR[1]	AR[2]	AR[3]	R^2 (%)
28	4.90	3	0.96	-0.39	0.17	58.9
29	4.39	3	1.07	-0.51	0.29	73.7
30	5.55	3	0.96	-0.33	0.13	61.3
31	4.90	1	0.71			51.7
32	8.68	2	0.79	-0.19		47.0
33	6.09	2	0.76	-0.15		45.9
34	4.39	3	0.79	-0.18	0.26	69.8
35	4.55	3	0.96	-0.54	0.34	57.7
36	4.73	3	0.53	-0.16	0.27	31.5
37	4.73	3	1.05	-0.49	0.27	70.1
38	5.35	3	1.04	-0.46	0.18	64.4
39	5.10	3	0.80	-0.32	0.14	45.0
40	5.10	3	0.86	-0.38	0.29	56.4
41	4.72	2	0.62	0.34		88.9
42	5.55	3	0.49	0.25	0.23	89.1
43	3.62	3	0.49	0.19	0.27	82.5
44	3.73	2	0.15	0.20		22.5
45	3.85	3	0.86	0.26	-0.13	99.0
46	4.90	3	0.31	0.20	0.29	43.3
47	3.62	3	0.50	0.30	0.24	93.1
48	4.71	3	0.28	0.26	0.28	49.9
49	5.81	3	0.37	0.36	0.16	70.3
50	6.09	3	0.73	0.41	-0.15	96.7
51	7.14	3	0.28	0.32	0.30	67.2
52	6.10	3	0.22	0.26	0.17	41.8
53	2.38	3	0.38	0.32	0.20	70.7
54	5.11	2	0.72	0.25		93.2
55	3.08	3	0.19	0.34	0.25	55.2

RUN#	f_D (Hz)	AR (n)	AR[1]	AR[2]	AR[3]	R^2 (%)
56	6.41	3	0.46	0.17	0.24	79.1
57	3.09	2	0.51	0.40		79.8
58	4.89	2	0.82	0.17		98.4
59	5.10	2	0.74	0.26		98.8
60	3.01	3	0.36	0.28	0.32	85.3
61		2	0.51	0.45		88.0
62	5.10	3	0.23	0.17	0.24	36.3
63		3	0.40	0.35	0.14	91.7
64	5.55	2	0.67	0.33		98.4
65	3.16	3	0.39	0.31	0.24	86.1
66	5.32	3	0.36	0.14	0.30	57.7
67	4.09	3	0.50	0.21	0.17	97.3
68	5.81	2	0.63	0.35		96.5
69	4.54	1	1.00			98.8
70	5.55	3	0.47	0.27	0.18	83.8
71	4.90	2	0.60	0.38		84.1
72	3.75					
73	4.23					
74	5.55					
75	2.21					
76	5.10	2	1.46	-0.58		90.0
77	6.76	2	0.23	0.22		14.8
78	5.55					
79	2.82	2	0.23	0.22		14.8
80	4.90	1	0.57			35.9
81	5.81	3	0.45	-0.07	0.24	
82	3.85	3	0.54	-0.13	0.28	30.0
83	2.22					

RUN#	f_D (Hz)	AR (n)	AR[1]	AR[2]	AR[3]	R^2 (%)
84	6.41	3	0.54	-0.36	0.21	24.0
85	2.13					
86	4.72	2	0.49	-0.20		19.6
87	5.81					
88	2.48					
89	2.53					
90	3.85					
91	5.10	2	0.51	0.18		42.7
92	7.57					
93	5.32	2	0.06	-0.23		15.9
94	4.39					
95	2.74	2	0.20	0.26		14.9
96	3.42					20.4
97	2.38	2	0.20	0.14		12.9
98	6.41					
99	4.54	2	0.20	0.14		12.9
100	5.81					
101	7.89					
102	6.09					
103	2.51					
104	5.47	2	1.46	-0.58		90.0
105	8.06	3	1.56	-0.86	0.20	90.3
106	5.55					
107	5.32	2	0.39	0.13		24.6
108	3.86	3	0.54	-0.36	0.21	24.0
109	6.09					
110	3.85	2	0.29	-0.14		9.5
111	3.95					

RUN#	f_D (Hz)	AR (n)	AR[1]	AR[2]	AR[3]	R^2 (%)
112	6.76					
113	3.01					
114	7.34					
115	3.95					
116	3.01					
117	4.90					
118	2.53					
119	6.09					
120	3.04	1	0.58			33.6
121	5.22	1	0.15			2.8
122	2.52					
123	3.33	1	0.15			2.8
124	5.55					20.4
125	4.22	1	0.20			4.1
126	6.41					
127	6.09	1	0.20			4.1
128	3.85					
129	5.32	2	0.52	-0.25		22.0
130	2.25					
131	4.89	1	0.13			7.5
132	5.32	2	0.97	-0.12		80.1
133	6.10	2	1.11	-0.27		82.5
134	5.32	2	1.20	-0.26		90.5
135	3 73	1	0.44			21.1
136	5.55	2	1.20	-0.33		87.5
137	6.75	2	1.17	-0.24		89.0
138	5.57	2	1.29	-0.35		93.4
139	6.09	1	0.78			61.0

RUN#	f_D (Hz)	AR (n)	AR[1]	AR[2]	AR[3]	R^2 (%)
140	5.32	2	1.17	-0.25		87.5
141	6.41	1	0.58			52.0
142	5.10	2	1.35	-0.42		92.0
143	5.31	3	1.17	-0.72	0.38	71.0
144	6.41	1	0.53			52.1
145	5.32	3	1.05	-0.24	0.12	86.9
146	3.73	1	0.20			11.7
147	5.10	2	1.00	-0.25		66.4
148	6.10	3	0.38	0.15	0.12	44.4
149	4.90	1	0.77			59.7
150	5.81	2	0.54	0.18	0.20	44.6
151	4.54	1	0.57			32.0
152	5.32	1	0.44			25.7
153	5.10	3	1.10	-0.43	0.16	74.0
154	4.90	3	0.56	-0.12	0.31	43.7
155	4.72	3	1.20	-0.52	0.22	86.3
156	5.55	3	0.39	0.27	0.17	58.3
157	5.10	3	1.16	-0.61	0.20	69.0
158	4.24	3	0.44	0.21	0.15	49.9
159	6.09	1	0.60			36.0
160	4.72	1	0.64			42.9
161	4.72	2	0.36	0.16		20.8
162	5.10	1	0.57			38.1
163	2.06	2	0.19	0.11		5.8
164	4.24	2	0.49	0.17		39.2
165	4.39	1	0.72			76.0
166	3.52	3	0.30	0.20	0.28	40.2
167	7.57	2	0.98	-0.22		67.0

RUN#	f_D (Hz)	AR (n)	AR[1]	AR[2]	AR[3]	R^2 (%)
168	5.15	2	0.43	0.20		31.7
169	6.76	1	0.51			30.8
170	5.10	2	0.35	0.20		21.8
171	4.72	1	0.91			83.5
172	4.55	2	0.23	0.19		11.4
173	5.10	3	1.12	-0.51	0.25	82.0
174	4.54	3	0.28	0.16	0.17	22.6
175	6.75	2	0.90	-0.30		52.0
176	3.96	2	0.29	0.14		20.6
177	5.10	1	0.79			61.0
178	4.90	1	0.84			69.8
179	6.41	3	1.08	-0.47	0.05	67.0
180	4.72	2	1.29	-0.44		86.5
181	4.72	1	0.40			16.5
182	5.82	1	0.69			79.4
183	4.72	2	0.19	0.11		5.8
184	4.72	2	1.12	-0.26		80.9
185	6.09	1	0.44			21.1
186	6.75	2	1.47	-0.55		91.9
187	5.32	3	1.10	-0.48	0.23	90.0
188	5.55	3	1.15	-0.51	0.15	72.1
189	4.18	2	-0.31	0.24		45.4
190	4.24	2	1.39	-0.58		85.6
191	5.35	1	0.64			40.0
192	4.54	3	1.36	-0.69	0.17	83.0
193	5.55	2	1.06	-0.25		73.3
194	3.96	3	1.50	-0.84	0.24	88.3
195	5.55	3	1.04	-0.43	0.14	64.4

RUN#	f_D (Hz)	AR (n)	AR[1]	AR[2]	AR[3]	R^2 (%)
196	8.62	2	1.31	-0.45		86.0
197	4.90	2				
198	5.32	3	1.08	-0.56	0.23	64.0
199	4.73	2	1.02	-0.14		80.7
200	4.93	3	1.39	-0.83	0.37	80.7
201	5.55	3	1.41	-0.74	0.32	86.6

APPENDIX H3 : PRESSURE GRADIENT RAW DATA FOR GLASS BEADS

RUN	Θ	W_s	U_g	α	STATIC PRESSURE	ΔP/L
#	(°)	kg/m²s	m/s	m³/m³	Pa	Pa/m
2	0	185.4	8.42	2.57	5251	580
3	0	174.3	8.27	2.45	4986	533
4	0	231.0	8.42	2.95	5789	680
5	0	199.0	8.47	2.83	5604	640
6	0	150.0	8.21	2.18	4456	454
7	0	172.5	8.30	1.31	4804	493
8	0	138.8	8.27	1.88	4198	411
9	0	95.4	8.22	1.14	3398	292
10	0	121.5	8.24	1.32	3810	344
11	0	76.5	8.15	0.95	2925	237
12	0	45.4	8.13	0.59	2411	165
13	0	142.9	7.45	4.98	7317	1033
14	0	152.5	7.39	4.87	7242	1001
15	0	147.5	7.42	3.67	6179	827
16	0	135.0	7.36	2.83	5545	718
17	0	123.8	7.27	2.69	4880	603
18	0	102.5	7.18	1.92	3901	435
19	0	127.5	7.24	2.37	4434	516
20	0	87.6	7.20	1.56	3462	354
21	0	64.6	7.10	1.17	2888	269
22	0	152.5	7.42	4.33	7182	1003
23	0	197.8	7.51	4.77	7807	1093
24	0	114.5	6.76	6.12	8591	1260
25	0	103.6	6.80	5.97	8576	1276
26	0	92.4	6.69	5.29	7213	1014
27	0	76.0	6.58	4.33	6571	903

28	0	38.6	6.40	2.26	3637	469
29	0	51.5	6.45	2.82	4597	586
30	0	45.0	6.52	3.10	5264	660
31	0	50.0	6.59	3.38	5800	757
32	0	95.3	9.68	1.56	3885	328
33	0	112.5	9.68	1.45	4137	368
34	0	77.9	9.58	1.23	3412	277
35	0	245.0	11.40	2.73	6303	587
36	0	217.5	11.28	2.41	5802	517
37	0	215.0	11.29	2.09	5884	518
38	0.	185.0	11.30	1.87	5333	451
39	0	123.8	11.21	1.39	4814	394
40	0	160.0	11.25	1.63	4850	412
41	0	125.0	11.18	1.27	4481	363
42	0	100.8	11.15	1.04	4109	318
43	0	79.3	11.02	0.85	3626	266
44	0	68.3	11.08	0.56	3072	202
45	0	127.9	7.96	4.39	6951	841
46	0	115.8	7.94	3.08	5686	764
47	0	116.5	7.82	2.30	4849	607
48	0	91.4	7.72	2.03	4019	471
49	0	112.0	7.75	2.50	4418	537
50	0	85.8	8.07	1.72	3472	378
51	0	77.3	7.66	1.49	3132	325
52	0	58.6	7.64	0.98	2516	227
53	0	68.1	7.22	0.77	2835	254
54	0	13.0	5.32	1.49	1851	263
55	0	18.3	5.38	1.94	2879	386
56	0	36.8	6.02	2.77	4645	620
57	0	33.5	6.05	3.30	5333	630

58	0	30.4	6.23	4.77	6418	924
59	0	16.9	5.37	4.03	4159	608
60	0	293.8	15.09	1.79	7445	540
61	0	201.1	14.95	2.01	6443	460
62	0	228.1	14.84	1.19	6790	483
63	0	175.8	14.72	0.91	5611	373
64	0	119.4	9.88	1.21	6496	334
65	0	119.8	9.81	1.42	6913	384
66	0	141.6	9.92	1.63	7207	416
67	0	177.9	9.97	2.04	8050	530
68	0	243.8	10.12	3.23	8679	742
69	0	207.9	10.00	2.14	8539	620
70	7	202.6	8.48	2.90	8914	825
71	7	187.5	8.47	2.34	7956	663
72	7	155.9	8.43	2.48	7301	562
73	7	143.5	8.30	2.24	6418	531
74	7	127.6	8.32	1.76	5868	442
75	7	102.8	8.25	1.48	5442	383
76	7	69.5	8.24	1.09	4904	296
77	7	64.0	8.16	0.91	4477	234
78	7	30.4	8.13	0.48	3863	140
79	7	14.6	7.09	0.52	3871	137
80	7	28.0	7.23	0.71	4513	204
81	7	58.9	7.25	1.12	5106	287
82	7	76.0	7.22	1.63	5549	378
83	7	114.3	7.38	1.93	6648	533
84	7	120.9	7.44	2.33	7436	649
85	7	148.0	7.36	3.06	8069	743
86	7	155.3	7.50	3.23	8516	805
87	7	200.0	8.15	3.43	9264	869

88	7	160.1	8.07	3.76	8944	880
89	7	160.1	8.01	3.21	8241	735
90	7	134.0	7.99	2.21	7287	588
91	7	149.3	7.95	2.88	7908	699
92	7	119.0	7.89	2.12	6704	131
93	7	99.3	7.82	1.74	6229	458
94	7	91.8	7.75	1.48	5811	382
95	7	74.4	7.82	1.21	5322	299
96	7	72.0	7.63	0.47	3943	138
97	17	74.1	8.31	1.92	6799	474
98	17	69.5	8.20	1.63	6322	410
99	17	38.9	8.20	0.58	4207	142
100	17	57.9	8.27		5515	314
101	17	166.3	10.04		9558	702
102	17	151.3	9.99	2.43	9097	631
103	17	104.4	9.84	1.5	7299	426
104	17	135.0	9.95	1.97	8072	502
105	17	87.5	9.27	1.09	6066	302

APPENDIX H4 : PRESSURE GRADIENT TIME SERIES DATA FOR GLASS BEADS

RUN #	f_D (Hz)	AR(n)	AR[1]	AR[2]	AR[3]	AR[4]	R^2 (%)
1	2.43	2	0.21	0.44			37
2	2.57	3	0.56	0.50	-0.40		56
3	2.22	4	0.31	0.56	-0.28	-0.13	37
4	7.14	1	0.75				56
5	2.00	3	0.60	0.48	-0.34		61
6	2.14	3	0.29	0.51	-0.24		35
7	2.74	3	0.20	0.51	-0.14		30
8	2.10	3	0.13	0.51	-0.27		31
9	2.81	2	-0.36	-0.19			12
10	2.43	3	-0.21	0.43	0.23		23
11	3.72	3	0.12	-0.29	0.27		15
12	5.32	3	0.17	-0.37	-0.39		41
13	3.85	2	0.58	0.26			66
14							
15	2.43	3	0.80	0.53	-0.40		89
16	3.25	3	0.74	0.54	-0.36		86
17	2.03	3	0.70	0.54	-0.34		83
18	2.17	3	0.35	0.71	-0.24		65
19	2.11	4	0.57	0.52	-0.44	0.13	63
20	2.57	2	0.12	0.35			18
21	3.42	3	0.22	-0.16	0.49		26
22	2.14	3	0.88	0.52	-0.44		91
23	5.55	3	0.97	0.27	-0.34		88
24	3.33	4	1.00	-0.19	0.29	-0.19	88
25	2.87	1	0.88				77
26	2.75	2	0.77	0.19			91
27	2.63	2	0.73	0.24			93

RUN #	f_D (Hz)	AR(n)	AR[1]	AR[2]	AR[3]	AR[4]	R^2 (%)
28	2.47	2	0.21	0.36			42
29							
30							
31							
32	2.38						
33	2.74	2	-0.10	0.24			8
34							
35	2.52						
36	2.21	3	-0.16	0.39	-0.12		
37	2.13	4	0.17	0.29	-0.30	0.13	19
38	2.03	2	-0.11	0.51			30
39		2	-0.18	0.53			39
40	2.48	3	-0.38	0.12	0.26		21
41	2.17	2	-0.24	0.50			42
42		2	-0.22	0.53			44
43	2.43	1	-0.31				10
44	3.73	2	-0.13	-0.58			41
45	2.57	4	.755	0.38	-0.38	0.16	83
46		5	0.67	0.38	-0.18	0.28	90
47	2.17	3	0.57	0.45	-0.14		73
48	2.33	4	0.31	0.62	0.19	-0.26	69
49	2.21	2	0.44	0.46			74
50	2.87	1	-0.10				1
51	3.52	3	0.15	-0.20	0.48		24
52	5.32	3	0.16	-0.35	-0.38		38
53	6.41	2	0.67	-0.16			39
54	5.32	3	0.23	-0.41	-0.30		45
55	3.52	0	-0.25	0.39			23

RUN #	f_D (Hz)	AR(n)	AR[1]	AR[2]	AR[3]	AR[4]	R^2 (%)
56	2.35	5	0.34	0.71	-0.26	-0.28	76
57	2.25	2	0.22	0.53			47
58	2.29	2	0.22	0.53			74
59	2.29	2	0.23	0.59			81
60	2.29	3	0.96	0.50	-0.58		91
61	2.14	3	0.86	0.31	-0.38		82
62	2.38	3	1.00	0.14	-0.34		82
63	2.47	5	0.75	0.55	-0.20	-0.52	81
64	4.39	5	0.21	-0.17	0.17	0.53	65
65	2.94	4	0.34	0.26	0.59	-0.10	72
66	3.09	4	0.53	0.13	0.55	-0.44	61
67	2.69	4	0.71	0.21	0.25	-0.34	77
68	2.94	5	1.08	-0.24	0.33	-0.53	82
69	3.09	1	0.87				76
70	3.01	4	0.93	-0.11	0.28	-0.30	76
71	2.75	5	0.70	0.21	0.24	-0.46	76
72	2.75	5	0.56	0.16	0.26	-0.48	63
73	4.39	4	0.55	-0.13	0.17	0.27	82
74	3.42	3	0.19	-0.10	0.65		45
75	3.01	2	-0.21	-0.19			13
76	2.14	2	-0.31	0.31			36
77							
78							
79		2	-0.21	0.59			64
80	2.57	4	-0.24	0.19	0.26	-0.22	74
81	2.81	3	-0.19	0.15	0.58		60
82	2.87	4	0.15	0.13	0.73	-0.14	70
83	2.87	4	0.31	0.22	0.32	-0.28	55

RUN #	f_D (Hz)	AR(n)	AR[1]	AR[2]	AR[3]	AR[4]	R^2 (%)
84	2.94	4	0.68	0.05	0.53	-0.45	76
85	2.87	3	0.80	0.08	0.25		72
86	2.75	2	1.06	-0.23			75
87	3.16	1	0.93				86
88	2.81	1	0.87				77
89	2.87	1	0.85				74
90	3.01	4	0.59	0.12	0.40	-0.35	60
91	2.81	1	0.84				77
92	2.57	3	0.58	-0.12	0.45		79
93	3.96	5	0.19	-0.13	0.21	0.33	74
94							
95	4.54	5	0.17	-0.14	-0.26	0.18	55
96	2.69	4	0.02	0.21	0.60	-0.19	51
97	3.84	4					
98	3.84	4	-0.01	-0.13	0.10	0.65	77
99	3.08	2	0.32	0.24			65
100	3.52	4	0.33	-0.10	0.55	0.17	96
101	3.42	4	1.00	-0.28	0.62	-0.41	91
102	3.52	4	0.86	-0.12	0.45	-0.27	89
103	3.42	2	0.64	0.30			85
104	3.52	1	0.93				85
105	3.42	3	0.80	-0.13	0.31		95